The Influence of Input Uncertainties on Remotely Sensed Estimates of Ocean Primary Productivity

The Influence of Input Uncertainties on Remotely Sensed Estimates of Ocean Primary Productivity

Svetlana Milutinović

Dissertation for the degree philosophiae doctor (PhD)
at the University of Bergen

April 2011

Geophysical Institute,
University of Bergen

Nansen Environmental and
Remote Sensing Center

Bjerknes Centre for
Climate Research

Abstract

Temporally and spatially dense estimates of oceanic phytoplankton net primary productivity (NPP), which are commonly derived by mathematical models from satellite observations of ocean colour, are a cornerstone of current research efforts focused on the state and variability of ecosystems, biogeochemical cycles and climate. Using two exemplary NPP models, it was examined how uncertainties in model input terms might affect the accuracy of the output.

In the first part of the dissertation, the response of NPP estimates to perturbing input values of mixed layer depth (MLD) was analyzed. Four series of NPP fields, two global and two covering the North Atlantic, were computed in monthly intervals during a period of several years. Each of the series resulted from identical remote sensing data but different MLD input. Due to the influence of MLD on the availability of light for photosynthesis, the NPP estimates were overall inversely related to MLD. However, the degree of this relationship varied considerably in space and time over most of the world ocean. During summer, NPP at middle and high latitudes was appreciably sensitive even to small MLD fluctuations, but had little or no response to large MLD perturbations in winter. On the other hand, subtropical regions were characterized by a largely opposite seasonal pattern. Tropical areas showed no seasonality and, apart from the equatorial Pacific, exhibited little sensitivity of NPP to MLD uncertainties. The observed variability in the NPP response was attributed not only to the model's nonlinearity, but also to the presence of the photosynthetic saturation/limitation thresholds, as well as to the coincident sea surface irradiance and, in particular, the diffuse attenuation coefficient for downward irradiance (K_d). It was shown that K_d could be used as an indicator of the NPP sensitivity to uncertainties in MLD, the greatest sensitivity being associated with very large K_d values. Maximum differences between areally integrated annual NPP estimates, based on different MLD input, were about 20–30% in the North Atlantic subpolar gyre, about 15–20% in the eastern part of the North Atlantic subtropical gyre, and less than 10% over the global ocean.

In the second part of the thesis, uncertainties in input terms were propagated through one of the most widely used NPP models via a Monte Carlo method, which enabled distinguishing between random and systematic uncertainty components. The study was based on monthly averaged global remote sensing observations from 2005. Although, due to computational requirements, the analysis was restricted to one year only, the results were remarkably stable in time and space, suggesting that they might also be valid for other years covered by the satellite observations. The typical distribution of uncertainty around the model output was lognormal-like. The average random uncertainty in NPP, expressed as the coefficient of variation, was 108%. The nominal NPP values in individual grid cells were typically overestimated by 6%, relative to the means of the associated uncertainty distributions. These positive systematic errors accumulated to an overestimate of 2.5 Pg C in the annual global NPP of 46.1 Pg C. The input quantity that contributed most to the systematic uncertainty in NPP

was the parameter representing irradiance-dependent vertical changes in chlorophyll-normalized photosynthetic rates. On the other hand, the largest contributor to the random uncertainty in NPP was the term describing the physiological state of phytoplankton. Thus, reductions in the respective uncertainties in these two input terms could improve the accuracy of the NPP model the most.

The final part of the thesis presents an analysis of uncertainty associated with a model of the euphotic depth (Z_{eu}), which was developed for remote sensing applications and computes Z_{eu} from the near-surface chlorophyll concentration. The analysis disregarded any uncertainty in the input chlorophyll values and concentrated only on the intrinsic uncertainty in the Z_{eu} model. The latter was quantified by comparisons between the Z_{eu} model output and reference values of Z_{eu}, derived from *in situ* measured vertical profiles of downward irradiance. The Z_{eu} model uncertainty, expressed in relative terms, complied well with a normal distribution. Due to an uneven geographical coverage of the *in situ* data set, the uncertainty statistics were weighted with a global Z_{eu} climatology, obtained from remote sensing. This provided an estimate of positive bias equal to 9%. The remaining part of Z_{eu} model uncertainty, which is associated with natural variability, amounted to 22% (expressed as the zero-centred root mean square difference).

Contents

Outline

This thesis is organized in six chapters. The first is an introductory chapter, which demonstrates the motivation for the thesis and presents the current state of relevant knowledge. The second chapter gives a synopsis of the author's original research work, while the third chapter synthesizes and discusses the major results of the thesis, and offers some thoughts on possible directions for related future scientific activities.

The original research is presented in a form of scientific papers, in Chapters 4–6. The papers are:

Milutinović S., M. J. Behrenfeld, J. A. Johannessen, and T. Johannessen (2009), Sensitivity of Remote Sensing–Derived Phytoplankton Productivity to Mixed Layer Depth: Lessons from the Carbon-based Productivity Model. *Global Biogeochemical Cycles, 23*, GB4005.

Milutinović S. and L. Bertino (2011), Assessment and Propagation of Uncertainties in Input Terms through an Ocean-Colour-Based Model of Primary Productivity. *Remote Sensing of Environment,* in press, doi: 10.1016/j.rse.2011.03.013.

Milutinović S. (2011), Uncertainty in a Model for Estimating Euphotic Depth from Satellite Observations of Chlorophyll. NERSC Special Report, No. 88, Nansen Environmental and Remote Sensing Center, Bergen, Norway.

Acknowledgements

At last, this years-long voyage is ending. The seas were rough at times, threatening to crush and swallow my little boat, and keep my goal forever out of my reach. Thankfully, those troubles are now behind me and I am sailing into the destination port, but the success is far from being just my own. There are many people I must thank for teaching me how to navigate, for helping me steer in the desired direction or simply for cheering me up in times of self-doubt.

I start with those without whom this particular voyage, in this particular boat, would never have been taken. I am indebted to Ola Johannessen for opening the door of the Nansen Center to me, and to Dominique Durand whose generous assistance with things formal and practical made sure that I could come to Bergen at all. I thank my supervisors, Truls Johannessen, Johnny Johannessen and Christoph Heinze, who, for reasons unclear to me, saw a potential scientist in me and gave me the opportunity to become one.

My special thanks are due to Ingo Bethke and Knut-Frode Dagestad, who unselfishly helped me transform myself from a computational illiterate into a fairly independent code writer, and to Laurent Bertino, for always being available for discussions and for making sure that my statistics hold water.

I am grateful to all those people at work and beyond who helped me find my way around Bergen and have made me feel welcome and accepted. Some of you have become greater friends to me than I could ever have hoped for.

I was fortunate to spend a part of my PhD studies at Oregon State University and have an honour and a pleasure of working with, and learning from, Mike Behrenfeld, Giorgio Dall'Olmo, Robert O'Malley and Toby Westberry. My stay in Oregon would not have been nearly as pleasant as it was without the friendship of Dawn Dauble and Brayden Criswell, who never have stopped showing their care about my well-being, and interest in the progress of my studies.

My utmost gratitude goes to those people who, from my very beginnings onwards, inspired and encouraged me to cultivate my talents and improve as a human being, above all my family: my parents, who helped me discover a passion for knowledge in my earliest years, took care that I keep it and gave me freedom to choose my own path, and my brother, who makes me laugh, gives me a sense of perspective and enriches my life.

<div align="right">

Svetlana Milutinović

Bergen, August 2010

</div>

CHAPTER 1 ——————————————

Introduction

1.1. Motivation

Phytoplankton, the drifting algae, are organisms usually so tiny that their presence is undetectable by the human eye, apart from the occasional periods of prosperity when they become so numerous that they discolour large areas of water surface. The total mass of all living phytoplankton in the oceans at any moment is $1/300$ to $1/1000$ that of all terrestrial plants [*Falkowski and Raven*, 2007]. Although these values may seem rather unimportant, phytoplankton played a crucial role in some major events in the Earth's history and continue to be a vital part of the Earth system today [*Falkowski et al.*, 1998].

Every year, phytoplankton absorb massive quantities of carbon dioxide (CO_2), nearly as much as land plants [*Field et al.*, 1998], and, with the help of sunlight, transform it into energy-dense organic substances that power their life processes and build their organisms. A by-product of this activity, known as photosynthesis, is oxygen, which in a distant geological past, before piling up in the atmosphere, was consumed in the oxidation of rocks. It allowed vast portions of phytoplankton organic material to sink to the sea bottom and later become fossilized [*Falkowski and Raven*, 2007]. About two centuries ago, the fossilized marine phytoplankton became fuel for a rapid technological and economic development, an unintended consequence of which has been a perturbation of the global carbon cycle at a level and rate unseen for at least the past 800,000 years [*Lüthi et al.*, 2008]. The human-triggered emissions of CO_2 trap extra heat in the atmosphere, leading to a change in the Earth's climate. So far, the ocean has abated the climate change to some extent by absorbing a large portion of the excess CO_2, but this has started to modify the ocean's chemical properties [*Doney et al.*, 2009]. Marine organisms, including phytoplankton, are exposed to both direct (chemical) and indirect (climatic) consequences of the human interference with the carbon cycle, and will have to adapt or risk a decline, some of them possibly even extinction [e.g. *Raven et al.*, 2005]. Superimposed on the abiotic (nonliving) environmental impacts are the biotic ones that arise from the intricate web of connections among all living creatures, in which phytoplankton have a fundamental position, because they are the immediate or ultimate source of food for practically all other marine microorganisms and animals. Hence, abiotic impacts on phytoplankton (e.g. shift in the availability of resources for photosynthesis) can, via nutritional relationships, reverberate throughout the network of marine life and thereby also affect the catches of fish and other economically important sea animals. Moreover, phytoplankton responses set off by the initial climate perturbation can act back on climate phenomena, primarily due to the pivotal role of these photosynthesizers in the sequestration of carbon in the deep ocean [*Denman et al.*, 2007].

The environmental factors are many, they operate simultaneously, with time lags or sequentially, can interact with one another directly or indirectly and often involve nonlinear behaviour, all leading to a great complexity that is presenting a major challenge to our understanding and, in turn, limiting our

3

ability to predict the consequences of the human-induced environmental change [*Lawton*, 2001]. A critical goal for the research concerned with these problems is to elucidate environmental regulations of phytoplankton photosynthetic productivity (primary productivity) and the associated responses and feedbacks [*Falkowski et al.*, 2000; *Geider et al.*, 2001]. To achieve this goal, it is essential to acquire routine, long-term and worldwide estimates of ocean primary productivity.

For over a decade, Earth-orbiting satellites have taken remote measurements from which estimates of ocean primary productivity can be derived. Naturally, these estimates must be sufficiently accurate to ensure valid scientific conclusions. The work presented here investigates how the accuracy of primary productivity estimates may be affected by the uncertainty in data they rest upon. In part, uncertainty is a consequence of an incomplete knowledge about the measured phenomenon or reductions in the complexity and detail of the knowledge built in a measurement model, which are often necessary to make the measurement practicable [*Curran*, 2002]. This portion of uncertainty shows how skilful a given primary productivity model is in representing the reality. It has been investigated in a number of studies by comparisons with field measurements of primary productivity [e.g. *Campbell et al.*, 2002; *Friedrichs et al.*, 2009]. The remaining part of uncertainty is brought about by uncertainties in model input terms and has not received much attention.

The following section presents an overview of some fundamental concepts and the current state of knowledge on the topic.

1.2. Background

1.2.1. What is Primary Productivity?

Primary productivity (PP) is the biochemical conversion of inorganic carbon, i.e. CO_2, into organic compounds, whereby carbon becomes a biologically usable building material and a source of energy for metabolism. Because this process takes carbon from a gaseous state and makes it nonvolatile by converting it into organic solutes and particles [*Falkowski et al.*, 1998], its alternative name is carbon fixation. PP is often used in the scientific literature to denote both the process itself and the rate at which it occurs, although some authors suggested that the latter be described by the term 'primary production' [see *Williams*, 1993]. On the other hand, *Falkowski and Raven* [2007] stated that 'productivity' indicates a time-dependent process or a rate (with dimensions of mass/time), while 'production' is a quantity expressed in dimensions of mass. In this work, PP is used with the intended meaning indicated by the context.

To yield the energy-rich organic matter from the reactant of a considerably lower energy content (CO_2), primary producers or autotrophs (from Greek *autos* 'self' + *trophē* 'nourishment') require a supply of free energy in one of two

forms. The first is chemical energy originating from oxidation of simple inorganic chemicals, such as H_2S or NH_4^+. PP based on this form of energy is referred to as chemosynthesis. Only a few species of bacteria, confined to hydrothermal vents or cold-water seeps at the sea-floor, are chemosynthetic (or chemoautotrophic) [*Libes*, 1992]. This marginalizes the importance of chemosynthesis in a global context, when compared to the other type of PP, that is, photosynthesis. Photosynthesis is fuelled by the energy of light and, although comprising a number of chemical reactions, can be summarized by the simple chemical equation

$$CO_2 + H_2O + light \xrightarrow{\text{chlorophyll } a} (CH_2O) + O_2. \tag{1.1}$$
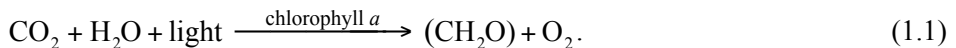
Chlorophyll *a* is the main photosynthetic pigment, responsible for the absorption of energy from light. The harvested energy is used to extract protons and electrons from water (H_2O), in order to pass them to CO_2, which yields carbohydrate, designated by the empirical chemical formula (CH_2O), and diatomic molecular oxygen (O_2). The energy and carbon incorporated during photosynthesis can subsequently be used (with addition of nutrients, such as nitrogen and phosphorus) to synthesize other important organic compounds, including proteins, lipids, and nucleic acids. Owing to the release of O_2, the process represented by the Equation (1.1) is called oxygenic photosynthesis. There are a few prokaryotic[1] photosynthesizers that perform another, more primitive, type of photosynthesis, which is based on different pigments, uses different electron donors instead of H_2O and therefore does not generate O_2 (hence named anoxygenic photosynthesis) [e.g. *Béjà et al.*, 2000; *Blankenship*, 1992; *Kolber et al.*, 2000]. However, the Equation (1.1) is representative of the vast majority of photosynthesizers (or photoautotrophs), including most of the cyanobacteria and all eukaryotic[2] photoautotrophs.

1.2.2. Importance of Primary Productivity: Food Webs, Elemental Cycles and Climate

Virtually all of the biologically usable energy on the Earth originates ultimately from the Sun. Sunlight, however, is not available without interruptions. In order to secure regular and sufficient supply of free energy, photoautotrophs manufacture carbohydrates and other organic compounds as storage molecules

---

[1] Pertaining to prokaryotes (from Greek *pro* 'before' + *karyon* 'nut, kernel'), which are microscopic, single-celled organisms that have no nucleus or other specialized intracellular structures bounded by membranes.

[2] Belonging to the group of organisms called eukaryotes (from Greek *eu* 'well' + *karyon* 'nut, kernel'), which consist of one or more cells with membrane-surrounded compartments or organelles, including the nucleus.

for the chemical energy yield resulting from the absorption of light. The newly formed organic matter may be used for the immediate energy requirements of the photosynthetic organisms. The set of biochemical reactions that break down organic matter to retrieve energy is known as cellular respiration [*del Giorgio and Williams*, 2005]. Although the respective metabolic pathways of photosynthesis and cellular respiration are different, respiration can be summarized by the chemical equation equivalent to that which represents photosynthesis (Equation (1.1)), but of the opposite direction:

$$(CH_2O) + O_2 \longrightarrow CO_2 + H_2O + energy .\qquad(1.2)$$
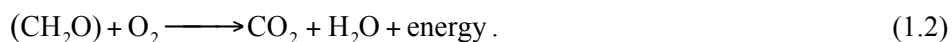
If the instantaneous energy requirements are not exhaustive, the excess organic molecules can be stockpiled as energy reserves or used for the autotrophs' growth and reproduction. The build-up of the unused organic matter in the environment is a *condicio sine qua non* for a nutritionally distinct group of organisms termed heterotrophs (from Greek *heteros* 'other' + *trophē* 'nourishment') or consumers, which encompasses all animals and fungi, as well as many bacteria. Unlike the autotrophs, the heterotrophs cannot extract energy from abiotic sources and instead meet their energy requirements by consuming prefabricated organic matter (living or dead, particulate or dissolved) that originates from either autotrophs or other heterotrophs. These trophic (i.e. nutritional) relationships among various populations in an ecosystem can be visualized as a network of connections, the food web [*Pomeroy*, 1974]. According to their general feeding habits, the members of a food web can be grouped into hierarchical categories named trophic levels. The nutritionally self-reliant primary producers form the foundation of any food web and therefore constitute the first trophic level. They are the direct source of food for grazers or herbivores, which are the primary consumers and represent the second trophic level. Heterotrophs that feed on herbivores are regarded as the third trophic level. These carnivorous (i.e. flesh-eating) organisms can themselves be prey for other carnivores, and so on, until the highest trophic level is reached. The nonliving organic matter, that results, for instance, from excretion and death at all trophic levels, is eventually consumed by heterotrophic microorganisms and thereby remineralized, i.e. returned to inorganic state.

This brief overview of trophic interrelationships reveals that the accumulation rate of the leftover organic material from autotrophs in the environment determines the maximum potential biomass and productivity of an ecological unit (such as an ecosystem, a biome or the entire biosphere) by constraining the overall flow of biological energy and cycling of biologically relevant chemical elements (biogeochemical cycles) [*Falkowski and Raven*, 2007]. The amount of organic matter that is made available to the second trophic level within a particular time period, because it has not been respired by

the autotrophs, is net primary productivity (NPP) [*Lindeman*, 1942; *Williams*, 1993]. NPP is usually expressed in terms of carbon, which is universally present in organic compounds. At a fundamental level, NPP might be thought of as the net amount of carbon fixed in an instant by a photoautotrophic cell [*Platt and Sathyendranath*, 1993a]. However, ecological and biogeochemical studies are concerned with comparatively large temporal and spatial scales. Within that framework, therefore, NPP is commonly presented as the net mass of carbon fixed in a unit volume (or per unit surface area) of the photoautotroph-containing medium during an entire day.

Around one half of the global annual NPP is accomplished by oxygenic photosynthesis in marine environments [*Field et al.*, 1998]. Marine photoautotrophs are a heterogeneous group of organisms, encompassing life forms of increasing complexity ranging from simple prokaryotes (e.g. cyanobacteria) and unicellular eukaryotes (e.g. diatoms, coccolithophores and dinoflagellates) to macroscopic algae (seaweeds) and highly evolved flowering plants (seagrasses). Virtually all macroscopic forms and some of the microscopic ones are benthic (i.e. inhabiting the sea bottom) [e.g. *Bernecker*, 2009; *Cahoon*, 1999; *Gattuso et al.*, 2006]. Since light fades away rapidly as it travels through the water, the benthic photoautotrophs are restricted to the relatively shallow sea bottoms of coastal regions and thus, although important for the local ecosystems, are not major contributors to the global ocean NPP [e.g. *Charpy-Roubaud and Sournia*, 1990; *Duarte and Chiscano*, 1999; *Field et al.*, 1998]. The bulk of the worldwide oceanic NPP is supplied by the photosynthetic activity of mainly unicellular photoautotrophs that float in the well-lit upper layer of the water column. They are called phytoplankton (from Greek *phuton* 'plant' + *planktos* 'wandering').

By dominating oceanic NPP, phytoplankton assume a critical role in the global cycling of vital chemical elements, such as carbon. In taking up CO_2 during photosynthesis, phytoplankton lower the partial pressure of this gas in the surrounding water. The created imbalance in CO_2 content at the atmosphere-ocean interface induces an influx of CO_2 into the surface layer of the ocean from the overlying air. Most of the photosynthetically fixed carbon enters the food web in the upper ocean, where it undergoes heterotrophic respiration that returns CO_2 into the water and potentially to the atmosphere. Nevertheless, a small proportion of organic carbon (approximately 15–20% of global ocean NPP [*Falkowski and Oliver*, 2007; *Laws et al.*, 2000]) escapes by sinking into the dark ocean interior. A tiny fraction of this organic material (~0.1% [*Falkowski and Oliver*, 2007; *Holligan*, 1992]) gets buried in marine sediments, while the rest is respired by deep ocean biota, releasing CO_2 into the ocean interior. In general, deep water is heavier than that at the surface and the two water layers are separated by a steep density gradient (the pycnocline) that presents a hindrance to the vertical exchange of matter. Hence, the return of the deep waters to the sea surface occurs very slowly and CO_2 is effectively trapped in the deep zone for centuries or even millennia [*Falkowski et al.*, 1998; *Sarma*

et al., 2007]. The sinking flux of organic carbon in concert with the vertical stratification makes the concentration of CO_2 in the deep ocean much higher than at the air-sea interface.

The biologically mediated sequestration of CO_2 or 'biological pump' [*Heinze et al.*, 1991] is responsible for keeping the atmospheric concentration of this greenhouse gas 300 parts per million by volume lower than would be the case if there were no life in the sea [*Falkowski and Oliver*, 2007], hence directly affecting the Earth's climate (Figure 1.1). On the other hand, climate-related physical and chemical processes strongly influence the abundance, diversity and distribution of ocean biota [e.g. *Longhurst*, 1998; *Mann and Lazier*, 1996]. In particular, these processes affect the very motor of the biological pump, i.e. NPP, by controlling the biotope conditions, such as temperature and availability of light and nutrients for phytoplankton photosynthesis [*Behrenfeld et al.*, 2002a; *Falkowski and Oliver*, 2007]. It is now practically indisputable that the anthropogenic emissions of CO_2 and other greenhouse gases will lead to a global warming in the coming decades [*Solomon et al.*, 2007]. A warming trend was already recorded in the upper layer of the world ocean during the second half of the previous century [*Levitus et al.*, 2000]. The projected continuation of this trend would, in general, intensify the vertical stratification of the ocean and therefore further constrain mixing between surface and deep waters [*Sarmiento et al.*, 1998]. While this would likely keep the already sequestered CO_2 below the pycnocline (and thus out of contact with the atmosphere) for a prolonged time, it would also slow down the return of nutrients essential for phytoplankton growth (which were lost from the upper layer in the form of sinking organic matter) to the nutrient-impoverished surface layer. At the same time, suppressed vertical mixing would keep phytoplankton above the depths that cannot be reached by sunlight, thus increasing the average exposure of phytoplankton to light. This would extend the phytoplankton growth season in the regions where light is in short supply [*Bopp et al.*, 2001; *Le Quéré et al.*, 2003]. Beside this indirect effect, ocean surface warming *per se* could also benefit phytoplankton in presently very cold regions by abating the direct temperature limitation of photosynthesis [*Steinacher et al.*, 2010]. Owing to the mutually opposing effects on phytoplankton growth, the ocean warming could equally lead to a rise or drop in oceanic NPP [*Behrenfeld et al.*, 2008; *Le Quéré et al.*, 2003] and, consequently, a strengthening or weakening of the biological pump.

The climate is not the only agent capable of modifying the biological pump. Any change in the biologically mediated oceanic absorption of CO_2 is superimposed on, and likely to interact with, changes in the physically and chemically driven CO_2 transfer at the air-sea interface. The physical CO_2 flux is determined by a propensity for equilibration of CO_2 concentrations between the air and the sea surface [*Takahashi et al.*, 2009]. The ability of the surface ocean to physically absorb CO_2 from the atmosphere is substantially enhanced by a chemical reaction between CO_2 and water that creates carbonic acid and its ions [*Sabine and Tanhua*, 2010]. While this chemical enhancement has greatly
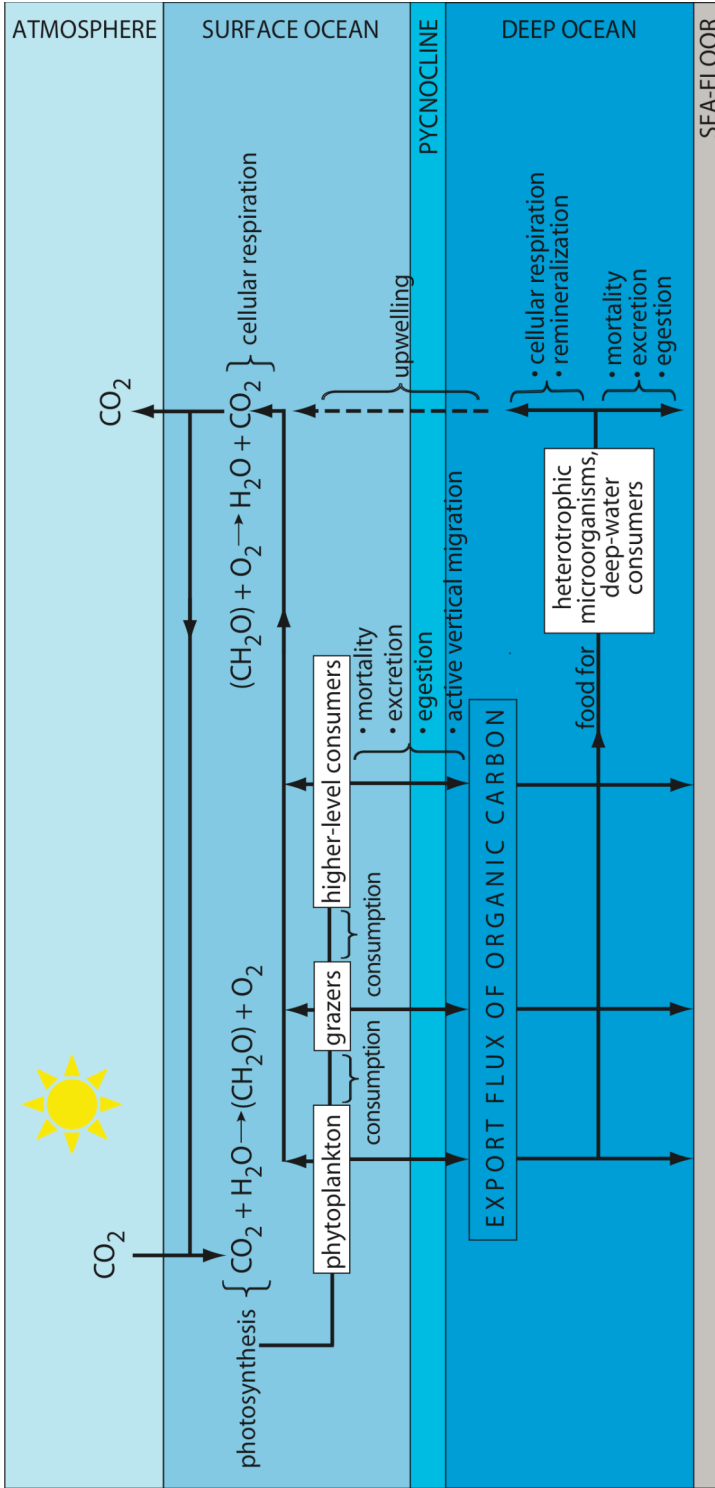
Figure 1.1. Diagram of the biological pump, i.e. the enrichment of the deep ocean with CO_2, relative to the surface ocean layer. Note that the vertical layers on the diagram are not shown in their natural relative proportions. The biological pump is initiated by the photosynthetic activity of phytoplankton, wherein sunlight is used to fix CO_2 into organic carbon substances, such as carbohydrates. A part of the organic matter is respired by phytoplankton, while the rest becomes available for consumption and subsequent respiration by heterotrophs. (Continued on next page.)

Figure 1.1. (Continued.) The collective cellular respiration of the surface ocean biota releases most of the previously fixed CO_2 back into the water (from where it can return to the atmosphere). However, a portion of the organic carbon slips away across the pycnocline into the deep ocean via sinking of nonliving biogenic material or via vertically migrating organisms. It is estimated that this portion, on average, amounts to about 15–20% of global NPP [*Falkowski and Oliver*, 2007; *Laws et al.*, 2000], but the regional values are very much dependent on the factors such as the phytoplankton taxa, cell size and abundance, as well as the structure of the surface ocean food web [*Chisholm*, 2000; *Falkowski and Oliver*, 2007; *Holligan*, 1992]. Most of the exported organic carbon is used as food by deep-ocean biota, thereby being oxidized into CO_2. Since, on the whole, it takes a large amount of energy, and hence time, to lift up the dense, CO_2-rich deep water through the pycnocline, CO_2 piles up and lingers at great depths for about 1,000 years on average [*Chisholm*, 2000]. This, together with the deep convection of cold and heavy surface waters in the polar regions, yields a sharp CO_2 gradient between the surface ocean (holding 9.2×10^{17} g of carbon in the form of CO_2 and its hydrated and ionic equivalents) and the deep ocean (containing about 3.7×10^{19} g petagrams of inorganic carbon) [*Sabine and Tanhua*, 2010]. A tiny fraction of organic carbon fixed in the surface ocean (about 0.1%) escapes oxidation and makes it all the way to the sea-floor, where it becomes integrated in sediments and sedimentary rocks, therefore enabling the accumulation of oxygen in the Earth's atmosphere over geological time scales [*Falkowski and Oliver*, 2007].

contributed to a mitigation of atmospheric CO_2 rise (the upper ocean currently absorbs about a third of the excess atmospheric CO_2), it has made the ocean surface water more acidic [*Doney et al.*, 2009]. Continued CO_2 emissions will make the surface ocean accumulate even more CO_2 and further acidify. These changes are expected to affect marine phytoplankton in various ways. Some of these effects are primarily associated with the increased ocean CO_2 content, while others are mainly ascribed to the rising ocean acidity, although these two environmental factors cannot be fully separated [*Raven et al.*, 2005].

Because most of marine phytoplankton species can actively concentrate CO_2 at the sites of carbon fixation, their growth is not limited by oceanic CO_2 concentration [*Giordano et al.*, 2005]. Indeed, a number of studies reviewed by *Doney et al.* [2009] found little change in algal photosynthetic rates during high-CO_2 exposure. Yet, some experiments resulted in a substantial increase in the productivity of studied species or phytoplankton communities under high-CO_2 conditions [e.g. *Iglesias-Rodriguez et al.*, 2008; *Riebesell et al.*, 1993; *Riebesell*, 2004; *Riebesell et al.*, 2007]. The reported inconsistencies in phytoplankton response may be caused by inherent differences among investigated phytoplankton strains/species/communities, as well as by

discrepancies in experimental design (e.g. duration, light and nutrient availability).

An additional consequence of increasing ocean CO_2 level could be a rise in the carbon content of the photosynthetically produced organic matter relative to nitrogen and phosphorus, respectively, and an increased leakage of dissolved organic substances from phytoplankton cells [*Bellerby et al.*, 2008; *Riebesell*, 2004; *Riebesell et al.*, 2007]. The increased carbon content of organic material may lead to an increased efficiency of the biological pump, provided that the material is sufficiently heavy, so it can sink in the deep ocean before it is degraded. This could be accomplished by the ability of dissolved organic matter to spontaneously assemble in polymer gels that enhance particle aggregation [*Riebesell*, 2004]. On the other hand, the formation and preservation of calcium carbonate ($CaCO_3$), a very important ballast mineral in sinking particles, is widely expected to be negatively affected by the acidification, which would act to reduce the efficiency of the biological pump [*Raven et al.*, 2005]. In today's oceans, $CaCO_3$ cannot be precipitated abiotically and is generated in large proportions by a group of phytoplankton called coccolithophores [*Raven et al.*, 2005]. However, the research on their ability to calcify in a more acid ocean has yielded very disparate results, although it has been focused on only four of about 250–500 extant coccolithophore species [*Doney et al.*, 2009]. In addition to being major calcifying organisms, coccolithophores are prominent primary producers, but it is unclear whether, and to what extent, a potential decrease in their calcification would negatively influence their contribution to overall ocean NPP. In fact, some studies show that the photosynthetic activity of a dominant coccolithophore species increases under high-CO_2 conditions [e.g. *Iglesias-Rodriguez et al.*, 2008; *Riebesell*, 2004]. Alongside its direct impact on calcification, the acidification may have an indirect effect on NPP in general by controlling the chemical forms and solubility, and hence bioavailability, of nutrients and toxins [*Doney et al.*, 2009; *Raven et al.*, 2005].

Clearly, the increasing surface ocean CO_2 content and the accompanying acidification affect a number of marine phytoplankton properties, but the nature of each of these effects seems to be highly inconsistent among various phytoplankton communities, species and even strains. Because the research in this area is still at an early stage, the understanding of the physiological mechanisms underlying the direct impacts of CO_2 rise is poor and it is unclear how they may interact with one another or with the impacts of other simultaneously changing environmental factors [*Raven et al.*, 2005]. It is the interplay of the various factors and their integrated effect that will decide the future changes in marine ecosystems. Much more research is needed to predict the net direction and magnitude of these alterations with confidence [*Raven et al.*, 2005]. This is required to know whether the initial climate perturbation will be mitigated (negative feedback) or amplified (positive feedback) by marine biosphere.

Variations in the strength of the biological pump present the principal potential feedback of phytoplankton to climate change (via increased or decreased CO_2 absorption by the ocean). In addition, phytoplankton might respond to climate variability by adjusting their emissions of dimethylsulphide, which is the main source of cloud seeds over the oceans [*Ayers and Cainey*, 2007; *Charlson et al.*, 1987]. Furthermore, climate-induced changes in the absorbing and scattering of sunlight by phytoplankton cells would influence the global radiation budget and the heat distribution in the water column [*Frouin and Iacobellis*, 2002; *Morel and Antoine*, 1994]. All of these feedbacks are, or may be, associated with NPP. Another related and important factor to consider is that, by acting on phytoplankton and their photosynthetic activity, environmental perturbations are likely to be relayed throughout the food webs and so have indirect effect on the biomass and productivity of any higher trophic level, including marine crustaceans, molluscs, fish, reptiles, birds and mammals [*International Ocean-Colour Coordinating Group (IOCCG)*, 2009]. This, in turn, may change the functioning and structure of ocean ecosystems and affect the related economic activities.

These issues can be investigated using combined mathematical representations of climate-relevant physical, chemical and biological processes that serve as virtual laboratories in which the future high-CO_2 world is simulated. Such coupled climate-ecosystem models generally suggest that the stratification will promote NPP in regions where light is the dominant limiting factor for photosynthesis (i.e. high latitudes), but will dampen NPP where nutrients are the scarcest resource (i.e. subtropics) [*Doney*, 2006]. A few recent large-scale studies have indeed observed an inverse relationship between sea surface temperature (SST) or the depth of the pycnocline and NPP or phytoplankton chlorophyll concentration in the oligotrophic (nutrient-poor) regions of the global ocean [*Behrenfeld et al.*, 2006; *Behrenfeld et al.*, 2008; *Behrenfeld et al.*, 2009a; *Martinez et al.*, 2009]. However, they failed to find a statistically significant support for the traditional view that upper layer warming should benefit phytoplankton at higher latitudes. In fact, *Behrenfeld et al.* [2008; 2009a] discovered that, over the past decade or so, higher latitudes also exhibited an inverse relationship between SST and chlorophyll levels in the upper ocean. This does not necessarily imply that the same kind of relationship exists between SST and phytoplankton biomass or photosynthesis, as it may merely be a consequence of phytoplankton acclimation to enhanced light exposure, which involves reduction in intracellular chlorophyll content [*Behrenfeld et al.*, 2005]. Notwithstanding, *Behrenfeld* [2010] found a very close correspondence between sea-surface chlorophyll concentration and phytoplankton biomass in the subpolar North Atlantic. Contrary to the stance that has prevailed for more than half a century [see *Sverdrup*, 1953], *Behrenfeld* [2010] postulated a mechanism that gives vertical mixing the central role in the formation of phytoplankton bloom (a rapid substantial increase in phytoplankton biomass) in this region, with deeper mixing potentially resulting in a greater bloom. Clearly, these findings are not

fully consistent with the results of coupled climate-ecosystem models. Moreover, the modelling studies themselves are not in a complete mutual agreement with regard to the global net effect of climate change on phytoplankton. Several studies that modelled the response of ocean productivity to rising atmospheric CO_2 content during the 21st century found a net reduction in global ocean NPP or biological pump [e.g. *Bopp et al.*, 2001; *Boyd and Doney*, 2002; *Cox et al.*, 2000; *Henson et al.*, 2010; *Steinacher et al.*, 2010]. In contrast, an approach by *Sarmiento et al.* [2004] yielded a net rise in world ocean NPP by 2050. Furthermore, a multimillennial simulation by *Schmittner et al.* [2008] resulted in a continuous net increase in ocean NPP, which culminated in about twice as large global annual values in the fourth millennium, compared to the present time. In addition, *Schmittner et al.* [2008] found an initial drop in the efficiency of the biological pump, but this was followed by its full recovery to the preindustrial values and even a slight rise after the second half of the third millennium.

The coupled climate-ecosystem models are the key tools to quantify the numerous interweaved, often nonlinear, relations within and between the Earth's abiotic and biotic realms, and predict the future state of the global climate and ecosystems. At the same time, they are limited by the accuracy of the knowledge on underlying dominant processes and their mutual feedbacks, as well as the availability of high-performance computational resources. Hence, the model output and, more fundamentally, the paradigms the models are based on must continually be evaluated against experimental and observational data. Regular, long-term and large-scale observations of ocean NPP are therefore an indispensable component of efforts to further elucidate climatic controls on ocean biology and the associated responses and feedbacks [*Henson et al.*, 2010].

1.2.3. Field Measurements of Oceanic NPP

There are several methods that can be used in oceanographic fieldwork to measure NPP [*Falkowski and Raven*, 2007; *Platt and Sathyendranath*, 1993a]. The most common of those is the ^{14}C method, involving the addition of a small amount of CO_2, labelled by the radioactive carbon isotope ^{14}C, into a sample of seawater from a certain depth, confined within a transparent container. After a period of incubation (hours), either *in situ* or onboard a research vessel, the radioactivity of filtered particulate organic material from the sample is measured to yield the rate at which ^{14}C is incorporated in phytoplankton. Thereafter, NPP is determined based on the assumption that the rates of incorporation of ^{14}C and the naturally prevailing non-radioactive isotope ^{12}C are proportional to their concentrations in the medium.

The ^{14}C method was introduced by *Steemann Nielsen* in 1952 and quickly became accepted by oceanographers worldwide, whose cumulative effort has contributed several thousand vertical profiles of NPP since [*Falkowski and Raven*, 2007]. The decades of intensive use permitted a build-up of detailed

understanding of the method's strengths and weaknesses [see e.g. *Barber et al.*, 2001; *Falkowski and Raven*, 2007; *Maestrini et al.*, 1993]. Notably, it was realized in the late 1970s that the measurement tools could easily contaminate the samples with trace metals, hence distorting the results [*Falkowski and Raven*, 2007]. The problem was widespread until this discovery and persisted even after that for a while. Moreover, it was found that individuals or laboratories performing the method were themselves a considerable source of uncertainty in the ^{14}C NPP estimates [*Richardson*, 1991]. These issues were subsequently addressed in large collective activities, such as Joint Global Ocean Flux Study, which helped in improving and converging the ^{14}C measurement procedures [*Barber et al.*, 2001].

While the ^{14}C method is very sensitive, precise and rather simple [*Williams et al.*, 2002], it is time-consuming, especially if recommendations are followed that the incubations be done *in situ* (to avoid uncertainties from on-deck simulations of ambient temperatures and particularly the intensity and spectral quality of light [*Lohrenz*, 1993]) and over the period between sunrise and sunset or even the full 24-hour cycle (to be able to make proper allowance for phytoplankton respiration [*Dandonneau*, 1993]). Hence, the field measurements can only cover an infinitesimal proportion of the vast ocean expanse and, apart from few stations with long-term dedicated monitoring programmes, hardly offer more than one isolated, static glance at a given location within a long stretch of time. On the other hand, ecological, biogeochemical and climatological applications require sustained regional and global mapping of spatial and temporal variability in oceanic NPP. Although maps yielded by interpolating between sporadic and pointwise field observations did provide historic insight into broad patterns of ocean NPP [e.g. *Koblentz-Mishke et al.*, 1970], they cannot meet the requirements of today's global change research.

1.2.4. Observations of Oceanic NPP from Space

Today, NPP maps can be provided by satellite remote sensing [e.g. *Antoine et al.*, 1996; *Behrenfeld et al.*, 2005; *Behrenfeld and Falkowski*, 1997a; *Longhurst et al.*, 1995; *Mélin and Hoepffner*, 2011; *Smyth et al.*, 2005]. Instead of involving a direct contact with the ocean, these measurements rely on satellite-borne sensors that receive and record electromagnetic radiation emanated from the ocean surface into the space. The electromagnetic signal bears an imprint of surface or near-surface oceanic properties and can be interpreted in a way that extracts useful information on these properties. The part of electromagnetic spectrum conveying information on phytoplankton is the segment visible to the human eye, which spans the wavelengths between 400 nm and 700 nm (Figure 1.2). The kind of remote sensing that provides the optical view of the ocean is generally known as ocean colour remote sensing, although it does not correspond exactly to the human colour vision, as it can collect much richer and more complex information than the human eye [*Morel*, 1980; *Robinson*, 2004].

frequency in hertz
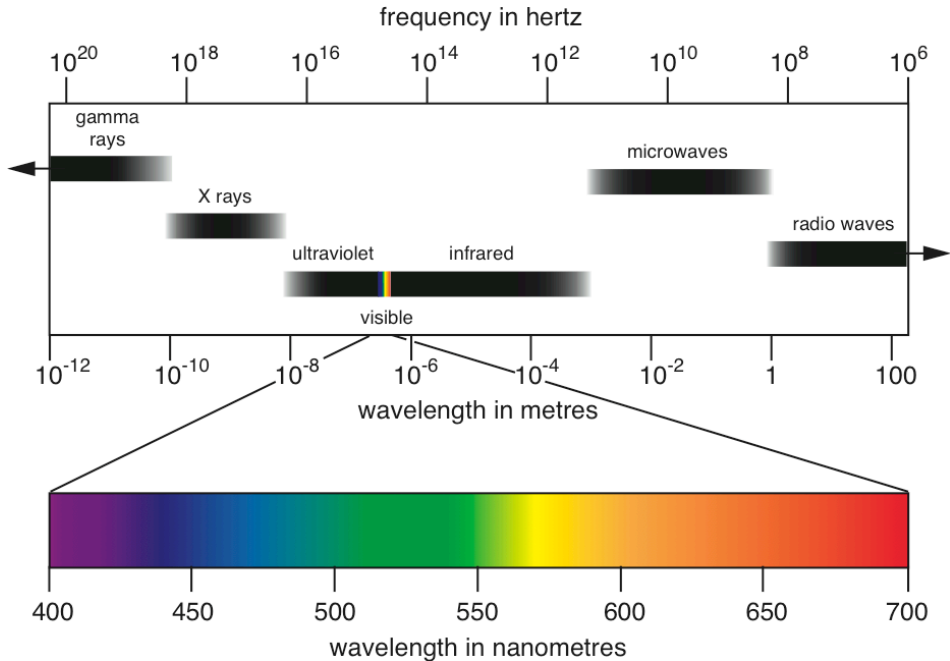
Figure 1.2. The electromagnetic spectrum. Note that the boundaries between the indicated spectral regions are approximate rather than precise. The visible radiation occupies a narrow band within the spectrum, which is shown magnified to illustrate the position of different colours.

Most of the satellites on which the ocean colour sensors are mounted have a near-polar orbit, i.e. the orientation of their overhead trajectory around the Earth is close to the orientation of the Earth's polar axis [*Robinson*, 2004]. Usually, the sensors do not merely observe the thin path straight below the spacecraft, but view a wide swath of the Earth's surface by rapidly scanning the surface strip that lies perpendicular to the direction of the flight [*Kirk*, 1994]. This capability, together with the satellite altitude of around 700–800 km, used commonly in this type of remote sensing, yields a swath width ranging from a few hundreds to thousands of kilometres [*IOCCG*, 1998]. While a polar-orbiting satellite flies above the Earth, the Earth rotates eastward. Therefore, each consecutive orbit covers a different swath within the satellite repeat cycle. The light signal that the spaceborne sensors are intended to measure is the portion of sunlight that reaches the ocean and, rather than being absorbed, gets scattered upward in the sensors' direction. This kind of sensors can thus view the ocean only when it is sun-lit. Nevertheless, as it takes only ~100 minutes to complete an orbit and the observed swath is very wide, the entire ocean surface area can be observed in one to three days [*IOCCG*, 1998]. However, a part of the ocean surface is usually concealed from the view of satellite ocean colour

sensors by clouds, which in practice extends the time needed for global coverage to about 5–10 days [*Campbell et al.*, 2002]. Even with those limitations, ocean colour remote sensing can still provide vastly better spatial coverage than could ever be achieved with field measurements.

The working principle of ocean colour remote sensing stems from the fact that light changes its behaviour as it passes through the water column, because it interacts with seawater. The optically active components of seawater, which are capable of obstructing or altering the propagation of photons by absorbing or scattering them, include phytoplankton cells, coloured dissolved organic matter and suspended debris [*Kirk*, 1994]. Each of these components interacts with light in a characteristic way. The changes they impose on light are evident in the magnitude and spectral composition of the upwelling photon flux, which can thus be translated into qualitative and quantitative information on the optically active substances.

It is generally taken that, apart from pure water itself, phytoplankton exert the most influence on light in the open ocean and that the optical effects of the remaining oceanic seawater components can be deduced from those of phytoplankton [*IOCCG*, 2000; *Morel*, 1988; *Morel*, 2009]. Phytoplankton cellular structures scatter light of all wavelengths relatively evenly [e.g. *Garver and Siegel*, 1997]. At the same time, phytoplankton contain a number of pigments that absorb light, namely chlorophylls, carotenoids and/or phycobilins. Some of those take part in photosynthesis, while others serve mainly to protect the cells from the damaging effects of light. Among the phytoplankton pigments, chlorophyll *a* is the only one found in all oxygenic phytoplankton and is necessary for photosynthesis to take place. Hence, the absorption of light by phytoplankton is typically expressed in terms of chlorophyll *a* [*Geider and MacIntyre*, 2002]. This pigment is most efficient in absorbing the blue light (the peak absorption occurs at ~443 nm) and, to a lesser extent, the red light (the absorption is strongest at the wavelength of ~675 nm) [*Robinson*, 2004]. It is considerably less successful at absorbing the green light, which imparts green colour to it [*Morel*, 1980].

To enable detecting the contributions of phytoplankton and other seawater components to the water-leaving light, satellite ocean colour sensors measure the magnitude of radiation in multiple distinct narrow wavebands across the visible domain. Such measurements are employed in bio-optical algorithms or ocean colour models, which relate the magnitude of signal in wavebands optically most representative of a given substance (such as chlorophyll *a*) to the concentration of the substance [e.g. *O'Reilly et al.*, 1998] (Figure 1.3). In the early days of satellite ocean colour remote sensing, bio-optical algorithms were commonly formulated empirically [*Sathyendranath and Platt*, 2010], i.e. by finding the equation of the line that best described (in the statistical sense) a collection of points yielded when *in situ* measurements of upwelling visible radiation at the ocean surface were plotted against coincidental concentrations of chlorophyll *a*. Improvements in the theoretical understanding of ocean optics
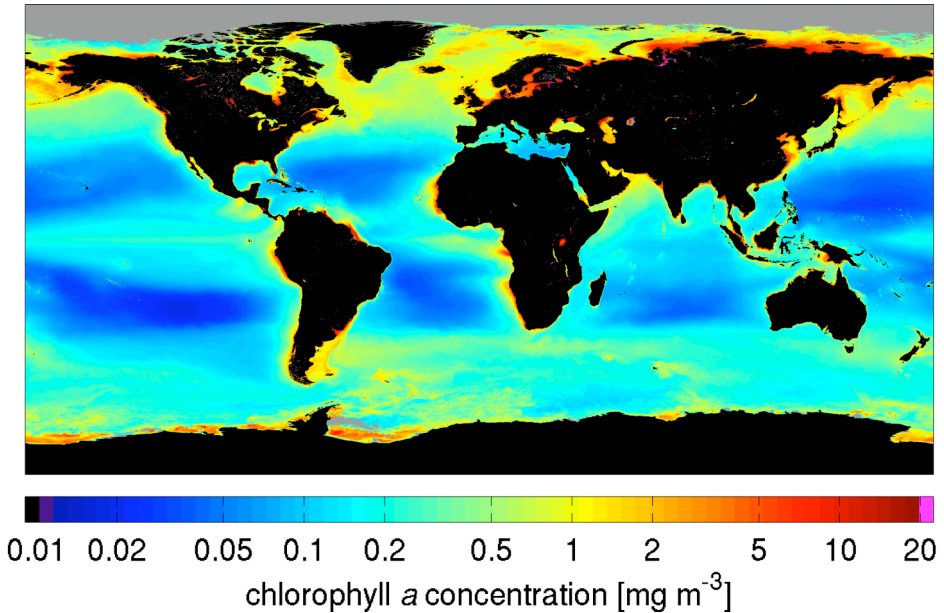
Figure 1.3. Average chlorophyll *a* concentration in the surface ocean, observed between 4th September 1997 and 30th June 2010 by the Sea-viewing Wide Field-of-view Sensor (SeaWiFS). Grey colour is assigned to the grid cells with no data. Data source: the NASA Ocean Biology Processing Group (http://oceancolor.gsfc.nasa.gov/cgi/l3).

and advances in remote sensing technology have enabled a development of ocean colour algorithms that are grounded in theoretical knowledge, although not completely independent of empirical data. Unlike the purely empirical algorithms [e.g. *O'Reilly et al.*, 2000], which are still widely used, the semi-empirical (or semi-analytical) ones can simultaneously derive more than one property, for instance both chlorophyll *a* concentration and backscattering (i.e. upward scattering) of sunlight by particles in the phytoplankton size domain [e.g. *Boss and Roesler*, 2006; *Garver and Siegel*, 1997; *Lee et al.*, 2002; *Loisel and Stramski*, 2000; *Maritorena et al.*, 2002; *Sathyendranath and Platt*, 1997; *Smyth et al.*, 2006].

These properties can be used to compute water-column NPP by mathematical models known as NPP algorithms (Figure 1.4). A myriad of NPP algorithms have been published over the past half a century or so [*Behrenfeld et al.*, 2002a; *Falkowski and Raven*, 2007]. They can be classified according to increasing levels of architectural complexity, from the simplest algorithms that treat the water column, photoperiod and radiation, respectively, as lumps, to the most elaborate ones that model photosynthesis at various wavelengths, day times and water depths [*Behrenfeld and Falkowski*, 1997b]. Other
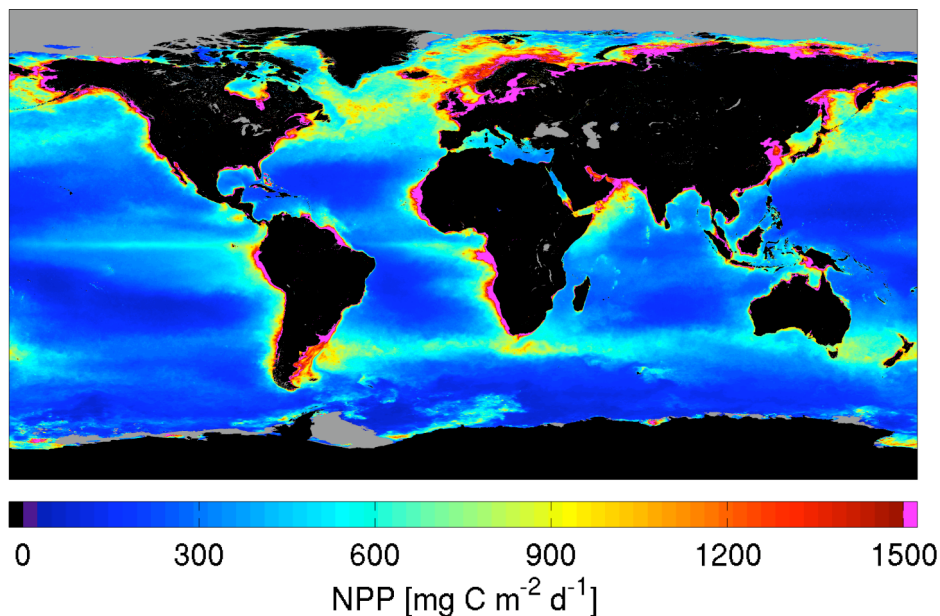
Figure 1.4. Average NPP for 2006, computed by the Vertically Generalized Productivity Model [*Behrenfeld and Falkowski*, 1997a] using SeaWiFS observations. Grey colour denotes missing values. Data source: http://orca.science.oregonstate.edu/2160.by.4320.yearly.hdf.land.ocean.merge.php.

classifications are possible, based on different criteria [e.g. *Joint and Groom*, 2000; *Sathyendranath and Platt*, 2007]. Regardless of classification, all NPP models share the same fundamental approach, computing NPP as a function of phytoplankton biomass [*Antoine and Morel*, 1996; *Behrenfeld et al.*, 2002a; *Morel*, 1991; *Platt and Sathyendranath*, 1993b]. Because, for a long while, the only property of phytoplankton discernable from ocean colour was chlorophyll *a* concentration, many NPP models embraced it as an index of phytoplankton biomass in the surface ocean. This chlorophyll-based approach has only recently got an alternative in carbon-based NPP models. They express phytoplankton biomass in terms of carbon, calculating it from ocean colour observations of particle backscattering [e.g. *Behrenfeld et al.*, 2005; *Westberry et al.*, 2008]. Whatever the model approach, NPP is estimated by multiplying phytoplankton biomass, which is a state variable, by a time-dependent variable. That variable can be expressed as the rate of carbon fixation per unit chlorophyll *a* (in chlorophyll-based models) or the rate of growth, i.e. cell divisions (in carbon-based models). It represents the physiological potential of phytoplankton to photosynthesize, which is largely governed by environmental factors, such as light conditions, nutrient concentrations and temperature. The photophysiological response to ambient

conditions is usually modelled as a function of one or more environmental variables that can be observed from satellites. Historically, it was most common to relate this response to remote sensing observations of SST. However, it has become apparent that light and nutrient availability are much stronger determinants of photophysiological variability than is temperature [*Behrenfeld et al.*, 2002a]. Therefore, novel methods for determining the photophysiological variable lean toward the products of ocean colour remote sensing and ocean modelling [e.g. *Behrenfeld et al.*, 2005; *Behrenfeld et al.*, 2002b; *Behrenfeld et al.*, 2009b; *Uitz et al.*, 2008; *Westberry et al.*, 2008].

NPP estimates derived as the product of remotely sensed phytoplankton biomass and photophysiological state relate only to the ocean layer that contributes to the optical signal detected by ocean colour sensors, which extends to one optical depth, i.e. the depth where light intensity is attenuated to e^{-1} or 37% of its surface value [*Gordon and McCluney*, 1975]. However, photosynthesis is appreciable down to the depth at which the intensity of light falls to 1% of the surface value, i.e. the euphotic depth [*Behrenfeld and Falkowski*, 1997b; *Kirk*, 1994]. NPP models must hence extrapolate the values of NPP pertinent to the first optical depth down to the euphotic depth [*Morel and Berthon*, 1989]. To achieve this, they must, based on some assumptions and ancillary data, imply or express vertical changes in phytoplankton biomass and photophysiological condition, that are primarily driven by the vertical attenuation of light, but also depend on other environmental factors, such as the vertical distribution of nutrients and mixing. The result of NPP modelling is therefore an integrated value for the entire euphotic layer.

References

Antoine, D., J. M. André, and A. Morel (1996), Oceanic primary production 2. Estimation at global scale from satellite (coastal zone color scanner) chlorophyll, *Global Biogeochemical Cycles*, *10*(1), 57-69.

Antoine, D., and A. Morel (1996), Oceanic primary production 1. Adaptation of a spectral light-photosynthesis model in view of application to satellite chlorophyll observations, *Global Biogeochemical Cycles*, *10*(1), 43-55.

Ayers, G. P., and J. M. Cainey (2007), The CLAW hypothesis: A review of the major developments, *Environmental Chemistry*, *4*(6), 366-374.

Barber, R. T., J. Marra, R. C. Bidigare, L. A. Codispoti, D. Halpern, Z. Johnson, M. Latasa, R. Goericke, and S. L. Smith (2001), Primary productivity and its regulation in the Arabian Sea during 1995, *Deep Sea Research Part II: Topical Studies in Oceanography*, *48*(6-7), 1127-1172.

Behrenfeld, M., E. Boss, D. Siegel, and D. Shea (2005), Carbon-based ocean productivity and phytoplankton physiology from space, *Global Biogeochemical Cycles*, *19*(1), GB1006.

Behrenfeld, M. J., and P. G. Falkowski (1997a), Photosynthetic rates derived from satellite-based chlorophyll concentration, *Limnology and Oceanography*, *42*(1), 1-20.

Behrenfeld, M. J., and P. G. Falkowski (1997b), A consumer's guide to phytoplankton primary productivity models, *Limnology and Oceanography*, *42*(7), 1479-1491.

Behrenfeld, M. J., W. E. Esaias, and K. R. Turpie (2002a), Assessment of primary production at the global scale, in *Phytoplankton productivity: Carbon assimilation in marine and freshwater ecosystems*, edited by P. J. leB. Williams, D. N. Thomas and C. S. Reynolds, pp. 156-186, Blackwell Science.

Behrenfeld, M. J., E. Maranon, D. A. Siegel, and S. B. Hooker (2002b), Photoacclimation and nutrient-based model of light-saturated photosynthesis for quantifying oceanic primary production, *Marine Ecology-Progress Series*, *228*, 103-117.

Behrenfeld, M. J., R. T. O'Malley, D. A. Siegel, C. R. McClain, J. L. Sarmiento, G. C. Feldman, A. J. Milligan, P. G. Falkowski, R. M. Letelier, and E. S. Boss (2006), Climate-driven trends in contemporary ocean productivity, *Nature*, *444*(7120), 752-755.

Behrenfeld, M. J., D. A. Siegel, and R. T. O'Malley (2008), Global ocean phytoplankton and productivity, in *State of the climate in 2007*, edited by D. H. Levinson and J. H. Lawrimore, pp. S56–S61, Bulletin of the American Meteorological Society.

Behrenfeld, M. J., D. A. Siegel, R. T. O'Malley, and S. Maritorena (2009a), Global ocean phytoplankton, in *State of the climate in 2008*, edited by T. C. Peterson and M. O. Baringer, pp. S68-S73, Bulletin of the American Meteorological Society.

Behrenfeld, M. J., T. K. Westberry, E. S. Boss, R. T. O'Malley, D. A. Siegel, J. D. Wiggert, B. A. Franz, C. R. McClain, G. C. Feldman, S. C. Doney, J. K. Moore, G. Dall'Olmo, A. J. Milligan, I. Lima, and N. Mahowald (2009b), Satellite-detected fluorescence reveals global physiology of ocean phytoplankton, *Biogeosciences*, *6*(5), 779-794.

Behrenfeld, M. J. (2010), Abandoning Sverdrup's critical depth hypothesis on phytoplankton blooms, *Ecology*, *91*(4), 977-989.

Béjà, O., L. Aravind, E. V. Koonin, M. T. Suzuki, A. Hadd, L. P. Nguyen, S. B. Jovanovich, C. M. Gates, R. A. Feldman, J. L. Spudich, E. N. Spudich, and E. F. DeLong (2000), Bacterial rhodopsin: Evidence for a new type of phototrophy in the sea, *Science*, *289*(5486), 1902-1906.

Bellerby, R. G. J., K. G. Schulz, U. Riebesell, C. Neill, G. Nondal, E. Heegaard, T. Johannessen, and K. R. Brown (2008), Marine ecosystem community carbon and nutrient uptake stoichiometry under varying ocean acidification during the PeECE III experiment, *Biogeosciences*, *5*(6), 1517-1527.

Bernecker, A. (2009), Marine benthic algae, in *Marine biodiversity of Costa Rica, central America*, edited by I. S. Wehrtmann and J. Cortés, pp. 109-118, Springer.

Blankenship, R. E. (1992), Origin and early evolution of photosynthesis, *Photosynthesis Research*, *33*(2), 91-111.

Bopp, L., P. Monfray, O. Aumont, J.-L. Dufresne, H. L. Treut, G. Madec, L. Terray, and J. C. Orr (2001), Potential impact of climate change on marine export production, *Global Biogeochemical Cycles*, *15*(1), 81-99.

Boss, E., and C. Roesler (2006), Over constrained linear matrix inversion with statistical selection, in *Remote sensing of inherent optical properties: Fundamentals, tests of algorithms and applications*, edited by Z. Lee, pp. 57-62, International Ocean-Colour Coordinating Group, Dartmouth, Canada.

Boyd, P. W., and S. C. Doney (2002), Modelling regional responses by marine pelagic ecosystems to global climate change, *Geophysical Research Letters*, *29*(16).

Cahoon, L. B. (1999), The role of benthic microalgae in neritic ecosystems, *Oceanography and Marine Biology: An Annual Review*, *37*, 47-86.

Campbell, J., D. Antoine, R. Armstrong, K. Arrigo, W. Balch, R. Barber, M. Behrenfeld, R. Bidigare, J. Bishop, M. Carr, W. Esaias, P. Falkowski, N. Hoepffner, R. Iverson, D. Kiefer, S. Lohrenz, J. Marra, A. Morel, J. Ryan, V. Vedernikov, K. Waters, C. Yentsch, and J. A. Yoder (2002), Comparison of algorithms for estimating ocean primary production from surface chlorophyll, temperature, and irradiance, *Global Biogeochemical Cycles*, *16*(3), 1035.

Charlson, R., J. E. Lovelock, M. O. Andreae, and S. G. Warren (1987), Oceanic phytoplankton, atmospheric sulphur, cloud albedo and climate, *Nature*, *326*(6114), 655-661.

Charpy-Roubaud, C., and A. Sournia (1990), The comparative estimation of phytoplanktonic, microphytobenthic and macrophytobenthic primary production in the oceans, *Marine Microbial Food Webs*, *4*(1), 31-57.

Chisholm, S. W. (2000), Oceanography: Stirring times in the Southern Ocean, *Nature*, *407*(6805), 685-687.

Cox, P. M., R. A. Betts, C. D. Jones, S. A. Spall, and I. J. Totterdell (2000), Acceleration of global warming due to carbon-cycle feedbacks in a coupled climate model, *Nature*, *408*(6809), 184-187.

Curran, P. J. (2002), Foreword, in *Uncertainty in remote sensing and GIS*, edited by G. M. Foody and P. M. Atkinson, pp. xi-xvi, John Wiley & Sons, Ltd.

Dandonneau, Y. (1993), Measurement of *in situ* profiles of primary production using an automated sampling and incubation device, in *Measurement of primary production from the molecular to the global scale*, edited by W. K. W. Li and S. Y. Maestrini, pp. 172-180, International Council for the Exploration of the Sea, Copenhagen, Denmark.

del Giorgio, P. A., and P. J. leB. Williams (Eds.) (2005), *Respiration in aquatic ecosystems*, 326 pp., Oxford University Press, Oxford.

Denman, K. L., G. Brasseur, A. Chidthaisong, P. Ciais, P. M. Cox, R. E. Dickinson, D. Hauglustaine, C. Heinze, E. Holland, D. Jacob, U.Lohmann, S. Ramachandran, P. L. d. S. Dias, S. C. Wofsy, and X. Zhang (2007), Couplings between changes in the climate system and biogeochemistry, in *Climate change 2007: The physical science basis. Contribution of Working Group I to the Fourth Assessment Report of the Intergovernmental Panel on Climate Change*, edited by S. Solomon, D. Qin, M. Manning, Z. Chen, M. Marquis, K.B. Averyt, M.Tignor and H.L. Miller, pp. 499-588, Cambridge University Press, Cambridge, United Kingdom and New York, USA.

Doney, S. C. (2006), Plankton in a warmer world, *Nature*, *444*, 695-696.

Doney, S. C., V. J. Fabry, R. A. Feely, and J. A. Kleypas (2009), Ocean acidification: The other CO_2 problem, *Annual Review of Marine Science*, *1*(1), 169-192.

Duarte, C. M., and C. L. Chiscano (1999), Seagrass biomass and production: A reassessment, *Aquatic Botany*, *65*(1-4), 159-174.

Falkowski, P., R. Scholes, E. Boyle, J. Canadell, D. Canfield, J. Elser, N. Gruber, K. Hibbard, P. Hogberg, S. Linder, F. Mackenzie, B. Moore, T. Pedersen, Y. Rosenthal, S. Seitzinger, V. Smetacek, and W. Steffen (2000), The global carbon cycle: A test of our knowledge of earth as a system, *Science*, *290*(5490), 291-296.

Falkowski, P. G., R. T. Barber, and V. Smetacek (1998), Biogeochemical controls and feedbacks on ocean primary production, *Science*, *281*(5374), 200-206.

Falkowski, P. G., and M. J. Oliver (2007), Mix and match: How climate selects phytoplankton, *Nature Reviews Microbiology*, *5*(10), 813-819.

Falkowski, P. G., and J. A. Raven (2007), *Aquatic photosynthesis*, 2nd ed., 500 pp., Princeton University Press.

Field, C. B., M. J. Behrenfeld, J. T. Randerson, and P. Falkowski (1998), Primary production of the biosphere: Integrating terrestrial and oceanic components, *Science*, *281*(5374), 237-240.

Friedrichs, M. A. M., M.-E. Carr, R. T. Barber, M. Scardi, D. Antoine, R. A. Armstrong, I. Asanuma, M. J. Behrenfeld, E. T. Buitenhuis, F. Chai, J. R. Christian, A. M. Ciotti, S. C. Doney, M. Dowell, J. Dunne, B. Gentili, W. Gregg, N. Hoepffner, J. Ishizaka, T. Kameda, I. Lima, J. Marra, F. Mélin, J. K. Moore, A. Morel, R. T. O'Malley, J. O'Reilly, V. S. Saba, M. Schmeltz, T. J. Smyth, J. Tjiputra, K. Waters, T. K. Westberry, and A. Winguth (2009), Assessing the uncertainties of model estimates of primary productivity in the tropical Pacific ocean, *Journal of Marine Systems*, *76*(1-2), 113-133.

Frouin, R., and S. F. Iacobellis (2002), Influence of phytoplankton on the global radiation budget, *Journal of Geophysical Research-Atmospheres*, *107*(D19).

Garver, S. A., and D. A. Siegel (1997), Inherent optical property inversion of ocean color spectra and its biogeochemical interpretation 1. Time series from the Sargasso Sea, *Journal of Geophysical Research-Oceans*, *102*(C8), 18607-18625.

Gattuso, J.-P., B. Gentili, C. M. Duarte, J. A. Kleypas, J. J. Middelburg, and D. Antoine (2006), Light availability in the coastal ocean: Impact on the distribution of benthic photosynthetic organisms and their contribution to primary production, *Biogeosciences*, *3*(4), 489-513.

Geider, R. J., E. H. Delucia, P. G. Falkowski, A. C. Finzi, J. P. Grime, J. Grace, T. M. Kana, J. La Roche, S. P. Long, B. A. Osborne, T. Platt, I. C. Prentice, J. A. Raven, W. H. Schlesinger, V. Smetacek, V. Stuart, S. Sathyendranath, R. B. Thomas, T. C. Vogelmann, P. Williams, and F. I. Woodward (2001), Primary productivity of planet earth: Biological determinants and physical constraints in terrestrial and aquatic habitats, *Global Change Biology*, *7*(8), 849-882.

Geider, R. J., and H. L. MacIntyre (2002), Physiology and biochemistry of photosynthesis and algal carbon acquisition, in *Phytoplankton productivity: Carbon assimilation in marine and freshwater ecosystems*, edited by P. J. l. B. Williams, D. N. Thomas and C. S. Reynolds, pp. 44-77, Blackwell Science.

Giordano, M., J. Beardall, and J. A. Raven (2005), CO_2 concentrating mechanisms in algae: Mechanisms, environmental modulation, and evolution, *Annual Review of Plant Biology*, *56*(1), 99-131.

Gordon, H. R., and W. R. McCluney (1975), Estimation of the depth of sunlight penetration in the sea for remote sensing, *Appl. Opt.*, *14*(2), 413-416.

Heinze, C., E. Maier-Reimer, and K. Winn (1991), Glacial pCO_2 reduction by the world ocean: Experiments with the Hamburg Carbon Cycle Model, *Paleoceanography*, *6*(4), 395-430.

Henson, S. A., J. L. Sarmiento, J. P. Dunne, L. Bopp, I. Lima, S. C. Doney, J. John, and C. Beaulieu (2010), Detection of anthropogenic climate change in satellite records of ocean chlorophyll and productivity, *Biogeosciences*, *7*(2), 621-640.

Holligan, P. M. (1992), Do marine phytoplankton influence global climate?, in *Primary productivity and biogeochemical cycles in the sea*, edited by P. G. Falkowski and A. D. Woodhead, pp. 487-501, Plenum Press, New York.

Iglesias-Rodriguez, M. D., P. R. Halloran, R. E. M. Rickaby, I. R. Hall, E. Colmenero-Hidalgo, J. R. Gittins, D. R. H. Green, T. Tyrrell, S. J. Gibbs, P. von Dassow, E. Rehm, E. V. Armbrust, and K. P. Boessenkool (2008), Phytoplankton calcification in a high-CO_2 world, *Science*, *320*(5874), 336-340.

International Ocean-Colour Coordinating Group (IOCCG) (1998), Minimum requirements for an operational ocean-colour sensor for the open ocean, 46 pp, IOCCG, Dartmouth, Canada.

International Ocean-Colour Coordinating Group (IOCCG) (2000), Remote sensing of ocean colour in coastal, and other optically-complex, waters, 140 pp, IOCCG, Dartmouth, Canada.

International Ocean-Colour Coordinating Group (IOCCG) (2009), Remote sensing in fisheries and aquaculture, 120 pp, IOCCG, Dartmouth, Canada.

Joint, I., and S. Groom (2000), Estimation of phytoplankton production from space: Current status and future potential of satellite remote sensing, *Journal of Experimental Marine Biology and Ecology*, *250*(1-2), 233-255.

Kirk, J. T. O. (1994), *Light and photosynthesis in aquatic ecosystems*, 2nd ed., 528 pp., Cambridge University Press.

Koblentz-Mishke, O. J., V. V. Volkovinsky, and J. G. Kabanova (1970), Plankton primary production of the world ocean, in *Scientific exploration of the South Pacific*, edited by W. S. Wooster, pp. 183-193, National Academy of Sciences, Washington, D.C.

Kolber, Z. S., C. L. Van Dover, R. A. Niederman, and P. G. Falkowski (2000), Bacterial photosynthesis in surface waters of the open ocean, *Nature*, *407*(6801), 177-179.

Laws, E. A., P. G. Falkowski, W. O. Smith, Jr., H. Ducklow, and J. J. McCarthy (2000), Temperature effects on export production in the open ocean, *Global Biogeochemical Cycles*, *14*(4), 1231-1246.

Lawton, J. (2001), Earth system science, *Science*, *292*(5524), 1965.

Le Quéré, C., O. Aumont, P. Monfray, and J. Orr (2003), Propagation of climatic events on ocean stratification, marine biology, and CO_2: Case studies over the 1979-1999 period, *Journal of Geophysical Research-Oceans*, *108*(C12), 3375.

Lee, Z., K. L. Carder, and R. A. Arnone (2002), Deriving inherent optical properties from water color: A multiband quasi-analytical algorithm for optically deep waters, *Applied Optics*, *41*(27), 5755-5772.

Levitus, S., J. I. Antonov, T. P. Boyer, and C. Stephens (2000), Warming of the world ocean, *Science*, *287*(5461), 2225-2229.

Libes, S. M. (1992), *An introduction to marine biogeochemistry*, 752 pp., John Wiley & Sons, Inc.

Lindeman, R. L. (1942), The trophic-dynamic aspect of ecology, *Ecology*, *23*(4), 399-417.

Lohrenz, S. E. (1993), Estimation of primary production by the simulated *in situ* method, in *Measurement of primary production from the molecular to the global scale*, edited by W. K. W. Li and S. Y. Maestrini, pp. 159-171, International Council for the Exploration of the Sea, Copenhagen, Denmark.

Loisel, H., and D. Stramski (2000), Estimation of the inherent optical properties of natural waters from the irradiance attenuation coefficient and reflectance in the presence of Raman scattering, *Applied Optics*, *39*(18), 3001-3011.

Longhurst, A., S. Sathyendranath, T. Platt, and C. Caverhill (1995), An estimate of global primary production in the ocean from satellite radiometer data, *Journal of Plankton Research*, *17*(6), 1245-1271.

Longhurst, A. R. (1998), *Ecological geography of the sea*, 398 pp., Academic Press, San Diego.

Lüthi, D., M. Le Floch, B. Bereiter, T. Blunier, J.-M. Barnola, U. Siegenthaler, D. Raynaud, J. Jouzel, H. Fischer, K. Kawamura, and T. F. Stocker (2008), High-resolution carbon dioxide concentration record 650,000-800,000 years before present, *Nature*, *453*(7193), 379-382.

Maestrini, S. Y., A. Sournia, and A. Herbland (1993), Measuring phytoplankton production in 1992 and the coming years: A dilemma?, in *Measurement of primary production from the molecular to the global scale*, edited by W. K. W. Li and S. Y. Maestrini, pp. 244-259, International Council for the Exploration of the Sea, Copenhagen, Denmark.

Mann, K. H., and J. R. N. Lazier (1996), *Dynamics of marine ecosystems: Biological-physical interactions in the oceans*, 2nd ed., 394 pp., Blackwell Science, Cambridge, Massachusetts.

Maritorena, S., D. A. Siegel, and A. R. Peterson (2002), Optimization of a semianalytical ocean color model for global-scale applications, *Applied Optics*, *41*(15), 2705-2714.

Martinez, E., D. Antoine, F. D'Ortenzio, and B. Gentili (2009), Climate-driven basin-scale decadal oscillations of oceanic phytoplankton, *Science*, *326*(5957), 1253-1256.

Mélin, F., and N. Hoepffner (2011), Monitoring phytoplankton productivity from satellite: An aid to marine resources management, in *Handbook of satellite remote sensing image interpretation: Applications for marine living resources conservation and management*, edited by J. Morales, V. Stuart, T. Platt and S. Sathyendranath, pp. 79-93, EU PRESPO and IOCCG.

Morel, A. (1980), In-water and remote measurements of ocean color, *Boundary-Layer Meteorology*, *18*(2), 177-201.

Morel, A. (1988), Optical modeling of the upper ocean in relation to its biogenous matter content (case i waters), *Journal of Geophysical Research-Oceans*, *93*(C9), 10,749-710,768.

Morel, A., and J. F. Berthon (1989), Surface pigments, algal biomass profiles, and potential production of the euphotic layer - relationships reinvestigated in view of remote-sensing applications, *Limnology and Oceanography*, *34*(8), 1545-1562.

Morel, A. (1991), Light and marine photosynthesis: A spectral model with geochemical and climatological implications, *Progress in Oceanography*, *26*(3), 263-306.

Morel, A., and D. Antoine (1994), Heating rate within the upper ocean in relation to its bio-optical state, *Journal of Physical Oceanography*, *24*(7), 1652-1665.

Morel, A. (2009), Are the empirical relationships describing the bio-optical properties of case 1 waters consistent and internally compatible?, *Journal of Geophysical Research-Oceans*, *114*, 15.

O'Reilly, J. E., S. Maritorena, B. G. Mitchel, D. A. Siegel, K. L. Carder, S. A. Garver, M. Kahru, and C. McClain (1998), Ocean color chlorophyll algorithms for SeaWiFS, *Journal of Geophysical Research-Oceans*, *103* (C11), 24937-24953.

O'Reilly, J. E., S. Maritorena, D. Siegel, M. C. O'Brien, D. Toole, B. G. Mitchell, M. Kahru, F. P. Chavez, P. Strutton, G. Cota, S. B. Hooker, C. R. McClain, K. L. Carder, F. Muller-Karger, L. Harding, A. Magnuson, D. Phinney, G. F. Moore, J. Aiken, K. R. Arrigo, R. Letelier, and M. Culver (2000), Ocean color chlorophyll *a* algorithms for SeaWiFS, OC2, and OC4: Version 4, in *SeaWiFS postlaunch technical report series, volume 11, SeaWiFS postlaunch calibration and validation analyses, part 3*, edited by S. B. Hooker and E. R. Firestone, pp. 9-23, NASA, Goddard Space Flight Center, Greenbelt, Maryland.

Platt, T., and S. Sathyendranath (1993a), Fundamental issues in measurement of primary production, in *Measurement of primary production from the molecular to the global scale*, edited by W. K. W. Li and S. Y. Maestrini, pp. 3-8, International Council for the Exploration of the Sea, Copenhagen, Denmark.

Platt, T., and S. Sathyendranath (1993b), Estimators of primary production for interpretation of remotely sensed data on ocean color, *Journal of Geophysical Research-Oceans*, *98*(C8), 14561-14576.

Pomeroy, L. R. (1974), The ocean's food web, a changing paradigm, *BioScience*, *24*(9), 499-504.

Raven, J., K. Caldeira, H. Elderfield, O. Hoegh-Guldberg, P. Liss, U. Riebesell, J. Shepherd, C. Turley, A. Watson, R. Heap, R. Banes, and R. Quinn (2005), *Ocean acidification due to increasing atmospheric carbon dioxide*, 68 pp., The Royal Society, London.

Richardson, K. (1991), Comparison of ^{14}C primary production determinations made by different laboratories, *Marine Ecology-Progress Series*, *72*, 189-201.

Riebesell, U., D. A. Wolf-Gladrow, and V. Smetacek (1993), Carbon dioxide limitation of marine phytoplankton growth rates, *Nature*, *361*(6409), 249-251.

Riebesell, U. (2004), Effects of CO_2 enrichment on marine phytoplankton, *Journal of Oceanography*, *60*(4), 719-729.

Riebesell, U., K. G. Schulz, R. G. J. Bellerby, M. Botros, P. Fritsche, M. Meyerhofer, C. Neill, G. Nondal, A. Oschlies, J. Wohlers, and E. Zollner (2007), Enhanced biological carbon consumption in a high CO_2 ocean, *Nature*, *450*(7169), 545-548.

Robinson, I. S. (2004), *Measuring the oceans from space: The principles and methods of satellite oceanography*, 669 pp., Praxis Publishing Ltd. /Springer Verlag.

Sabine, C. L., and T. Tanhua (2010), Estimation of anthropogenic CO_2 inventories in the ocean, *Annual Review of Marine Science*, *2*(1), 175-198.

Sarma, V., M. Dileep Kumar, and T. Saino (2007), Impact of sinking carbon flux on accumulation of deep-ocean carbon in the northern Indian Ocean, *Biogeochemistry*, *82*(1), 89-100.

Sarmiento, J. L., T. M. C. Hughes, R. J. Stouffer, and S. Manabe (1998), Simulated response of the ocean carbon cycle to anthropogenic climate warming, *Nature*, *393*(6682), 245-249.

Sarmiento, J. L., R. Slater, R. Barber, L. Bopp, S. C. Doney, A. C. Hirst, J. Kleypas, R. Matear, U. Mikolajewicz, P. Monfray, V. Soldatov, S. A. Spall, and R. Stouffer (2004), Response of ocean ecosystems to climate warming, *Global Biogeochemical Cycles*, *18*(3), GB3003.

Sathyendranath, S., and T. Platt (1997), Analytic model of ocean color, *Applied Optics*, *36*(12), 2620-2629.

Sathyendranath, S., and T. Platt (2007), Spectral effects in bio-optical control on the ocean system, *Oceanologia*, *49*(1), 5-39.

Sathyendranath, S., and T. Platt (2010), Ocean-colour radiometry: Achievements and future perspectives, in *Oceanography from space: Revisited*, edited by V. Barale, J. F. R. Gower and L. Alberotanza, pp. 349-359, Springer, Dordrecht, The Netherlands.

Schmittner, A., A. Oschlies, H. D. Matthews, and E. D. Galbraith (2008), Future changes in climate, ocean circulation, ecosystems, and biogeochemical cycling simulated for a business-as-usual CO_2 emission scenario until year 4000 AD, *Global Biogeochemical Cycles*, *22*(1), GB1013.

Smyth, T. J., G. H. Tilstone, and S. B. Groom (2005), Integration of radiative transfer into satellite models of ocean primary production, *Journal of Geophysical Research-Oceans*, *110*(C10), C10014.

Smyth, T. J., G. F. Moore, T. Hirata, and J. Aiken (2006), Semianalytical model for the derivation of ocean color inherent optical properties: Description, implementation, and performance assessment, *Applied Optics*, *45*(31), 8116-8131.

Solomon, S., D. Qin, M. Manning, Z. Chen, M. Marquis, K. B. Averyt, M. Tignor, and H. L. Miller (Eds.) (2007), *Climate change 2007: The physical science basis. Contribution of Working Group I to the Fourth Assessment Report of the Intergovernmental Panel on Climate Change*, 996 pp., Cambridge University Press, Cambridge, UK and New York, USA.

Steemann Nielsen, E. (1952), The use of radio-active carbon (C^{14}) for measuring organic production in the sea, *Journal du Conseil International pour l' Exploration de la Mer*, *18*(2), 117-140.

Steinacher, M., F. Joos, T. L. Frölicher, L. Bopp, P. Cadule, V. Cocco, S. C. Doney, M. Gehlen, K. Lindsay, J. K. Moore, B. Schneider, and J. Segschneider (2010), Projected 21st century decrease in marine productivity: A multi-model analysis, *Biogeosciences*, *7*(3), 979-1005.

Sverdrup, H. U. (1953), On conditions for the vernal blooming of phytoplankton, *Journal du Conseil International pour l' Exploration de la Mer*, *18*(3), 287-295.

Takahashi, T., S. C. Sutherland, R. Wanninkhof, C. Sweeney, R. A. Feely, D. W. Chipman, B. Hales, G. Friederich, F. Chavez, C. Sabine, A. Watson, D. C. E. Bakker, U. Schuster, N. Metzl, H. Yoshikawa-Inoue, M. Ishii, T. Midorikawa, Y. Nojiri, A. Körtzinger, T. Steinhoff, M. Hoppema, J. Olafsson, T. S. Arnarson, B. Tilbrook, T. Johannessen, A. Olsen, R. Bellerby, C. S. Wong, B. Delille, N. R. Bates, and H. J. W. de Baar (2009), Climatological mean and decadal change in surface ocean pCO_2, and net sea-air CO_2 flux over the global oceans, *Deep Sea Research Part II: Topical Studies in Oceanography*, *56*(8-10), 554-577.

Uitz, J., Y. Huot, F. Bruyant, M. Babin, and H. Claustre (2008), Relating phytoplankton photophysiological properties to community structure on large scales, *Limnology and Oceanography*, *53*(2), 614-630.

Westberry, T., M. J. Behrenfeld, D. A. Siegel, and E. Boss (2008), Carbon-based primary productivity modeling with vertically resolved photoacclimation, *Global Biogeochemical Cycles*, *22*, GB2024.

Williams, P. J. leB. (1993), On the definition of plankton production terms, in *Measurement of primary production from the molecular to the global scale*, edited

by W. K. W. Li and S. Y. Maestrini, pp. 9-19, International Council for the Exploration of the Sea, Copenhagen, Denmark.

Williams, P. J. leB., D. N. Thomas, and C. S. Reynolds (Eds.) (2002), *Phytoplankton productivity: Carbon assimilation in marine and freshwater ecosystems*, 400 pp., Blackwell Science.

CHAPTER 2 ————————————

Objectives and Summary of the Original Research

II

This thesis aims at gaining a detailed knowledge on the impact that input uncertainties have on NPP assessments from ocean colour data. The thesis includes three papers, which make use not only of satellite observations, but also of physical ocean modelling and *in situ* measurements. The first paper [*Milutinović et al.*, 2009] investigates the sensitivity of an NPP algorithm to variations in input values of mixed layer depth. The second paper [*Milutinović and Bertino*, 2011] quantifies the uncertainty in NPP estimates by Monte Carlo simulations. The third paper [*Milutinović*, 2011] assesses the uncertainty associated with a method for determining the euphotic depth.

2.1. Paper I – Sensitivity of Remote Sensing–Derived Phytoplankton Productivity to Mixed Layer Depth: Lessons from the Carbon-based Productivity Model

Being in direct contact with the atmosphere, the surface of the ocean is constantly exposed to atmospheric boundary layer conditions, such as the near-surface wind, temperature, humidity and precipitation. Their interaction with the ocean surface influences the density of the top ocean layer and creates turbulent and convective motions that penetrate to a certain depth, to which phytoplankton-containing seawater is well mixed and thus of nearly uniform density. This depth is known as the mixed layer depth (MLD). The vertical mixing strongly influences the exposure of phytoplankton to light. If the mixing is shallow, phytoplankton can be positioned close to the sea surface, which, provided the surface illumination is sufficiently strong, makes photosynthesis saturate with respect to light and proceed at a maximum rate possible for given nutrient and temperature conditions. On the other hand, if the mixing penetrates towards greater depths, phytoplankton experience decrease in light levels, which leads to reduced photosynthetic rates.

The knowledge of MLD can be used in NPP algorithms to model the exposure of phytoplankton to light. While a few previously published brief analyses indicated that uncertainties in MLD could severely impact the performance of NPP models [*Carr et al.*, 2006; *Friedrichs et al.*, 2009], no elaborate studies of this issue have been available. The objective of this study was therefore to examine in detail how sensitive the output of an NPP algorithm [*Behrenfeld et al.*, 2005] is to fluctuating MLD. NPP was computed in monthly time steps over a multiyear period. For every month, the NPP algorithm was run four times, each time with the same ocean colour data but new MLD input. The MLD values were generated by four physical ocean models. The models differed in horizontal and vertical resolution, environmental forcing, parameterization of vertical mixing, and definitions of MLD. Owing to this, the MLD fields displayed considerable variability. Nevertheless, the range of MLD estimates at a particular time and location was considered more realistic than would be the case if MLD had simply been perturbed by an arbitrary value. Two of the modelled MLD data sets covered the entire world ocean, while the others covered the North Atlantic only.

Thus, the resulting NPP fields were analyzed and compared globally, as well as in the subpolar and eastern subtropical North Atlantic.

Generally, MLD and NPP were inversely related, because the NPP algorithm determines the amount of light available for photosynthesis as a negative exponential function of MLD. However, different patterns were observed in distinct latitudinal bands. At high and middle latitudes, NPP was practically insensitive to particularly large uncertainties in MLD encountered during winter. In contrast, great sensitivity, even to subtle MLD perturbations, was revealed during summer. In the subtropics, on the other hand, the magnitude of NPP response to MLD uncertainties followed the opposite trend, being negligible in summer and relatively large in winter. Tropical regions exhibited no seasonal variations and, apart from the equatorial Pacific, were characterized by robustness of NPP to uncertainties in MLD. The maximum discrepancy among annual spatially integrated NPP values, which were based on varied MLD input, was 20–30% in the subpolar North Atlantic, 15–20% in the eastern subtropical North Atlantic and <10% over the entire global ocean.

The observed regional and seasonal differences in the response of NPP to MLD perturbations were explained not only by the nonlinear relationship between MLD and light exposure of phytoplankton, as specified by the NPP algorithm, but also by the existence of thresholds beyond which the impact of MLD ceases. The first threshold signifies the light saturation of photosynthesis. When the mixed layer becomes so shallow that the light saturation is accomplished, its continued shoaling will have no further effect. The second threshold designates the full light limitation of photosynthesis. When the mixed layer deepens so much that the complete light limitation is reached, any deeper mixing will exert no further impact. In addition, the influence of uncertainties in MLD on the estimates of light levels experienced by phytoplankton is modified by the intensity of surface illumination and especially by the rate at which light diminishes as it travels down the water column (expressed as the coefficient of attenuation for downward light). The interplay among the two last-mentioned input terms and MLD was analyzed to identify conditions under which the accuracy of MLD is particularly important. It was shown that the value of the attenuation coefficient, a standard product of ocean colour remote sensing, could be used to diagnose the instances when NPP is particularly sensitive to uncertainties in MLD, the sensitivity being greatest for the very large coefficient values (i.e. in turbid waters).

2.2. Paper II – Assessment and Propagation of Uncertainties in Input Terms through an Ocean-Colour-Based Model of Primary Productivity

Every quantity that serves as input for an NPP algorithm is associated with some uncertainty. Two components of uncertainty can be distinguished. One component, termed bias, is caused by the effects that make measurements or

model estimates systematically too high or too low. The remaining uncertainty component, here called imprecision, is related to natural variability. It incorporates uncontrollable random variations in apparently stable conditions that make repeated quantifications of the same variable nonidentical. These two classes of uncertainties in input quantities are likely to yield biased and imprecise NPP estimates. The magnitude of the resulting bias and imprecision, however, depends not only on the analogous values for the input terms, but also on the degree of the algorithm complexity and nonlinearity, as well as the level of correlation between the input terms.

The goal of this study was to quantify the bias and imprecision of estimates from an NPP algorithm [*Behrenfeld and Falkowski*, 1997] that result from uncertainties in its input terms. To this end, a Monte Carlo method was used, the principle of which is generation of random numbers that follow a prescribed distribution of probability. The probability distribution represented the uncertainty in a particular input quantity. If possible, the properties of the input uncertainty distribution were acquired from literature. Otherwise, they were evaluated statistically. Nominal NPP values were computed using monthly averaged remote sensing data from one calendar year. Thereafter, uncertainty in each nominal NPP value was determined by repeating the algorithm calculations a large number of times, each time using a set of input values that were drawn at random from the assigned input uncertainty distributions. For each location and time step, this resulted in a frequency distribution, i.e. a collection of algorithm output values that were sorted and counted according to their magnitude. Such distribution represented uncertainty in a particular nominal NPP value. The difference between the nominal NPP value and the distribution's average was chosen as a measure of the NPP bias. The standard deviation of the distribution was used as a measure of the NPP imprecision. To simplify the analysis, these statistics were normalized with regard to the average of the distribution and expressed as percentages.

It was found that the characteristic NPP uncertainty distribution had a relatively pronounced peak and was skewed to the right, thus resembling a lognormal distribution. The nominal NPP values were typically overestimated by 6%, while their imprecision was 108% on average. The individual overestimates combined additively, yielding a positive bias of 2.5 petagrams of carbon (Pg C = 10^{15} g C) in the annual global NPP of 46.1 Pg C. The input terms were rated based on their individual contributions to the NPP uncertainties. The input parameter that accounts for the relative vertical distribution of photosynthesis was most responsible for the bias of NPP estimates. On the other hand, the input term that represents the photophysiological state of phytoplankton contributed most to the imprecision of NPP. The largest reduction in the input-related NPP uncertainty for the analyzed algorithm would therefore be achieved if the accuracy of these two input terms were improved.

2.3. Paper III – Uncertainty in a Model for Estimating Euphotic Depth from Satellite Observations of Chlorophyll

The ocean layer that is well illuminated by sunlight, thereby allowing appreciable photosynthetic activity, spans from the sea surface to the euphotic depth (Z_{eu}), where photoautotrophic productivity and respiration are considered to be more or less in balance. Since the output of NPP modelling commonly represents the vertical integral of NPP over this euphotic layer, it is important that uncertainty in Z_{eu} be assessed. Various approaches have been developed to estimate Z_{eu} from remotely sensed properties. This paper quantifies the uncertainty in the approach from *Morel and Berthon* [1989], updated by *Morel and Maritorena* [2001], which models Z_{eu} as a function of satellite-derived chlorophyll. In contrast to the second paper [*Milutinović and Bertino*, 2011], this paper disregards the uncertainty contribution from remotely sensed chlorophyll and focuses solely on the uncertainty that is inherent in the Z_{eu} model.

This uncertainty was evaluated by comparing the Z_{eu} model output, derived from field measurements of surface chlorophyll concentrations, with reference Z_{eu} values, determined from vertically resolved *in situ* measurements of underwater light in various geographic regions. It was found that the relative uncertainty (i.e. uncertainty expressed in percentage terms) could be represented by a normal distribution. Because the geographic coverage of the *in situ* data set was inhomogeneous, and hence not globally representative, the uncertainty estimates were statistically weighted against an ensemble of 8-year average Z_{eu} estimates from satellite observations of chlorophyll. This procedure resulted in bias equal to 9% and imprecision equal to 22%.

References

Behrenfeld, M., E. Boss, D. Siegel, and D. Shea (2005), Carbon-based ocean productivity and phytoplankton physiology from space, *Global Biogeochemical Cycles*, *19*(1), GB1006.

Behrenfeld, M. J., and P. G. Falkowski (1997), Photosynthetic rates derived from satellite-based chlorophyll concentration, *Limnology and Oceanography*, *42*(1), 1-20.

Carr, M.-E., M. A. M. Friedrichs, M. Schmeltz, M. Noguchi Aita, D. Antoine, K. R. Arrigo, I. Asanuma, O. Aumont, R. Barber, M. Behrenfeld, R. Bidigare, E. T. Buitenhuis, J. Campbell, A. Ciotti, H. Dierssen, M. Dowell, J. Dunne, W. Esaias, B. Gentili, W. Gregg, S. Groom, N. Hoepffner, J. Ishizaka, T. Kameda, C. L. Quéré, S. Lohrenz, J. Marra, F. Mélin, K. Moore, A. Morel, T. E. Reddy, J. Ryan, M. Scardi, T. Smyth, K. Turpie, G. Tilstone, K. Waters, and Y. Yamanaka (2006), A comparison of global estimates of marine primary production from ocean color, *Deep Sea Research Part II: Topical Studies in Oceanography*, *53*(5-7), 741- 770.

Friedrichs, M. A. M., M.-E. Carr, R. T. Barber, M. Scardi, D. Antoine, R. A. Armstrong, I. Asanuma, M. J. Behrenfeld, E. T. Buitenhuis, F. Chai, J. R.

Christian, A. M. Ciotti, S. C. Doney, M. Dowell, J. Dunne, B. Gentili, W. Gregg, N. Hoepffner, J. Ishizaka, T. Kameda, I. Lima, J. Marra, F. Mélin, J. K. Moore, A. Morel, R. T. O'Malley, J. O'Reilly, V. S. Saba, M. Schmeltz, T. J. Smyth, J. Tjiputra, K. Waters, T. K. Westberry, and A. Winguth (2009), Assessing the uncertainties of model estimates of primary productivity in the tropical Pacific ocean, *Journal of Marine Systems*, *76*(1-2), 113-133.

Milutinović, S., M. J. Behrenfeld, J. A. Johannessen, and T. Johannessen (2009), Sensitivity of remote sensing-derived phytoplankton productivity to mixed layer depth: Lessons from the carbon-based productivity model, *Global Biogeochemical Cycles*, *23*, GB4005.

Milutinović, S. (2011), Uncertainty in a model for estimating euphotic depth from satellite observations of chlorophyll, NERSC Special Report, No. 88, Nansen Environmental and Remote Sensing Center, Bergen, Norway.

Milutinović, S., and L. Bertino (2011), Assessment and propagation of uncertainties in input terms through an ocean-colour-based model of primary productivity, *Remote Sensing of Environment*, in press, doi: 10.1016/j.rse.2011.03.013.

Morel, A., and J. F. Berthon (1989), Surface pigments, algal biomass profiles, and potential production of the euphotic layer - relationships reinvestigated in view of remote-sensing applications, *Limnology and Oceanography*, *34*(8), 1545-1562.

Morel, A., and S. Maritorena (2001), Bio-optical properties of oceanic waters: A reappraisal, *Journal of Geophysical Research-Oceans*, *106*(C4), 7163-7180.

CHAPTER 3

Synthesis and Outlook

III

This chapter brings together the major findings of the thesis, while placing them in a wider context of current knowledge. The unavoidable limitations of the present research are discussed and, building upon this, possible directions for future studies and research-related activities are suggested. Topics addressed here include: the characteristics of *in situ* measurements and satellite ocean colour data; the reliability of modelled mixed layer depth (MLD); the quality of studied net primary productivity (NPP) models; and methods for deriving the euphotic depth (Z_{eu}). The chapter concludes with a short summary of the main points.

3.1. Characteristics of *In Situ* and Remote Sensing Data

3.1.1. Availability of Field Data

For lack of access to a comprehensive collection of field data, the data set employed in the study by *Milutinović and Bertino* [2011] was characterized by weaknesses that inevitably affected the findings. Notably, there was a considerable overlap between the data exploited to formulate some of the input functions and the data used to quantify the associated uncertainties. Consequently, the uncertainties attributed to those input functions are most likely smaller than would be the case if completely independent data were used in the uncertainty evaluations. Furthermore, the spatial coverage by the *in situ* data was adequate only in very few regions, implying that the results of the study might not be representative of the entire world ocean. The temporal coverage was also poor, making it impossible to explore potential geographic and temporal variations in uncertainties.

The lack of appropriate field measurements is a widespread limitation for research dealing with the global marine biosphere [*Richardson and Poloczanska*, 2008] and the problem can be aggravated by restricted access to some of the *in situ* data repositories. This situation would be improved not only by relaxing the restrictions on data access, but also by establishing long-term multinational observational undertakings, such as Joint Global Ocean Flux Study (JGOFS) [*Abbott*, 2001]. In more than a decade, JGOFS collected various field measurements (including those of NPP) that made an invaluable contribution to our current understanding of oceanic biogeochemical cycles and their relationship with climate phenomena [*Dickey*, 2001]. Regrettably, due to technical problems, most of the JGOFS field-work was unaccompanied by satellite observations of ocean colour [*Yoder et al.*, 2001]. Today, with several ocean colour sensors in orbit, a technologically and strategically improved JGOFS-like global *in situ* observational network would be much more valuable. It would, however, require considerable resources and organizational efforts. A more feasible action would be to set up an international point of reference, which would offer an updated index of all existing data archives anywhere in the world, including the metadata, if not the data themselves (for example,

within the framework of the Group on Earth Observations that is coordinating efforts to build the Global Earth Observation System of Systems; see http://www.earthobservations.org/about_geo.shtml). This would be a major step towards ensuring that studies reliant on *in situ* data have a fully adequate foundation, which would enhance the robustness and value of their results, as well as open new research possibilities (e.g. for analyses of spatial and seasonal to decadal variability in uncertainties). Of course, this implies that sustained commitment to field data collection activities must be secured in future [e.g. *Birdsey et al.*, 2009], with simultaneous measurements of all physical, chemical and biological variables necessary for improved understanding of environmental processes, as well as their complex interactions and feedbacks. This new knowledge could, in turn, be integrated in models concerned with climate and ecosystems, while some modelling efforts could also benefit from data assimilation. Moreover, high-quality multidisciplinary *in situ* measurements are imperative for evaluation and support of satellite remote sensing observations, such as ocean colour.

3.1.2. Accuracy of Field Data

Model uncertainty analyses often treat *in situ* measurements as true values [*Boss and Maritorena*, 2006], and this dissertation is no exception in that respect. While such an approach is practical, it is also idealized, because no measurement is devoid of uncertainty [*Bureau International des Poids et Mesures (BIPM) et al.*, 2008; *Taylor*, 1997]. For example, the method for deriving *in situ* values of the euphotic depth (Chapter 6) was based on optical measurements that were themselves associated with some (unknown) uncertainty. Moreover, the method involved interpolation among irradiances at discrete wavelengths and depths, and, in some cases, extrapolation to the depth of 1% photosynthetically available radiation (PAR), each of which was a potential source of uncertainty. The problem of PAR definition (i.e. basing it on plane, rather than scalar, irradiance) and units (μW cm^{-2} versus μmol photons cm^{-2} s^{-1}) could have added to the *in situ* euphotic depth uncertainty, although the study by *Morel and Gentili* [2004] suggests that those effects might be negligible.

Vertical interpolation could also have contributed uncertainty to *in situ* estimates of the *F* parameter by *Milutinović and Bertino* [2011]. More fundamentally, however, the *in situ* assessments of *F*, as well as the phytoplankton photophysiological state (P^b_{opt}), were potentially affected by uncertainties in the field measurements of NPP and chlorophyll concentrations, respectively. Many of the measurements in the NPP data set used by *Milutinović and Bertino* [2011] were taken before the contamination of samples with trace metals from collection and handling procedures was recognized, and addressed, as a serious source of bias (M. J. Behrenfeld, personal communication, 2007) [see also *Falkowski and Raven*, 2007;

Sanderson et al., 1995]. Furthermore, that data set was methodologically heterogeneous, consisting of measurements from both *in situ* and simulated *in situ* ^{14}C incubations, which lasted anywhere between 2 and 24 hours [*Behrenfeld and Falkowski*, 1997b]. It is recognized that the duration of incubations can introduce biases to NPP measurements [*Maestrini et al.*, 1993]. When respiration rates are low, short-term (2–4 h) incubations approximate gross, rather than net, primary productivity [*Falkowski and Raven*, 2007], so the incubation period of 24 h is preferred, as it allows the respiration of radioactively labelled organic C to catch up with that of non-labelled one, takes into account diel periodicity in photosynthetic and respiratory rates and incorporates respiratory losses during night [*Dandonneau*, 1993; *Lohrenz*, 1993, and references therein]. In addition, simulated *in situ* incubations involve uncertainties related to the replications of underwater light field and temperature in on-deck incubators [*Lohrenz*, 1993]. Many other sources of uncertainties concerning the ^{14}C method have been identified [e.g. *Lohrenz*, 1993; *Maestrini et al.*, 1993; *Williams*, 1993], with so-called 'bottle effects' emerging as one of the major problems [*Falkowski and Raven*, 2007]. These are the effects that arise from phytoplankton being isolated in a relatively small volume of water, within an enclosed container, instead of being freely exposed to the natural environment. For instance, in the confinement, phytoplankton are not subject to the naturally occurring light oscillations associated with vertical mixing [*MacIntyre et al.*, 2000]. Also, algal cells within a sample cannot be separated from heterotrophs, which implies that some phytoplankton can be consumed by grazers, with the concomitant return of ^{14}C to inorganic form via heterotrophic respiration [*Falkowski and Raven*, 2007]. Unfortunately, no uncertainties were provided with *in situ* NPP data set employed by *Milutinović and Bertino* [2011], but the order of magnitude of those uncertainties might be surmised based on information from literature. For example, *Pemberton et al.* [2006] analyzed 7 primary productivity measurements, acquired in May 2000 in the Celtic Sea using ^{14}C incubations, and found that the associated uncertainty (expressed as a 95% confidence interval) was up to ±20%. *Friedrichs et al.* [2009] assumed a 10–30% uncertainty level for their tropical Pacific NPP data set, although they cautioned that the actual measurement errors could have been larger. Based on unpublished information, *Saba et al.* [2011] inferred that uncertainty values between ±20% and ±50% were representative for their NPP data, collected in a variety of ocean regions. Neither *Friedrichs et al.* [2009] nor *Saba et al.* [2011] specified the confidence level for their uncertainty values. Besides, none of the three cited sources of quantitative information related to *in situ* productivity data uncertainty made a distinction between bias and imprecision. Finally, it must be emphasized that the studies by *Pemberton et al.* [2006], *Friedrichs et al.* [2009] and *Saba et al.* [2011] were concerned with daily depth-integrated productivity. For that reason, their findings can

serve as no more than a rough guide to uncertainties in the hourly depth-resolved productivity measurements used by *Milutinović and Bertino* [2011].

As already mentioned, *in situ* P^b_{opt} and *F* values in the study by *Milutinović and Bertino* [2011] were also affected by uncertainties in chlorophyll concentrations (Chl). The Chl measurements were obtained from either fluorometry or high performance liquid chromatography (HPLC) [*Behrenfeld and Falkowski*, 1997b]. Fluorometry is generally recognized as a less accurate method of Chl measurement than HPLC [*Gieskes and Kraay*, 1983; *Mantoura and Llewellyn*, 1983; *Mantoura et al.*, 1997; *Pinckney et al.*, 1994; *Wiltshire et al.*, 1998], but the Chl data set applied by *Milutinović and Bertino* [2011] contained no information on the corresponding uncertainties. Moreover, the definition of Chl in the data set was not precise, but it was most likely restricted to chlorophyll *a*, in which case an informed assumption on the magnitude of Chl uncertainties can be derived from literature. *Mantoura and Llewellyn* [1983] reported that the reproducibility of their HPLC technique was 4.8%, based on triplicate samples. A linear regression of actual chlorophyll concentrations in standard pigment mixtures against HPLC measurements by the same technique, performed by *Mantoura et al.* [1997, Figure 14.1], demonstrated an excellent analytical accuracy of HPLC (r^2 = 0.998; slope of the regression line = 1.019). The accuracy of fluorometric methods is affected by the presence and concentration of accessory chlorophylls *b* and *c* and, in particular, chlorophyll degradation products, all of which interfere with fluorescence signal from chlorophyll *a*, thereby resulting in bias [*Gieskes and Kraay*, 1983]. Varying levels of the fluorometric bias have been reported. For illustration, *Gieskes and Kraay* [1983, Table 2] recorded fluorometric chlorophyll *a* overestimates ranging from 1% to 500% with reference to HPLC data in a variety of natural environments (the North Sea, the Caribbean, the North Equatorial Current and the Gulf of Guinea). On the other hand, *Mantoura et al.* [1997] found that, in comparison to HPLC-derived values, fluorometry both over- and underestimated chlorophyll *a* concentrations in mixed pigment standards, microalgal cultures and field samples. In the field samples of seawater, mainly from the North Atlantic, the most extreme over- and underestimates documented by *Mantoura et al.* [1997] were +37% and −69%, respectively. In comparison, fluorometric and HPLC chlorophyll *a* measurements used in Chapter 6 of this thesis were in very good agreement (see Figure 6.3). This literature overview shows that uncertainties in Chl measurements can vary widely, thus making it impossible to speculate on what uncertainty level is reasonable to assume for the Chl data set employed by *Milutinović and Bertino* [2011]. Therefore, uncertainties associated with the corresponding *in situ* P^b_{opt} and *F* values cannot be quantified. To facilitate this and similar kinds of analyses in future, the *in situ* data providers should be encouraged to routinely accompany their measurements with relevant information on uncertainties [*Boss and Maritorena*, 2006].

3.1.3. Availability and Quality of Remotely Sensed Data on Ocean Colour

Ocean colour has been proclaimed as one of currently 45 Essential Climate Variables, in support of the climate monitoring requirements linked to the United Nations Framework Convention on Climate Change [*Global Climate Observing System (GCOS)*, 2009]. Owing to relatively short satellite lifetimes, no single satellite sensor can acquire a sufficiently long time series of measurements that is needed to successfully monitor the effects of changing climate on the ocean biosphere. By comparing the results from three coupled climate-ecosystem models with a 10-year-long satellite ocean colour data set, *Henson et al.* [2010] found that about 40 years of uninterrupted satellite observations are necessary before a response of Chl and NPP to long-term climate trend can undoubtedly be distinguished from interannual to multidecadal oscillations. A gap in the satellite record would extend the time required for detecting the long-term trend to around 60 years [*Henson et al.*, 2010]. Recently, some concerns have been expressed regarding disruption in good-quality ocean colour data record [*Birdsey et al.*, 2009; *Hammann and Puschell*, 2009; *Henson et al.*, 2010; *Kintisch*, 2008; *Siegel and Yoder*, 2007; *Wilson*, 2011]. The main reason for those concerns is that the principal sources of ocean colour data for climate-related research are now either operating beyond their planned mission lifetimes [*Birdsey et al.*, 2009; *Wilson*, 2011] or have completely ceased to operate. Moreover, the performance of an instrument that will succeed two extremely important U.S. sensors (launch scheduled for 2012 [*Wilson*, 2011]) has been questioned in a letter signed by a number of eminent ocean biologists and biogeochemists [*Siegel and Yoder*, 2007]. Fortunately, the European Space Agency is now well under way to ensure a continuity of high-quality ocean colour data over at least 2 decades, starting from 2013, when the first in a series of Sentinel-3 satellites is planned to be launched (see http://www.esa.int/esaLP/SEMTST4KXMF_LPgmes_0.html). Ocean colour missions from other space agencies will follow soon thereafter (Table 3.1). It is necessary, however, that data from at least one of the existing sensors (Table 3.1) be available for the next few years, to enable intercalibrations [*Wilson*, 2011]. This will be crucial for achieving a seamless string of ocean colour observations required to separate out the climate-change-driven trends in ocean biosphere from shorter-term variability.

The intrinsic strengths and weaknesses of ocean colour remote sensing data are roughly opposite to those of *in situ* measurements. While satellite ocean colour sensors can provide frequent and routine observations of vast ocean expanses, they are restricted to measuring the near-surface optical signal, with no ability to achieve vertical profiling [e.g. *Gordon and McCluney*, 1975; *Longhurst et al.*, 1995]. Furthermore, they are incapable of viewing through clouds, whereas in cloudless conditions the largest part (up to ~90%) of the signal they receive is of atmospheric origin [*Longhurst et al.*, 1995; *Robinson*, 2004; *Sathyendranath*, 2000]. The atmospheric component of the signal must

Table 3.1. Current and scheduled satellite ocean colour missions[a]

Sensor	Agency	Satellite	Launch date	Orbit
		Current missions		
COCTS, CZI	CNSA (China)	HY-1B	11 Apr 2007	Polar
GOCI	KARI / KORDI (South Korea)	COMS	26 Jun 2010	Geostationary
HICO	ONR and DOD Space Test Programme	JEM-EF International Space Station	18 Sep 2009	51.6°, 15.8 orbits p/d
MERIS	ESA (Europe)	ENVISAT	1 Mar 2002	Polar
MODIS	NASA (USA)	Terra (EOS-AM1)	18 Dec 1999	Polar
MODIS	NASA (USA)	Aqua (EOS-PM1)	4 May 2002	Polar
OCM	ISRO (India)	IRS-P4	26 May 1999	Polar
OCM-2	ISRO (India)	Oceansat-2	23 Sep 2009	Polar
POLDER-3	CNES (France)	Parasol	18 Dec 2004	Polar
		Scheduled missions		
VIIRS	NOAA / NASA (USA)	NPP	2012	Polar
OLCI	ESA (Europe)	Sentinel-3A	2013	Polar
HSI	DLR (Germany)	EnMAP	2013	Polar
SGLI	JAXA (Japan)	GCOM-C	2014	Polar
COCTS, CZI	CNSA (Japan)	HY-1C/D (China)	2014	Polar
Multispectral Optical Camera	INPE / CONAE (Brazil, Argentina)	SABIA-MAR	2015	Polar
Ocean Colour Scanner, Coastal Zone Scanner	ROSCOSMOS (Russia)	Meteor-3M(3)	2015	Polar
VIIRS	NOAA / NASA (USA)	JPSS-1	2015	Polar
OLCI	ESA (Europe)	Sentinel-3B	2017	Polar
COCTS, CZI	CNSA (Japan)	HY-1E/F (China)	2017	Polar
GOCI-II	KARI / KORDI (South Korea)	KMGS-B	2018	Geostationary
OES	NASA (USA)	PACE	2019	Polar
OES	NASA (USA)	ACE	After 2020	Polar
Coastal Ocean Colour Imaging Spectrometer	NASA (USA)	GEO-CAPE	After 2020	Geostationary

[a]Based on information from the International Ocean-Colour Coordinating Group (http://www.ioccg.org/sensors_ioccg.html).

be removed before any application of bio-optical models, and the accuracy of this so-called atmospheric correction is critical, because even small errors at

this stage can give rise to large errors in the estimates of oceanic optical properties [*Morel*, 1980]. The negative impact of cloudiness on spatial coverage can be lessened by using monthly averages of ocean colour data, although a persistent cloud cover can reduce the number of contributing daily values to considerably fewer than 30. This thesis follows the common practice of estimating NPP from monthly averaged input fields [*Campbell*, 2004]. A more suitable approach for NPP algorithms that involve nonlinear relationships, such as the Vertically Generalized Productivity Model (VGPM) and the depth- and wavelength integrated Carbon-based Productivity Model (DWI CbPM), would be to employ Level-2 remote sensing data in NPP calculations and then average the daily results to obtain monthly mean NPP [*Campbell*, 2004]. Such an approach was not used, partly because of too large requirements for data storage and computational capacity. In addition, NPP algorithms generally rest on the simplistic assumption of balanced (or steady-state) phytoplankton growth [*Siegel et al.*, 2001], implying complete physiological acclimation to instantaneous environmental conditions, such as light availability and nutrient levels [*Behrenfeld et al.*, 2005]. However, a fully acclimated state cannot be established at once, that is, physiological responses lag behind their environmental determinants. Time required for a full physiological adjustment can be as long as several days and depends on such factors as the direction of environmental perturbation, initial growth rate, phytoplankton taxon and property under consideration [e.g. *Cullen and Lewis*, 1988; *MacIntyre et al.*, 2000; *Prézelin et al.*, 1991]. Consequently, the steady-state assumption can be deemed largely valid at time scales over which the short-term occurrences of unbalanced growth more or less average out, but the approach would be inadequate at a temporal resolution matching fluctuations in environmental conditions that are more rapid than the associated physiological responses [*Behrenfeld et al.*, 2005].

Monthly resolution also increases confidence in the suitability of the CbPM expression for deriving algal carbon biomass (Equation (4.2) in Chapter 4) by ensuring that potential transient deviations from the contribution of phytoplankton to particulate backscattering (i.e. $b_{bp}(443)$), set by the scaling factor of 13,000 mg C m^{-2}, are smoothed out [*Behrenfeld et al.*, 2005]. Nonetheless, *Westberry et al.* [2008] found that NPP estimates from the depth- and wavelength resolved (DWR) CbPM were largely robust to variations in the scaling factor between 10,000 and 20,000 mg C m^{-2}, which prompted them to conclude that the selection of the scaling factor value is a second-order problem. Hence, it is probable that the CbPM carbon biomass estimates are more severely affected by uncertainties in $b_{bp}(443)$.

This optical property was derived from remote sensing measurements of water-leaving radiance using the Garver-Siegel-Maritorena semianalytical ocean colour model, version 1 (GSM01), which is optimized for global use [*Garver and Siegel*, 1997; *Maritorena et al.*, 2002]. Unfortunately, a thorough evaluation of GSM01 $b_{bp}(443)$ estimates has been hampered by a shortage of

in situ $b_{bp}(443)$ measurements [*International Ocean-Colour Coordinating Group (IOCCG)*, 2006; *Maritorena et al.*, 2002; *Maritorena et al.*, 2010; *Siegel et al.*, 2005]. Therefore, assessments of uncertainties in $b_{bp}(443)$ output of GSM01 and other bio-optical models have often resorted to synthetic or quasi-real data, generated by independent bio-optical relationships whose uncertainty is assumed to be negligible [see e.g. *Lee et al.*, 2010]. *Maritorena et al.* [2002] reported only a moderate agreement (on a $\log_{10}$ scale: $r^2 = 0.426$; RMSD = 0.2525; bias = 0.04125; $n = 1071$) between GSM01-derived $b_{bp}(443)$ and $b_{bp}(443)$ estimated from *in situ* Chl using formulations devised by *Loisel and Morel* [1998] and *Morel and Maritorena* [2001]. However, the empirical character of the employed relationship between Chl and $b_{bp}(443)$ raises doubts about the usefulness of the corresponding synthetic data set in this context [*Siegel et al.*, 2005]. A more credible synthetic data set ($n = 500$), covering a wide range of natural variability, was simulated by *IOCCG* [2006] and used to evaluate $b_{bp}(443)$ (along with other modelled variables) from GSM01, as well as from bio-optical algorithms by *Loisel and Stramski* [2000], *Boss and Roesler* [2006], *Lee et al.* [2002] and *Sathyendranath and Platt* [1997] (some of the models computed $b_{bp}(440)$ rather than $b_{bp}(443)$, but the small difference in wavelength can be disregarded [*Lee et al.*, 2010; *Maritorena and Siegel*, 2006]). Various metrics of performance, including the linear regression statistics, applied to logarithmically transformed $b_{bp}(443)$ values indicated an overall high skill of all the models in reproducing the quasi-real $b_{bp}(443)$ data (intercept from −0.186 to +0.198; slope from 0.902 to 1.133; r^2 from 0.898 to 0.981; RMSD from 0.081 to 0.168; bias from −0.062 to +0.056). Although the *IOCCG* [2006] synthetic data set had a significant coastal component, while GSM01 was intended for noncoastal applications, its performance was not very much different from that of the model by *Lee et al.* [2002], which was designed to handle a broader range of environments and had the best score in four out of five afore-mentioned statistical measures of model performance. It is also worth noting that *Maritorena et al.* [2010] observed a fairly good agreement of GSM01 with a small number of *in situ* $b_{bp}(443)$ data ($n = 175$) on a $\log_{10}$ scale (intercept = 0.2528; slope = 1.123; $r^2 = 0.503$; RMSD = 0.1973; bias = −0.053), despite the fact that most of the *in situ* values came from coastal regions. Importantly, GSM01 is seemingly the first and, so far, the only ocean colour model to have its satellite-derived output accompanied by routinely available pixel-by-pixel uncertainty estimates [*Maritorena et al.*, 2010], even though methods for creating uncertainty maps have been developed for a few other bio-optical algorithms as well [see *Lee et al.*, 2010; *Wang et al.*, 2005]. While the current approach that produces uncertainty maps for GSM01 output assumes that uncertainties associated with the satellite-observed water-leaving radiances and the model are unbiased and do not vary in space and/or time [*Maritorena et al.*, 2010], it lays the foundation for a future propagation of $b_{bp}(443)$ uncertainties through both versions of the CbPM.

3.2. Quality of Modelled MLD

3.2.1. Influence of Defining Criteria and Ocean Model Characteristics on MLD

A shortage of hydrographical measurements during the period of the study by *Milutinović et al.* [2009] did not allow a statistically rigorous determination of uncertainty in the mixed layer depth (MLD) by comparison of model-derived MLD with MLD derived from *in situ* observations of temperature and salinity. Still, the strengths and weaknesses of the model MLD fields can be explored, to some extent, based solely on model characteristics and MLD definitions. These definitions were developed from a variety of published criteria, which is a known cause of disagreements in MLD assessments [e.g. *de Boyer Montégut et al.*, 2004; *Dong et al.*, 2008]. In the case of Hybrid Coordinate Ocean Model (HYCOM) [*Bleck*, 2002], MLD was calculated from the vertical profiles of seawater density, while the Thermodynamic Ocean Prediction System (TOPS) model [*Clancy and Martin*, 1981; *Clancy and Pollak*, 1983; *Clancy and Sadler*, 1992] used temperature profiles. In both cases, MLD was computed as the depth at which the defining property changed by a given threshold value in reference to the sea-surface value. In contrast to the indirect approach of HYCOM and TOPS, the two versions of Miami Isopycnic Coordinate Ocean Model (MICOM) [*Bleck and Smith*, 1990; *Bleck et al.*, 1992; *Hátún et al.*, 2005] determined MLD as the penetration depth of mixing motions, created by fluxes of momentum, heat and freshwater at the air-sea interface and quantified by a turbulent kinetic energy formulation from *Gaspar et al.* [1990]. In the context of phytoplankton light exposure modelling (see Equation (4.3), Chapter 4), MLD should be defined based on active mixing rather than the near-uniformity of vertical density/temperature profiles, because the latter may be due to past, rather than present, mixing events [e.g. *Huisman et al.*, 1999; *Townsend et al.*, 1994; *Yamazaki and Kamykowski*, 1991]. In that sense, the MLD computation approach applied in MICOM would appear preferable. However, the mixing parameterization by *Gaspar et al.* [1990] is crude, as it assumes a 'slab' mixed layer, with perfect vertical mixing occurring instantaneously whenever static instability (relatively dense water above lighter one) appears in the upper ocean. A more realistic vertical mixing parameterization [*Large et al.*, 1994] was used in HYCOM, where turbulent mixing is a time-dependent process whose strength and penetration is determined by estimated vertical profiles of eddy diffusivity. Being predicated on empirical approach, however, this parameterization has been argued to be inferior to statistically based mixing formulations [*Burchard and Bolding*, 2001], such as that applied in TOPS [*Mellor and Yamada*, 1974]. While TOPS used physically the soundest mixing formulation among those discussed here, its temperature-based approach to deriving MLD is unsatisfactory in situations in which MLD is principally governed by salinity [*de Boyer Montégut et al.*, 2004]. In such circumstances, MLD should be derived from density profiles, as was the case for HYCOM, since density integrates both the effects of

salinity and temperature. On the other hand, the density criterion may lead to overestimated MLD in regions where so-called vertically compensated layers occur (see the paper by *de Boyer Montégut et al.* [2004] and Figure 10 within). In the compensated layers, vertical gradients in temperature and salinity (i.e. the thermocline and halocline, respectively) run in parallel, so that no gradient in density (i.e. the pycnocline) appears. Errors arising from such situations can be avoided by following the advice of *Dong et al.* [2008] that MLD should be computed both from density and temperature profiles, and the shallower of the two estimates selected as representative of the depth of active mixing. The accuracy of this estimate depends not only on the choice between temperature and density, but also on the use of appropriate threshold difference for the selected property. According to the global climatological study by *de Boyer Montégut et al.* [2004], the threshold values of 0.03 kg m^{-3} or 0.2°C are best suited for estimating the depth of mixing over the timescale of a daily cycle, whereas the thresholds applied in HYCOM (0.125 kg m^{-3}) and TOPS (0.5°C), respectively, are too large and yield particularly large MLD overestimates when stratification is relatively weak.

Along with the criteria for MLD definition and the mixing parameterizations, different atmospheric surface forcing fields, as well as the horizontal and vertical resolutions of ocean models, contributed further to discrepancies among MLD estimates employed in this dissertation. Both versions of MICOM had a limit prescribed to MLD, so that it could not become shallower than ~20 m, implying potential overestimates in summer. In contrast, HYCOM and TOPS did not suffer from such a limitation, owing to their good vertical resolutions. Although the vertical axis in TOPS extended only to the depth of 400 m, that was practically irrelevant for NPP estimates, because MLD values greater than 400 m generally take place in high latitude regions in winter, when little or no light is available for photosynthesis (Figure 4.7, Chapter 4). Of all the models, HYCOM had the best ability to resolve ocean variability on the mesoscale (i.e. the spatial scale on the order of magnitude from 100 km down to 10 km [*Danabasoglu et al.*, 1994]), due to the relatively fine horizontal grid spacing (~11–16 km). Being associated with the most vigorous oceanic flows [*Danabasoglu et al.*, 1994], which affect the large-scale transport of heat, salinity and momentum [*Hallberg and Gnanadesikan*, 2006; *McClean et al.*, 2008; *Oschlies*, 2002], the mesoscale should be adequately resolved to allow for a more realistic representation of mixing. For example, *Oschlies* [2002] compared two configurations of a North Atlantic ocean model that differed only in the horizontal resolution (1/3° versus 1/9°, the latter being mesoscale-resolving) and found that the higher resolution resulted in much shallower winter MLD, later surface restratification in spring and earlier autumn deepening of the mixed layer. More reliable global MLD products can also be expected, owing to recent refinements in the horizontal spacing of several global ocean circulation models to 1/10° or better [e.g. *Scott et al.*, 2010].

3.2.2. Benefits of Data Assimilation

An outstanding example of the power of international collaborations in building and sustaining global networks of field observations that are dense in coverage, quality assured and freely and timely available to everyone is the Argo programme [*Roemmich et al.*, 2009]. This programme has created a global array of autonomous profiling floats that measure temperature, salinity and pressure in the ocean's upper 2000 m, which can be used to derive MLD. Unfortunately, the Argo programme was only in its pilot phase during the period of the study by *Milutinović et al.* [2009], i.e. prior to 2004, and could not provide sufficient data to support a statistical analysis of model MLD uncertainties therein. Instead, the uncertainty in MLD was represented by a range of MLD estimates from the selected ocean models. Although the number of Argo floats brought into service rose steadily from 1999 to 2004 (Figure 3.1), many of them failed to function properly (Figure 3.2.) and the programme goal of at least 3000 active floats was not reached before November 2007 [*Roemmich et al.*, 2009]. By now, the floats have rendered hundreds of thousands of profiles in the open ocean [*Roemmich et al.*, 2009]. Thus, a statistically rigorous approach to propagating uncertainties in MLD through NPP algorithms would be achievable today, bringing an additional advantage of differentiation between imprecision
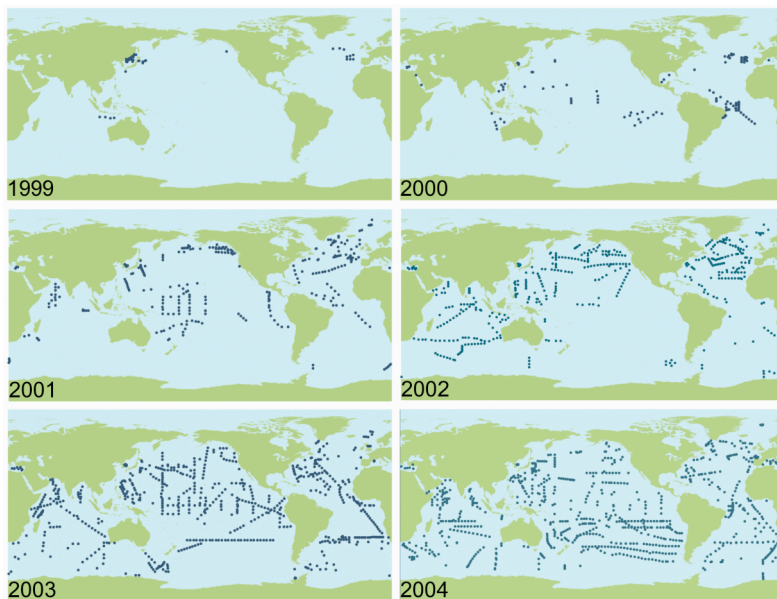

Figure 3.1. Locations where the Argo floats were deployed between 1999 and 2004. (Figure based on maps provided by the Argo Information Centre at ftp://ftp.jcommops.org/Argo/Maps/.)
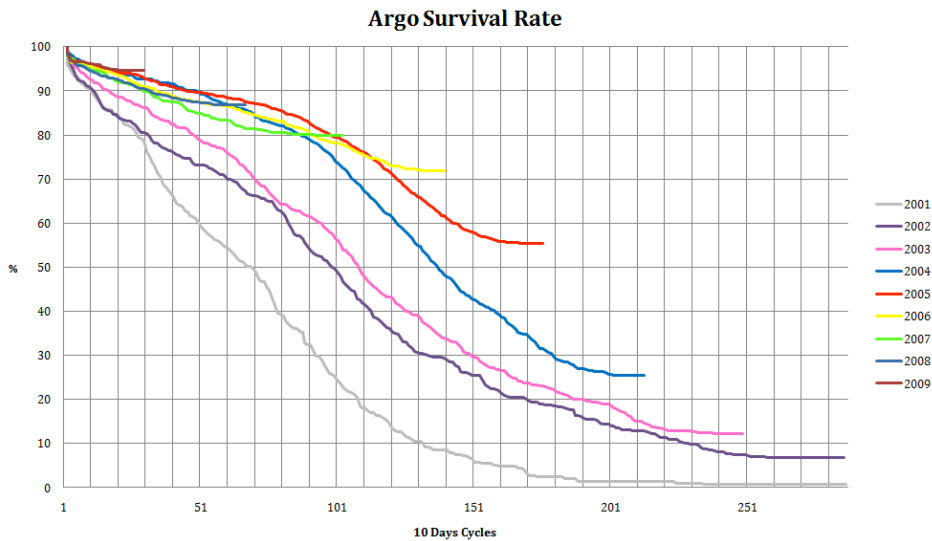
Figure 3.2. Decrease in the proportion of functional Argo floats with time in years 2001–2009. (Figure provided by the Argo Information Centre at ftp://ftp.jcommops.org/Argo/Status/YearlySurvivalRate.png.)

and bias. Such a task, however, exceeds the scope of this thesis, as it would have to be performed entirely *de novo*, using new sets of inputs coinciding with the operational phase of the Argo programme, and the resulting uncertainty statistics for the modelled MLD fields would not necessarily be valid for the time covered by the work of *Milutinović et al.* [2009], due to a development of the underlying ocean models meanwhile. On the other hand, ocean modelling has started to directly benefit from the Argo programme via data assimilation [*Roemmich et al.*, 2009], which ensures that model outputs are consistent with observations [e.g. *Evensen*, 2009]. Figures 3.3a–3.3d and 3.4a–3.4b illustrate how MLD estimates from the Nansen Environmental and Remote Sensing Center's version of HYCOM were modified by assimilating the Argo data in March and July 2008, respectively (note that residual errors after the assimilation are neglected in further discussion). The overall patterns of these estimates, as well as the difference between the respective MLD fields from an assimilation run and a non-assimilation run (i.e. free run) of HYCOM (ΔMLD), are very similar to the comparisons of MLD fields from several ocean models in the study by *Milutinović et al.* [2009] (cf. Figures 4.1, 4.3 and 4.5 in Chapter 4, but note the difference in the colour scales, relative to Figures 3.3a–3.3d and 3.4a–3.4b). The assimilation run departed most conspicuously from the free run of HYCOM in the middle and high latitudes
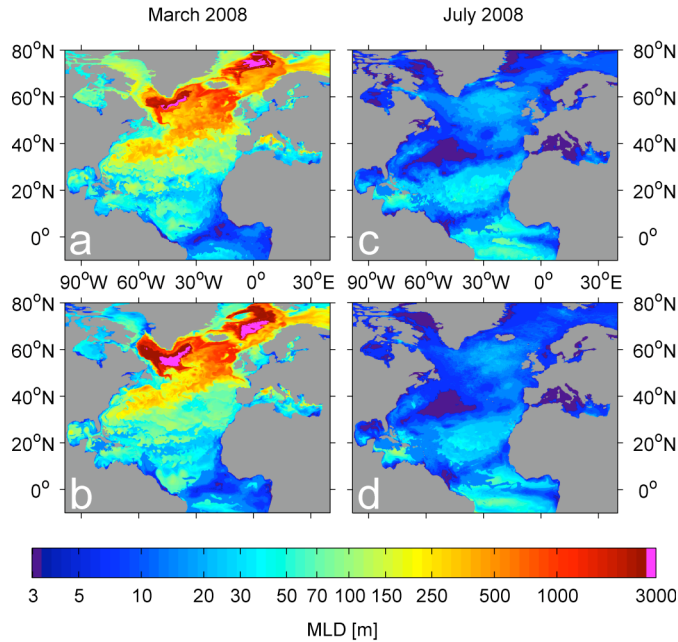
Figure 3.3. Monthly mean mixed layer depth (MLD [m]) in March and July 2008, in the part of the Atlantic covered by HYCOM run at the Nansen Environmental and Remote Sensing Center, Bergen, Norway. Top: The output of the HYCOM run in data assimilation mode. Bottom: The output of the HYCOM run in free mode (i.e. without assimilating the Argo observations). (MLD fields courtesy of Laurent Bertino and François Counillon.)
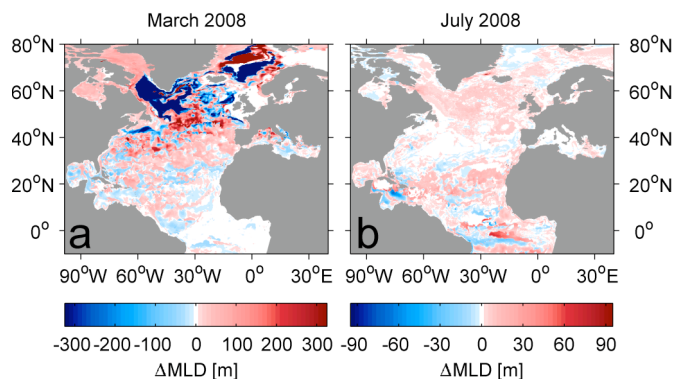

Figure 3.4. Difference between the mean monthly MLD fields from the assimilation run and the free run of HYCOM (ΔMLD [m]) in (a) March and (b) July 2008 (Figure 3.4a = Figure 3.3a – Figure 3.3b; Figure 3.4b = Figure 3.3c – Figure 3.3d). Note that the two maps have different colour scales.

51

in March 2008 (see Figures 3.3a–3.3b and 3.4a), revealing three main weak points (L. Bertino, personal communication, 2011). First, HYCOM run in the free mode overestimated the extent of sea-ice cover east of Greenland (close to 70°N) and therefore placed a region of deep vertical mixing too far south. Secondly, in the free run, the northward inflow of high-salinity Atlantic water to the Nordic Seas was excessively recirculated (cf. Figure 1a by *Skjelvan et al.* [2005]), i.e. returned into the subpolar gyre, thereby giving rise to overly deep mixing south of Greenland. Finally, the free-run HYCOM allowed the Gulf Stream to overshoot Cape Hatteras. Rather than being unique to HYCOM, the overshoot is a widespread problem of ocean modelling [e.g. *Mellor and Ezer*, 1991] and could possibly also apply to other ocean models used by *Milutinović et al.* [2009]. Only the last-mentioned of the salient ΔMLD features had a prominent effect on NPP estimates from the DWI CbPM (see Figures 3.5a–3.5b and 3.6a). This was anticipated, based on the outcome of the analysis by *Milutinović et al.* [2009].

That is to say, in the high latitudes in the month of March, the gain in the accuracy of the HYCOM MLD through the Argo data assimilation (Figure 3.4a) was not expected to have a significant bearing on the NPP assessments, since surface illumination was relatively modest, while the mixed layer from both HYCOM runs was so deep that the full light limitation of photosynthesis was the most likely result in either case (compare Figures 3.3a–3.3b with Figure 4.7 in Chapter 4). In summer, however, even the small change in the model MLD (Figure 3.4b) was highly important for the DWI CbPM NPP estimates in this part of the North Atlantic (Figure 3.6b), due to the combination of generally shallow mixed layer estimates (Figures 3.3c–3.3d) with abundant daylight and relatively high water turbidity (see Figure 4.7 in Chapter 4). In contrast, ΔMLD in the subtropical North Atlantic (Figure 3.4b) was inconsequential for the DWI CbPM NPP estimates in summer (Figure 3.6b), when these oligotrophic waters are characterized by remarkable clarity and plentiful sunlight that could make photosynthesis run at the light-saturated level, regardless of which of the two HYCOM MLD inputs was used (compare Figures 3.3c–3.3d and Figure 4.7 from Chapter 4). On the other hand, such neutralization of ΔMLD effect on NPP estimates was not possible in the colder period in the subtropics (see Figure 3.6a), not only because ΔMLD was more pronounced (compare Figures 3.4a and 3.4b), but also because it was combined with deeper mixing (Figures 3.3a–3.3d), diminished water clarity and less insolation (Figure 4.7 in Chapter 4).

This brief investigation confirms that the effects of uncertainties in MLD on NPP depend on location and season, i.e. on actual MLD value together with concurrent surface irradiance and vertical light attenuation rate, as discussed by *Milutinović et al.* [2009]. It remains unclear, though, whether the overall MLD uncertainties, suggested by this analysis, can be extrapolated to the period from 1997 to 2003, studied by *Milutinović et al.* [2009]. However,
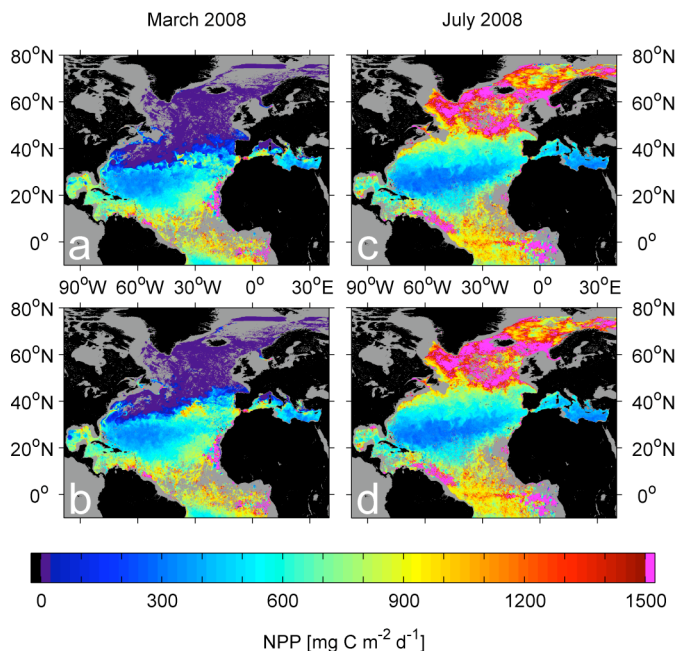
Figure 3.5. Monthly mean net primary productivity (NPP [mg C m^{-2} d^{-1}]) in March and July 2008, computed by the DWI CbPM using the corresponding HYCOM MLD fields from the assimilation run (top) and the free run (bottom), presented in Figure 3.3. NPP computations were based on monthly Level-3 binned remote sensing data (reprocessing version 2009.1) from the Moderate Resolution Imaging Spectroradiometer (MODIS) on board the Aqua satellite. (Note that Sea-viewing Wide Field-of-view Sensor (SeaWiFS) observations were used for the DWI CbPM computations in Chapter 4, but were not available for the months considered here.) Photosynthetically available radiation and diffuse vertical attenuation coefficient at 490 nm resulted from standard MODIS algorithms and were provided by the NASA Ocean Biology Processing Group (http://oceancolor.gsfc.nasa.gov/cgi/l3). Chlorophyll and particulate backscattering coefficient at 443 nm were generated by the Garver-Siegel-Maritorena bio-optical model [*Garver and Siegel*, 1997; *Maritorena et al.*, 2002] and were downloaded from http://www.science.oregonstate.edu/ocean.productivity/inputData.php.

if the MLD biases indicated in Figures 3.4a–3.4b are correct and valid for that time interval, it could be claimed that the regionally integrated annual NPP estimates by *Milutinović et al.* [2009] based on HYCOM MLD were somewhat too high in both the subpolar and subtropical gyres of the North Atlantic (see Figures 3.6a–3.6b).
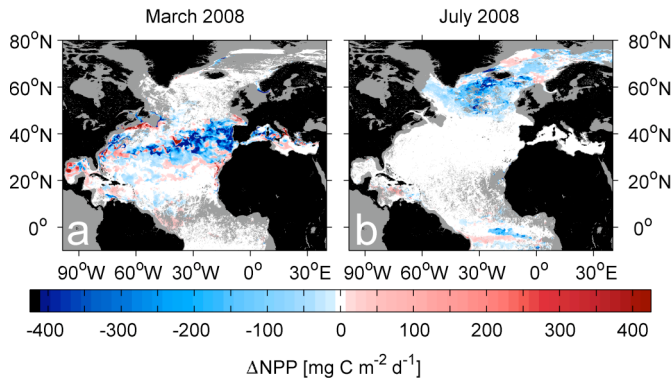
Figure 3.6. Difference between the monthly mean NPP values (ΔNPP [mg C m^{-2} d^{-1}]) based on MLD fields from the assimilation run and the free run of HYCOM in (a) March and (b) July 2008 (Figure 3.6a = Figure 3.5a – Figure 3.5b; Figure 3.6b = Figure 3.5c – Figure 3.5d).

3.3. Quality of the Studied NPP Models

Contrary to the results by *Friedrichs et al.* [2009], *Milutinović et al.* [2009] observed little or no difference in sensitivity to MLD perturbations between the DWI CbPM and the DWR CbPM. Reasons for the disagreement between the two studies are unclear. At the same time, the similarity in the models' behaviour is not surprising, considering that the resolved version is an extension of the integrated one. Still, NPP estimates from the DWI CbPM were often substantially higher. This was caused primarily by the DWI CbPM methodology for assessing the euphotic depth (Z_{eu}), which is based on blue light (see the fifth term in the Equation (4.1), Chapter 4), rather than the entire photosynthetic waveband (as is the case in the DWR CbPM [*Westberry et al.*, 2008]), and thus yields overestimates. Substituting the overestimated Z_{eu} values in the DWI CbPM with those from the method of *Westberry et al.* [2008] lowered the DWI CbPM NPP estimates considerably and made them nearly identical to the DWR CbPM results in cases when MLD exceeded Z_{eu} (for example, this was the situation in January 2000 at the location covered by Figure S4.2, Chapter 4). In such cases, the formulations of the two CbPM versions correspond most closely to one another, since the DWR CbPM returns uniform vertical profiles of all properties other than light [*Westberry et al.*, 2008], which, in effect, is equivalent to having no vertical resolution in the model. However, when the mixed layer was shallower than the euphotic zone (as, for instance, in July 2000 at the site considered by Figure S4.3, Chapter 4), the Z_{eu} substitution rendered the DWI CbPM NPP estimates lower than those from the DWR CbPM. This was most likely caused by the ability

Table 3.2. Respective global annual NPP estimates [Pg C yr^{-1}] by the DWI CbPM and VGPM from several sources, including the present thesis

Source	Model	NPP	Period
Milutinović et al. [2009]	DWI CbPM	64.5	Oct 1997 – Sep 2004
Milutinović and Bertino [2011]	VGPM	46.1	2005
Behrenfeld et al. [2005]	DWI CbPM	67	1997–2002
Behrenfeld et al. [2005]	VGPM	60	1997–2002

of the DWR CbPM to model a gradual reduction in nutrient stress underneath MLD, depending on the distance from the nitracline (the sharp vertical gradient of nitrate and nitrite concentrations) [*Westberry et al.*, 2008], whereas the DWI CbPM lacks such a feature and assumes constant nutrient limitation of photosynthesis throughout the euphotic layer.

The results of the Z_{eu} substitution additionally suggest that divergent methodologies for Z_{eu} assessment (see also Section 3.4) were probably the primary source of the large discrepancy between global annual NPP estimates from the VGPM and the DWI CbPM, presented in this dissertation (Table 3.2). This presumption is further corroborated by the study of *Behrenfeld et al.* [2005], wherein a much better agreement between the VGPM and the DWI CbPM (Table 3.2) was achieved by using Z_{eu} assessments from the DWI CbPM in both of these models. The respective estimates by *Behrenfeld et al.* [2005] and *Milutinović et al.* [2009] are on the higher end of the range of global estimates from various NPP models reported by *Carr et al.* [2006] for six months of 1998, while the assessment by *Milutinović and Bertino* [2011] lies closer to the average output value of all models analyzed by *Carr et al.* [2006] (50.7 Pg C yr^{-1}). However, the proximity of any particular estimate to this average should not serve as a measure of model performance, because model skill could only be quantified through testing against *in situ* data [*Carr et al.*, 2006]. Interestingly, a comparison of Figure 4.1 (Chapter 4) with Figure 5.8 (Chapter 5) shows that the patterns of regional and seasonal differences between the DWI CbPM and the VGPM assessments in this thesis are consistent with the analogous patterns observed by *Behrenfeld et al.* [2005; cf. their Figure 5], as summarized in Table 3.3. This consistency indicates that these patterns are not driven by differences in how the models estimate Z_{eu} (i.e. although Z_{eu} can influence the magnitude of the differences between the NPP values considerably, it does not seem responsible for the sign of the differences). It is clear from the models' formulations (Equations (4.1) and (5.1) in Chapters 4 and 5, respectively) that the differences in NPP from the VGPM and the DWI CbPM remaining after removing divergences in Z_{eu} must be due to disagreements in the models' respective estimates of phytoplankton biomass and physiological capacity to fix carbon.

Table 3.3. Qualitative comparison of seasonal NPP estimates from the DWI CbPM relative to the VGPM, in various regions of the global ocean[a]

Region	Winter	Summer
Tropics and subtropics	↑	↑
Temperate and subpolar North Atlantic	↓	↓
Temperate and subpolar North Pacific	↓	↑
Southern Ocean	↓	↑↓[b]

[a]Based on the sources listed in Table 3.2.
[b]Upward arrows symbolize higher NPP estimates from the DWI CbPM with respect to the VGPM. Downward arrows designate the opposite. Both types of arrows (the case of the Southern Ocean in summer) denote spatial irregularities in difference between the outputs from the two models.

While revealing substantial differences in the output of the deployed NPP models, this thesis does not attempt to rank the model performances, because it does not incorporate any evaluations of the model NPP estimates against *in situ* measurements. However, a few recently published studies [*Friedrichs et al.*, 2009; *Saba et al.*, 2010; *Saba et al.*, 2011], which evaluated a large number of NPP models by comparing their output with *in situ* NPP data obtained by the ^{14}C-uptake method, offer some insights into the skill of the VGPM and the DWI CbPM. In the study by *Friedrichs et al.* [2009], which was focused on the tropical Pacific, a variant of the VGPM apparently identical to that used by *Milutinović and Bertino* [2011] scored highly on various statistical measures of model performance (it had comparatively low bias and zero-centred root mean square difference, provided a very good fit to the cumulative frequency distribution of the test data and showed a relatively high correlation with those data). This model was less successful in the geographically most extensive NPP model evaluation so far [*Saba et al.*, 2011] (it was among the best performing models in only two out of ten studied regions), although another VGPM variant was identified as one of the most skilful NPP algorithms. *Saba et al.* [2011] did not evaluate the DWI CbPM, because one of its input quantities, namely particulate backscattering coefficient ($b_{bp}(443)$), was not available in their test data set. On the other hand, *Friedrichs et al.* [2009] bypassed the lack of *in situ* $b_{bp}(443)$ by using monthly climatological means of remotely sensed $b_{bp}(443)$ values. While this put the DWI CbPM at a disadvantage, its performance was not much lower than that of the best VGPM variant. Furthermore, *Friedrichs et al.* [2009] analyzed the sensitivity of NPP models to uncertainties in input quantities and, even without considering uncertainties in $b_{bp}(443)$, found that the root mean square difference (RMSD) would have decreased more for the DWI CbPM than any other model if there had been no uncertainties in input

variables. Similarly to *Friedrichs et al.* [2009], *Saba et al.* [2010] circumvented the absence of *in situ* b_{bp}(443) in their NPP model evaluations at the respective locations of Hawaii Ocean Time-series (HOT) and Bermuda Atlantic Time-series Study (BATS). At both sites, the VGPM outperformed the DWI CbPM in terms of RMSD. At the HOT site, the latter model's RMSD was dominated by bias. At the BATS location, the DWI CbPM performance was particularly poor, which, in agreement with *Milutinović et al.* [2009], might be explained by an increased sensitivity of the NPP model to MLD uncertainties owing to a deeper winter mixed layer compared to HOT [*Saba et al.*, 2010]. In addition, MLD uncertainties were possibly larger at BATS, due to MLD being derived by an ocean model, whereas at HOT MLD was determined from *in situ* estimated vertical density profiles.

The two NPP models analyzed in this dissertation are of the simplest kind [see *Behrenfeld and Falkowski*, 1997a] and one might be tempted to expect more accuracy from NPP models of greater complexity. It may, therefore, come as a surprise that none of the large intercomparisons of NPP algorithms to date [*Campbell et al.*, 2002; *Carr et al.*, 2006; *Friedrichs et al.*, 2009; *Saba et al.*, 2010; *Saba et al.*, 2011] found any evidence to support such an expectation. A general lack of association between the performance and the complexity of the models was among the main findings of those intercomparisons that evaluated the models' skill using *in situ* data [*Campbell et al.*, 2002; *Friedrichs et al.*, 2009; *Saba et al.*, 2010; *Saba et al.*, 2011]. While *Carr et al.* [2006] did not employ *in situ* NPP measurements, their pair-wise comparisons of 24 NPP models showed that model structure was not a good predictor of relationship between model results. Even so, dismissing the model complexity as entirely unnecessary could be misguided, since complex models are more closely related to the fundamental concepts of photosynthesis and could probably quite readily absorb the advances in theory and remote sensing technology [*Campbell et al.*, 2002; *Carr et al.*, 2006], which would be less feasible for the simple models that are commonly more empirical in nature.

This thesis separates the uncertainty of the VGPM NPP estimates into bias and imprecision. The impact of imprecision is important if interest is focused on single NPP values at specific points in space and time. However, in applications that do not demand the finest possible resolution, imprecision could be reduced by considering greater spatial/temporal scales. The reason for this is that adding the individual NPP values together to produce an integrated or averaged value for a chosen larger portion of space/time implies a summation of the associated randomly governed errors. If sufficiently many individual NPP values participate in the spatial/temporal integration or averaging, the distribution of their corresponding errors represents the underlying uncertainty distribution and, as a result, the sum of the negative errors is more or less balanced by the sum of the positive ones. Hence, the random uncertainty of a seasonally/annually and/or regionally/globally

integrated or averaged NPP should approach zero. The integration or averaging, however, cannot reduce bias (assuming that bias is stable in space and time, which was true in the study of *Milutinović and Bertino* [2011]). Hence, *Milutinović and Bertino* [2011] found that the bias of individual NPP estimates joined into an overestimate of 2.5 Pg C in the annually and globally integrated NPP value of 46.1 Pg C for 2005. This has important implications for studies that make use of NPP estimates derived from remote sensing. For example, the output of the VGPM has been frequently used to evaluate the output of coupled climate-ecosystem models [see e.g. *Schlitzer*, 2002; *Schneider et al.*, 2008; *Steinacher et al.*, 2010]. Furthermore, it has also been employed to infer the amount of organic carbon exported from the surface into the deep ocean by the biological pump [e.g. *Falkowski et al.*, 1998; *Laws et al.*, 2000]. While the knowledge of imprecision in NPP is not absolutely necessary for those applications to work reasonably well, as long as averaging/integration is acceptable, NPP bias must be known to make sure that the ensuing conclusions are not adversely affected.

Based on a comparison of the output of twelve unnamed NPP algorithms with *in situ* NPP estimates from 89 stations across the world ocean, *Campbell et al.* [2002] identified bias as a major problem for most of the algorithms. *Friedrichs et al.* [2009] carried out a similar analysis in the tropical Pacific for 21 NPP algorithms, using ~1000 stations. They found that the simplest algorithms (including the one used by *Milutinović and Bertino* [2011]) were generally associated with the lowest bias, which was also a characteristic of the best-performing algorithms in their study. The bias found by *Milutinović and Bertino* [2011] is similarly low (6%). Even so, there is room for improvement, primarily by addressing the bias in the input function that accounts for the shape of the vertical profile of photosynthesis, but also by making progress in the representation of photophysiological state, which contributed almost as large a bias as the former input function (albeit of the opposite sign) and was by far the largest contributor to the imprecision in NPP.

The photophysiological input functions have long been recognized as the 'Achilles heel' of NPP modelling [e.g. *Behrenfeld and Falkowski*, 1997a; *Campbell et al.*, 2002; *Siegel et al.*, 2001]. The weakness of the VGPM photophysiological (i.e. P^b_{opt}) function (Equation (5.4) in Chapter 5) is also strongly evident from the comparisons with field data in this thesis (Figures 5.2 and 5.3 in Chapter 5). It is, therefore, not surprising that this input function contributed most to the imprecision of the VGPM estimates in the study by *Milutinović and Bertino* [2011]. Moreover, other P^b_{opt} functions of temperature studied by *Milutinović and Bertino* [2011], such as that from *Antoine et al.* [1996], were at least equally unsuccessful (Figure 5.4 in Chapter 5). None of the P^b_{opt} functions analyzed here explained more than 9% of variance in the observations, a result consistent with a similar analysis by *Behrenfeld et al.* [2002b]. This general underperformance stems, foremost, from the historically

limited access to the photophysiologically relevant observations with sufficient spatiotemporal coverage, which compelled NPP modellers to resort to either the satellite observations of sea surface temperature [e.g. *Antoine et al.*, 1996; *Balch et al.*, 1992; *Behrenfeld and Falkowski*, 1997b; *Megard*, 1972] or the climatological averages of phytoplankton photophysiological state in biogeographic regions [e.g. *Longhurst et al.*, 1995]. While the latter approach has a stronger oceanographic and ecological foundation [*Behrenfeld et al.*, 2002a], it is compromised by the extent of small scale variability within a given region that can easily surpass the climatological differences among various regions [e.g. *Marañón and Holligan*, 1999]. On the other hand, temperature is a poor predictor of P^b_{opt}, since a direct effect of temperature above ~5°C on P^b_{opt} is unlikely, whereas its indirect effect arises from generally weak correlation with the photophysiologically more influential factors (i.e. prevailing light field and nutrient concentrations) [e.g. *Behrenfeld et al.*, 2002a]. The recent progress in ocean colour modelling has begun to provide additional information, such as phytoplankton carbon biomass, solar-induced fluorescence and algal community composition [*Sathyendranath and Platt*, 2010], that can help improve photophysiological formulations in NPP algorithms [e.g. *Behrenfeld et al.*, 2005; *Behrenfeld et al.*, 2009; *Uitz et al.*, 2008]. The DWI CbPM incorporates a novel approach to representing phytoplankton photophysiology that is much more connected to the mechanistic understanding of photosynthesis, but is shown to be very sensitive to uncertainties in MLD [*Milutinović et al.*, 2009]. It is therefore important, as discussed earlier, to minimize the uncertainty in MLD estimates, which are used for deducing the physiological adjustment of photosynthetic machinery to changes in light exposure governed by vertical mixing.

3.4. Methodology for Determining Z_{eu}

Whereas MLD was the only input quantity whose uncertainty was considered by *Milutinović et al.* [2009], *Milutinović and Bertino* [2011] took into account uncertainties in all input terms for the NPP algorithm they selected. However, in the latter study, uncertainty in one particular input term, namely Z_{eu}, was treated differently than uncertainties in the other input quantities. The reason for this was that Z_{eu} uncertainty, unlike the other input uncertainties, reflects not only the fundamental skill of the function that provided Z_{eu} values, but also uncertainty in another input term, i.e. Chl. This was, in turn, a consequence of Z_{eu} being determined as a function of Chl (following the method of *Morel and Berthon* [1989] in a revised form [*Morel and Maritorena*, 2001]). The uncertainty in this function was quantified by comparing its output with a number of matching *in situ* estimates (Chapter 6), and was found to be small relative to the rest of input uncertainties. This allowed *Milutinović and Bertino* [2011] to disregard the uncertainty in the Z_{eu} function, in order to make the propagation of uncertainties and the analysis of results simpler. In other words,

the Z_{eu} function was treated as completely accurate and only the portion of Z_{eu} uncertainty that originated from Chl uncertainty was propagated through the NPP algorithm. Therefore, the future refinements should include the uncertainty related to the Z_{eu} function in the Monte Carlo simulations.

The Chl-based method used here to quantify Z_{eu} was developed exclusively for Case-1 waters [*Morel and Berthon*, 1989], which are the waters whose optical properties are dominated by phytoplankton (and their accompanying degradation products) and can therefore be quantitatively related to Chl (serving as a proxy for phytoplankton content) [*Mobley et al.*, 2004; *Morel and Prieur*, 1977]. This is not to say that phytoplankton are the only optically active ingredient of Case-1 waters, but merely that other optically important substances, such as detritus and dissolved organic matter, are present in comparatively small concentrations and covary with phytoplankton [*Sathyendranath*, 2000]. In all other waters, named Case-2 waters, agents unrelated to phytoplankton are at least as important in controlling the waters' optical properties[1]. Case-2 situations arise, for instance, when mineral particles and/or coloured dissolved organic matter enter the water column via river runoff, coastal erosion, wind deposition of dust or agitation of underlying sediments by tides and storms [*Mobley et al.*, 2004]. Although it has been shown that the Case-1 and Case-2 classification is not a geographic concept [*Lee and Hu*, 2006], for the sake of simplicity in this thesis the customary approach that equates all oceanic waters to Case 1 is followed, while the waters over the continental shelves are disregarded as Case 2. In the paper of *Milutinović et al.* [2009], the distinction was required to avoid the instances when phytoplankton are not the dominant contributor to backscattering of light, which would invalidate the method for estimating phytoplankton biomass, used therein. In the study by *Milutinović and Bertino* [2011], the untenability of the method for inferring Z_{eu} in Case-2 waters demanded that they be omitted. Recently, however, *Lee et al.* [2007] presented a new method for quantifying Z_{eu} in all waters, regardless of their optical complexity. The preliminary analysis of the method's accuracy was encouraging, indicating that it may be superior to the method used by *Milutinović and Bertino* [2011], even when only Case-1 waters were considered. If this is confirmed by more extensive analyses, the method of *Lee et al.* [2007] could be employed in NPP assessments, which would be doubly beneficial, as it would both eliminate the need to exclude Case-2 waters and would reduce uncertainties in NPP.

A few remarks are due with regard to the exclusion of the continental shelves, which served as the proxy for Case-2 waters. The shelves occupy only

---

[1] Note that blooms of coccolithophores bring about high concentrations of suspended mineral particles ($CaCO_3$ platelets detached from the cells) [*Gordon et al.*, 2009; *Smyth et al.*, 2002]. Although being a product of the phytoplankters, these particles cause an excessive scattering of light that is incompatible with the Case-1 definition [*Morel*, 1988]. Waters affected by such blooms are therefore classified as Case 2.

~7% of the world ocean surface area [*Gattuso et al.*, 1998], but are generally estimated to have a more prominent share in the global marine primary productivity (PP). The published estimates of that share vary widely (~10–30% of the total marine PP) and are very difficult to compare, due to reasons such as different definitions of the area of interest, the type of PP (i.e. gross versus net PP) serving as the starting point for estimation and the groups of primary producers considered (e.g. phytoplankton, benthic algae, seagrasses) [see *Cotrim da Cunha et al.*, 2007; *Ducklow and McCallister*, 2005; *Gattuso et al.*, 1998; *Muller-Karger et al.*, 2005; *Wollast*, 1998]. Nevertheless, it seems unquestionable that including the shelves would enhance areally-integrated NPP values estimated by *Milutinović et al.* [2009] and *Milutinović and Bertino* [2011], respectively, beyond the proportion of the corresponding surface area. For example, assuming that missing values had a negligible impact on the annual open-ocean NPP of 46.1 Pg C, assessed by *Milutinović and Bertino* [2011], and using the conservative estimate of 10% for the shelf contribution to the overall marine NPP, one can arrive at the combined estimate of 51.2 Pg C. However, deducing the overestimate in the all-inclusive annual global ocean NPP from the open-ocean value of 2.5 Pg C [*Milutinović and Bertino*, 2011] by using the same logic would not be credible due to two reasons. First, standard ocean colour algorithms, which are developed for global ocean applications, are expected to be associated with greater uncertainties in Case-2 than Case-1 waters [see e.g. *Neumann et al.*, 2000; *Saba et al.*, 2011]. This is confirmed by the finding of *Gregg et al.* [2009] that the standard SeaWiFS Chl product gives much larger overestimates and reproduces *in situ* observed Chl variability much more poorly in regions with shallow sea bottoms (<200 m). Second, the evaluation study of 21 NPP models in ten marine regions around the world by *Saba et al.* [2011] showed that waters shallower than 250 m are characterized by a significantly poorer average model skill (indicated by RMSD) and a generally pronounced positive bias in the modelled NPP, even though the NPP assessments were based on *in situ* Chl input. Consequently, the increase resulting from adding the continental shelf contribution to the annual open-ocean NPP overestimate would most probably exceed the expectations based solely on the shelf NPP value and could only be quantified by performing a separate uncertainty analysis for the shelf area.

3.5. Summary

Saba et al. [2011] recommended that the publicly available estimates of NPP from ocean colour observations be accompanied by information on uncertainties originating from input data, such as Chl and MLD. This thesis might pave the way for such efforts in the future. It could also provide some guidance for attempts aimed at improving the accuracy of ocean-colour-derived NPP. The key suggestions for achieving these goals, which have been laid out in this chapter, are summarized in Box 3.1.

Box 3.1. Suggestions for future activities with respect to quantification and minimization of uncertainties in ocean-colour-based NPP estimates

Steps regarding *in situ* data

- Ensuring sustained measurement activities with sufficient temporal and spatial coverage
- Taking concurrent multidisciplinary measurements for increased process understanding, model development and improvement, and support to remote sensing observations
- Selecting the most accurate measurement methodologies and harmonizing protocols
- Encouraging prompt submission of new measurements to public data bases
- Reporting measurement uncertainties
- Integrating individual data bases

Steps regarding modelled MLD

- Preferably, modelling the depth of active mixing
- Alternatively, computing MLD from both density and temperature profiles (respective thresholds equalling 0.03 kg m^{-3} and 0.2°C) and choosing the shallower of the two values
- Ensuring fine vertical resolution
- Resolving mesoscale variability
- Assimilating data into ocean models

Steps regarding modelled Z_{eu} and NPP

- Improving modelling of photophysiology and parameterization of vertical changes in photosynthetic rates
- Using method for Z_{eu} quantification that works well in both Case-1 and Case-2 waters
- Propagating complete Z_{eu} uncertainty (i.e. combining contributions from remote sensing input and Z_{eu} quantification methodology)
- Propagating uncertainty in $b_{bp}(443)$ to quantify its effect on phytoplankton biomass estimates
- Performing separate uncertainty analysis for the continental shelves
- Investigating why NPP models tend to underperform in shelf areas

References

Abbott, M. R. (2001), Challenges and opportunities for interdisciplinary oceanography, *Oceanography*, *14*(4), 121.

Antoine, D., J. M. André, and A. Morel (1996), Oceanic primary production 2. Estimation at global scale from satellite (coastal zone color scanner) chlorophyll, *Global Biogeochemical Cycles*, *10*(1), 57-69.

Balch, W., R. Evans, J. Brown, G. Feldman, C. McClain, and W. Esaias (1992), The remote-sensing of ocean primary productivity - use of a new data compilation to test satellite algorithms, *Journal of Geophysical Research-Oceans*, *97*(C2), 2279-2293.

Behrenfeld, M., E. Boss, D. Siegel, and D. Shea (2005), Carbon-based ocean productivity and phytoplankton physiology from space, *Global Biogeochemical Cycles*, *19*(1), GB1006.

Behrenfeld, M. J., and P. G. Falkowski (1997a), A consumer's guide to phytoplankton primary productivity models, *Limnology and Oceanography*, *42*(7), 1479-1491.

Behrenfeld, M. J., and P. G. Falkowski (1997b), Photosynthetic rates derived from satellite-based chlorophyll concentration, *Limnology and Oceanography*, *42*(1), 1-20.

Behrenfeld, M. J., W. E. Esaias, and K. R. Turpie (2002a), Assessment of primary production at the global scale, in *Phytoplankton productivity: Carbon assimilation in marine and freshwater ecosystems*, edited by P. J. leB. Williams, D. N. Thomas and C. S. Reynolds, pp. 156-186, Blackwell Science.

Behrenfeld, M. J., E. Maranon, D. A. Siegel, and S. B. Hooker (2002b), Photoacclimation and nutrient-based model of light-saturated photosynthesis for quantifying oceanic primary production, *Marine Ecology-Progress Series*, *228*, 103-117.

Behrenfeld, M. J., T. K. Westberry, E. S. Boss, R. T. O'Malley, D. A. Siegel, J. D. Wiggert, B. A. Franz, C. R. McClain, G. C. Feldman, S. C. Doney, J. K. Moore, G. Dall'Olmo, A. J. Milligan, I. Lima, and N. Mahowald (2009), Satellite-detected fluorescence reveals global physiology of ocean phytoplankton, *Biogeosciences*, *6*(5), 779-794.

Birdsey, R., N. Bates, M. Behrenfeld, K. Davis, S.C. Doney, R. Feely, D. Hansell, L. Heath, E. Kasischke, H. Kheshgi, B. Law, C. Lee, A.D. McGuire, P. Raymond, and C. J. Tucker (2009), Carbon cycle observations: Gaps threaten climate mitigation policies, *Eos, Transactions*, *90*(34), 292-293.

Bleck, R., and L. T. Smith (1990), A wind-driven isopycnic coordinate model of the north and equatorial Atlantic-ocean 1. Model development and supporting experiments, *Journal of Geophysical Research-Oceans*, *95*(C3), 3273-3285.

Bleck, R., C. Rooth, D. Hu, and L. T. Smith (1992), Salinity-driven thermocline transients in a wind- and thermohaline-forced isopycnic coordinate model of the North Atlantic, *Journal of Physical Oceanography*, *22*(12), 1486-1505.

Bleck, R. (2002), An oceanic general circulation model framed in hybrid isopycnic-Cartesian coordinates, *Ocean Modelling*, *4*(1), 55-88.

Boss, E., and S. Maritorena (2006), Uncertainties in the products of ocean-colour remote sensing, in *Remote sensing of inherent optical properties: Fundamentals, tests of algorithms and applications*, edited by Z. Lee, pp. 19-26, International Ocean-Colour Coordinating Group, Dartmouth, Canada.

Boss, E., and C. Roesler (2006), Over constrained linear matrix inversion with statistical selection, in *Remote sensing of inherent optical properties: Fundamentals, tests of algorithms and applications*, edited by Z. Lee, pp. 57-62, International Ocean-Colour Coordinating Group, Dartmouth, Canada.

Burchard, H., and K. Bolding (2001), Comparative analysis of four second-moment turbulence closure models for the oceanic mixed layer, *Journal of Physical Oceanography*, *31*(8), 1943-1968.

Bureau International des Poids et Mesures (BIPM), International Electrotechnical Commission (IEC), International Federation of Clinical Chemistry (IFCC), International Organization for Standardization (ISO), International Union of Pure and Applied Chemistry (IUPAC), International Union of Pure and Applied Physics (IUPAP), and Organisation Internationale de Métrologie Légale (OIML) (2008), *Evaluation of measurement data — guide to the expression of uncertainty in measurement (GUM 1995 with minor corrections)*, Joint Committee for Guides in Metrology, Bureau International des Poids et Mesures, Sèvres, France. Available at http://www.bipm.org/utils/common/documents/jcgm/JCGM_100_2008_E.pdf.

Campbell, J., D. Antoine, R. Armstrong, K. Arrigo, W. Balch, R. Barber, M. Behrenfeld, R. Bidigare, J. Bishop, M. Carr, W. Esaias, P. Falkowski, N. Hoepffner, R. Iverson, D. Kiefer, S. Lohrenz, J. Marra, A. Morel, J. Ryan, V. Vedernikov, K. Waters, C. Yentsch, and J. A. Yoder (2002), Comparison of algorithms for estimating ocean primary production from surface chlorophyll, temperature, and irradiance, *Global Biogeochemical Cycles*, *16*(3), 1035.

Campbell, J. (2004), Issues linked to the use of binned data in models: An example using primary production, in *Guide to the creation and use of ocean-colour, level-3, binned data products*, edited by D. Antoine, pp. 47-57, International Ocean-Colour Coordinating Group, Dartmouth, Canada.

Carr, M.-E., M. A. M. Friedrichs, M. Schmeltz, M. Noguchi Aita, D. Antoine, K. R. Arrigo, I. Asanuma, O. Aumont, R. Barber, M. Behrenfeld, R. Bidigare, E. T. Buitenhuis, J. Campbell, A. Ciotti, H. Dierssen, M. Dowell, J. Dunne, W. Esaias, B. Gentili, W. Gregg, S. Groom, N. Hoepffner, J. Ishizaka, T. Kameda, C. L. Quéré, S. Lohrenz, J. Marra, F. Mélin, K. Moore, A. Morel, T. E. Reddy, J. Ryan, M. Scardi, T. Smyth, K. Turpie, G. Tilstone, K. Waters, and Y. Yamanaka (2006), A comparison of global estimates of marine primary production from ocean color, *Deep Sea Research Part II: Topical Studies in Oceanography*, *53*(5-7), 741- 770.

Clancy, R. M., and P. J. Martin (1981), Synoptic forecasting of the oceanic mixed layer using the navy's operational environmental data base: Present capabilities and future applications, *Bulletin of the American Meteorological Society*, *62*(6), 770-770.

Clancy, R. M., and K. D. Pollak (1983), A real-time synoptic ocean thermal analysis/forecast system, *Progress in Oceanography*, *12*(4), 383-424.

Clancy, R. M., and W. D. Sadler (1992), The Fleet Numerical Oceanography Center suite of oceanographic models and products, *Weather and Forecasting*, *7*(2), 307-327.

Cotrim da Cunha, L., E. T. Buitenhuis, C. Le Quéré, X. Giraud, and W. Ludwig (2007), Potential impact of changes in river nutrient supply on global ocean biogeochemistry, *Global Biogeochemical Cycles*, *21*(4), GB4007.

Cullen, J. J., and M. R. Lewis (1988), The kinetics of algal photoadaptation in the context of vertical mixing, *Journal of Plankton Research*, *10*(5), 1039-1063.

Danabasoglu, G., J. C. McWilliams, and P. R. Gent (1994), The role of mesoscale tracer transports in the global ocean circulation, *Science*, *264*(5162), 1123-1126.

Dandonneau, Y. (1993), Measurement of *in situ* profiles of primary production using an automated sampling and incubation device, in *Measurement of primary production from the molecular to the global scale*, edited by W. K. W. Li and S. Y. Maestrini, pp. 172-180, International Council for the Exploration of the Sea, Copenhagen, Denmark.

de Boyer Montégut, C., G. Madec, A. S. Fischer, A. Lazar, and D. Iudicone (2004), Mixed layer depth over the global ocean: An examination of profile data and a profile-based climatology, *Journal of Geophysical Research-Oceans*, *109*(C12).

Dickey, T. D. (2001), The role of new technology in advancing ocean biogeochemical research, *Oceanography*, *14*(4), 108-120.

Dong, S., J. Sprintall, S. T. Gille, and L. Talley (2008), Southern Ocean mixed-layer depth from Argo float profiles, *Journal of Geophysical Research-Oceans*, *113*(C6), C06013.

Ducklow, H. W., and S. L. McCallister (2005), The biogeochemistry of carbon dioxide in the coastal oceans, in *The sea: The global coastal ocean—multiscale interdisciplinary processes*, edited by A. R. Robinson and K. H. Brink, pp. 269-315, Harvard University Press, Cambridge, Massachusetts, USA.

Evensen, G. (2009), *Data assimilation: The ensemble Kalman filter*, 2nd ed., 307 pp., Springer-Verlag, Berlin, Germany.

Falkowski, P. G., R. T. Barber, and V. Smetacek (1998), Biogeochemical controls and feedbacks on ocean primary production, *Science*, *281*(5374), 200-206.

Falkowski, P. G., and J. A. Raven (2007), *Aquatic photosynthesis*, 2nd ed., 500 pp., Princeton University Press.

Friedrichs, M. A. M., M.-E. Carr, R. T. Barber, M. Scardi, D. Antoine, R. A. Armstrong, I. Asanuma, M. J. Behrenfeld, E. T. Buitenhuis, F. Chai, J. R. Christian, A. M. Ciotti, S. C. Doney, M. Dowell, J. Dunne, B. Gentili, W. Gregg, N. Hoepffner, J. Ishizaka, T. Kameda, I. Lima, J. Marra, F. Mélin, J. K. Moore, A. Morel, R. T. O'Malley, J. O'Reilly, V. S. Saba, M. Schmeltz, T. J. Smyth, J. Tjiputra, K. Waters, T. K. Westberry, and A. Winguth (2009), Assessing the uncertainties of model estimates of primary productivity in the tropical Pacific ocean, *Journal of Marine Systems*, *76*(1-2), 113-133.

Garver, S. A., and D. A. Siegel (1997), Inherent optical property inversion of ocean color spectra and its biogeochemical interpretation 1. Time series from the Sargasso Sea, *Journal of Geophysical Research-Oceans*, *102*(C8), 18607-18625.

Gaspar, P., Y. Grégoris, and J.-M. Lefevre (1990), A simple eddy kinetic energy model for simulations of the oceanic vertical mixing: Tests at station papa and long-term upper ocean study site, *Journal of Geophysical Research-Oceans*, *95*(C9), 16,179-116,193.

Gattuso, J. P., M. Frankignoulle, and R. Wollast (1998), Carbon and carbonate metabolism in coastal aquatic ecosystems, *Annual Review of Ecology and Systematics*, *29*, 405-434.

Gieskes, W. W., and G. W. Kraay (1983), Unknown chlorophyll *a* derivatives in the north sea and the tropical Atlantic ocean revealed by HPLC analysis, *Limnology and Oceanography*, *28*(4), 757-766.

Global Climate Observing System (GCOS) (2009), Guideline for the generation of satellite-based datasets and products meeting GCOS requirements, GCOS-128

(WMO/TD No. 1488), GCOS Secretariat, World Meteorological Organization, Geneva, Switzerland.

Gordon, H. R., and W. R. McCluney (1975), Estimation of the depth of sunlight penetration in the sea for remote sensing, *Appl. Opt.*, *14*(2), 413-416.

Gordon, H. R., T. J. Smyth, W. M. Balch, G. C. Boynton, and G. A. Tarran (2009), Light scattering by coccoliths detached from Emiliania huxleyi, *Applied Optics*, *48*(31), 6059-6073.

Gregg, W. W., N. W. Casey, J. E. O'Reilly, and W. E. Esaias (2009), An empirical approach to ocean color data: Reducing bias and the need for post-launch radiometric re-calibration, *Remote Sensing of Environment*, *113*(8), 1598-1612.

Hallberg, R., and A. Gnanadesikan (2006), The role of eddies in determining the structure and response of the wind-driven southern hemisphere overturning: Results from the modeling eddies in the Southern Ocean (MESO) project, *Journal of Physical Oceanography*, *36*(12), 2232-2252.

Hammann, M. G., and J. J. Puschell (2009), SeaWiFS-2: An ocean color data continuity mission to address climate change, in *Remote sensing system engineering II, Proceedings of SPIE, 7458(745804)*, edited by P. E. Ardanuy and J. J. Puschell.

Hátún, H., A. B. Sandø, H. Drange, B. Hansen, and H. Valdimarsson (2005), Influence of the Atlantic subpolar gyre on the thermohaline circulation, *Science*, *309*(5742), 1841-1844.

Henson, S. A., J. L. Sarmiento, J. P. Dunne, L. Bopp, I. Lima, S. C. Doney, J. John, and C. Beaulieu (2010), Detection of anthropogenic climate change in satellite records of ocean chlorophyll and productivity, *Biogeosciences*, *7*(2), 621-640.

Huisman, J., P. van Oostveen, and F. J. Weissing (1999), Critical depth and critical turbulence: Two different mechanisms for the development of phytoplankton blooms, *Limnology and Oceanography*, *44*(7), 1781-1787.

International Ocean-Colour Coordinating Group (IOCCG) (2006), Remote sensing of inherent optical properties: Fundamentals, tests of algorithms and applications, 126 pp, IOCCG, Dartmouth, Canada.

Kintisch, E. (2008), U.S. Prepares to launch flawed satellite, *Science*, *319*(5865), 886.

Large, W. G., J. C. McWilliams, and S. C. Doney (1994), Oceanic vertical mixing - a review and a model with a nonlocal boundary-layer parameterization, *Reviews of Geophysics*, *32*(4), 363-403.

Laws, E. A., P. G. Falkowski, W. O. Smith, Jr., H. Ducklow, and J. J. McCarthy (2000), Temperature effects on export production in the open ocean, *Global Biogeochemical Cycles*, *14*(4), 1231-1246.

Lee, Z., K. L. Carder, and R. A. Arnone (2002), Deriving inherent optical properties from water color: A multiband quasi-analytical algorithm for optically deep waters, *Applied Optics*, *41*(27), 5755-5772.

Lee, Z., and C. M. Hu (2006), Global distribution of Case-1 waters: An analysis from SeaWiFS measurements, *Remote Sensing of Environment*, *101*(2), 270-276.

Lee, Z., A. Weidemann, J. Kindle, R. Arnone, K. L. Carder, and C. Davis (2007), Euphotic zone depth: Its derivation and implication to ocean-color remote sensing, *Journal of Geophysical Research-Oceans*, *112*(C3), C03009.

Lee, Z., R. Arnone, C. M. Hu, P. J. Werdell, and B. Lubac (2010), Uncertainties of optical parameters and their propagations in an analytical ocean color inversion algorithm, *Applied Optics*, *49*(3), 369-381.

Lohrenz, S. E. (1993), Estimation of primary production by the simulated *in situ* method, in *Measurement of primary production from the molecular to the global scale*, edited by W. K. W. Li and S. Y. Maestrini, pp. 159-171, International Council for the Exploration of the Sea, Copenhagen, Denmark.

Loisel, H., and A. Morel (1998), Light scattering and chlorophyll concentration in case 1 waters: A reexamination, *Limnology and Oceanography*, *43*(5), 847-858.

Loisel, H., and D. Stramski (2000), Estimation of the inherent optical properties of natural waters from the irradiance attenuation coefficient and reflectance in the presence of Raman scattering, *Applied Optics*, *39*(18), 3001-3011.

Longhurst, A., S. Sathyendranath, T. Platt, and C. Caverhill (1995), An estimate of global primary production in the ocean from satellite radiometer data, *Journal of Plankton Research*, *17*(6), 1245-1271.

MacIntyre, H. L., T. M. Kana, and R. J. Geider (2000), The effect of water motion on short-term rates of photosynthesis by marine phytoplankton, *Trends in Plant Science*, *5*(1), 12-17.

Maestrini, S. Y., A. Sournia, and A. Herbland (1993), Measuring phytoplankton production in 1992 and the coming years: A dilemma?, in *Measurement of primary production from the molecular to the global scale*, edited by W. K. W. Li and S. Y. Maestrini, pp. 244-259, International Council for the Exploration of the Sea, Copenhagen, Denmark.

Mantoura, R. F. C., and C. A. Llewellyn (1983), The rapid determination of algal chlorophyll and carotenoid pigments and their breakdown products in natural waters by reverse-phase high-performance liquid chromatography, *Analytica Chimica Acta*, *151*, 297-314.

Mantoura, R. F. C., S. W. Jeffrey, C. A. Llewellyn, C. H., and C. E. Morales (1997), Comparison between spectrophotometric, fluorometric and HPLC methods for chlorophyll analysis, in *Phytoplankton pigments in oceanography: Guidelines to modern methods*, edited by S. W. Jeffrey, R. F. C. Mantoura and S. W. Wright, pp. 361-380, UNESCO Publishing, Paris, France.

Marañón, E., and P. M. Holligan (1999), Photosynthetic parameters of phytoplankton from 50°n to 50°s in the Atlantic ocean, *Marine Ecology-Progress Series*, *176*, 191-203.

Maritorena, S., D. A. Siegel, and A. R. Peterson (2002), Optimization of a semianalytical ocean color model for global-scale applications, *Applied Optics*, *41*(15), 2705-2714.

Maritorena, S., and D. Siegel (2006), The GSM semi-analytical bio-optical model, in *Remote sensing of inherent optical properties: Fundamentals, tests of algorithms and applications*, edited by Z. Lee, pp. 81-85, International Ocean-Colour Coordinating Group, Dartmouth, Canada.

Maritorena, S., O. H. Fanton d'Andon, A. Mangin, and D. A. Siegel (2010), Merged satellite ocean color data products using a bio-optical model: Characteristics, benefits and issues, *Remote Sensing of Environment*, *114*(8), 1791-1804.

McClean, J., S. Jayne, M. Maltrud, and D. Ivanova (2008), The fidelity of ocean models with explicit eddies, in *Ocean modeling in an eddying regime*, edited by M. W. Hecht and H. Hasumi, pp. 149–163, American Geophysical Union.

Megard, R. O. (1972), Phytoplankton, photosynthesis, and phosphorus in lake Minnetonka, Minnesota, *Limnology and Oceanography*, *17*(1), 68-87.

Mellor, G. L., and T. Yamada (1974), A hierarchy of turbulence closure models for planetary boundary layers, *Journal of the Atmospheric Sciences*, *31*(7), 1791-1806.

Mellor, G. L., and T. Ezer (1991), A Gulf Stream model and an altimetry assimilation scheme, *Journal of Geophysical Research-Oceans*, *96*(C5), 8779-8795.

Milutinović, S., M. J. Behrenfeld, J. A. Johannessen, and T. Johannessen (2009), Sensitivity of remote sensing-derived phytoplankton productivity to mixed layer depth: Lessons from the carbon-based productivity model, *Global Biogeochemical Cycles*, *23*, GB4005.

Milutinović, S., and L. Bertino (2011), Assessment and propagation of uncertainties in input terms through an ocean-colour-based model of primary productivity, *Remote Sensing of Environment*, in press, doi: 10.1016/j.rse.2011.03.013.

Mobley, C. D., D. Stramski, W. P. Bissett, and E. Boss (2004), Optical modeling of ocean waters: Is the Case 1 - Case 2 classification still useful?, *Oceanography*, *17*(2), 60-67.

Morel, A., and L. Prieur (1977), Analysis of variations in ocean color, *Limnology and Oceanography*, *22*(4), 709-722.

Morel, A. (1980), In-water and remote measurements of ocean color, *Boundary-Layer Meteorology*, *18*(2), 177-201.

Morel, A. (1988), Optical modeling of the upper ocean in relation to its biogenous matter content (case i waters), *Journal of Geophysical Research-Oceans*, *93*(C9), 10,749-710,768.

Morel, A., and J. F. Berthon (1989), Surface pigments, algal biomass profiles, and potential production of the euphotic layer - relationships reinvestigated in view of remote-sensing applications, *Limnology and Oceanography*, *34*(8), 1545-1562.

Morel, A., and S. Maritorena (2001), Bio-optical properties of oceanic waters: A reappraisal, *Journal of Geophysical Research-Oceans*, *106*(C4), 7163-7180.

Morel, A., and B. Gentili (2004), Radiation transport within oceanic (case 1) water, *Journal of Geophysical Research-Oceans*, *109*, C06008.

Muller-Karger, F. E., R. Varela, R. Thunell, R. Luerssen, C. Hu, and J. J. Walsh (2005), The importance of continental margins in the global carbon cycle, *Geophysical Research Letters*, *32*(1), L01602.

Neumann, A., R. Doerffer, H. Krawczyk, M. D. Dowell, R. Arnone, C. O. Davis, M. Kishino, A. Tanaka, C. Hu, R. P. Bukata, H. R. Gordon, J. Campbell, and S. Sathyendranath (2000), Algorithms for Case 2 waters, in *Remote sensing of ocean colour in coastal, and other optically-complex, waters*, edited by S. Sathyendranath, pp. 47-76, International Ocean-Colour Coordinating Group, Dartmouth, Canada.

Oschlies, A. (2002), Improved representation of upper-ocean dynamics and mixed layer depths in a model of the North Atlantic on switching from eddy-permitting to eddy-resolving grid resolution, *Journal of Physical Oceanography*, *32*(8), 2277-2298.

Pemberton, K. L., K. R. Clarke, and I. Joint (2006), Quantifying uncertainties associated with the measurement of primary production, *Marine Ecology-Progress Series*, *322*, 51-59.

Pinckney, J., R. Papa, and R. Zingmark (1994), Comparison of high-performance liquid chromatographic, spectrophotometric, and fluorometric methods for determining chlorophyll a concentrations in estaurine sediments, *Journal of Microbiological Methods*, *19*(1), 59-66.

Prézelin, B. B., M. M. Tilzer, O. Schofield, and C. Haese (1991), The control of the production process of phytoplankton by the physical structure of the aquatic environment with special reference to its optical properties, *Aquatic Sciences*, *53*(2-3), 136-186.

Richardson, A. J., and E. S. Poloczanska (2008), Under-resourced, under threat, *Science*, *320*(5881), 1294-1295.

Robinson, I. S. (2004), *Measuring the oceans from space: The principles and methods of satellite oceanography*, 669 pp., Praxis Publishing Ltd. /Springer Verlag.

Roemmich, D., G. C. Johnson, S. Riser, R. Davis, J. Gilson, W. B. Owens, S. L. Garzoli, C. Schmid, and M. Ignaszewski (2009), The Argo program: Observing the global ocean with profiling floats, *Oceanography*, *22*(2), 34-43.

Saba, V. S., M. A. M. Friedrichs, M.-E. Carr, D. Antoine, R. A. Armstrong, I. Asanuma, O. Aumont, N. R. Bates, M. J. Behrenfeld, V. Bennington, L. Bopp, J. Bruggeman, E. T. Buitenhuis, M. J. Church, A. M. Ciotti, S. C. Doney, M. Dowell, J. Dunne, S. Dutkiewicz, W. Gregg, N. Hoepffner, K. J. W. Hyde, J. Ishizaka, T. Kameda, D. M. Karl, I. Lima, M. W. Lomas, J. Marra, G. A. McKinley, F. MÈlin, J. K. Moore, A. Morel, J. O'Reilly, B. Salihoglu, M. Scardi, T. J. Smyth, S. Tang, J. Tjiputra, J. Uitz, M. Vichi, K. Waters, T. K. Westberry, and A. Yool (2010), Challenges of modeling depth-integrated marine primary productivity over multiple decades: A case study at bats and hot, *Global Biogeochemical Cycles*, *24*(3), GB3020.

Saba, V. S., M. A. M. Friedrichs, D. Antoine, R. A. Armstrong, I. Asanuma, M. J. Behrenfeld, A. M. Ciotti, M. Dowell, N. Hoepffner, K. J. W. Hyde, J. Ishizaka, T. Kameda, J. Marra, F. Mélin, A. Morel, J. O'Reilly, M. Scardi, W. O. Smith Jr, T. J. Smyth, S. Tang, J. Uitz, K. Waters, and T. K. Westberry (2011), An evaluation of ocean color model estimates of marine primary productivity in coastal and pelagic regions across the globe, *Biogeosciences*, *8*(2), 489-503.

Sanderson, M. P., C. N. Hunter, S. E. Fitzwater, R. M. Gordon, and R. T. Barber (1995), Primary productivity and trace-metal contamination measurements from a clean rosette system versus ultra-clean go-flo bottles, *Deep Sea Research Part II: Topical Studies in Oceanography*, *42*(2-3), 431-440.

Sathyendranath, S., and T. Platt (1997), Analytic model of ocean color, *Applied Optics*, *36*(12), 2620-2629.

Sathyendranath, S. (2000), General introduction, in *Remote sensing of ocean colour in coastal, and other optically-complex, waters*, edited by S. Sathyendranath, pp. 5-21, International Ocean-Colour Coordinating Group, Dartmouth, Canada.

Sathyendranath, S., and T. Platt (2010), Ocean-colour radiometry: Achievements and future perspectives, in *Oceanography from space: Revisited*, edited by V. Barale, J. F. R. Gower and L. Alberotanza, pp. 349-359, Springer, Dordrecht, The Netherlands.

Schlitzer, R. (2002), Carbon export fluxes in the Southern Ocean: Results from inverse modeling and comparison with satellite-based estimates, *Deep Sea Research Part II: Topical Studies in Oceanography*, *49*(9-10), 1623-1644.

Schneider, B., L. Bopp, M. Gehlen, J. Segschneider, T. L. Frölicher, P. Cadule, P. Friedlingstein, S. C. Doney, M. J. Behrenfeld, and F. Joos (2008), Climate-induced interannual variability of marine primary and export production in three global coupled climate carbon cycle models, *Biogeosciences*, *5*(2), 597-614.

Scott, R. B., B. K. Arbic, E. P. Chassignet, A. C. Coward, M. Maltrud, W. J. Merryfield, A. Srinivasan, and A. Varghese (2010), Total kinetic energy in four global eddying ocean circulation models and over 5000 current meter records, *Ocean Modelling*, *32*(3-4), 157-169.

Siegel, D. A., T. K. Westberry, M. C. O'Brien, N. B. Nelson, A. F. Michaels, J. R. Morrison, A. Scott, E. A. Caporelli, J. C. Sorensen, S. Maritorena, S. A. Garver, E. A. Brody, J. Ubante, and M. A. Hammer (2001), Bio-optical modeling of primary production on regional scales: The Bermuda BioOptics project, *Deep Sea Research Part II: Topical Studies in Oceanography*, *48*(8-9), 1865-1896.

Siegel, D. A., S. Maritorena, N. B. Nelson, and M. J. Behrenfeld (2005), Independence and interdependencies among global ocean color properties: Reassessing the bio-optical assumption, *Journal of Geophysical Research-Oceans*, *110*, C07011.

Siegel, D. A., and J. Yoder (2007), Community letter to NASA and NOAA regarding concerns over NPOESS Preparatory Project VIIRS sensor, in *Ensuring the climate record from the NPOESS and GOES-R spacecraft: Elements of a strategy to recover measurement capabilities lost in program restructuring*, edited by N. R. C. o. t. N. A. Space Studies Board, pp. 167-169, The National Academies Press, Washington, D.C.

Skjelvan, I., A. Olsen, L. G. Anderson, R. G. J. Bellerby, E. Falck, Y. Kasajima, C. Kivimäe, A. Omar, F. Rey, K. A. Olsson, T. Johannessen, and C. Heinze (2005), A review of the inorganic carbon cycle of the Nordic Seas and Barents Sea, in *The Nordic Seas: An integrated perspective*, edited by H. Drange, T. Dokken, T. Furevik, R. Gerdes and W. Berger, pp. 157-175, American Geophysical Union.

Smyth, T. J., G. F. Moore, S. B. Groom, P. E. Land, and T. Tyrrell (2002), Optical modeling and measurements of a coccolithophore bloom, *Applied Optics*, *41*(36), 7679-7688.

Steinacher, M., F. Joos, T. L. Frölicher, L. Bopp, P. Cadule, V. Cocco, S. C. Doney, M. Gehlen, K. Lindsay, J. K. Moore, B. Schneider, and J. Segschneider (2010), Projected 21st century decrease in marine productivity: A multi-model analysis, *Biogeosciences*, *7*(3), 979-1005.

Taylor, J. R. (1997), *An introduction to error analysis: The study of uncertainties in physical measurements*, 327 pp., University Science Books.

Townsend, D. W., L. M. Cammen, P. M. Holligan, D. E. Campbell, and N. R. Pettigrew (1994), Causes and consequences of variability in the timing of spring phytoplankton blooms, *Deep Sea Research Part I: Oceanographic Research Papers*, *41*(5-6), 747-765.

Uitz, J., Y. Huot, F. Bruyant, M. Babin, and H. Claustre (2008), Relating phytoplankton photophysiological properties to community structure on large scales, *Limnology and Oceanography*, *53*(2), 614-630.

Wang, P., E. S. Boss, and C. Roesler (2005), Uncertainties of inherent optical properties obtained from semianalytical inversions of ocean color, *Applied Optics*, *44*(19), 4074-4085.

Westberry, T., M. J. Behrenfeld, D. A. Siegel, and E. Boss (2008), Carbon-based primary productivity modeling with vertically resolved photoacclimation, *Global Biogeochemical Cycles*, *22*, GB2024.

Williams, P. J. leB. (1993), Chemical and tracer methods of measuring plankton production, in *Measurement of primary production from the molecular to the*

global scale, edited by W. K. W. Li and S. Y. Maestrini, pp. 20-36, International Council for the Exploration of the Sea, Copenhagen, Denmark.

Wilson, C. (2011), The rocky road from research to operations for satellite ocean-colour data in fishery management, *ICES Journal of Marine Science: Journal du Conseil*, *68*(4), 677-686.

Wiltshire, K. H., S. Harsdorf, B. Smidt, G. Blocker, R. Reuter, and F. Schroeder (1998), The determination of algal biomass (as chlorophyll) in suspended matter from the elbe estuary and the german bight: A comparison of high-performance liquid chromatography, delayed fluorescence and prompt fluorescence methods, *Journal of Experimental Marine Biology and Ecology*, *222*(1-2), 113-131.

Wollast, R. (1998), Evaluation and comparison of the global carbon cycle in the coastal zone and in the open ocean, in *The sea: The global coastal ocean processes and methods*, edited by K. H. Brink and A. R. Robinson, pp. 213-252, John Wiley & Sons, Inc., New York, USA.

Yamazaki, H., and D. Kamykowski (1991), The vertical trajectories of motile phytoplankton in a wind-mixed water column, *Deep Sea Research Part I: Oceanographic Research Papers*, *38*(2), 219-241.

Yoder, J. A., J. K. Moore, and R. N. Swift (2001), Putting together the big picture: Remote-sensing observations of ocean color, *Oceanography*, *14*(4), 33-40.

CHAPTER 4 ———————————

Sensitivity of Remote Sensing–Derived Phytoplankton Productivity to Mixed Layer Depth: Lessons from the Carbon-based Productivity Model

IV

Sensitivity of Remote Sensing–Derived Phytoplankton Productivity to Mixed Layer Depth: Lessons from the Carbon-based Productivity Model

Svetlana Milutinović [1,2,3,*], Michael J. Behrenfeld [4], Johnny A. Johannessen [1,3], and Truls Johannessen [3,2]

[1] *Nansen Environmental and Remote Sensing Center, Bergen, Norway*
[2] *Bjerknes Centre for Climate Research, Bergen, Norway*
[3] *Geophysical Institute, University of Bergen, Bergen, Norway*
[4] *Department of Botany and Plant Pathology, Oregon State University, Corvallis, Oregon, USA*

Abstract Mixed layer depth (MLD) has long been recognized as having an important influence on underwater light budget and, thus, net primary productivity (NPP) of phytoplankton. The depth- and wavelength-integrated Carbon-based Productivity Model (DWI CbPM) is one of a few productivity algorithms that explicitly use information on MLD to estimate ocean NPP from remote sensing observations. This study evaluates the sensitivity of NPP estimates from the DWI CbPM to MLD input by using MLD fields from four different ocean models. Owing to the effect of MLD on light availability, the model NPP is generally inversely related to MLD, but the strength of this relationship is highly variable. In most of the ocean, it exhibits a seasonal character. In summer, NPP at middle and high latitudes can show substantial sensitivity to subtle changes in MLD, but is largely robust to strong MLD variability in winter. An opposite seasonal pattern is encountered in subtropical ocean gyres. A lack of seasonality is observed in tropical areas, among which only the equatorial Pacific displays strong response of NPP to small or moderate changes in MLD. We find that the spatial and temporal variability of the MLD-NPP relationship can be explained by nonlinearity and light saturation/limitation thresholds indicated in the DWI CbPM, as well as the influence of surface irradiance (I_0) and diffuse attenuation coefficient for downwelling light at 490 nm ($K_d(490)$). NPP is sensitive to varying MLD only if coincidental I_0 and $K_d(490)$ values are such that combined with the coexisting differences in MLD estimates, they have potential to give effective differences in light saturation/limitation of photosynthesis.

---

[*] Corresponding author. Address: NERSC, Thormøhlensgate 47, 5006 Bergen, Norway; phone: +47 55 20 58 34; fax: +47 55 20 58 01; e-mail: svetlana.milutinovic@nersc.no.

4.1. Introduction

The dominant primary producers in the ocean are phytoplankton, microscopic photosynthetic organisms suspended in the illuminated part of water column. They are responsible for roughly half of the global annual photosynthetic net primary productivity (NPP), which is the amount of fixed carbon available for the first heterotrophic level in an ecosystem [*Field et al.*, 1998]. Environmental forcing controls spatiotemporal changes in phytoplankton abundance and community composition by affecting the key determinants of marine photosynthesis: mixed-layer light availability, concentration of macronutrients and micronutrients, and the ambient temperature [*Behrenfeld et al.*, 2002a; *Field et al.*, 1998]. Owing to a tight coupling between photosynthesizers and higher trophic levels via transfer of matter and energy, any environmental changes imposed on phytoplankton are bound to resonate across food webs, thereby potentially affecting functioning and structure of marine ecosystems [*Cloern and Dufford*, 2005; *Duffy and Stachowicz*, 2006; *Riebesell et al.*, 2007]. Phytoplankton are also likely to impose feedbacks on the future climate system [*Falkowski et al.*, 1998; *Frouin and Iacobellis*, 2002; *Gabric et al.*, 2004]. Physical-chemical-biological interactions often involve a high degree of complexity and nonlinearity [*Jickells et al.*, 2005], making them complicated to understand. The present lack of understanding restricts our ability to predict future consequences of ongoing man-made climate perturbations. Clarifying controls on primary productivity and related responses and feedbacks has been identified as a key goal of global change research [*Falkowski et al.*, 2000; *Geider et al.*, 2001].

An essential requirement for achieving this goal is measurements of NPP and quantification of its variability in space and time. However, ship-based NPP measurements are insufficient [*Carr et al.*, 2006] and need to be complemented with satellite observations [*Behrenfeld et al.*, 2002a]. Satellite ocean colour sensors have been routinely producing a global optical view of the ocean surface. The sensors measure spectral characteristics of water-leaving radiance, which are influenced by the type and concentration of optically active materials in seawater, such as chlorophyll and suspended particles [*International Ocean Colour Coordinating Group* (*IOCCG*), 2000]. It is thus possible, by deploying inversion models of optical properties, to quantify these materials from remotely sensed optical signal [*Garver and Siegel*, 1997]. Most NPP models use chlorophyll as an index of phytoplankton biomass, because it is easily obtainable from remote sensing and is the only pigment found in all phytoplankton taxa [*Geider and MacIntyre*, 2002]. However, there are two main issues associated with this chlorophyll-based approach. First, variations in chlorophyll are not exclusively a result of variations in biomass, but can also be caused by physiological adjustment of intracellular pigment concentrations to nonoptimal light, nutrient, and temperature levels [*Behrenfeld et al.*, 2005]. Second, the direct conversion of chlorophyll concentration to NPP requires an

empirically established scaling parameter, which should account for variability in carbon assimilation efficiency. This parameter cannot be assessed with sufficient accuracy [*Behrenfeld and Falkowski*, 1997a] and is considered responsible for the poor performance of chlorophyll-based algorithms [*Behrenfeld and Falkowski*, 1997b; *Behrenfeld et al.*, 2002b; *Campbell et al.*, 2002].

Recently, *Behrenfeld et al.* [2005] developed an alternative, carbon-based, approach to NPP calculations. This was made possible by the advent of semianalytical ocean colour models, which are able to simultaneously quantify both chlorophyll and backscattering by particles [*Garver and Siegel*, 1997; *Maritorena et al.*, 2002; *Siegel et al.*, 2002]. The Carbon-based Productivity Model (CbPM) of *Behrenfeld et al.* [2005] bypasses the main weaknesses of chlorophyll-based algorithms by deriving information on phytoplankton physiology directly from remote sensing products. The CbPM calculates phytoplankton biomass from particulate backscattering coefficient, which shows an empirical correlation with particulate organic carbon in Case-1 waters, i.e. open ocean [*Loisel et al.*, 2001; *Stramski et al.*, 1999]. Physiological information is then extracted from variability in chlorophyll:carbon (Chl:C) ratios, on the basis of the extensive laboratory-derived knowledge on ecophysiology.

Physiological responses to varying growth irradiance (I_g) are an important factor influencing both phytoplankton Chl:C ratios and photosynthetic assimilation efficiencies. Mixed layer depth (MLD) is a crucial regulator of I_g, as well as nutrient availability [*Mann and Lazier*, 1996]. While accurate MLD estimates are vitally important for NPP estimates [*Westberry et al.*, 2008], few studies have examined the sensitivity of NPP models to MLD perturbations. *Carr et al.* [2006] analyzed sensitivity of six NPP models to widely varying MLD at 11 representative locations in all ocean basins and reported up to a factor of 2 impact. *Friedrichs et al.* [2009] investigated the effect of uncertainties in MLD input (±20 m) on productivity estimates in the tropical Pacific for seven NPP models. They found that MLD uncertainties severely limit the skills of most of the studied models. Among them, both depth- and wavelength-integrated (DWI) [*Behrenfeld et al.*, 2005] and depth- and wavelength-resolved (DWR) [*Westberry et al.*, 2008] versions of the CbPM were considered. Interestingly, the DWR CbPM was largely robust to MLD perturbations in the region of interest, while the DWI CbPM was the most sensitive among the inspected models.

Motivated by those findings, here we address more extensively and in more detail the sensitivity of the DWI CbPM to changes in input MLD. While our study focuses on a particular NPP model, its results may also contribute to better understanding of similar NPP models that use MLD to describe phytoplankton physiological acclimation to changing light conditions (i.e. photoacclimation). Furthermore, the importance of mixing depth variability is intrinsic to all NPP estimates, regardless of whether photoacclimation is

included in a given model formulation. In other words, NPP models that do not include light dependence in their formulation of assimilation efficiencies are subject to large errors associated with the full range of photoacclimation, whereas those models that do include a photoacclimation term are subject to smaller errors associated with uncertainties in assessing I_g.

Sensitivity of the DWI CbPM–derived NPP estimates is examined using MLD fields produced by four different ocean models. Results of the sensitivity experiments are analyzed both globally and in two oceanographically and ecologically distinct North Atlantic provinces: the subpolar and subtropical gyres.

4.2. Methods

4.2.1. Productivity Algorithm

The DWI version of the CbPM is presented by the following expression [*Behrenfeld et al.*, 2005]:

$$\text{NPP} = C_{\text{sat}} \times \left[2 \text{ cell divisions d}^{-1} \times \frac{\text{Chl}:C_{\text{sat}}}{0.022 + (0.045 - 0.022)e^{-3I_g}} \times (1 - e^{-3I_g}) \right]$$
$$\times \frac{-\ln(0.01)}{K_d(490)} \times \frac{0.66125 I_0}{I_0 + 4.1},$$
(4.1)

where the terms C_{sat} and I_g are defined as

$$C_{\text{sat}} = \left(b_{\text{bp}}(443) - 0.00035 \text{ m}^{-1} \right) \times 13{,}000 \text{ mg C m}^{-2},$$
(4.2)

$$I_g = I_0 \times e^{-K_d(490) \times \text{MLD}/2}.$$
(4.3)

Vertically integrated net primary productivity (NPP [mg C m^{-2} d^{-1}]) is calculated as a product of satellite-derived surface phytoplankton carbon biomass (C_{sat} [mg C m^{-3}]) and growth rate, scaled to the depth of the euphotic zone, while taking into account changes in photosynthetic rate with depth. C_{sat} (see Equation (4.2)) is determined from particulate backscattering coefficient at 443 nm ($b_{\text{bp}}(443)$ [m^{-1}]), which is first corrected for a stable background contribution from nonalgal particles (0.00035 m^{-1}), and then multiplied by a scaling factor (13,000 mg C m^{-2}) that relates $b_{\text{bp}}(443)$ to algal biomass. Phytoplankton growth rate (expressed in cell divisions per day) is computed from a maximum growth rate estimate based on observations in natural communities (2 cell divisions d^{-1}) [*Banse*, 1991], then adjusted to account for decreases in growth caused by suboptimal nutrient, temperature, and light

conditions. The third term in Equation (4.1) embodies reductions in growth rate due to combined effects of nutrient and temperature limitation, using the ratio between surface chlorophyll (Chl [mg Chl m^{-3}]) and C_{sat} (Chl:C_{sat}, given in the numerator) relative to the maximum possible Chl:C ratio at a given irradiance (in the denominator). The fourth term determines the degree of light limitation from growth irradiance (I_g [mol photons m^{-2} h^{-1}]), which is taken to be the median light intensity for phytoplankton in the mixed layer. I_g (see Equation (4.3)) is a function of photosynthetically available radiation at the sea surface (I_0 [mol photons m^{-2} h^{-1}]), the diffuse attenuation coefficient for downward irradiance at 490 nm (K_d(490) [m^{-1}]), and mixed layer depth (MLD [m]). The DWI CbPM uses MLD explicitly to determine average exposure of phytoplankton to light, while the indirect influence of MLD on nutrient availability is captured by Chl:C_{sat} variability for a given I_g. K_d(490) is also used to calculate the euphotic depth, defined here as the depth at which irradiance is reduced to 1% of its sea surface value (the fifth term in Equation (4.1)). Finally, the sixth term in Equation (4.1) accounts for the loss in potential NPP due to light limitation.

4.2.2. Satellite Data

Remote sensing input variables for the DWI CbPM were Level-3 composites based on the fifth reprocessing of satellite ocean colour observations taken by the Sea-viewing Wide Field-of-view Sensor (SeaWiFS). These data sets consist of global monthly mean values, presented on an equal area grid with the bin size of approximately 9 km × 9 km. The grid characteristics are discussed in detail by *IOCCG* [2004]. I_0 and K_d(490) are standard SeaWiFS products distributed by the Ocean Color Web at ftp://oceans.gsfc.nasa.gov/SeaWiFS/Binned/Monthly/. Chl and b_{bp}(443) were computed by the Garver-Siegel-Maritorena model version 1 (GSM01) [*Garver and Siegel*, 1997; *Maritorena et al.*, 2002; *Siegel et al.*, 2002]. GSM01 Chl exhibits similar agreement with coincidental *in situ* measurements of chlorophyll as the standard SeaWiFS chlorophyll product [*Siegel et al.*, 2005]. Too few reliable *in situ* observations of b_{bp}(443) in the open ocean are available to enable estimates of the uncertainty in GSM01 b_{bp}(443) retrievals (S. Maritorena, personal communication, 2006).

4.2.3. Model-Based MLD Fields

Although MLD climatologies could be used in the DWI CbPM, it is more advisable to use MLD generated by ocean models, in order to capture information on interannual variability [*Behrenfeld et al.*, 2005]. MLD data sets generated by four different ocean models were used in the sensitivity experiments. Key model characteristics and methods for calculation of MLD are summarized in Table 4.1. Daily model MLD values were averaged to produce monthly mean fields collocated with the satellite products. Since all MLD data

Table 4.1. Overview of the main features of mixed layer depth data sets used in this study

Model acronym	Spatial coverage	Temporal coverage	Horizontal resolution	Vertical coordinates	Basis of MLD definition	Vertical mixing scheme
TOPS	global	October 1997 to September 2004	1°×1°	fixed depth	temperature	level-2 turbulence closure theory of *Mellor and Yamada* [1974]
MICOM1	global	October 1997 to September 2004	location-dependent (~40 to ~200 km)	isopycnic	heat, salinity, and momentum fluxes	kinetic energy (KE) parameterization of *Gaspar et al.* [1990]
MICOM2	North Atlantic	October 1997 to September 2003	location-dependent (~20 to ~40 km)	isopycnic	heat, salinity, and momentum fluxes	kinetic energy (KE) parameterization of *Gaspar et al.* [1990]
HYCOM	North Atlantic	October 1997 to September 2004	location-dependent (~11 to ~16 km)	hybrid (fixed depth in the mixed layer)	density	*K* profile parameterization (KPP) of *Large et al.* [1994]

sets had coarser horizontal resolution than the remote sensing data sets, the nearest-neighbour interpolation scheme was used to place them on the SeaWiFS 9-km grid prior to the experiments.

The first MLD data set was produced by the Thermodynamic Ocean Prediction System (TOPS), a model of the Fleet Numerical Meteorology and Oceanography Center (FNMOC), Monterey, California [*Clancy and Martin*, 1981; *Clancy and Pollak*, 1983; *Clancy and Sadler*, 1992]. This data set was used in the original DWI CbPM calculations by *Behrenfeld et al.* [2005]. TOPS provides global coverage on 1°×1° horizontal grid, while the vertical axis extends down to 400 m, with coordinates constrained to fixed depths. The upper boundary conditions (i.e. surface wind stress and heat fluxes) are provided by the Navy Operational Global Atmospheric Prediction System (NOGAPS). The Level-2 turbulence closure theory of *Mellor and Yamada* [1974] is used to represent the effects of vertical mixing. MLD is the depth at which the temperature drops by 0.5˚C from the value at the sea surface.

The second MLD data set is an output of a global version of the Miami Isopycnic Coordinate Ocean Model (MICOM) [*Bleck and Smith*, 1990; *Bleck et al.*, 1992], run at the Nansen Environmental and Remote Sensing Center (NERSC), Bergen, Norway. This data set is supplied on an irregular grid, with two poles placed over North America and Eurasia, respectively. Such grid design provides enhanced spatial resolution (~40 km) in the Nordic Seas, while grid cells in the Southern Ocean are ~200 km. This MLD data set is referred to here as the MICOM1 MLD data set. MICOM represents the ocean water column with 26 isopycnal layers. While the 25 interior layers have prescribed densities, the uppermost layer is the thermodynamically active mixed layer. Its density is vertically uniform, but varies horizontally and in time. MICOM does not allow the mixed layer to get shallower than ~20 m. MICOM is forced by daily mean fluxes of fresh water, heat and momentum from the NCEP/NCAR Reanalysis Project at the National Oceanic and Atmospheric Administration

(NOAA). MLD is determined as a prognostic variable, based on the available turbulent energy, by means of a simple eddy kinetic energy model from *Gaspar et al.* [1990].

The third MLD data set, covering only the North Atlantic, is a product of a North Atlantic version of MICOM from NERSC [*Hátún et al.*, 2005]. This data set is generated in a similar manner as MICOM1 but has an improved spatial resolution in the North Atlantic (from ~20 km in the Nordic Seas to ~40 km in the subtropical gyre). This third MLD model is referred to here as MICOM2.

The fourth MLD data set, also limited to the North Atlantic, is generated by NERSC's version of the Hybrid Coordinate Ocean Model (HYCOM) [*Bleck*, 2002]. In the mixed layer, this particular version of HYCOM employs constant depth vertical coordinates. Owing to a curvilinear grid used by HYCOM, horizontal resolution of this data set varies from ~11 km to ~16 km, depending on the ocean region. HYCOM uses forcing fields in the form of wind stress, heat, and freshwater fluxes from the European Centre for Medium Range Weather Forecasts (ECMWF). Upper ocean mixing processes are parameterized using the vertical mixing scheme of *Large et al.* [1994]. MLD is calculated as the depth at which the density of seawater increases by 0.125 g dm^{-3} compared to the surface value.

Scarcity of hydrographic measurements precludes us from making any definitive evaluation of the accuracy of MLD estimates from the four models. While today measurements from Argo floats have reached a very good spatial coverage, it was not the case during the time period of this study (1997–2004).

4.2.4. Sensitivity Experiments

MLD fields from the four models described above exhibit significant differences because they are generated on different horizontal and vertical grids, using different environmental forcing, mixing parameterizations and definitions of MLD. This range of variability in MLD assessments serves the purpose of our sensitivity experiments.

To examine the influence of MLD variability on NPP, four sensitivity experiments were performed. Each DWI CbPM run was executed using the same data sets of SeaWiFS-derived monthly mean $b_{bp}(443)$, Chl, $K_d(490)$ and I_0. The runs differed only in the choice of MLD data set.

The DWI CbPM expression for phytoplankton carbon biomass (Equation (4.2)) is likely to fail in optically complex waters, where suspended inorganic particles load is not functionally related to phytoplankton [*Behrenfeld et al.*, 2005]. Thus, exclusion of shelf regions (here defined as shallower than 200 m) from the analysis was used as a simple way to delineate those waters. In addition, the Arctic waters (i.e. latitudes higher than 75°N) were disregarded owing to poor satellite coverage and persistent sea ice. No correction for missing satellite data was employed.

In Section 4.3, we first present results of sensitivity experiments with the two global MLD data sets (TOPS and MICOM1) over the entire world ocean. Subsequently, results based on all four MLD data sets are presented for the North Atlantic subpolar gyre and the eastern part of the North Atlantic subtropical gyre.

4.3. Results

4.3.1. Global Ocean

To facilitate the analysis of the results, twelve respective monthly mean MLD and NPP fields were produced by averaging over the 7-year period from October 1997 to September 2004. The boreal winter/austral summer is presented by average January values (Figures 4.1a, 4.1b, 4.1g and 4.1h). July averages represent the boreal summer/austral winter (Figures 4.1d, 4.1e, 4.1j and 4.1k). On further mention of seasons, both hemispheres are implied (e.g. 'summer' means both boreal and austral summer), unless specified otherwise. The mixed layer from either model is considerably deeper in winter in each hemisphere, particularly at high and middle latitudes, where NPP is extremely low. On the other hand, these latitudes become very productive in summer, which coincides with shoaling of the mixed layer. In contrast, lower latitudes show more moderate seasonal variability in MLD and NPP. Whereas equatorial waters are highly productive throughout the year, subtropical regions exhibit sustained low NPP.

To compare results from the different MLD and NPP estimates, difference values (hereafter denoted by Δ) for each average month were calculated by subtracting MICOM1 MLD and NPP mean from the equivalent TOPS mean. In general, comparison of ΔMLD (Figures 4.1c and 4.1f) with corresponding ΔNPP (Figures 4.1i and 4.1l) reveals an inverse relationship between MLD and NPP. As indicated in Equations (4.1) and (4.3), an increase in MLD can only cause a decrease in estimated I_g, and hence in NPP. However, there are instances in which even a very strong ΔMLD makes little difference for NPP estimates. For example, the pronounced wintertime ΔMLD in the North Atlantic Current (Figure 4.1c) bears little effect on NPP (Figure 4.1i). Also, there are regions having clearly distinguishable ΔMLD values, but similar ΔNPP values. Such a case can be easily identified in average January in the middle- to high-latitude South Atlantic (Figures 4.1c and 4.1i), where there are two distinct areas with comparable ΔNPP (~-700 mg C m^{-2} d^{-1}), yet differing in terms of ΔMLD values by an order of magnitude (~30 m in the equatorward area versus ~300 m in the poleward area). Moreover, it is possible that a slight variability in MLD gives rise to a large variability in NPP, as for example in the middle- to high-latitude North Atlantic in summer (Figures 4.1f and 4.1l). All such cases can be explained by the nonlinearity of the relationship between I_g and MLD, as well as the influence of I_0 and $K_d(490)$ on it (Equation (4.3)), and the existence
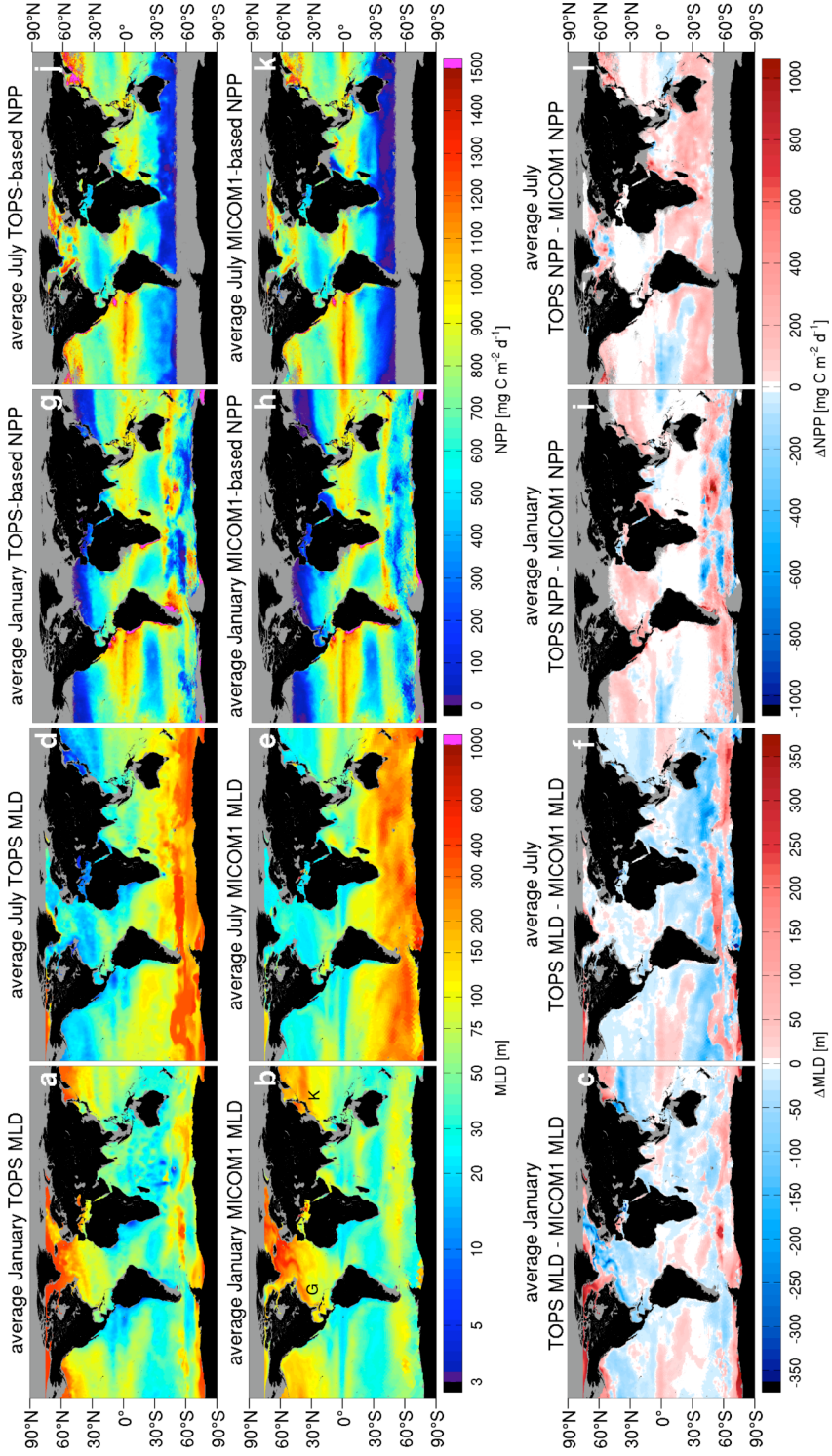
Figure 4.1. (Caption on next page.)

Figure 4.1. Temporal averages for the months of January and July between 1998 and 2004 of the mixed layer depth values modelled by TOPS and MICOM1 (MLD [m]), the associated net primary productivity estimates from the DWI CbPM (NPP [mg C m^{-2} d^{-1}]), and the corresponding differences in MLD (ΔMLD [m]) and NPP (ΔNPP [mg C m^{-2} d^{-1}]), respectively. The differences are calculated by subtracting a given MICOM1 estimate from the equivalent TOPS estimate (Figure 4.1c = Figure 4.1a – Figure 4.1b; Figure 4.1f = Figure 4.1d – Figure 4.1e; Figure 4.1i= Figure 4.1g – Figure 4.1h; Figure 4.1l = Figure 4.1j – Figure 4.1k). Thus, negative ΔMLD means that TOPS MLD is shallower than MICOM1 MLD, while positive ΔMLD means the opposite. Grey colour indicates shelf (<200 m), the Arctic (>75°N) and pixels with no MLD data or ocean colour observations (e.g. due to cloud cover, polar darkness, or sea ice). Letters G and K in Figure 4.1b denote the Gulf Stream and the Kuroshio Current, respectively.

of light saturation and limitation thresholds (indicated in the fourth term of Equation (4.1)). A detailed discussion of these effects will follow in Section 4.4.

Figures 4.1c and 4.1f show that the prominent ΔMLD values are frequent in winter, especially at high latitudes, where the mixed layer is particularly deep. The absolute values of ΔMLD ($|\Delta$MLD$|$) in the sub-Arctic regions and the Southern Ocean sometimes reach more than 300 m. However, the observed effect of large $|\Delta$MLD$|$ at high to middle latitudes is modest, as $|\Delta$NPP$|$ spans from zero to maximally a few hundred mg C m^{-2} d^{-1} (Figures 4.1i and 4.1l). For example, at a location along the North Atlantic Current track, average January ΔMLD of ~−360 m leads to a ΔNPP ranging between ~40 and ~70 mg C m^{-2} d^{-1}.

In summer, a shallow mixed layer is fully developed and MLD variability at middle to high latitudes becomes more restrained, particularly in the northern hemisphere, where $|\Delta$MLD$|$ is often on the order of only a few metres (Figure 4.1f). However, at these latitudes NPP is much more responsive to the summer ΔMLD (Figure 4.1l). For instance, at some locations in the North Pacific, average July ΔNPP reaches more than 1000 mg C m^{-2} d^{-1}, which corresponds to ΔMLD of merely ~−15 m. Similarly, in the Southern Atlantic, average January ΔMLD of ~45 m leads to ΔNPP of nearly −1000 mg C m^{-2} d^{-1}.

In contrast to middle and high latitudes, subtropical gyres are characterized by moderate winter $|\Delta$MLD$|$ (Figures 4.1c and 4.1f). Only along the Gulf Stream and the Kuroshio Current does $|\Delta$MLD$|$ reach above 100 m. Elsewhere in the subtropical gyres, $|\Delta$MLD$|$ rarely surpasses 50 m and often takes up values of ~25 m or less. Even so, winter $|\Delta$NPP$|$ values in the subtropics are generally similar to the largest $|\Delta$NPP$|$ values at higher latitudes (i.e. up to ~300 mg C m^{-2} d^{-1}; Figures 4.1i and 4.1l). In comparison, summer $|\Delta$MLD$|$ in the subtropical gyres is very subtle and rarely goes beyond 10 m. Its influence on ΔNPP is negligible, which contrasts with the effect observed during summer at higher latitudes.

Contrary to the above-mentioned regions, tropical areas show little seasonality in ΔMLD (Figures 4.1c and 4.1f) and ΔNPP (Figures 4.1i and 4.1l). In the equatorial zone of the Atlantic and Indian Oceans, |ΔMLD| is most often significantly below ~30 m, while |ΔNPP| is usually close to zero. Central equatorial Pacific, on the other hand, features larger |ΔMLD| (up to ~60 m), concurrent with |ΔNPP| of ~300 to ~400 mg C m^{-2} d^{-1}. This result agrees with the pronounced sensitivity of the DWI CbPM to MLD perturbations (±20 m) in the tropical Pacific, found by *Friedrichs et al.* [2009]. They reported the removal of MLD uncertainties might reduce the total root mean square difference for the DWI CbPM by as much as 40% and hence greatly improve the skill of the model in this region.

Overall, findings reveal a clear pattern. In winter, |ΔMLD| increases substantially from the subtropics polewards, while an opposite and much weaker meridional gradient is found for |ΔNPP|. In summer, smaller |ΔMLD| is observed at all latitudes, with no distinct meridional gradient. However, summer ΔNPP in the subtropics is negligible, while it attains considerable values at middle and high latitudes. In comparison, equatorial regions display little seasonal variability in either ΔNPP or ΔMLD.

Figure 4.2 presents global annual average MLD values from TOPS and MICOM1 along with related globally integrated annual NPP estimates. The TOPS MLD averages are consistently shallower and thus associated with higher NPP estimates. However, the interannual progression of global MLD values from either model is not perfectly mirrored in the direction of corresponding NPP, although the inverse relationship is largely obvious. This is, nevertheless, not unexpected, bearing in mind the nonlinearity involved in the DWI CbPM (Equations (4.1) and (4.3)). The annual NPP values based on MICOM1 MLD are 5–7% lower than those based on TOPS MLD. This is not incompatible with the results of the sensitivity analysis performed by *Carr et al.* [2006] on six NPP models. They systematically varied MLD over a wide but realistic range of values at 11 geographically representative points in the world ocean. Some NPP models were largely insensitive to changes in MLD, but most showed up to a factor of 2 response, which is comparable with small-scale variability in NPP we discovered. However, the relative differences in global annual NPP estimates (Figure 4.2) are generally considerably smaller, because local short-term positive and negative differences are to a large extent cancelled out in the process of temporal and spatial integration. Over the period October 1997 to September 2004, the TOPS-based annual NPP averages to slightly more than 64.5 Pg C, which is about 2.5 Pg C less than *Behrenfeld et al.* [2005] reported for the period 1997-2002. This difference is caused by not applying interpolation in cloudy regions in this study, while different time period, exclusion of certain parts of the global ocean and version of SeaWiFS data used for the DWI CbPM are likely of secondary importance.
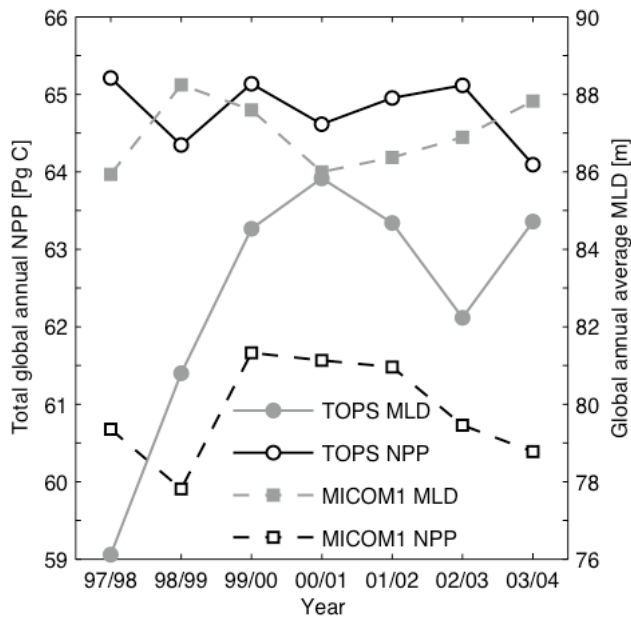
Figure 4.2. Global annual mean MLD [m] from TOPS and MICOM1, with corresponding total global annual NPP calculated by the DWI CbPM, presented in petagrams (10^{15} grams) of carbon [Pg C]. The MLD values were calculated as global averages over seven consecutive 12-month periods ranging from October to September between 1997 and 2004 (e.g. year 1997/1998 is the period October 1997 to September 1998). The NPP values were computed by summing up global monthly NPP over the same 12-month periods. Note that the y axes do not start from zero. No interpolation for cloudy bins has been performed, and MLD values in those bins have been disregarded. Thus, these global values should not be regarded as complete, and any conclusions about interannual trends should be made with caution. However, cloudiness does not present a problem when values from the same time step are compared. Data from shelf regions (<200 m) and the Arctic (>75°N) have been omitted.

In the following text, regional characteristics of the relationship between MLD and NPP are examined in more detail by focusing on the North Atlantic subpolar and subtropical gyres.

4.3.2. North Atlantic Subpolar Gyre

The North Atlantic subpolar gyre (NASPG) is defined as the area stretching from 44°N to 70°N and 10°W to 60°W. Regional analysis is limited to the 6-

year period October 1997 to September 2003, because of a shorter temporal coverage of MICOM2 MLD. March averages are used to illustrate typical winter conditions instead of January owing to the lack of ocean colour information in January poleward of ~50°N. Summer conditions are represented by July averages, as for the global analysis.

TOPS only considers the upper 400 m of water column, and hence produces the shallowest winter mixed layer (Table 4.2). In contrast, HYCOM MLD is by far the deepest. Despite the pronounced differences in average March MLD among the models, the related NPP values are remarkably similar. This is notable in most of the statistics for average March NPP shown in Table 4.2. In average July, on the other hand, the mean and median of HYCOM MLD are ~10 m smaller than the equivalent statistics of TOPS, MICOM1 and MICOM2 MLD data sets (Table 4.2). Being the shallowest, HYCOM mixed layer results in the highest NPP, with the mean and median ~150 to ~200 mg C m^{-2} d^{-1} above average July NPP based on MLD input from the other three models.

The seasonal character of the relationship between MLD and NPP in NASPG is clearly evident on maps of average differences between pairs of modelled MLD fields and the resulting differences in NPP fields (Figures 4.3a–4.3l). The key results for comparison between TOPS and MICOM1 in NASPG are same as outlined in Section 4.3.1 for middle to high latitudes. Findings for the remaining pairs of models also generally agree with the results reported in the global analysis (remarkable ΔMLD during winter accompanied by insignificant ΔNPP; small ΔMLD in summer cooccurring with pronounced ΔNPP). Here, we focus on the summer findings.

In average July, the two versions of MICOM show close agreement in their MLD values so that |ΔMLD| is mostly less than 10 m (Figure 4.3g). The largest difference occurs in the Iceland Sea, where MICOM1 estimates ~70 m deeper mixed layer. Despite the generally high level of similarity in MLD estimates, considerable differences in NPP values are present over a large part of the gyre area (Figure 4.3h). Even a difference in MLD of less than one metre can lead to more than 100 mg C m^{-2} d^{-1} difference in NPP. Thus, |ΔNPP| is largest in the Iceland Sea (up to ~1000 mg C m^{-2} d^{-1}). However, looking at the whole gyre region, the comparison of the two MICOM-based NPP data sets does not reveal as strong differences as those found when MICOM1 is compared with TOPS (Figure 4.3d).

While the comparisons between TOPS and MICOM1, as well as MICOM1 and MICOM2, show both regions of negative and positive ΔMLD, average July mixed layer from HYCOM is almost invariably shallower than that from MICOM2 (Figure 4.3k). The bulk of ΔMLD values range up to ~20 m. In contrast, the majority of ΔNPP values are negative, spreading mostly between about −10 and −600 mg C m^{-2} d^{-1}, with only a small number of values over −1000 mg C m^{-2} d^{-1} (Figure 4.3l). Positive ΔNPP is very rare and close to zero.

Table 4.2. Descriptive statistics of respective mixed layer depth values (MLD [m]) from TOPS, MICOM1, MICOM2 and HYCOM, and their associated net primary productivity values (NPP [mg C m^{-2} d^{-1}]) in NASPG in average March and July of the period 1998–2003[a]

	MLD				NPP			
	TOPS	MICOM1	MICOM2	HYCOM	TOPS	MICOM1	MICOM2	HYCOM
	Average March							
Mean	294.1	380.3	366.8	652.5	14.3	12.7	18.3	6.2
Median	321.6	341.6	290.0	500.1	2.6	1.5	3.2	0.1
Minimum	47.5	47.4	23.4	40.8	0.0	0.0	0.0	0.0
Maximum	400.0	1305.4	1817.9	3206.3	1422.9	2908.4	1202.1	1119.7
2nd percentile	88.7	109.0	115.3	106.0	0.1	0.0	0.0	0.0
98th percentile	398.5	882.6	965.2	2177.5	119.3	104.4	129.3	63.9
	Average July							
Mean	32.0	30.3	29.5	20.1	867.8	836.3	845.1	1048.1
Median	28.1	29.5	28.8	20.7	871.7	836.1	838.2	1034.7
Minimum	3.8	20.3	20.2	2.9	0.0	46.1	149.1	359.6
Maximum	263.3	95.5	71.1	35.0	6017.3	6062.8	7088.0	8536.4
2nd percentile	9.9	21.9	21.1	10.4	70.6	443.7	523.4	678.1
98th percentile	105.3	46.8	42.3	25.3	1422.7	1208.9	1232.2	1486.8

[a]Shelf regions (<200 m) are not taken into account.

The substantial differences in NPP values, characteristic of summer in NASPG, translate into considerable differences in regionally integrated annual NPP (Figure 4.4). The consistently lowest annual NPP arises from MICOM2 MLD. MICOM1 MLD yields only slightly higher annual NPP. In comparison, total annual NPP values based on TOPS MLD are substantially larger (~10–17%), except in years 1999/2000 and 2001/2002. The HYCOM MLD results in the highest annual NPP values for the whole period, between ~5 and ~20% above the corresponding annual NPP estimates based on TOPS MLD. We have found that peaks in all annual NPP estimates during the years 1997/1998 and 2000/2001 seem to be mostly due to larger average values of $b_{bp}(443)$ in those years. The contribution of other input variables to the observed annual NPP peaks, particularly those that have a highly nonlinear relationship with the model-derived NPP (i.e. $K_d(490)$ and MLD), is less clear.

4.3.3. Eastern North Atlantic Subtropical Gyre

As in the case of NASPG, only the 6-year period between October 1997 and September 2003 is considered for the eastern part of the North Atlantic subtropical gyre (NASTG-E), defined as the area between 20°W–40°W and 25°N–40°N. Differences in monthly MLD averages between June and October are found to be very small, while the accompanying NPP differences are almost nonexistent. Average ΔMLD and ΔNPP in winter and early spring months are,
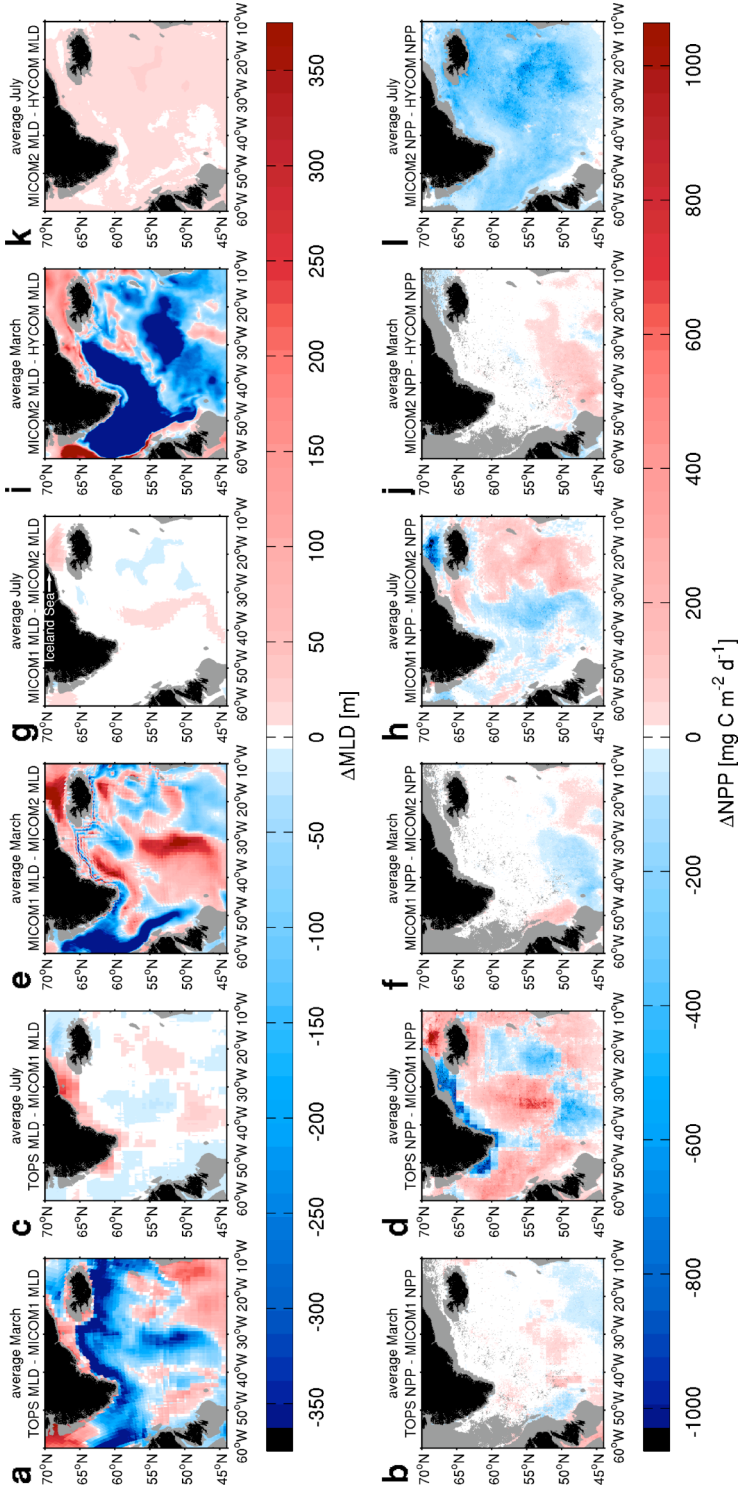
Figure 4.3. Differences in average March and July MLD (ΔMLD [m]) and the corresponding differences in NPP (ΔNPP [mg C m^{-2} d^{-1}]) in NASPG, for the period 1998–2003, between (a–d) TOPS and MICOM1, (e–h) MICOM1 and MICOM2, and (i–l) MICOM2 and HYCOM. Grey colour denotes shelf (<200 m) and locations without available MLD or ocean colour data.
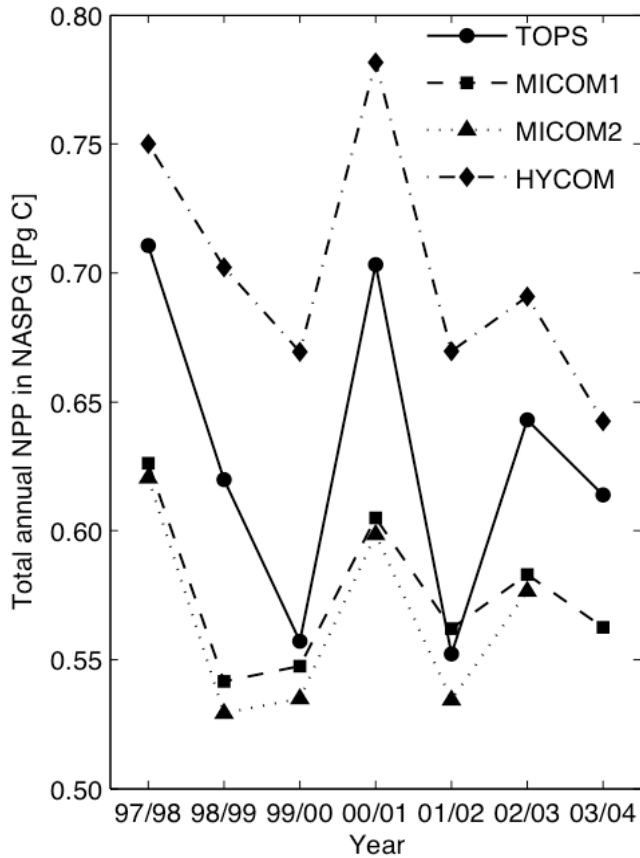
Figure 4.4. Areally integrated annual NPP [Pg C] in the North Atlantic subpolar gyre, calculated by the DWI CbPM, using MLD input from TOPS, MICOM1, MICOM2 and HYCOM, respectively. Note that the *y* axis does not start from zero. Each year is defined as a 12-month period from October to September, starting with October 1997. There are no data from MICOM2 for the last year in the time series. Shelf regions (<200 m) are not taken into account. Cloud correction has not been performed. Thus, these NPP estimates are somewhat lower than they would be if cloudiness were 'removed'.

in comparison, much stronger. Thus, we focus on results for winter represented by average February, which is the month when the NPP estimates generally reach annual minimum and disagree the most.

TOPS produces the shallowest mixed layer estimates (centred at ~105 m), which result in overall the highest average February NPP values (clustered around ~390 mg C m^{-2} d^{-1}; Table 4.3). MLD data from the two versions of MICOM are somewhat larger, thus resulting in lower NPP. Finally, HYCOM

MLD values are largest (with the median ~90 m greater than that of TOPS MLD) and translate into the lowest NPP values, with the median nearly 280 mg C m^{-2} d^{-1} lower than that of TOPS-based NPP.

Figures 4.5a–4.5f illustrate the average February relationship between ΔMLD and ΔNPP geographically. Average February ΔMLD values between TOPS and MICOM1 in NASTG-E are predominantly negative, but do not go beyond about –60 m (Figure 4.5a). A narrow band with positive ΔMLD reaching up to ~40 m is encountered in the northern part of the region. Figure 4.5b reveals a dominant pattern of positive ΔNPP values, majority of which extend up to ~270 mg C m^{-2} d^{-1}, and a minor patch of negative ΔNPP ranging down to ~–65 mg C m^{-2} d^{-1}.

In comparison, ΔMLD and ΔNPP values between MICOM1 and MICOM2 display roughly opposite structures (Figures 4.5c–4.5d). The majority of ΔMLD values are located between about –50 and +50 m. Only a small portion of ΔNPP reaches beyond about –175 or +95 mg C m^{-2} d^{-1}.

Average February ΔMLD is most pronounced between MICOM2 and HYCOM data (Figure 4.5e), from about –170 to +35 m and negative values predominate. The corresponding ΔNPP values lie mainly between about –65 and +340 mg C m^{-2} d^{-1} and are mostly positive (Figure 4.5f). However, in the northwestern corner of NASTG-E both ΔMLD and ΔNPP are negative. Examination of the data from each February between 1998 and 2003 reveals that negative ΔMLD predominates in this part of the gyre. However, it often fails to exert much effect on NPP. On the other hand, positive ΔMLD is

Table 4.3. Descriptive statistics of respective MLD values [m] from TOPS, MICOM1, MICOM2 and HYCOM, and their associated NPP values [mg C m^{-2} d^{-1}] in NASTG-E in average February and July of the period 1998–2003[a]

	MLD				NPP			
	TOPS	MICOM1	MICOM2	HYCOM	TOPS	MICOM1	MICOM2	HYCOM
Average February								
Mean	109.0	137.4	130.3	191.6	359.6	238.4	276.3	142.5
Median	105.4	137.5	125.5	196.0	392.4	210.2	285.7	115.0
Minimum	81.0	104.8	99.7	98.7	14.0	24.7	8.4	0.7
Maximum	176.2	201.6	211.6	294.3	4307.5	2066.8	3824.5	925.2
2nd percentile	87.7	108.9	107.4	118.2	55.3	75.9	36.9	3.9
98th percentile	155.6	171.4	189.9	263.8	575.6	481.6	522.0	394.5
Average July								
Mean	22.4	26.8	25.9	16.6	570.6	570.6	570.6	570.9
Median	18.7	25.9	24.7	14.5	569.2	569.4	569.5	569.7
Minimum	12.7	21.1	20.5	7.2	366.7	367.2	367.3	367.4
Maximum	51.2	41.0	45.0	38.1	1512.4	1504.0	1504.0	1510.9
2nd percentile	14.3	21.5	21.0	8.4	412.9	413.0	413.0	413.1
98th percentile	45.4	38.4	40.2	32.3	730.8	730.5	730.5	731.1

[a]Locations shallower than 200 m are not taken into account.

regularly associated with fairly pronounced negative ΔNPP. Consequently, the process of averaging obscures the true nature of the relationship between ΔMLD and ΔNPP here.

Table 4.3 shows that all models produce considerably shallower mixed layer in summer than in winter. Summer MLD exceeds 50 m in few cases. HYCOM MLD is the shallowest. TOPS MLD is the second shallowest (both in terms of mean and median). Data sets from the two versions of MICOM are not very much different (see also Table 4.4). NPP estimates differ at most by a few milligrams of carbon per square metre per day (Table 4.4).

The findings in NASTG-E are largely opposed to those reported for NASPG. During winter, which is the season of the deepest mixed layer and strongest ΔMLD, ΔNPP is most pronounced. During summer, the mixed layer is at its shallowest and NPP at its highest. However, ΔMLD and particularly ΔNPP are insignificant.

Regionally integrated annual NPP estimates in NASTG-E are presented in Figure 4.6. TOPS-based NPP estimates are highest during the whole period of the study. They exceed the estimates based on MLD from the two MICOM versions by 2–7%. TOPS-based values are 15–23% above the consistently lowest HYCOM-based values.

4.4. Discussion

Accurate assessments of ocean NPP depend, *inter alia*, on representation of phytoplankton exposure to light. Growth irradiance (I_g) is strongly influenced by variations in vertical mixing [e.g. *MacIntyre et al.*, 2000, 2002]. Our study focused on the part of uncertainty in I_g (and thus NPP) arising from uncertainty in MLD, by applying a selection of modelled MLD estimates to the DWI CbPM. The global analysis of modelled MLD fields and associated NPP fields reveals a generally inverse relationship. It is specified in Equations (4.1) and (4.3) that shallower mixed layer results in higher average irradiances, leading to higher growth rates and hence increased NPP. In contrast, large MLD limits light availability and, in turn, NPP. It is important to note that mixed layer depth affects NPP both by influencing the availability of light and nutrients for photosynthesis. However, there is a trade-off between the two effects, as light availability drops, whereas nutrient availability increases with deepening mixing [*Mann and Lazier*, 1996]. In the model considered here, MLD is used explicitly to determine growth irradiance only. On the other hand, the model takes into account the effect of MLD on nutrient levels indirectly via Chl:C ratio. Here, we investigated the relationship between MLD and NPP that is explicit in the DWI CbPM. Our findings show the influence of MLD uncertainties on NPP assessments is highly variable, ranging from no effect to a strong inverse relationship. Our analysis suggests that this can be explained by the following factors: (1) The dependence of I_g on MLD (Equation (4.3)) is not linear; (2) The impact of MLD on I_g is conditioned by $K_d(490)$ and I_0. These
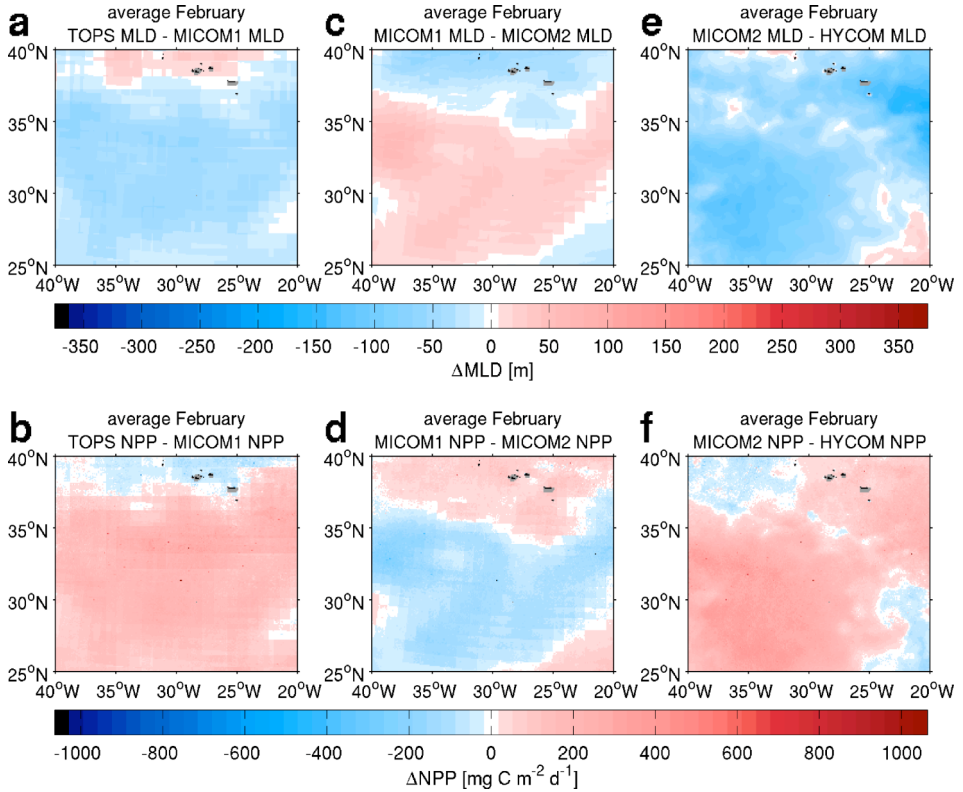
Figure 4.5. Differences in average February MLD (ΔMLD [m]) and the corresponding differences in NPP (ΔNPP [mg C m^{-2} d^{-1}]) in NASTG-E for the period 1998–2003. (a) ΔMLD between TOPS and MICOM1 and (b) the associated ΔNPP; (c) ΔMLD between MICOM1 and MICOM2 and (d) the related ΔNPP; (e) ΔMLD between MICOM2 and HYCOM and (f) the corresponding ΔNPP. Grey colour represents locations shallower than 200 m and grid cells where MLD or ocean colour data are unavailable.

conclusions are robust to the influence of cloudiness on NPP averages, on which this analysis is based.

The relationship between ΔMLD and ΔNPP is found to have a seasonal character. In general, greater absolute values of ΔMLD (|ΔMLD|) are present during winter. Middle and high latitudes in the winter hemisphere have more pronounced ΔMLD than lower latitudes. In contrast, winter |ΔNPP| at middle to high latitudes is minor, while summer |ΔNPP| is considerably larger. In subtropical ocean gyres, on the other hand, a different seasonal regime is encountered. In summer, when |ΔMLD| is minimal, there is virtually no difference in NPP. In winter, ΔMLD is much more prominent and ΔNPP is

93

Table 4.4. Descriptive statistics of respective differences in mixed layer depth fields (ΔMLD [m]) produced by TOPS, MICOM1, MICOM2 and HYCOM, and the associated differences in net primary productivity fields (ΔNPP [mg C m^{-2} d^{-1}]) in NASTG-E, in average July of the period 1998–2003[a]

	ΔMLD			ΔNPP		
	TOPS – MICOM1	MICOM1 – MICOM2	MICOM2 – HYCOM	TOPS – MICOM1	MICOM1 – MICOM2	MICOM2 – HYCOM
Mean	−4.4	0.8	9.3	0.0	0.0	−0.3
Median	−6.1	0.9	10.0	0.1	0.0	−0.2
Minimum	−11.9	−4.8	−3.4	−7.7	−2.3	−14.0
Maximum	17.1	4.1	15.4	8.4	6.1	4.0
2nd percentile	−10.3	−2.1	0.8	−1.9	−0.2	−1.4
98th percentile	10.1	2.7	13.6	0.8	0.5	0.0

[a]Locations shallower than 200 m are not taken into account.

more distinct. A rare region that does not display seasonal differences is the equatorial Pacific, where persistently small or moderate |ΔMLD| is coupled with large |ΔNPP|.

Two previous studies have addressed the influence of MLD perturbations on several NPP models [*Carr et al.*, 2006; *Friedrichs et al.*, 2009]. *Carr et al.* [2006] studied the impact of wide-range variations in MLD on six NPP models at 11 points representative of conditions in different ocean basins. Two models were relatively insensitive to ΔMLD, while the rest showed considerable sensitivity, but usually less than a factor of two. They found the sensitivity was largest during respective summer at locations in the temperate North Atlantic (51.3°N, 21.8°W), subtropical North Pacific (33.8°N, 153.9°E) and subtropical Indian Ocean (36.6°S, 83.7°E), where initial MLD was 10–15 m. Our results agree with those of *Carr et al.* [2006] at the mid-latitude North Atlantic location, but we found no sensitivity in NPP at the subtropical latitudes.

A recent study by *Friedrichs et al.* [2009] analyzed the effect of uncertainties in MLD on seven NPP models, including the DWI CbPM, in the tropical Pacific. The skill of most NPP models was seriously affected by MLD perturbations of ±20 m. The impact on the DWI CbPM was largest. *Friedrichs et al.* [2009] found that eliminating MLD uncertainties would greatly improve the DWI CbPM performance in the tropical Pacific, as it may lower the related total root mean square difference by up to 40%. This is consistent with our results in the same region. It should be noted that the CbPM has recently been significantly expanded to include spectral- and depth-dependent variations in light properties, phytoplankton biomass and growth rate [*Westberry et al.*, 2008]. This depth- and wavelength-resolved (DWR) CbPM was also subjected to MLD perturbations by *Friedrichs et al.* [2009]. Unlike its predecessor, it showed little sensitivity. We compared the sensitivity of NPP estimates from
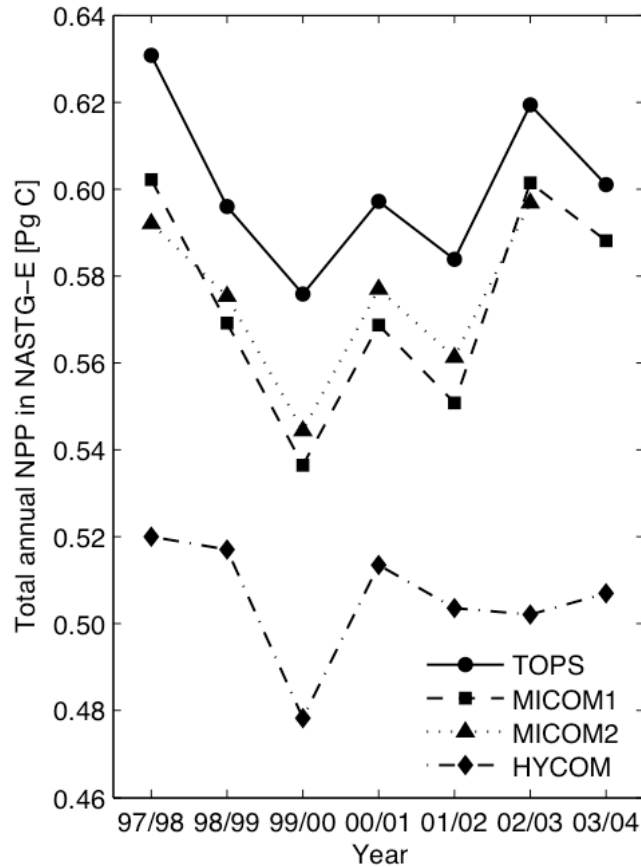
Figure 4.6. Areally integrated annual NPP [Pg C] in the eastern part of the North Atlantic subtropical gyre, calculated by the DWI CbPM using MLD input from TOPS, MICOM1, MICOM2 and HYCOM, respectively. Note that the y axis does not start from zero. Each year is defined as a 12-month period from October to September, starting with October 1997. Data from MICOM2 are unavailable for the last 12 months of the time period. Although NPP fields have not been corrected for cloudiness, cloud presence in this region is rather small, especially in summer months. Therefore, these estimates are probably not very much lower than they would be if cloud correction were performed.

both versions of the CbPM at three respective locations in NASPG (48.81°N, 43.80°W), NASTG-E (33.06°N, 37.05°W) and the equatorial Pacific (0.88°S, 150.99°W). Each location corresponds to a 9-km SeaWiFS bin and is representative of seasonal variability in input values and model response in a given region. Values of input variables were taken from March and July 2000 in NASPG, while January and July 2000 were used elsewhere. The model runs

95

were performed as described in Section 4.2.4, with the addition of nitracline depth as input for the DWR CbPM (computed by the method of *Westberry et al.* [2008], but based on more recent climatological nutrient fields [*Garcia et al.*, 2006]). Figures S4.1–S4.3 (Appendix) show that while the two CbPM versions give rather different results, their sensitivity to uncertainties in MLD is generally comparable. A somewhat smaller sensitivity of the DWR CbPM is observed in July 2000 in NASPG and the equatorial Pacific. The tendency of the DWI CbPM to give higher NPP is mainly due to overestimated Z_{eu} values in this model version [*Westberry et al.*, 2008]. When Z_{eu} values estimated by the method of *Westberry et al.* [2008] are used instead to get the total water-column NPP from the surface NPP estimates of the DWI CbPM, the results are much closer to those of the DWR CbPM (Figures S4.1–S4.3, Appendix). The findings of our brief analysis in the equatorial Pacific do not seem to comply with those of *Friedrichs et al.* [2009], perhaps because they used smaller MLD perturbations. Thus, a separate study is required to analyze the sensitivity of the DWR CbPM to MLD in more detail and so fully identify the corresponding differences and similarities between the two model versions.

Mechanisms responsible for the observed difference in seasonal regimes between higher and lower latitudes are revealed by a closer inspection of the NASPG and NASTG-E results. In NASPG, winter ΔMLD is very distinct and often reaches several hundred metres. However, this yields minor difference in NPP due to generally unfavourable irradiance conditions. Photoperiod during winter is short, while surface photosynthetically available radiation (I_0) is low. These circumstances, combined with large MLD, suppress productivity. In order to illustrate reasons for this finding, we rearranged Equation (4.3):

$$\text{MLD} = \frac{2}{K_d(490)} \times \Big[\ln(I_0) - \ln(I_g) \Big]. \tag{4.4}$$

The fourth term in Equation (4.1), ($1 - e^{-3I_g}$), implies a threshold value of I_g below which productivity is limited by light. We approximated this threshold to 2 mol photons m^{-2} h^{-1}. Applying it to Equation (4.4) for a range of I_0 and $K_d(490)$ gives a set of MLD values on the verge of light limitation (see Figure 4.7a). If modelled MLD for a given pair of coincident I_0 and $K_d(490)$ values is smaller than the associated threshold MLD value in Figure 4.7a, the presence of light saturation is indicated. Regardless of how much MLD estimates differ among the models, if they are all smaller than the threshold MLD, NPP values derived from them will be equal (i.e. highest possible for particular nutrient and temperature levels). When modelled MLD exceeds the threshold MLD value, light limitation is at work. The larger the modelled MLD gets, the stronger the light limitation becomes. However, this is only true until MLD renders I_g so small that we can regard it as being effectively 0 mol photons m^{-2} h^{-1}. Figure 4.7b shows MLD values at which this critical point is reached, for an array of I_0
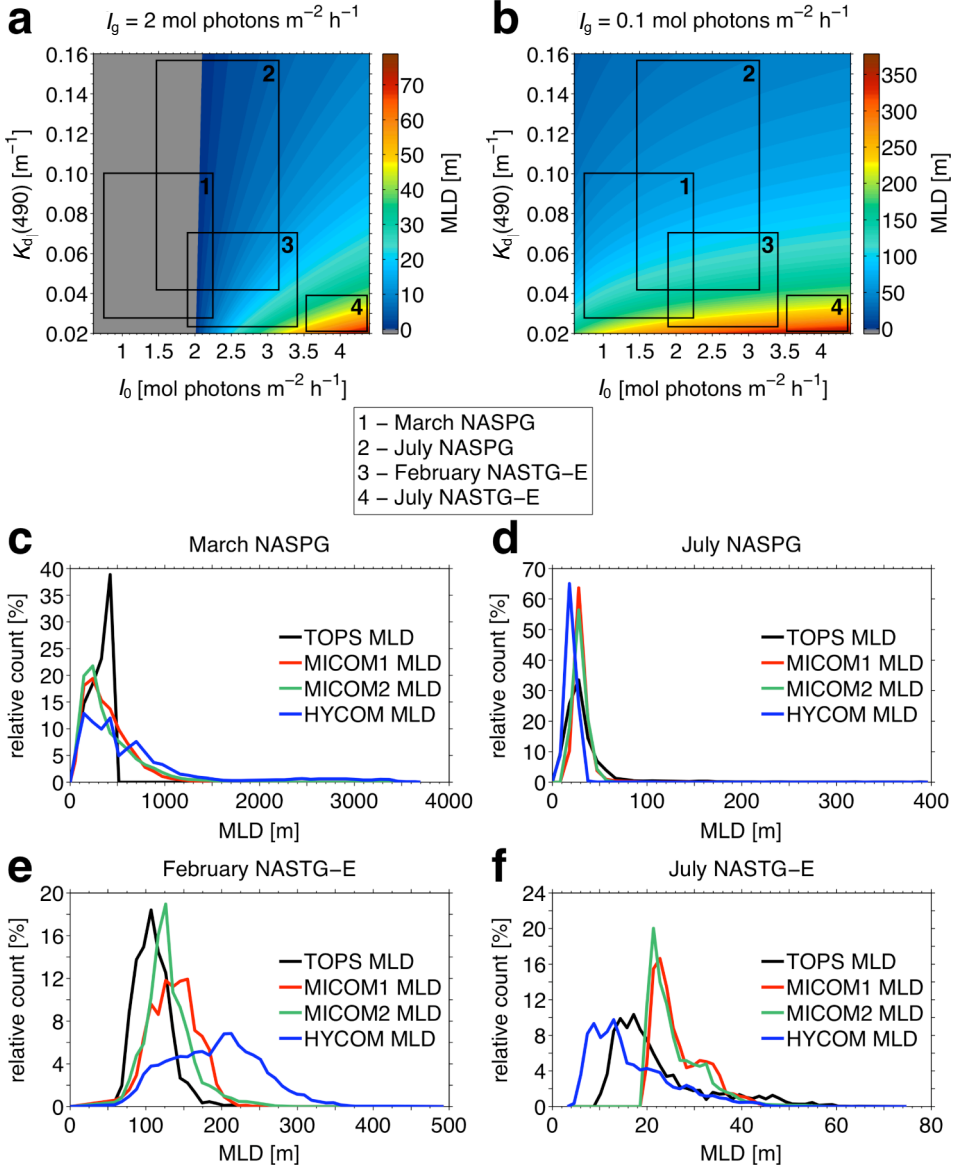
Figure 4.7. (a) Two-dimensional filled contour graph showing critical MLD as a function of I_0 [mol photons m^{-2} h^{-1}] and $K_d(490)$ [m^{-1}] for $I_g = 2$ mol photons m^{-2} h^{-1} (see Equation (4.4)). (b) Same as previous, but for $I_g = 0.1$ mol photons m^{-2} h^{-1}. The rectangles superimposed on the graphs show typical ranges of I_0 and $K_d(490)$ values for (1) March and (2) July in NASPG, and (3) February and (4) July in NASTG-E, respectively. These ranges are defined as 95% quantile intervals between 2.5% and 97.5% quantiles of the observed I_0 and $K_d(490)$ values for each respective month between 1998 and 2003. (Continued on next page.)

Figure 4.7. (Continued.) Note that the colour scales in Figures 4.7a and 4.7b have different extent. Grey in Figure 4.7a denotes circumstances in which no light saturation is possible. Figures 4.7c–4.7f show relative count (i.e. relative frequency distributions) of MLD values modelled by TOPS, MICOM1, MICOM2, and HYCOM, respectively, in representative months from 1998 to 2003: (c) March in NASPG; (d) July in NASPG; (e) February in NASTG-E; (f) July in NASTG-E. Relative counts were calculated as follows: In a particular region, MLD values estimated by a given ocean model in a certain month from 1998 to 2003 were collected together. Values from shelf areas were omitted. The range of MLD values was divided into equally spaced class intervals. Number of values in each class interval was determined and then divided by the total number of values.

and $K_d(490)$. At and beyond this point, light limitation can be considered complete. Thus, when MLD estimates from different models enter the realm of full light limitation, their associated NPP estimates must be the same, namely 0 mg C m^{-2} d^{-1}.

In NASPG in March, I_0 is usually so low that full light saturation cannot be achieved (Figure 4.7a). Full light limitation may be reached at depths between ~40 and ~200 m (Figure 4.7b), depending on the combination of typical I_0 and $K_d(490)$ values. The vast majority of MLD estimates are ≥~200 m (see Figure 4.7c), making the related NPP values negligible. Therefore, the largest part of NASPG is characterized by zero ΔNPP during winter. Toward summertime, MLD becomes shallower owing to the combined effect of rising sea surface temperatures, weaker winds and increased freshwater (meltwater) fluxes. All ocean models estimate this shoaling and ΔMLD becomes less prominent. NPP and |ΔNPP|, however, soar to summer maxima. Figures 4.7a–4.7b illustrate how the coexisting I_0 and $K_d(490)$ values characteristic of July in NASPG influence the threshold MLD values. Figure 4.7d shows that MLD from the two MICOM models is too large for full light saturation to be achieved. On the other hand, TOPS and particularly HYCOM MLD can theoretically often result in I_g equal to or larger than the saturation threshold. Nevertheless, we have found that matching I_0 and $K_d(490)$ are seldom favourable enough and only ~4% of MLD estimates from the latter two models give light saturated photosynthesis. Full light limitation is similarly rare. Depending on model, 90 to 99% of MLD estimates result in partial light limitation. Differences between these estimates, although small, have potential to trigger rather large differences in I_g because they are often coupled with rapid decay of light in the water column (see the range of $K_d(490)$ in Figures 4.7a–4.7b). This is in turn translated into considerable ΔNPP.

In comparison, the largest winter |ΔMLD| values in NASTG-E are accompanied by the largest |ΔNPP|. Figures 4.7a–4.7b reveal the interactions among MLD, I_0 and $K_d(490)$ underlying this finding. No model estimates a

sufficiently shallow mixed layer for full light saturation to be accomplished (Figure 4.7e). The range of winter MLD values from TOPS, MICOM1 and MICOM2 is such that, combined with the prevalent illumination conditions, partial light limitation occurs in 70 to 80% of cases. HYCOM MLD is considerably deeper and leads to full light limitation in more than 50% of instances. In summer, ΔMLD in NASTG-E is small and ΔNPP practically zero (Table 4.4), which differs from the relationship in NASPG. This is explained by the combination of shallow summer mixed layer (Figure 4.7f) with high I_0 and low $K_d(490)$ values, which in almost all cases leads to I_g exceeding the saturation threshold value (see Figure 4.7a), thus causing no difference in NPP.

To recapitulate, seasonal development of $|\Delta$NPP$|$ in NASPG runs in parallel with the seasonal cycle of NPP, rising from a winter minimum to a summer maximum. In this regime, it is the summer MLD values that bear most importance for NPP estimates, whereas winter ΔMLD makes little difference. On the other hand, the seasonal cycle of ΔNPP in NASTG-E is in antiphase with the seasonal changes in NPP itself: most distinct ΔNPP occurs in low productivity period, while summertime ΔNPP is virtually zero. In this case, variability in MLD between June and October has practically no discernable influence on NPP, while winter ΔMLD has the largest impact.

$K_d(490)$ can be used to indicate how sensitive NPP is to changes in MLD. For the same I_0, increase in $K_d(490)$ causes the depth of transition from saturating to limiting I_g to be shallower (Figure 4.7a). The same is valid for the depth at which total light limitation arises (Figure 4.7b). Also, the difference between the two critical MLD values for a given I_0 becomes smaller as $K_d(490)$ increases. For example, for $I_0 = 3$ mol photons m^{-2} h^{-1} and $K_d(490) = 0.02$ m^{-1}, the progression from full light saturation (MLD = 40.5 m) to full light limitation (MLD = 340 m) occurs over a range of ~300 m (compare Figures 4.7a and 4.7b). However, the critical depth difference becomes only 37.5 m (i.e. 42.5 m − 5 m) for the same I_0 when $K_d(490)$ is 0.16 m^{-1}. It follows that a unit of change in MLD between the two critical values produces a steeper gradient in I_g for larger $K_d(490)$.

The highest annual productivity estimates are about 20–30% above the lowest ones in NASPG, ~15 to ~20% in NASTG-E and less than 10% in the global ocean. These results are well within the factor of 2 boundaries reported for differences in global or regional annual NPP estimates in studies that compared performance of a number of different productivity algorithms [*Campbell et al.*, 2002; *Carr et al.*, 2006; *Friedrichs et al.*, 2009]. In other words, uncertainties in global or regional NPP estimates that originate from using different input MLD in a particular NPP model are much more constrained than those stemming from using different productivity models.

4.5. Future Directions

The newly developed, more complex version of the CbPM [*Westberry et al.*, 2008] is capable of resolving vertical profiles of optical and biological

properties below the mixed layer. While *Friedrichs et al.* [2009] reported its sensitivity to MLD perturbations in the tropical Pacific was much lower compared to the simpler CbPM version, we found no similar disparity between the two versions. However, as we only performed a brief comparison, further more detailed and extensive analysis is needed to fully quantify and understand the response of the more recent version of the CbPM to MLD uncertainties in various ecological regimes across the ocean.

Turbulent mixing has a strong influence on vertical motion of phytoplankton cells and light intensity they experience [*MacIntyre et al.*, 2000]. However, the aim of phytoplankton productivity models to improve NPP estimates by explicitly taking the effects of vertical mixing into account is currently limited by the availability of alternatives to MLD. The concept of the mixed layer is based on the homogeneity of vertical density profile, while identification of the mixing layer depends on the dissipation rate of turbulent kinetic energy [*Dewey and Moum*, 1990]. Hence, vertical mixing of phytoplankton may be considerably shallower than MLD [e.g. *Townsend et al.*, 1994]. In other words, a deep mixed layer does not inevitably imply a severe light limitation of photosynthesis [*Backhaus et al.*, 2003; *D'Asaro*, 2008; *Huisman et al.*, 1999; *Townsend et al.*, 1994; *Yamazaki and Kamykowski*, 1991]. While the depth of active turbulent mixing would be a more adequate indicator of average growth irradiance than MLD, it is not yet a routine product of ocean modelling. Global and regional ocean models typically have too coarse horizontal resolutions to adequately resolve small-scale turbulent and convective processes that are responsible for vertical mixing [*Marshall and Schott*, 1999]. The horizontally averaged effects of these 'subgrid' processes thus have to be parameterized. A number of vertical mixing parameterizations have been developed [*Burchard and Petersen*, 1999], but they are not equally skilful in realistic representation of mixing for various applications [*Burchard*, 2002]. Future activities towards advancing representation of phytoplankton light exposure should focus on selecting a theoretically sound and computationally economic turbulent mixing scheme that is best suited for this purpose.

Moreover, further studies are needed to verify the existence and extensiveness of the mechanism of 'phyto-convection' [*Backhaus et al.*, 2003; *D'Asaro*, 2008], which is claimed to promote phytoplankton productivity in a deep convective mixed layer during winter at high latitudes. If the importance of phyto-convection is shown to be fundamental, the widespread view that virtually no net productivity is possible at subpolar latitudes during winter will have to be reexamined.

Finally, it is important to recognize that input variables other than MLD contribute to the uncertainty in model NPP estimates. For example, *Friedrichs et al.* [2009] evaluated response of a number of NPP models, including the two CbPM versions, to perturbations in Chl and I_0 in the tropical Pacific. More studies of that kind are necessary to direct future research aimed at reducing uncertainties in ocean NPP modelling.

Acknowledgements

We thank Robert T. O'Malley and Toby K. Westberry for their help with the CbPM computations. The GSM01 products were kindly provided by Stéphane Maritorena. We acknowledge Yongqi Gao, Anne Britt Sandø and Knut Arild Lisæter for supplying MLD fields from MICOM1, MICOM2 and HYCOM, respectively. We are grateful to Ingo Bethke, Knut-Frode Dagestad, Anton Korosov and Lars-Gunnar Persson for their technical assistance. We also thank Laurent Bertino, Annette Samuelsen and Kjetil Lygre for their advice regarding the analysis of the results. Finally, we thank Vincent S. Saba and an anonymous reviewer, whose constructive comments have helped us improve the manuscript. This work was supported by the Research Council of Norway grant 177269/V10. This is publication A235 from the Bjerknes Centre for Climate Research.

Appendix: Supplementary Figures
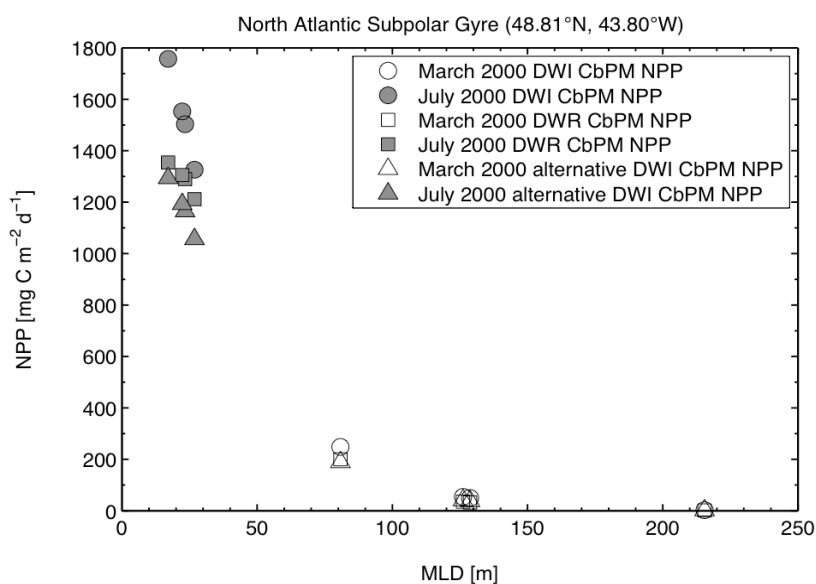
Figure S4.1. Net primary productivity estimates (NPP [mg C m^{-2} d^{-1}]), based on monthly Level-3 SeaWiFS observations at a location in the North Atlantic Subpolar Gyre (48.81°N, 43.80°W) in March and July 2000, plotted against mixed layer depth values (MLD [m]) from TOPS, MICOM1, MICOM2 and HYCOM. Circles represent NPP estimated by the depth- and wavelength-integrated CbPM (DWI CbPM). Squares symbolize NPP computed by the depth- and wavelength-resolved CbPM (DWR CbPM). Triangles denote NPP estimates from the DWI CbPM with the parameterization for the euphotic depth taken from the DWR CbPM (alternative DWI CbPM).
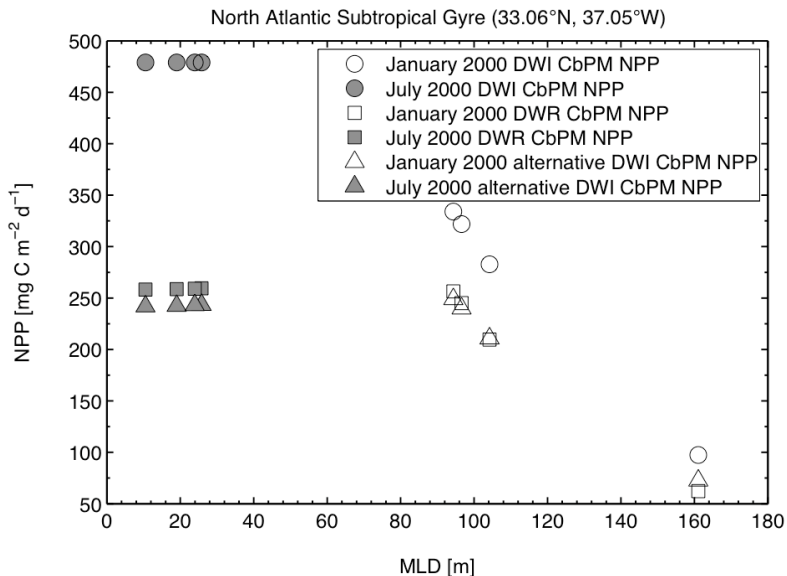
Figure S4.2. Same as the previous figure, but at a location in the North Atlantic Subtropical Gyre (33.06°N, 37.05°W) in January and July 2000.
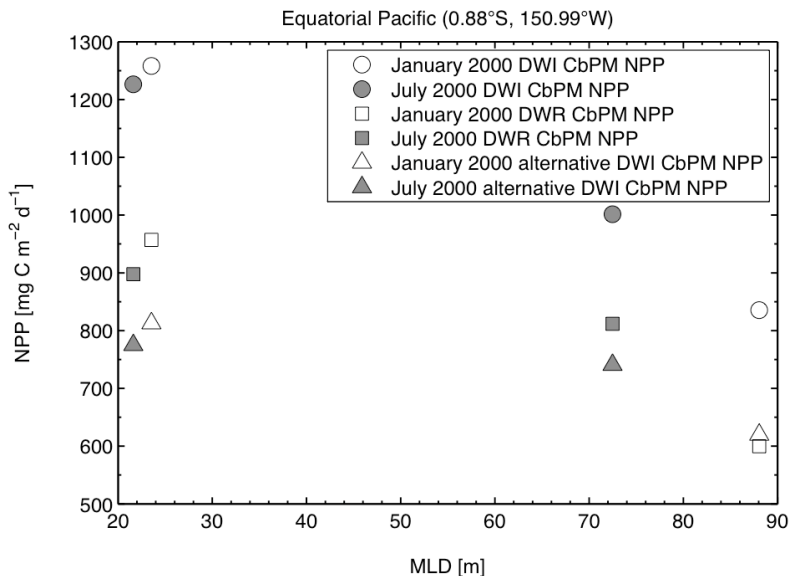
Figure S4.3. Same as the previous figure, but at a location in the equatorial Pacific (0.88°S, 150.99°W). Note that MLD estimates at this location were available from TOPS and MICOM1 only.

References

Backhaus, J. O., E. N. Hegseth, H. Wehde, X. Irigoien, K. Hatten, and K. Logemann (2003), Convection and primary production in winter, *Marine Ecology-Progress Series*, *251*, 1-14.

Banse, K. (1991), Rates of phytoplankton cell division in the field and in iron enrichment experiments, *Limnology and Oceanography*, *36*(8), 1886-1898.

Behrenfeld, M., E. Boss, D. Siegel, and D. Shea (2005), Carbon-based ocean productivity and phytoplankton physiology from space, *Global Biogeochemical Cycles*, *19*(1), GB1006.

Behrenfeld, M. J., W. E. Esaias, and K. R. Turpie (2002a), Assessment of primary production at the global scale, in *Phytoplankton productivity: Carbon assimilation in marine and freshwater ecosystems*, edited by P. J. leB. Williams, et al., pp. 156-186, Blackwell Science, Oxford, UK.

Behrenfeld, M. J., and P. G. Falkowski (1997a), A consumer's guide to phytoplankton primary productivity models, *Limnology and Oceanography*, *42*(7), 1479-1491.

Behrenfeld, M. J., and P. G. Falkowski (1997b), Photosynthetic rates derived from satellite-based chlorophyll concentration, *Limnology and Oceanography*, *42*(1), 1-20.

Behrenfeld, M. J., E. Maranon, D. A. Siegel, and S. B. Hooker (2002b), Photoacclimation and nutrient-based model of light-saturated photosynthesis for quantifying oceanic primary production, *Marine Ecology-Progress Series*, *228*, 103-117.

Bleck, R. (2002), An oceanic general circulation model framed in hybrid isopycnic-Cartesian coordinates, *Ocean Modelling*, *4*(1), 55-88.

Bleck, R., C. Rooth, D. Hu, and L. T. Smith (1992), Salinity-driven thermocline transients in a wind- and thermohaline-forced isopycnic coordinate model of the North Atlantic, *Journal of Physical Oceanography*, *22*(12), 1486-1505.

Bleck, R., and L. T. Smith (1990), A wind-driven isopycnic coordinate model of the north and equatorial Atlantic Ocean: 1. Model development and supporting experiments, *Journal of Geophysical Research-Oceans*, *95*(C3), 3273-3285.

Burchard, H. (2002), *Applied turbulence modelling in marine waters*, 229 pp., Springer, Berlin, Germany.

Burchard, H., and O. Petersen (1999), Models of turbulence in the marine environment: A comparative study of two-equation turbulence models, *Journal of Marine Systems*, *21*(1-4), 29-53.

Campbell, J., D. Antoine, R. Armstrong, K. Arrigo, W. Balch, R. Barber, M. Behrenfeld, R. Bidigare, J. Bishop, M. Carr, W. Esaias, P. Falkowski, N. Hoepffner, R. Iverson, D. Kiefer, S. Lohrenz, J. Marra, A. Morel, J. Ryan, V. Vedernikov, K. Waters, C. Yentsch, and J. Yoder (2002), Comparison of algorithms for estimating ocean primary production from surface chlorophyll, temperature, and irradiance, *Global Biogeochemical Cycles*, *16*(3), 1035.

Carr, M.-E., M. A. M. Friedrichs, M. Schmeltz, M. Noguchi Aita, D. Antoine, K. R. Arrigo, I. Asanuma, O. Aumont, R. Barber, M. Behrenfeld, R. Bidigare, E. T. Buitenhuis, J. Campbell, A. Ciotti, H. Dierssen, M. Dowell, J. Dunne, W. Esaias, B. Gentili, W. Gregg, S. Groom, N. Hoepffner, J. Ishizaka, T. Kameda, C. L. Quéré, S. Lohrenz, J. Marra, F. Mélin, K. Moore, A. Morel, T. E. Reddy, J. Ryan, M. Scardi, T. Smyth, K. Turpie, G. Tilstone, K. Waters, and Y. Yamanaka (2006),

A comparison of global estimates of marine primary production from ocean color, *Deep Sea Research Part II: Topical Studies in Oceanography*, *53*(5-7), 741- 770.

Clancy, R. M., and P. J. Martin (1981), Synoptic forecasting of the oceanic mixed layer using the Navy's operational environmental data base: Present capabilities and future applications, *Bulletin of the American Meteorological Society*, *62*(6), 770-770.

Clancy, R. M., and K. D. Pollak (1983), A real-time synoptic ocean thermal analysis/forecast system, *Progress in Oceanography*, *12*(4), 383-424.

Clancy, R. M., and W. D. Sadler (1992), The Fleet Numerical Oceanography Center suite of oceanographic models and products, *Weather and Forecasting*, *7*(2), 307-327.

Cloern, J. E., and R. Dufford (2005), Phytoplankton community ecology: Principles applied in San Francisco Bay, *Marine Ecology-Progress Series*, *285*, 11-28.

D'Asaro, E. A. (2008), Convection and the seeding of the North Atlantic bloom, *Journal of Marine Systems*, *69*(3-4), 233-237.

Dewey, R. K., and J. N. Moum (1990), Enhancement of fronts by vertical mixing, *Journal of Geophysical Research-Oceans*, *95*(C6), 9433-9445.

Duffy, J. E., and J. J. Stachowicz (2006), Why biodiversity is important to oceanography: Potential roles of genetic, species, and trophic diversity in pelagic ecosystem processes, *Marine Ecology-Progress Series*, *311*, 179-189.

Falkowski, P., R. Scholes, E. Boyle, J. Canadell, D. Canfield, J. Elser, N. Gruber, K. Hibbard, P. Hogberg, S. Linder, F. Mackenzie, B. Moore, T. Pedersen, Y. Rosenthal, S. Seitzinger, V. Smetacek, and W. Steffen (2000), The global carbon cycle: A test of our knowledge of Earth as a system, *Science*, *290*(5490), 291-296.

Falkowski, P. G., R. T. Barber, and V. Smetacek (1998), Biogeochemical controls and feedbacks on ocean primary production, *Science*, *281*(5374), 200-206.

Field, C. B., M. J. Behrenfeld, J. T. Randerson, and P. Falkowski (1998), Primary production of the biosphere: Integrating terrestrial and oceanic components, *Science*, *281*(5374), 237-240.

Friedrichs, M. A. M., M.-E. Carr, R. T. Barber, M. Scardi, D. Antoine, R. A. Armstrong, I. Asanuma, M. J. Behrenfeld, E. T. Buitenhuis, F. Chai, J. R. Christian, A. M. Ciotti, S. C. Doney, M. Dowell, J. Dunne, B. Gentili, W. Gregg, N. Hoepffner, J. Ishizaka, T. Kameda, I. Lima, J. Marra, F. MÈlin, J. K. Moore, A. Morel, R. T. O'Malley, J. O'Reilly, V. S. Saba, M. Schmeltz, T. J. Smyth, J. Tjiputra, K. Waters, T. K. Westberry, and A. Winguth (2009), Assessing the uncertainties of model estimates of primary productivity in the tropical Pacific ocean, *Journal of Marine Systems*, *76*(1-2), 113-133.

Frouin, R., and S. F. Iacobellis (2002), Influence of phytoplankton on the global radiation budget, *Journal of Geophysical Research-Atmospheres*, *107*(D19).

Gabric, A. J., R. Simo, R. A. Cropp, A. C. Hirst, and J. Dachs (2004), Modeling estimates of the global emission of dimethylsulfide under enhanced greenhouse conditions, *Global Biogeochemical Cycles*, *18*(2), GB2014.

Garcia, H. E., R. A. Locarnini, T. P. Boyer, and J. I. Antonov (2006), World ocean atlas 2005, vol. 4: Nutrients (phosphate, nitrate, silicate), in *NOAA Atlas NESDIS*, vol. 64, edited by S. Levitus, 396 pp., NOAA, Silver Spring, Maryland, USA.

Garver, S. A., and D. A. Siegel (1997), Inherent optical property inversion of ocean color spectra and its biogeochemical interpretation: 1. Time series from the Sargasso Sea, *Journal of Geophysical Research-Oceans*, *102*(C8), 18,607-18,625.

Gaspar, P., Y. Grégoris, and J.-M. Lefevre (1990), A simple eddy kinetic energy model for simulations of the oceanic vertical mixing: Tests at station Papa and long-term upper ocean study site, *Journal of Geophysical Research-Oceans*, *95*(C9), 16,179-116,193.

Geider, R. J., E. H. Delucia, P. G. Falkowski, A. C. Finzi, J. P. Grime, J. Grace, T. M. Kana, J. La Roche, S. P. Long, B. A. Osborne, T. Platt, I. C. Prentice, J. A. Raven, W. H. Schlesinger, V. Smetacek, V. Stuart, S. Sathyendranath, R. B. Thomas, T. C. Vogelmann, P. Williams, and F. I. Woodward (2001), Primary productivity of planet Earth: Biological determinants and physical constraints in terrestrial and aquatic habitats, *Global Change Biology*, *7*(8), 849-882.

Geider, R. J., and H. L. MacIntyre (2002), Physiology and biochemistry of photosynthesis and algal carbon acquisition, in *Phytoplankton productivity: Carbon assimilation in marine and freshwater ecosystems*, edited by P. J. leB. Williams, et al., pp. 44-77, Blackwell Science, Oxford, UK.

Hátún, H., A. B. Sandø, H. Drange, B. Hansen, and H. Valdimarsson (2005), Influence of the Atlantic Subpolar Gyre on the thermohaline circulation, *Science*, *309*(5742), 1841-1844.

Huisman, J., P. van Oostveen, and F. J. Weissing (1999), Critical depth and critical turbulence: Two different mechanisms for the development of phytoplankton blooms, *Limnology and Oceanography*, *44*(7), 1781-1787.

International Ocean-Colour Coordinating Group (IOCCG) (2000), Remote sensing of ocean colour in coastal, and other optically-complex, waters, edited by S. Sathyendranath, *Rep. 3*, 140 pp, IOCCG, Dartmouth, Canada.

International Ocean-Colour Coordinating Group (IOCCG) (2004), Guide to the creation and use of ocean-colour, level-3, binned data products, edited by D. Antoine, *Rep. 4*, 88 pp, IOCCG, Dartmouth, Canada.

Jickells, T. D., Z. S. An, K. K. Andersen, A. R. Baker, G. Bergametti, N. Brooks, J. J. Cao, P. W. Boyd, R. A. Duce, K. A. Hunter, H. Kawahata, N. Kubilay, J. laRoche, P. S. Liss, N. Mahowald, J. M. Prospero, A. J. Ridgwell, I. Tegen, and R. Torres (2005), Global iron connections between desert dust, ocean biogeochemistry, and climate, *Science*, *308*(5718), 67-71.

Large, W. G., J. C. McWilliams, and S. C. Doney (1994), Oceanic vertical mixing: A review and a model with a nonlocal boundary-layer parameterization, *Reviews of Geophysics*, *32*(4), 363-403.

Loisel, H., E. Bosc, D. Stramski, K. Oubelkheir, and P. Y. Deschamps (2001), Seasonal variability of the backscattering coefficient in the Mediterranean Sea based on satellite SeaWiFS imagery, *Geophysical Research Letters*, *28*(22), 4203-4206.

MacIntyre, H. L., T. M. Kana, and R. J. Geider (2000), The effect of water motion on short-term rates of photosynthesis by marine phytoplankton, *Trends in Plant Science*, *5*(1), 12-17.

Mann, K. H., and J. R. N. Lazier (1996), *Dynamics of marine ecosystems: Biological-physical interactions in the oceans*, 2nd ed., XII, 394 pp., Blackwell Science, Cambridge, Massachusetts, USA.

Maritorena, S., D. A. Siegel, and A. R. Peterson (2002), Optimization of a semianalytical ocean color model for global-scale applications, *Applied Optics*, *41*(15), 2705-2714.

Marshall, J., and F. Schott (1999), Open-ocean convection: Observations, theory, and models, *Reviews of Geophysics*, *37*(1), 1-64.

Mellor, G. L., and T. Yamada (1974), A hierarchy of turbulence closure models for planetary boundary layers, *Journal of the Atmospheric Sciences*, *31*(7), 1791-1806.

Riebesell, U., K. G. Schulz, R. G. J. Bellerby, M. Botros, P. Fritsche, M. Meyerhofer, C. Neill, G. Nondal, A. Oschlies, J. Wohlers, and E. Zollner (2007), Enhanced biological carbon consumption in a high CO_2 ocean, *Nature*, *450*(7169), 545-548.

Siegel, D. A., S. Maritorena, N. B. Nelson, D. A. Hansell, and M. Lorenzi-Kayser (2002), Global distribution and dynamics of colored dissolved and detrital organic materials, *Journal of Geophysical Research-Oceans*, *107*(C12), 3228.

Siegel, D. A., S. Maritorena, N. B. Nelson, and M. J. Behrenfeld (2005), Independence and interdependencies among global ocean color properties: Reassessing the bio-optical assumption, *Journal of Geophysical Research-Oceans*, *110*, C07011.

Stramski, D., R. A. Reynolds, M. Kahru, and B. G. Mitchell (1999), Estimation of particulate organic carbon in the ocean from satellite remote sensing, *Science*, *285*(5425), 239-242.

Townsend, D. W., L. M. Cammen, P. M. Holligan, D. E. Campbell, and N. R. Pettigrew (1994), Causes and consequences of variability in the timing of spring phytoplankton blooms, *Deep Sea Research Part I: Oceanographic Research Papers*, *41*(5-6), 747-765.

Westberry, T., M. J. Behrenfeld, D. A. Siegel, and E. Boss (2008), Carbon-based primary productivity modeling with vertically resolved photoacclimation, *Global Biogeochemical Cycles*, *22*, GB2024.

Yamazaki, H., and D. Kamykowski (1991), The vertical trajectories of motile phytoplankton in a wind-mixed water column, *Deep Sea Research Part A: Oceanographic Research Papers*, *38*(2), 219-241.

CHAPTER 5 ————————————

Assessment and Propagation of Uncertainties in Input Terms through an Ocean-Colour-Based Model of Primary Productivity

V

Assessment and Propagation of Uncertainties in Input Terms through an Ocean-Colour-Based Model of Primary Productivity

Svetlana Milutinović [1,2,3,*] and Laurent Bertino [1]

[1] *Nansen Environmental and Remote Sensing Center, Bergen, Norway*
[2] *Bjerknes Centre for Climate Research, Bergen, Norway*
[3] *Geophysical Institute, University of Bergen, Bergen, Norway*

Abstract Net primary productivity (NPP) fields, derived from satellite observations of ocean colour, are commonly published without relevant information on uncertainties. In this study, we assessed the uncertainty in NPP estimates of the Vertically Generalized Productivity Model using a Monte Carlo approach. We did not consider the uncertainty stemming from the basic model formulation, but restricted the uncertainty analysis to input terms, which were generated by, or related to, remote sensing. The study was based on global monthly remote sensing data from 2005. We found that the typical distribution of uncertainty around the model output could be approximated by a lognormal probability density function. On average, NPP value in a grid cell was overestimated by 6%, relative to the mean of the corresponding uncertainty distribution. The random component of uncertainty in NPP, expressed as the coefficient of variation, amounted to an average of 108%. The systematic positive errors in individual grid cells built up to an overestimate of 2.5 Pg C in the annual global NPP of 46.1 Pg C. The largest individual contributor to the random uncertainty in NPP was the input term that describes the physiological state of phytoplankton. However, the biggest contribution to the systematic uncertainty in the model output came from the parameter that represents changes in the rate of chlorophyll-normalized photosynthesis with depth. Therefore, improvements in the accuracy of these two terms would have the largest potential to decrease the input-related uncertainty in the model NPP estimates.

5.1. Introduction

Primary productivity, the biological conversion of carbon dioxide into energy-rich organic carbon compounds, is a process central to the sustainment of all life

---

* Corresponding author. Address: NERSC, Thormøhlensgate 47, 5006 Bergen, Norway; phone: +47 55 20 58 34; fax: +47 55 20 58 01; e-mail: svetlana.milutinovic@nersc.no.

on Earth. In marine ecosystems, the greatest part of organic carbon stems ultimately from the photosynthetic activity of phytoplankton, mostly unicellular organisms afloat in the sun-lit layer of the water column. Phytoplankton use only a part of the photosynthetically produced organic matter to meet their own energy requirements. The surplus of organic carbon, called net primary productivity (NPP), is available as fuel and building material to primary consumers (i.e. grazers) and, via them, to more remote consumers [*Lindeman*, 1942]. NPP is, therefore, an indispensable diagnostic of the state and development of ecosystems and biogeochemical cycles, which are intimately connected with climate processes [*Arrigo*, 2005; *Charlson et al.*, 1987; *Falkowski et al.*, 1998; *Frouin and Iacobellis*, 2002; *Montes-Hugo et al.*, 2009].

Traditionally, oceanic NPP has been measured from ships, but the duration and cost of the shipboard measurements severely restrict their geographic and temporal coverage [*Carr et al.*, 2006]. Fortunately, for more than a decade, satellite-borne ocean colour sensors have routinely provided large-scale observations of the world oceans. These instruments measure spectral characteristics of water-leaving optical signal, which are influenced by the type and concentration of seawater components that interact with light, such as phytoplankton [*Kirk*, 1994]. The properties of phytoplankton, notably chlorophyll concentration, can thus be inferred from ocean colour remote sensing [*O'Reilly et al.*, 1998] and employed in mathematical models in combination with other remotely sensed quantities, such as sea surface temperature and photosynthetically available radiation, to estimate NPP [*Behrenfeld and Falkowski*, 1997a]. NPP estimates based on remote sensing make for much more reliable quantification of spatial and temporal variability in phytoplankton productivity than would be possible by interpolating among the sporadic *in situ* measurements [*Friedrichs et al.*, 2009].

Nevertheless, model assessments of NPP derived from remote sensing observations are subject to uncertainty, just as is any other sort of measurement [*Bureau International des Poids et Mesures* (*BIPM*) *et al.*, 2009]. Uncertainty related to a measurement function, as in the case of NPP models, stems partly from imperfections in our understanding of the measured phenomenon and the approximations or simplifications employed in the function to make the measurement feasible [*Curran*, 2002]. This part of uncertainty is inherent in the models and indicates the level of success in modelling the reality. A number of studies have assessed this intrinsic uncertainty in NPP models by comparison with shipboard measurements of NPP, such as ^{14}C uptake [e.g. *Campbell et al.*, 2002; *Friedrichs et al.*, 2009; *Saba et al.*, 2010; *Saba et al.*, 2011].

Another important part of uncertainty in satellite-based estimates of NPP is the one resulting from uncertainties in model input terms. *Carr et al.* [2006] documented a range of responses to successive wide-interval perturbations of a few input terms for 24 NPP models at 11 locations in one selected month. Covering a broader spatial and temporal scope, but focusing on the sensitivity of one NPP model to perturbations of mixed layer depth (MLD) input only,

Milutinović et al. [2009] found that varying the MLD input fields, generated by different ocean models, gave rise to less than 10% difference in global annual NPP estimates, while the maximum analogous difference over two North Atlantic regions was 20–30%. However, neither of the two studies provided a measure of uncertainty in the strict sense of the term, as the perturbation bounds were chosen either arbitrarily [*Carr et al.*, 2006] or based on the range of estimates from the selected ocean models [*Milutinović et al.*, 2009]. *Friedrichs et al.* [2009] examined how input uncertainties affected NPP estimates from 21 models in the tropical Pacific during a multiyear period, by perturbing input variables with simple addition or subtraction of a given assumed typical uncertainty value. They found that uncertainties in all input values and *in situ* NPP data together explained more than a half of the mismatch between the model estimates and field observations. Similarly, using a comparable methodology and the same number of models in 10 ocean regions around the world, *Saba et al.* [2011] found that 50% of the model-observation disagreement was due to the simultaneous effect of input uncertainties. While each of these studies showed that uncertainties in input variables contributed considerably to NPP model uncertainties, they did not provide information on what probability distribution or level of confidence the uncertainty bounds were related to, nor did they distinguish between different components of uncertainty (e.g. systematic and random).

In this study, we propagated input uncertainties through the Vertically Generalized Productivity Model (VGPM) of *Behrenfeld and Falkowski* [1997b], one of the most widely used oceanic NPP models [*Friedrichs et al.*, 2009]. We associated each of the input terms in the VGPM with a particular uncertainty, either by performing comparisons with reference data sets or using already published evaluations. The input uncertainties were represented by probability distributions and propagated through the VGPM using a Monte Carlo method [*BIPM et al.*, 2008a], i.e. random values were repeatedly drawn from the input distributions and introduced into the VGPM, yielding an output frequency distribution that described the uncertainty in the modelled NPP. Our approach distinguished between bias and uncertainty related to natural variability. We quantified not only the simultaneous impact of all input uncertainties, but also evaluated individual uncertainty contributions. This enabled identification of those steps in the NPP estimation that, if improved, have the largest potential to reduce the overall output uncertainty.

5.2. Primary Productivity Model and Input Data

The Vertically Generalized Productivity Model (VGPM) [*Behrenfeld and Falkowski*, 1997b] computes integral water-column net primary productivity (NPP [mg C m^{-2} d^{-1}]) as the product of surface phytoplankton chlorophyll concentration (Chl [mg Chl m^{-3}]), depth of the euphotic layer (Z_{eu} [m]), daylength (DL [h]), maximum chlorophyll-specific carbon fixation rate in a

111

water column (P^{b}_{opt} [mg C (mg Chl)$^{-1}$ h^{-1}]) and a parameter representing relative vertical profile of photosynthesis (F; unitless):

$$\mathrm{NPP} = \mathrm{Chl} \times Z_{eu} \times \mathrm{DL} \times P^{b}_{opt} \times F. \tag{5.1}$$

In this study, all input quantities to the VGPM, except daylength, were produced by, or related to, satellite remote sensing. We used three types of coincident global monthly Level-3 binned data products from 2005, provided by the NASA Ocean Biology Processing Group (http://oceancolor.gsfc.nasa.gov), namely Chl, photosynthetically available radiation at the sea surface (PAR [mol photons m^{-2} d^{-1}]) and daytime sea surface temperature (SST [°C]). The choice of the temporal coverage is explained in Section 5.5. Chl and PAR were generated in the reprocessing 5.1 of observations from the Sea-viewing Wide Field-of-view Sensor (SeaWiFS). SST resulted from the reprocessing 1.1 of the data set acquired by the Moderate Resolution Imaging Spectroradiometer (MODIS) aboard the Aqua platform. MODIS SST fields were originally provided at twice the longitude and latitude resolution of SeaWiFS Chl and PAR fields, and were thus subsampled to fit the SeaWiFS equal-area grid with the bin size of about 9.28 km × 9.28 km. We did not apply correction for missing data to avoid introducing additional biases to the input fields.

Besides being a direct input variable for the VGPM, Chl was also used to determine Z_{eu}, based on a two-step procedure originally developed by *Morel and Berthon* [1989]. First, total chlorophyll content within the productive water column (Chl$_{tot}$) was determined as

$$\mathrm{Chl}_{tot} = 40.6 \times \mathrm{Chl}^{0.459}. \tag{5.2}$$

Secondly, Z_{eu} was calculated from Chl$_{tot}$. The latter step was revised by *Morel and Maritorena* [2001] and hence we used their fourth-order polynomial that relates common logarithms of Z_{eu} and Chl$_{tot}$:

$$\begin{aligned} \log_{10}(Z_{eu}) = {} & 2.1236 + 0.932468\log_{10}(\mathrm{Chl}_{tot}) - 1.4264[\log_{10}(\mathrm{Chl}_{tot})]^2 \\ & + 0.52776[\log_{10}(\mathrm{Chl}_{tot})]^3 - 0.07617[\log_{10}(\mathrm{Chl}_{tot})]^4 \end{aligned} \tag{5.3}$$

This polynomial is reliable when it yields Z_{eu} between 5 m and 180 m [*Morel and Maritorena*, 2001]. Thus, in a few cases when Z_{eu} values were not in that range, they were excluded from further calculations. Inference of Z_{eu} from Chl is compromised when other optically active seawater components (coloured dissolved organic matter and suspended particles) cannot be functionally related to Chl, i.e. when Case-1 assumption does not hold [*Lee et al.*, 2007]. As a simple way for omitting Case-2 waters, we disregarded regions shallower than

200 m (continental shelf). The implications of omitting these regions are addressed in Section 5.5.

Daylength was computed as a function of latitude and day number [*Kirk*, *1994*]. It was adjusted to the temporal resolution of the rest of the input fields by finding the mean daylength value for a particular bin (i.e. grid cell) in a given month.

SST was employed in an empirically derived seventh-order polynomial function [*Behrenfeld and Falkowski*, 1997b] to compute P^b_{opt}:

$$P^b_{opt} = 1.2956 + 0.2749 SST + 0.0617 SST^2 - 0.0205 SST^3$$

$$+2.462 \times 10^{-3} SST^4 - 1.348 \times 10^{-4} SST^5 + 3.4132 \times 10^{-6} SST^6 \qquad (5.4)$$

$$-3.27 \times 10^{-8} SST^7.$$

This function is valid in the SST range from $-1°C$ to $28.5°C$. For $SST < -1°C$, it is prescribed that $P^b_{opt} = 1.13$ mg C (mg Chl)$^{-1}$ h^{-1}, while for $SST > 28.5°C$ the P^b_{opt} value of 4.00 mg C (mg Chl)$^{-1}$ h^{-1} is specified.

Daily downward surface irradiance in the photosynthetic waveband (400–700 nm), or PAR, was required as input to the function accounting for relative changes in photosynthetic rates due to the vertical decline of light [*Behrenfeld and Falkowski*, 1997b]:

$$F = \frac{0.66125 \times PAR}{PAR + 4.1}. \qquad (5.5)$$

Uncertainty associated with the output of a model can be evaluated by finding theoretical probability distributions that best describe contributing uncertainties in input quantities and propagating those distributions through the model [*BIPM et al.*, 2009]. In the next two sections, we present the assignment of the input uncertainty distributions and their propagation through the VGPM by a Monte Carlo approach.

5.3. Evaluation of Uncertainties in Input Quantities

There is more than one way to classify the uncertainty of a measurement (or a model estimate). For example, we can distinguish between an uncertainty component stemming from model imperfection and a component originating from an inexact knowledge of input values. Although the VGPM, as any other model, is not perfect (e.g. it rests on a simplistic assumption of a vertical homogeneity of chlorophyll concentration), for the purpose of this study we assumed that the VGPM itself was flawless, and that uncertainties in the model input were the only source of uncertainty in the output. We distinguished between two components of the input uncertainty, one describing a tendency to

make estimates of a given variable consistently too high or too low (known as bias), and the other related to success (or lack thereof) in reproducing natural variability.

We quantified both portions of uncertainty, associated with an estimate of a particular quantity derived from a given functional relationship, using simultaneous co-located *in situ* observations of the same quantity as reference values. To that end, we determined discrepancy (δ) between a model result and the coincident reference value, assembled all individual discrepancies and found their frequency distribution, which we regarded as the uncertainty distribution. Its mean represented the bias (*B*), while its standard deviation served as a measure of the remaining uncertainty component. The latter statistic is equivalent to the centred-pattern (or zero-centred) root mean square difference (see the work of *Taylor* [2001] and Equation 2 therein), which we denote by $RMSD_0$. A detailed explanation of this methodological approach with accompanying notation and equations can be found in Appendix A.

5.3.1. Uncertainty in Estimates of Chl

An approach similar to that described above has already been used by *Gregg et al.* [2009] to evaluate the uncertainty of a standard SeaWiFS Chl product. In this study, we used weighted uncertainty statistics that they reported for the open ocean, since the methodology of acquiring Z_{eu} estimates limited our study to Case-1 waters. As Chl values tend to be lognormally distributed [*Campbell*, 1995], normal probability density function is a suitable model for frequency distribution of $\delta^{LOG}(Chl)$ (definitions of δ^{LOG} and the corresponding statistics are given in Appendix A). We therefore worked with the Chl uncertainty statistics that *Gregg et al.* [2009, Figure 6] expressed on $\log_{10}$ scale: bias ($B^{LOG}(Chl)$) of 0.077 and root mean square $\log_{10}$ difference ($RMSD^{LOG}(Chl)$) of 0.249. From $RMSD^{LOG}(Chl)$, we computed $RMSD_0^{LOG}(Chl)$ as $\sqrt{[RMSD^{LOG}(Chl)]^2 - [B^{LOG}(Chl)]^2}$, which is 0.237.

5.3.2. Uncertainty in Estimates of Z_{eu} and DL

A preliminary analysis (presented in thesis Chapter 6) of uncertainty associated with the basic skill of the Z_{eu} model (Equations (5.2) and (5.3)) yielded $B^{REL}(Z_{eu})$ of 9% and $RMSD_0^{REL}(Z_{eu})$ of 22% (the reason for choosing the relative scale – denoted by the superscript 'REL' and defined in Appendix A – to express the Z_{eu} uncertainty was a good fit of the underlying frequency distribution to normality). When subsequently compared to uncertainties in the remaining input terms, these values were found to be relatively small. Thus, to simplify the Monte Carlo simulations and the following analysis of results, we regarded the Z_{eu} model as entirely accurate and only considered that part of Z_{eu} uncertainty which was implied in Chl uncertainty.
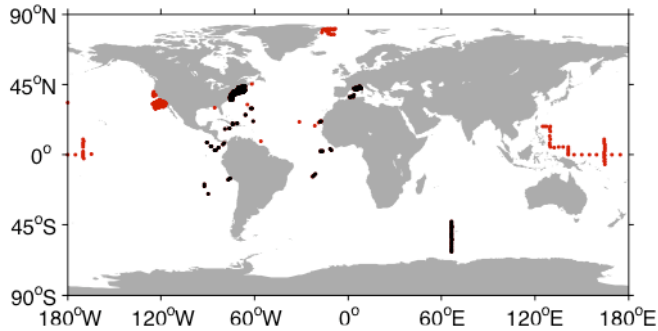
Figure 5.1. Locations of the *in situ* data used to determine the respective predictive uncertainties of the P^b_{opt} model (both black and red dots) and the function of PAR (black dots only).

In comparison to other input data, daylength estimates were deemed to have sufficiently high accuracy for this kind of application and were therefore treated as having no uncertainty.

5.3.3. Uncertainty in Estimates of P^b_{opt}

To estimate uncertainty of P^b_{opt} (Equation (5.4)), we applied the already described statistical approach (see also Appendix A) using field data available at http://www.science.oregonstate.edu/ocean.productivity/field.data.c14.online.php. More particularly, *in situ* measured SST was introduced into Equation (5.4) and the outcome was compared with measurements of P^b_{opt}, which served as reference values. Field estimates of $P^b_{opt} > 20$ mg C (mg Chl)$^{-1}$ h^{-1} were disregarded, since, due to physiological limitations of photosynthesis, values higher than that are rarely achievable [*Behrenfeld et al.*, 2002a] and might be an artefact caused by erroneous Chl data [*Behrenfeld and Falkowski*, 1997b]. Thereafter, 1823 simultaneous field measurements of P^b_{opt} and SST remained. A map in Figure 5.1 shows geographical distribution of the measurement stations.

Although the focus of this section is on the performance of the P^b_{opt} model by *Behrenfeld and Falkowski* [1997b] (see Equation (5.4)), we also provide a brief comparison with three other models that relate P^b_{opt} to temperature, which were respectively published by *Megard* [1972], *Balch et al.* [1992] and *Antoine et al.* [1996]. The last-mentioned model is a transform of *Eppley*'s [1972] expression for maximum phytoplankton growth rates. The corresponding equations can be found in the work of *Behrenfeld and Falkowski* [1997a, p. 1489].

Estimates of P^b_{opt} from Equation (5.4) are compared with reference P^b_{opt} values in Figures 5.2 and 5.3. Frequency distributions of the two sets of values are markedly different (Figure 5.2). The scattering of points around the line of

115
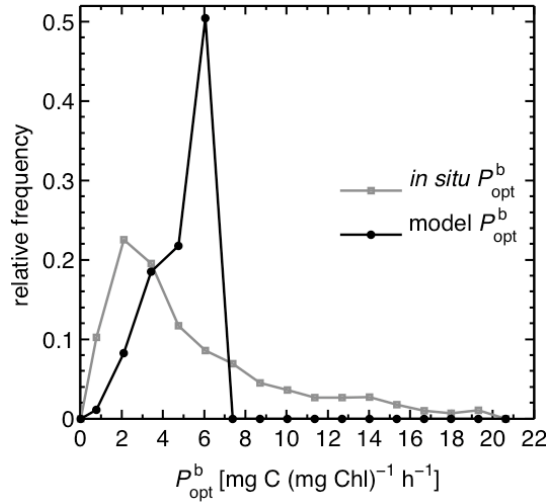
Figure 5.2. Relative frequency polygons for observations and model estimates (from Equation (5.4)) of maximum Chl-normalized carbon fixation rate in a vertical profile (P^b_{opt}). The highest possible model P^b_{opt} (6.63 mg C (mg Chl)$^{-1}$ h^{-1}) is relatively low, compared to the *in situ* data, because Equation (5.4) was constructed as a fit to the median values of otherwise highly dispersed training data set (see Figure 7 in the work of *Behrenfeld and Falkowski* [1997b]).

perfect agreement in Figure 5.3 is considerable, especially for the upper half of the model P^b_{opt} range. Correlation coefficient of 0.29 is slightly above that reported by *Behrenfeld and Falkowski* [1997a] ($r = 0.24$, $n = 1041$) and even higher than what *Behrenfeld et al.* [2002a] found using an appreciably smaller data set ($r = 0.1$; $n = 199$). In the latter study, the P^b_{opt} model of *Behrenfeld and Falkowski* [1997b] performed less well than the three remaining temperature-dependent functions, but in our analysis it was the best performing model. Nevertheless, our results agreed with the finding of *Behrenfeld et al.* [2002b] that none of the four P^b_{opt} models could explain more than 9% of variability in observations (the respective correlation coefficients for the P^b_{opt} models of *Megard* [1972], *Balch et al.* [1992] and *Antoine et al.* [1996] were 0.21, −0.26 and 0.14). Such poor predictive capabilities indicate that temperature alone is not enough to achieve adequate P^b_{opt} estimates [*Behrenfeld et al.*, 2002b]. This issue is discussed in Section 5.5.

To evaluate the P^b_{opt} model of *Behrenfeld and Falkowski* [1997b], we determined $\delta^{REL}(P^b_{opt})$ as shown by Equation (A5.2) in Appendix A. Mean, median, standard deviation and semi-interquartile range of $\delta^{REL}(P^b_{opt})$ were 0.69 (69%), 0.13 (13%), 2.23 (223%) and 0.58 (58%), respectively. Regional weighting of these statistics would be preferable, because data stations were
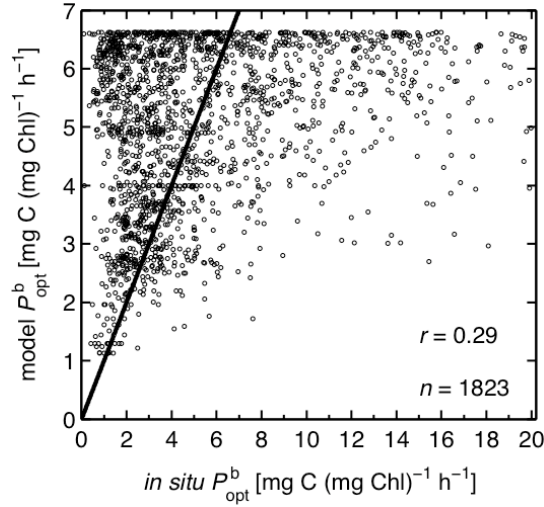
Figure 5.3. Estimates of maximum Chl-specific carbon fixation rate in a water column (P^b_{opt}) from the temperature-dependent function of *Behrenfeld and Falkowski* [1997b], compared with observations. The line indicates one-to-one relationship between the model and reference values. Correlation coefficient (r) and the number of data points (n) are included.

neither selected randomly, nor was the sampling uniform and sufficiently dense to be regarded as globally representative (see Figure 5.1). However, while there were two large clusters of data points in the north-western Atlantic (849 observations) and the north-eastern Pacific (633 observations), considerably fewer data were available in the rest of the ocean (341 observations). The inhomogeneity of the spatial distribution is reflected in a particularly poor coverage in certain classes of SST by the rest-of-the-ocean subset of data (Figure S5.1, Appendix B). Hence, a meaningful partition into oceanic regions, which would result in reliable regionally weighted statistics, was not possible.

The frequency distribution of $\delta^{REL}(P^b_{opt})$ is strongly skewed to the right (Figure S5.2, Appendix B). Following recommendation of *Sokal and Rohlf* [1995], we made it more symmetrical by logarithmic transformation, using Equation (A5.3) (Appendix A). Besides simplifying the simulation of uncertainty, this ensured that no negative (i.e. physically impossible) values were obtained after transforming logarithms back to linear scale, prior to uncertainty propagation. Frequency distribution of $\delta^{LOG}(P^b_{opt})$ resembles a normal distribution (shown by thick full black line in Figure 5.4) with mean (i.e. $B^{LOG}(P^b_{opt})$) 0.08 and standard deviation (i.e. $RMSD_0^{LOG}(P^b_{opt})$) 0.33. A graphical test of normality (Figure S5.3, Appendix B) confirmed that the distribution of $\log_{10}$ uncertainties in P^b_{opt} resulting from Equation (5.4) could be
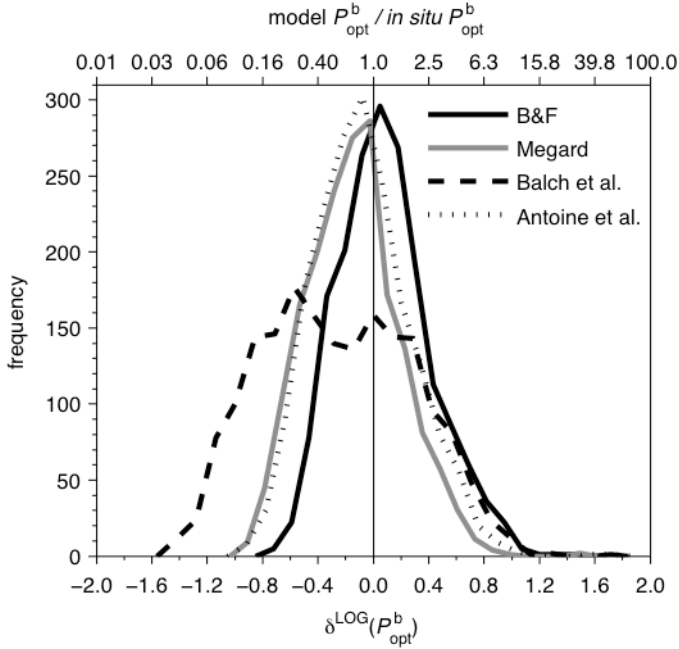
Figure 5.4. Frequency distributions of difference between common logarithms of model estimates and matching observed values of P^b_{opt} ($\delta^{LOG}(P^b_{opt})$) for the models of (a) *Behrenfeld and Falkowski* [1997b] (mean = 0.08, standard deviation = 0.33), (b) *Megard* [1972] (mean = –0.14, standard deviation = 0.34), (c) *Balch et al.* [1992] (mean = –0.26, standard deviation = 0.54) and (d) *Antoine et al.* [1996] (mean = –0.08, standard deviation = 0.35). For easier interpretation, $\log_{10}$ values (presented at the bottom of the figure) are accompanied by the corresponding antilogarithms (at the top).

reasonably well approximated by the normal distribution having the same mean and standard deviation.

For comparative purposes, we determined uncertainties associated with P^b_{opt} estimates from the rest of temperature-dependent functions, too. Their respective $\delta^{REL}(P^b_{opt})$ frequency distributions were also positively skewed. We thus performed the logarithmic transformation, which yielded more symmetrical distributions, displayed in Figure 5.4. As opposed to what was found for the P^b_{opt} model of *Behrenfeld and Falkowski* [1997b], the results for these three functions indicate negative bias. Absolute values of $B^{LOG}(P^b_{opt})$ and $RMSD_0^{LOG}(P^b_{opt})$ for the models of *Megard* [1972] and *Antoine et al.* [1996] are comparable to those for Equation (5.4), but those for the model of *Balch et al.* [1992] are substantially larger (Figure 5.4). The above-mentioned graphical test supported the assumption of normality for the uncertainty distributions

associated with the equations of *Megard* [1972] and *Antoine et al.* [1996]. However, we found that such an assumption would be less sound for the equation of *Balch et al.* [1992], due to pronounced platykurtosis.

5.3.4. Uncertainty in Estimates of F

The irradiance-dependent function devised by *Behrenfeld and Falkowski* [1997b] (Equation (5.5)) was evaluated using the statistical procedure described at the beginning of Section 5.3 (see also Appendix A). The role of this function is linked to the fact that the VGPM belongs to the simplest category in the classification system of *Behrenfeld and Falkowski* [1997a], that of the depth-integrated models (DIMs). As their name suggests, DIMs cannot explicitly resolve changes in the rate of photosynthesis with depth, which are, to a large extent, governed by the vertical attenuation of irradiance [*Behrenfeld et al.*, 2002b]. The depth-dependent variability in photosynthesis thus has to be represented in a DIM by the parameter *F*. To grasp its meaning, we may consider a strictly hypothetical situation of irradiance not being attenuated with depth, but remaining at a photosynthetically saturating level for the largest part of the day throughout the entire euphotic zone. In such a case, primary productivity normalized to the phytoplankton chlorophyll content 'b' at any given depth in the euphotic layer (P^b [mg C (mg Chl)$^{-1}$ h^{-1}]) would be identical to P^b_{opt}, i.e. the maximum P^b value achievable for the particular irradiance under prevailing nutrient and temperature conditions. In reality, however, light does diminish with depth and so only a portion of the hypothetical maximum integral water-column chlorophyll-normalized productivity is realized. *F* represents the dimensionless ratio of the actual integral chlorophyll-specific productivity to that hypothetical maximum. It can be modelled as a function of surface irradiance, such as that given by Equation (5.5).

We assessed the uncertainty associated with this function by using 973 *in situ* measurements of PAR from the afore-mentioned online database, together with accompanying reference estimates of *F* (REF(*F*)) (Figure 5.1). REF(*F*) values were based on field estimates of P^b at a number of depths within the upper water column. To avoid potential errors due to extrapolation, only those P^b data spanning the entire euphotic zone were considered. Also, the batches of P^b estimates containing $P^b_{opt} > 20$ mg C (mg Chl)$^{-1}$ h^{-1} were omitted for the reason already stated. It must be emphasized that a considerable number of the data employed here, as well as in the uncertainty analysis of P^b_{opt}, had been used to devise the VGPM.

To determine REF(*F*), we estimated a vertical profile of P^b by interpolating between the P^b values measured at discrete depths in the productive layer of the water column (Figure S5.4, Appendix B). Subsequently, the integral value (IP^b) was found for the vertical profile of P^b on the interval of optical depths (ζ) between zero and 4.6 (which is equivalent to the euphotic zone):
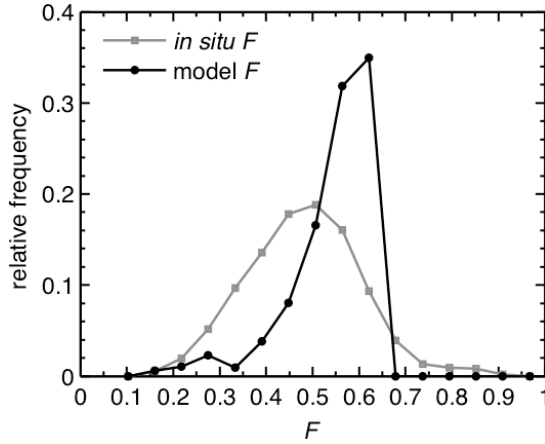
Figure 5.5. Relative frequency polygons of reference values and model estimates of F derived from Equation (5.5).

$$\mathrm{IP}^{\mathrm{b}} = \int_{\zeta=0}^{4.6} P^{\mathrm{b}} \mathrm{d}\zeta .$$

(5.6)

Finally, REF(F) was calculated as:

$$\mathrm{REF}(F) = \frac{\mathrm{IP}^{\mathrm{b}}}{P_{\mathrm{opt}}^{\mathrm{b}} \times 4.6} .$$

(5.7)

Figures 5.5 and 5.6 illustrate how values resulting from the irradiance-dependent function of *Behrenfeld and Falkowski* [1997b] (see Equation (5.5)) relate to coincident reference values of the parameter F. The reference data seem to follow a normal distribution, but the frequency distribution of the model results is skewed to the left (Figure 5.5). The relatively modest linear correlation ($r = 0.37$; see Figure 5.6) may partly be due to the effect of methodological inconsistencies among the *in situ* data (such as variable sample incubation periods and different techniques for measuring chlorophyll [*Behrenfeld and Falkowski*, 1997b]) on the reference values derived from them.

While many of the published functions that estimate F exhibit a similar shape, their discrepancies stem from choosing whether or not to take into account losses in productivity due to photoinhibition and, to a smaller degree, from the assumed kinetics of photosynthesis at subsaturating light intensities (see the work of *Behrenfeld and Falkowski* [1997a] and Figure 2 therein). For reasons of comparison, we selected another irradiance-dependent function, that of *Talling* [1957], as an alternative to the function presented by Equation (5.5).
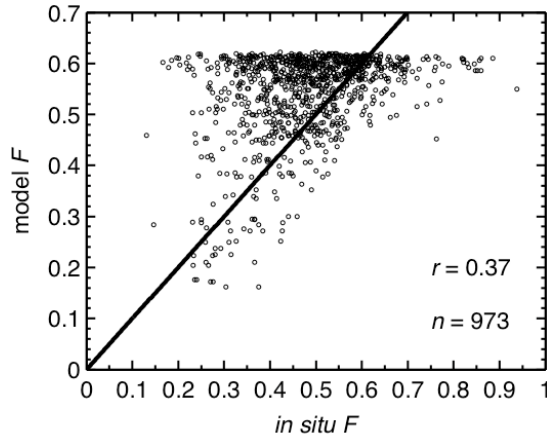
Figure 5.6. Estimates of *F* yielded from Equation (5.5), plotted against reference values. The line denotes perfect agreement between the two groups of values. Coefficient of linear correlation (*r*) and the number of data points (*n*) are inserted.

The performance of *Talling*'s [1957] empirically derived function can also indicate the capabilities of the equivalent function of *Platt and Sathyendranath* [1993], who found the former was the best approximation to their analytical approach. Following the reformulation of *Talling*'s [1957] depth-integrated productivity model by *Behrenfeld and Falkowski* [1997a], we arrived at this expression:

$$F = 0.22 \times \ln\left(\frac{PAR}{0.046 \times PAR + 0.68}\right) + 0.15,$$
(5.8)

which generates realistic, non-negative results for PAR $\geq$ ~0.4 mol photons m^{-2} d^{-1}.

We do not show a scatterplot of the output of Equation (5.8) against matching reference values, because its shape was not distinguishable from that in Figure 5.6, which was reflected in the same magnitude of linear correlation (*r* = 0.37). However, compared with Figure 5.6, the cloud of points related to Equation (5.8) appeared geometrically translated by a distance of ~ +0.15, whereby an overwhelming majority of the points moved above the one-to-one line. This result suggests that Equation (5.8) is much more prone to overestimation than Equation (5.5). That is possibly because the former, unlike the latter, assumes no photoinhibition.

We quantified uncertainties in the outcome of the two irradiance-dependent functions by determining δ(*F*), as described by Equation (A5.1) in Appendix A

121

(the reason for using $\delta(F)$ rather than $\delta^{REL}(F)$ or $\delta^{LOG}(F)$ lies in a good compliance of the underlying frequency distribution with normality, as shown below). Note that the absolute uncertainties presented here have no units, because F is a dimensionless quantity. Frequency distribution of $\delta(F)$ for Equation (5.5) appears normal, indicates a positive bias ($B(F) = 0.06$) and $RMSD_0(F)$ of 0.12 (Figure 5.7). In comparison, frequency distribution of $\delta(F)$ related to Equation (5.8) had a very similar shape and identical standard deviation (i.e. $RMSD_0$), but a larger positive bias (0.22). Normal probability plot in Figure S5.5 (Appendix B) confirms that the normal distribution with mean equal to $B(F)$ and standard deviation equal to $RMSD_0(F)$ is a suitable model of the uncertainty distribution for Equation (5.5). Analogous assumption holds for Equation (5.8).

Due to the uneven and very sparse *in situ* data coverage (see Figure 5.1), weighting of the statistics that describe the uncertainty in model estimates of F would be desirable. This requires dense global observations of F values from which population benchmarks could be derived. Such observations, however, are not available. Therefore, we decided to use the unweighted uncertainty statistics in further work.

5.4. Propagation of Uncertainties through the VGPM

5.4.1. Monte Carlo Approach

A variety of approaches can be taken to propagate uncertainties through a model [*BIPM et al.*, 2009]. Among them, Monte Carlo method has the widest domain of validity [*BIPM et al.*, 2008a]. The core of the method is random sampling from uncertainty distributions previously assigned to the input quantities. The model calculations are repeated a number of times with each set of the random input values, to obtain uncertainty distribution for the output quantity.

The quality (i.e. statistical precision) of results obtained from the Monte Carlo method increases with the number of randomly drawn values [*BIPM et al.*, 2008a], because the shape of the underlying probability density function gets increasingly better approximated. To achieve a compromise between sufficient quality and required computer processing time, we used 1500 realizations.

In any given bin (i.e. grid cell), bias was subtracted from the nominal value of each input quantity. This enabled us to quantify bias in nominal NPP, at a later stage. The remaining uncertainty (due to random effects) was simulated as a frequency distribution of 1500 random values that followed the earlier identified normal probability distribution, having mean equal to the bias-corrected nominal value and standard deviation equal to the zero-centred RMSD. When the results of uncertainty analysis led us to assume normal
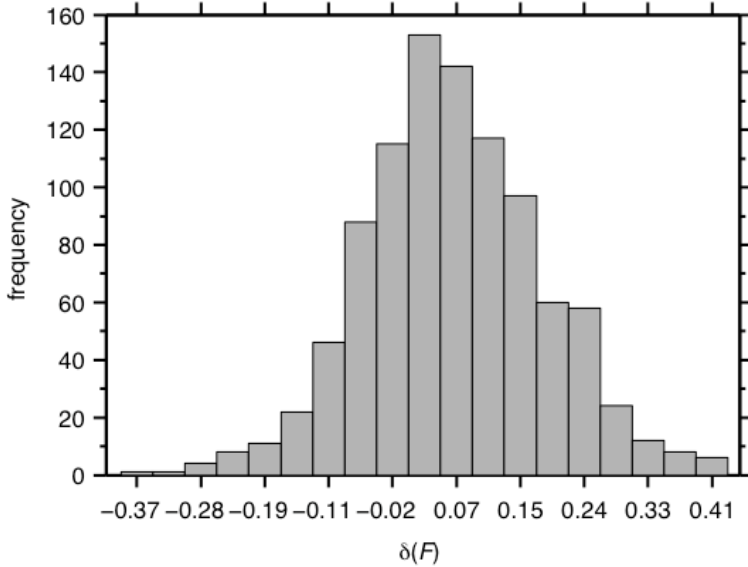
Figure 5.7. Histogram of discrepancies between model estimates from Equation (5.5) and matching reference values of F ($\delta(F)$).

uncertainty distribution on $\log_{10}$ scale (as was done for Chl and P^b_{opt} – see Sections 5.3.1 and 5.3.3), common logarithm of the nominal value was the simulation starting point. In this case, simulated frequency distribution had to be transformed to the original, linear scale by finding antilogarithms. Assuming normal uncertainty distribution on the linear scale, which was the case for F (see Section 5.3.4), meant that negative values could arise in the simulation. Being physically impossible, those values were discarded, but such occasions were rare, taking place only at high latitudes in winter hemisphere, where light availability was very limited. Even then, the number of acceptable values hardly ever fell below 1425 (i.e. 95% of the initial number of items). Also, unrealistically high values of F (>1) could be yielded in the simulation only very infrequently. Thus, while we made all such values equal one, it had a negligible impact on the consequent frequency distribution. Similarly, the limited validity of the polynomial by *Morel and Maritorena* [2001] (Equation (5.3)) was accommodated by removing unreliable Z_{eu} values (<5 m or >180 m). Only a small minority of all bins that contained data had >5% of Z_{eu} values rejected. Most of those bins were in the South Pacific subtropical gyre. As daylength was assumed to carry no uncertainty, its nominal value was reused in each model rerun. For each individual set of randomly generated input values, NPP was computed by the VGPM, resulting in an ensemble of up to 1500 NPP values in every bin. Their frequency distribution represented the uncertainty

Table 5.1. Summary of uncertainties in input quantities that were propagated through the VGPM[a]

Input quantity	Scale	Component of input uncertainty	
		Bias	*Zero-centred RMSD*
Chl	logarithmic	0.077	0.237
P^b_{opt}	logarithmic	0.08	0.33
F	linear	0.06	0.12

[a]Section 5.3 and Appendix A contain the relevant definitions and describe the methodology used to quantify the bias and the zero-centred RMSD. Note that uncertainties in F, although expressed on the linear scale, have no units because F is a dimensionless quantity.

associated with the nominal NPP value in the same bin. Because rejection of a large portion of invalid items from a frequency distribution can be misleading, as it can greatly affect descriptive statistics, the bins where <1425 (i.e. <95%) values remained after the rejection were omitted from the analysis. Of the entire 2005 collection of bins (not counting in the bins over land, shelf and cloudy areas), 1.4% was disregarded. A summary of this method is presented using mathematical notation in Appendix C.

5.4.2. Uncertainty in NPP Estimates by the VGPM

Table 5.1 presents a summary of uncertainties in input terms, namely Chl, P^b_{opt} (Equation (5.4)) and F (Equation (5.5)). The simultaneous propagation of these uncertainties through the VGPM resulted in a frequency distribution that represented uncertainty in the model NPP estimate in any given bin in a given month. The properties of the distribution in a particular bin were summarized using the mean, the coefficient of variation (i.e. the standard deviation stated as percentage of the mean), skewness (g_1) and kurtosis (g_2). The coefficient of variation, g_1 and g_2 were determined as explained by *Sokal and Rohlf* [1995, see their Equation (4.8) and Box 6.2, respectively]. The statistics were mapped and juxtaposed with the corresponding maps of NPP estimates, which were obtained by driving the VGPM with nominal values of input quantities (i.e. the input values that were not corrected for bias).

   Figures 5.8a–5.8b show maps of NPP for January and July 2005, illustrating typical findings for boreal winter/austral summer and boreal summer/austral winter, respectively. In broad terms, both months were characterized by high NPP in the coastal upwelling regions at the eastern boundaries of the Pacific and Atlantic Oceans and in the Arabian Sea, while low NPP persisted in the subtropical gyres of all ocean basins. In contrast, the largest seasonal amplitude was observed between winter NPP minima and summer NPP maxima at temperate and subpolar latitudes in both hemispheres.
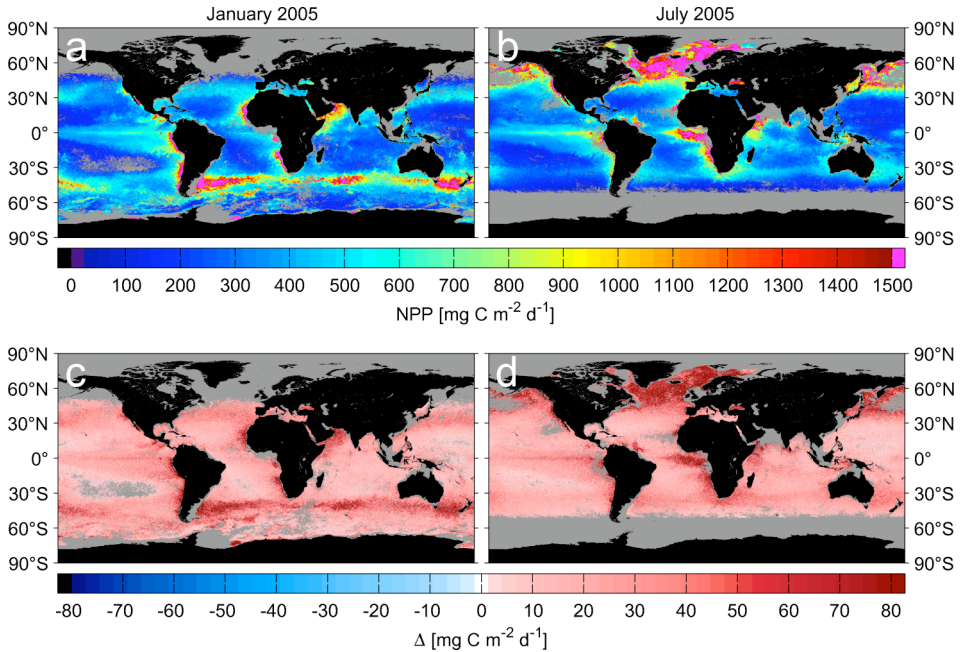
Figure 5.8. Top: Net primary productivity (NPP [mg C m^{-2} d^{-1}]) estimated using the Vertically Generalized Productivity Model (VGPM) for (a) January and (b) July 2005. Bottom: Difference between nominal NPP values (presented above in (a) and (b), respectively) and the mean values of corresponding NPP uncertainty distributions (Δ [mg C m^{-2} d^{-1}]) for (c) January and (d) July 2005. Note that the nominal NPP values were computed from input data that had not been corrected for bias, while the uncertainty distributions were simulated using bias-corrected input. Grey colour represents locations with no available remote sensing observations, continental shelf (<200 m) and bins with unreliable statistics.

The NPP uncertainty distributions in every bin and month were skewed to the right (annual average g_1 = 4) and leptokurtic (annual average g_2 = 32), i.e. they had lognormal-like shape. We do not present the maps of g_1 and g_2 here, because they had a uniform appearance across the global ocean throughout the year.

Although it may be argued that the mean is not a robust statistic of location for skewed distributions, we use it because it incorporates the influence of large errors that would not be accounted for by other estimators of central tendency. Furthermore, the mean is a logical complement to the standard deviation, which is commonly used to describe dispersion of errors [*BIPM et al.*, 2008b; *Taylor*, 1997].
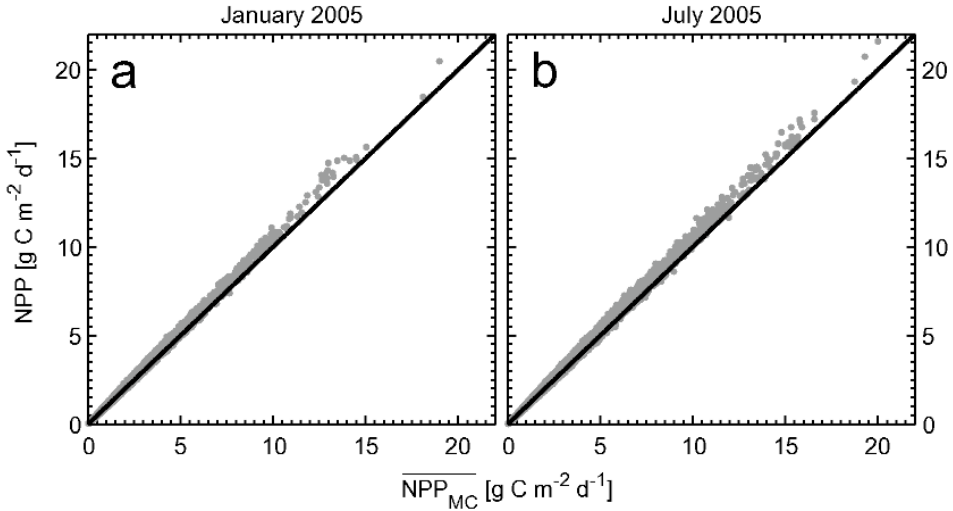
Figure 5.9. Nominal NPP [g C m^{-2} d^{-1}] plotted against the mean of associated NPP uncertainty distribution [g C m^{-2} d^{-1}] in (a) January and (b) July 2005 (grey dots). The black line in each scatterplot represents perfect agreement between the two sets of values.

When maps of the mean values for uncertainty distributions of NPP (hereafter labelled $\overline{NPP}_{MC}$, where MC signifies the Monte Carlo method) were generated, they were visually indistinguishable from the corresponding maps of NPP (Figures 5.8a–5.8b). To establish whether the two quantities differed at all and, if so, to what extent, we mapped the difference between NPP and the associated $\overline{NPP}_{MC}$ (Δ [mg C m^{-2} d^{-1}]) (Figures 5.8c–5.8d). Note that NPP was calculated from input values that were not corrected for bias, whereas $\overline{NPP}_{MC}$ represents the value that NPP would adopt if there were no bias in the input quantities, because Chl, P^{b}_{opt} and F had been corrected for bias before the Monte Carlo simulations were carried out. In other words, NPP incorporates the effects of bias in input quantities, whereas $\overline{NPP}_{MC}$ does not. Therefore, the sign and magnitude of Δ indicate by how much, if at all, NPP is over- or underestimated. Figures 5.8c–5.8d suggest that, overall, NPP is overestimated and the magnitude of this generally positive bias in NPP is proportional to NPP itself (see Figures 5.8a–5.8b). Underestimates occurred too, but just sporadically, which can only be spotted when the maps of Δ are magnified to the extent that makes the individual pixels clearly distinguishable. Figures 5.9a–5.9b present scatterplots of NPP against the matching $\overline{NPP}_{MC}$ values in the two representative months. To complement the information contained in Figures 5.8a–5.8d and 5.9a–5.9b, we expressed the bias in NPP estimates as percentage

of $\overline{\text{NPP}_{\text{MC}}}$, i.e. we divided the values of Δ by the related values of $\overline{\text{NPP}_{\text{MC}}}$ and multiplied the resulting quotient by 100. Not only in January and July, but in other months too, the bulk of percentage bias values spanned between $\sim -3\%$ and $\sim +15\%$. Maps of the percentage bias look mostly invariant in time and space (Figures S5.6a–S5.6b, Appendix B). High values of the percentage bias were somewhat more frequent at the weakly illuminated high latitudes in winter, because the bias of F in the Monte Carlo simulations was held fixed, rather than proportional to a given F value, and was thus relatively large for low F, which coincided with low irradiance. Because this situation was rare and occurred only where NPP was extremely low, its effect on the conclusions of the analysis is negligible. The average percentage bias in any given month was ~6%, which, after spatial and temporal integration, compounded to an overestimate of 2.5 Pg C in the global annual NPP of 46.1 Pg C (Pg = petagram = 10^{15} grams) for 2005. It should not be forgotten that cloudy areas, shelf regions and bins with unreliable statistics did not contribute to this figure. The average percentage bias would be larger if defined relative to a more robust statistic of central tendency, rather than the mean. We found that replacing the mean by the median of the NPP uncertainty distributions in this sense yielded, on average, a nearly 10 times larger percentage bias. However, we regard the mean (i.e. $\overline{\text{NPP}_{\text{MC}}}$) as a more appropriate statistic in this context because, beside representing the most frequent values in NPP uncertainty distributions, it takes into account those that are less frequent but important nevertheless.

Since the standard deviation for uncertainty distributions of NPP varied in proportion to the mean, it is more informative and convenient to present the random uncertainty of NPP estimates in relative terms, i.e. by the coefficient of variation (CV). In any month of 2005, the vast majority of the CV values spanned between ~90% and ~125%, yielding an annual average of 108%. Maps of the CV showed little geographic and temporal variability and are thus not displayed here.

As the mean (i.e. $\overline{\text{NPP}_{\text{MC}}}$) and standard deviation of NPP uncertainty distributions (i.e. random uncertainty of NPP, RU(NPP)) were linearly related to the nominal NPP (Figures S5.7 and S5.8, Appendix B), we used the least-squares linear regression to devise equations that describe the observed relationships:

$$\overline{\text{NPP}_{\text{MC}}} = -1.67 \times 10^{-3} \text{ g C m}^{-2} \text{ d}^{-1} + 0.95 \times \text{NPP}; \tag{5.9}$$

$$\text{RU(NPP)} = 6.01 \times 10^{-3} \text{ g C m}^{-2} \text{ d}^{-1} + \text{NPP}. \tag{5.10}$$

These equations may enable approximate but fast evaluations of bias and random uncertainty in the VGPM NPP estimates derived from remote sensing. However,

Table 5.2. Overall and individual contributions of uncertainties in input quantities to the uncertainty in NPP, expressed as global annual averages for 2005[a]

Input quantity	Component of NPP uncertainty	
	Total percentage bias	*Total coefficient of variation*
All	6%	108%
	Partial percentage bias	*Partial coefficient of variation*
Chl	3%	59%
Chl×Z_{eu}	6%	37%
P^b_{opt}	−10%	90%
F	12%	23%

[a]The component of uncertainty due to systematic effects is represented as percentage bias, while coefficient of variation represents the uncertainty component originating from random effects. Explanation on how these components were determined is given in the text (Section 5.4.2).

we advise some caution related to this, because the limitations of our *in situ* data set compelled us to assume that the input uncertainties were not variable in time and space, which may be too simplistic (as will be discussed in Section 5.5). For example, *Siegel et al.* [2001] found a similar bias (4%) for the VGPM when evaluating its output against a global *in situ* NPP data set, but the bias was much more pronounced (–38%) when only a subset of the data corresponding to low chlorophyll concentrations was considered.

To assess the respective individual contributions of Chl, P^b_{opt} and F to the overall uncertainty in NPP estimates, we used the Monte Carlo method in a manner that allowed the input quantities to vary randomly one at a time, following the predetermined probability density functions. While uncertainty in a particular input quantity was simulated as explained in Section 5.4.1, all the remaining input terms were kept fixed at their nominal values for each repeat calculation of NPP. This way, for a given bin in a given month, we arrived at a frequency distribution that illustrated the component of the overall uncertainty (i.e. the partial uncertainty) in NPP stemming from the uncertainty in that input quantity only. This frequency distribution was described by the mean and CV and, in turn, the mean was used to compute (as explained above) the percentage bias in NPP estimates that was solely due to the bias in the particular input quantity. Table 5.2 lists the annual averages of NPP uncertainty components (partial percentage bias and partial CV) originating from uncertainties in (i) Chl, (ii) the product of Chl and Z_{eu}, (iii) P^b_{opt} and (iv) F. The annual averages are generally very similar to the analogous monthly averages throughout 2005.

When only uncertainty in Chl was considered, Z_{eu} was held fixed at the value computed from the nominal value of Chl. The outcoming partial CV would constitute the contribution of Chl to the random part of uncertainty in NPP if there

were no correlation between Chl and Z_{eu}. The two, however, tend to be inversely related. In our study, an explicit mathematical description of this relationship was employed in NPP calculations (see Equations (5.2) and (5.3)). From this description, it follows that an overestimate in Chl leads to an underestimate in Z_{eu}, and vice versa. Therefore, when Z_{eu} was allowed to follow the randomly varying Chl in Monte Carlo simulations, it counteracted the impact of Chl uncertainty, i.e. partial CV resulting from the random uncertainty in the product Chl×Z_{eu} was smaller than that due to Chl alone. However, no counteracting effect was found for the partial percentage bias. In fact, the bias was larger when Z_{eu} was allowed to vary than when it was fixed (Table 5.2). Possible reasons for this may be the nonlinearity of the function describing the relationship between Chl and Z_{eu}, as well as the nonlinear nature of multiplication between the two variables.

Another counterintuitive finding is that negative partial percentage bias in NPP originated from a positive bias in P^b_{opt}. This is explained by the fact that uncertainty in P^b_{opt} was simulated using the assumption of normality on $\log_{10}$ scale, but the normal distribution had to be antilogarithmically transformed to enable the VGPM calculations. The mean of the normally distributed $\log_{10}$ values was determined by subtracting $B^{LOG}(P^b_{opt})$ from the logarithm of the nominal P^b_{opt} value (see Equations (A5.9) and (A5.12) in Appendices A and C, respectively). However, this correction for bias in P^b_{opt} was outweighed by the impact of the antilogarithmic transformation on the mean of the resulting lognormal distribution. This statistic is defined not only by the mean, but also by the standard deviation, of the corresponding normal distribution [*Thöni*, 1969]. Generally, if the mean and standard deviation of a normal distribution are respectively symbolized as $\bar{x}$ and s, and the logarithm base equals 10, then the mean of the analogous lognormal distribution ($\bar{y}$) is given by the relation $\bar{y} = 10^{\bar{x}+0.5\ln(10)s^2}$. Since s (i.e. $RMSD_0^{LOG}$; see Equation (A5.6) in Appendix A) of the normal distribution that described the uncertainty in P^b_{opt} was rather large (0.33), the term $0.5\ln(10)s^2$ exceeded the correction for bias B^{LOG}. Therefore, $\bar{y}$ surpassed the nominal value of P^b_{opt} and, in turn, the mean of NPP uncertainty distribution was greater than the associated nominal NPP value. Whereas the same method was used to simulate and propagate the uncertainty in Chl, in that case s (or $RMSD_0^{LOG}$) was appreciably smaller and thus able to only partially offset (but not outbalance) the effect of bias correction.

5.5. Discussion and Conclusions

We restricted our analysis of uncertainty propagation through the VGPM to one arbitrarily chosen calendar year, due to substantial computational demands of the Monte Carlo simulations. Nevertheless, we do not expect that multiannual simulations would bring any significant changes to our results, because the relative measures of NPP bias and random uncertainty, as well as the statistics

describing the shape of NPP uncertainty distributions, were generally uniform both in time and space.

The analysis showed that an output value of the VGPM was typically overestimated by 6%, whereas the representative measure of its random uncertainty was 108%. These values apply to a period of 1 month and 9 km × 9 km bin size. Considering greater spatial/temporal scales would reduce the random uncertainty. However, there is no analogous possibility of reducing the bias. We thus found that the systematic positive errors in the individual NPP estimates accumulated to yield an overestimate of 2.5 Pg C in the annual global NPP for 2005. This figure could have been even larger if we had performed cloud correction and taken into account the continental shelf, whose relative contribution to global marine NPP exceeds the associated share in global ocean surface area [*Ducklow and McCallister*, 2005; *Wollast*, 1998]. Besides, shallow waters generally present an additional challenge to both NPP algorithms [*Saba et al.*, 2011] and ocean colour remote sensing (e.g. *Gregg et al.* [2009] found a larger bias in SeaWiFS Chl over the coastal ocean).

While a number of NPP algorithms were shown to be substantially biased [e.g. *Campbell et al.*, 2002; *Friedrichs et al.*, 2009; *Saba et al.*, 2010; *Saba et al.*, 2011], the relatively low average bias of 6%, which we found for the VGPM, is in good agreement with the findings of a few previous studies for this model. *Siegel et al.* [2001] compared the VGPM NPP estimates with the global *in situ* NPP data set used in the model development, and reported a mean bias of 4%. *Friedrichs et al.* [2009], who evaluated the skill of several VGPM variants using ~1000 *in situ* NPP measurements in the tropical Pacific, found that the variant apparently analogous to the one used in our study was associated with the median bias of 6% (i.e. the median of the ratio between the modelled and *in situ* NPP values equalled 1.06)

The adverse effect of bias in NPP estimates derived from remote sensing on, for example, ensuing estimates of the anthropogenic carbon uptake by ocean biota or assessments of export production, is obvious. It is, therefore, of particular importance to identify and neutralize the sources of such a bias. *Campbell et al.* [2002] suggested that bias in satellite-based NPP fields may be removed by blending them with *in situ* data, following a method used by *Gregg and Conkright* [2001]. Nevertheless, it should be noted that *in situ* NPP assessments themselves are not entirely free from uncertainties [e.g. *Falkowski and Raven*, 2007; *Maestrini et al.*, 1993; *Pemberton et al.*, 2006].

The common shape of uncertainty distribution around the VGPM output resembled a lognormal probability density function. This result supports the implicit assumption of lognormality in the studies of *Campbell et al.* [2002], *Friedrichs et al.* [2009], *Saba et al.* [2010] and *Saba et al.* [2011], which evaluated the performance of a group of NPP models by comparing $\log_{10}$ transforms of coincident modelled and *in situ* NPP values.

P^b_{opt}, which encapsulates the limitative effects of environment on phytoplankton's physiological capacity to fix carbon, contributed the most to the

random uncertainty in the VGPM NPP estimates. This result is not unexpected, as several studies have indicated that P^b_{opt} is the least well accounted for among the input terms in any depth-integrated model of NPP [*Behrenfeld and Falkowski*, 1997a; *Behrenfeld et al.*, 2002a; *Siegel et al.*, 2001]. The reasons for this were discussed in detail by *Behrenfeld et al.* [2002b]. In short, it is common to model P^b_{opt} as a function of sea surface temperature (SST) alone, since this is the only environmental determinant of phytoplankton's physiological state that is measured routinely and synoptically. Yet, the potential of temperature to directly limit algal photosynthetic capacity is far weaker compared to the analogous physiological effects of light- and nutrient availability. At the same time, SST can generally be related to the availability of light and nutrients for photosynthesis. Thus, SST in P^b_{opt} models acts primarily as a proxy for the other two environmental factors. For instance, warm, permanently stratified ocean regions are usually associated with plenty of light and nutrient scarcity, while the opposite is largely true for cooler areas. Consequently, the success of a temperature-dependent P^b_{opt} function hinges on how well it correlates with the effect of the main photosynthesis-limiting factor in a given moment and location.

Recently, efforts have been made to improve the description of phytoplankton physiology in NPP algorithms by taking a more direct approach to the modelling of the light- and nutrient-limitation effects [*Behrenfeld et al.*, 2005; *Behrenfeld et al.*, 2002b; *Westberry et al.*, 2008]. This approach, however, is not free from uncertainties either, not least because it lacks appropriate observations and instead must rely on climatological fields and products of ocean modelling (i.e. mixed layer depth) to respectively determine nutrient- and light-stress conditions. For example, *Milutinović et al.* [2009] showed that uncertainties in mixed layer depth input may considerably affect assessment of photoacclimation and, in turn, quantification of NPP. *Saba et al.* [2010] also suggested the sensitivity to inaccuracies in mixed layer depth as a likely reason for a reduced skill of this NPP modelling approach, which they observed at the location of Bermuda Atlantic Time-series Study, relative to the site of Hawaii Ocean Time-series. Nevertheless, abandoning the temperature-only approach represents an important step forward, with potential for improvements as sustained autonomous profiling of oceanic nutrient concentrations, temperature and salinity [*Dickey et al.*, 2009; *Roemmich et al.*, 2009] becomes available with sufficient temporal and spatial coverage, and as the modelling of ocean mixing advances.

The average contribution of Chl to the random uncertainty in NPP estimates was two thirds of that from P^b_{opt}. We must mention that the uncertainty metrics ascribed to the monthly Level-3 Chl were evaluated for daily Level-3 values (for details, see the report of *Gregg et al.* [2009]). Ideally, a monthly Level-3 value is produced by averaging 30 daily Level-3 values. This would most probably narrow the random uncertainty of the monthly average by counterbalancing of individual errors. In an ideal case of errors being normally distributed, the reduction in the uncertainty would be proportional to $1/\sqrt{30}$. Nevertheless, cloudiness often reduces the number of SeaWiFS 're-views' to appreciably less

than 30 [*Campbell et al.*, 2002]. We therefore assume that this counterbalancing effect is relatively weak.

The Chl-related random uncertainty became smaller when examined jointly with Z_{eu}, due to the effect known as 'compensating errors' [*Taylor*, 1997], i.e. some of the uncertainty was cancelled by using Chl as the predictor of Z_{eu}. Sensitivity analyses, respectively performed by *Campbell et al.* [2002], *Carr et al.* [2006] and *Friedrichs et al.* [2009] on a suite of NPP models, found that the typical model response to perturbations in input Chl is less than proportional. This implies that NPP models in general involve some nonlinear behaviour, which, by and large, dampens the impact of Chl uncertainty. Predicting Z_{eu} from Chl meant that Z_{eu} uncertainty was implicit in Chl uncertainty. However, recent progress in inference of water's inherent optical properties from ocean colour remote sensing makes it possible to relate Z_{eu} directly to absorption and backscattering coefficients [*Lee et al.*, 2005]. Being applicable to both Case-1 and Case-2 waters, this analytical approach is, in principle, superior to the empirical, Chl-based methods. Indeed, the results of *Lee et al.* [2007], based on a small data set ($n = 64$), suggest that the new 'Chl-bypassing' methodology may substantially decrease uncertainties associated with Z_{eu} estimates. Nonetheless, a much larger number of globally representative *in situ* data are needed to assess these uncertainties with confidence, as well as to estimate the covariance between Z_{eu} and Chl, before they can be propagated through an NPP model.

In comparison to other input quantities, F was responsible for the smallest part of the random uncertainty in NPP. Moreover, the results of the two F functions we analyzed showed identical $RMSD_0$. These findings are in agreement with those of *Behrenfeld and Falkowski* [1997a], who tested the effect of various irradiance-dependent functions by comparing analogous modelled NPP values with coincident *in situ* NPP data. They reported the same high correlation between the modelled and observed NPP ($r^2 = 0.86$) for nearly all of the F functions, including those considered in our study. However, while correlation analysis does indicate, albeit indirectly, $RMSD_0$ related to an F function, it does not carry any information on the function's bias. *Behrenfeld and Falkowski* [1997a] did not present any measure of such a bias, but our results suggest that irradiance-dependent functions may differ substantially in their tendency to overestimate F. This could perhaps be related to the assumptions about photoinhibition, which are built into those functions. Although, in comparison to P^b_{opt} and Chl, decreasing the $RMSD_0$ of F promises just a modest improvement in NPP estimates, our findings lead us to expect a considerably larger benefit from reducing bias associated with F functions.

The ranking order of the input quantities in terms of their contributions to the bias in NPP differed from the analogous ranking related to the random uncertainty in NPP (see Table 5.2). This, in itself, is not peculiar, because the bias and random uncertainty of a quantity need not be correlated. However, we observed unintuitive outcomes in the propagation of bias for the product $Chl \times Z_{eu}$ and P^b_{opt}, respectively, that could be related to nonlinear effects

involved in both the VGPM and our statistical approach. The nonlinearity can explain, for example, the remarkable difference in the separate contributions of Chl and P^b_{opt} to the NPP bias (3% versus −10% on average), a result that could not be foreseen from the similarity in the respective biases of the two input terms (Table 5.1). Although Chl alone was the least prominent source of the NPP bias, its average contribution to the bias of NPP doubled when regarded together with Z_{eu}. In that respect, it may prove helpful to replace the standard SeaWiFS Level-3 Chl with Chl estimated using an approach devised by *Gregg et al.* [2009], which, they reported, leads to a great reduction in Chl bias. The bias of F was not assessed for logarithmic transforms, but rather for values on a linear scale, and thus cannot be compared with the individual biases of Chl and P^b_{opt} to determine whether it ranks the same as its contribution to the bias of NPP.

Sources of uncertainty prior to the level of the direct input terms for the VGPM were not considered, i.e. we regarded PAR and SST as uncertainty-free. Although this assumption is idealized, some previous studies lead us to believe that including uncertainties in PAR and SST would not change our results considerably. For instance, *Behrenfeld and Falkowski* [1997a] argued that variability in PAR, in its capacity to dictate the relative depth of light saturation, has a rather small impact on changes in NPP. *Carr et al.* [2006] found an overall minor response of the VGPM to perturbing PAR at 11 locations representative of all ocean basins. Similarly, the VGPM was much less sensitive to PAR perturbations than the rest of NPP models analyzed by *Friedrichs et al.* [2009] in the tropical Pacific. This is also suggested by our results for propagation of uncertainty in F, the explicit function of PAR in the VGPM. The relative insensitivity of the VGPM NPP to PAR can be explained as follows: The F functions analyzed here (Figure S5.9, Appendix B), as well as many others (cf. Figure 2 in the work of *Behrenfeld and Falkowski* [1997a]) display a steep, nearly linear increase at the low end of PAR range, but inflect at PAR of ~5 to ~10 mol photons m^{-2} d^{-1}, after which the rate of increase in F with PAR gradually approaches a plateau. An inspection of monthly Level-3 PAR values observed by SeaWiFS during 2005 showed that a major part of the world ocean receives more than 10 mol photons m^{-2} d^{-1} of solar radiation in the photosynthetic waveband. As a consequence, NPP estimates in most of the ocean are quite robust to fluctuations of PAR on the order of ±3.3 mol photons m^{-2} d^{-1}, which is the RMSD yielded in an evaluation of monthly-averaged SeaWiFS PAR by *Frouin et al.* [2003]. In the tropical Pacific, even PAR perturbations as large as ±10 mol photons m^{-2} d^{-1}, to which *Friedrichs et al.* [2009] exposed the VGPM, did not change the RMSD between the VGPM and *in situ* NPP by more than 5%. The simple sensitivity analysis of *Friedrichs et al.* [2009] also involved perturbations of SST by ±1°C. Again, this had only a small impact on the VGPM performance in the tropical Pacific, yielding at most 7% change in the RMSD (although the impact was twice as large on some VGPM variants). *Carr et al.* [2006] observed a larger sensitivity of the VGPM

NPP to altering SST at the selected 11 representative points, but their SST alterations were on the order of several °C and thus appreciably larger than the typical uncertainty in daytime MODIS Aqua SST observations (bias = −0.02 K, $RMSD_0$ = 0.52 K), estimated by *Minnett et al.* [2004] in a global evaluation study (n = 8211).

The statistical approach applied here relies on the selection of reference data, which imposed constraints on the outcome of our study. Unfortunately, we did not have access to a sufficiently large number of independent data and so a sizeable portion of the data set we used consisted of field measurements employed in the development of the VGPM. Consequently, our evaluation can be considered to have placed lower bounds on the uncertainty estimates for the P^b_{opt} and F functions devised by *Behrenfeld and Falkowski* [1997b]. Another limitation of the data set was its uneven spatial distribution. This left us with no possibility to statistically weight the uncertainty estimates, in order to make them more representative of the entire ocean. Since the skill of various NPP models has been shown to vary regionally [*Campbell et al.*, 2002; *Saba et al.*, 2011], a good data coverage of all major ocean basins would have also presented us with an opportunity to look for potential regional patterns of over- and underestimates. An ideal reference data set would also have enabled an exploration of possible seasonal biases in NPP estimates. Instead, we had to assume the uncertainties were not spatially and temporally autocorrelated. Furthermore, our data set encompassed measurements taken mostly prior to the 1990s. The analysis would have benefited from a larger number of more recent reference data, since we would have been able to investigate whether the uncertainties in P^b_{opt} and F changed interdecadally. This is a likely possibility, judging from the study of *Friedrichs et al.* [2009], which analyzed the performance of 21 satellite-based NPP models in the tropical Pacific and found that none of them was successful in reproducing interdecadal changes observed *in situ*. Such data set limitations are a common problem facing globally oriented studies of the marine biosphere [*Richardson and Poloczanska*, 2008]. Concerted, dedicated efforts, such as building of long-term international observational networks and liberalization of data-sharing policies, are needed to ameliorate this situation.

Acknowledgements

Appendix A: Methodological Details of Determining Uncertainties in Input Quantities for the VGPM

For the purpose of quantifying uncertainty in a given input term, we compared a particular input model estimate (MOD) with a coincident in situ measurement of the same quantity, which served as reference (REF), by finding simple difference (δ), relative difference (δ^{REL}) and logarithmic difference (δ^{LOG}):

$$\delta = \text{MOD} - \text{REF}; \tag{A5.1}$$

$$\delta^{REL} = \frac{\text{MOD} - \text{REF}}{\text{REF}}; \tag{A5.2}$$

$$\delta^{LOG} = \log_{10}(\text{MOD}) - \log_{10}(\text{REF}) = \log_{10}\left(\frac{\text{MOD}}{\text{REF}}\right) = \log_{10}(\delta^{REL} + 1). \tag{A5.3}$$

All individual differences related to a given variable were collected and arranged in a frequency distribution, which we treated as the uncertainty distribution. The properties of the distribution determined what difference (i.e. δ, δ^{REL} or δ^{LOG}) was selected for further work. We chose the type of difference whose distribution complied best with normal probability distribution, because it can be reproduced easily in Monte Carlo simulations. Another advantage of using a normal distribution is that its standard deviation has a clear meaning in terms of probability (68% of the discrepancies fall within ±1 standard deviation of the mean discrepancy). The standard deviation of a particular frequency distribution is, in fact, the zero-centred root mean square difference. It was used as a measure of the portion of input uncertainty associated with the natural variability, and expressed either in measurement units of a given quantity (RMSD_0), in relative terms (RMSD_0^{REL}) or on a $\log_{10}$ scale (RMSD_0^{LOG}), depending on the selected type of difference between MOD and REF:

$$\text{RMSD}_0 = \sqrt{\frac{1}{n-1}\sum_{i=1}^{n}\left(\delta_i - B\right)^2}; \tag{A5.4}$$

$$\text{RMSD}_0^{REL} = \sqrt{\frac{1}{n-1}\sum_{i=1}^{n}\left(\delta_i^{REL} - B^{REL}\right)^2}; \tag{A5.5}$$

$$\text{RMSD}_0^{\text{LOG}} = \sqrt{\frac{1}{n-1}\sum_{i=1}^{n}\left(\delta_i^{\text{LOG}} - B^{\text{LOG}}\right)^2}, \qquad\qquad\qquad (A5.6)$$

where n is the sample size and i the ordinal number of an item within the sample. B, B^{REL} and B^{LOG} in Equations (A5.4) to (A5.6) represent the respective values of bias, i.e. the mean discrepancy between MOD and REF:

$$B = \bar{\delta} = \frac{1}{n}\sum_{i=1}^{n}\left(\text{MOD}_i - \text{REF}_i\right); \qquad\qquad\qquad (A5.7)$$

$$B^{\text{REL}} = \overline{\delta^{\text{REL}}} = \frac{1}{n}\sum_{i=1}^{n}\left(\frac{\text{MOD}_i - \text{REF}_i}{\text{REF}_i}\right); \qquad\qquad (A5.8)$$

$$B^{\text{LOG}} = \overline{\delta^{\text{LOG}}} = \frac{1}{n}\sum_{i=1}^{n}\left[\log_{10}(\text{MOD}_i) - \log_{10}(\text{REF}_i)\right]. \qquad (A5.9)$$

Appendix B: Supplementary Figures
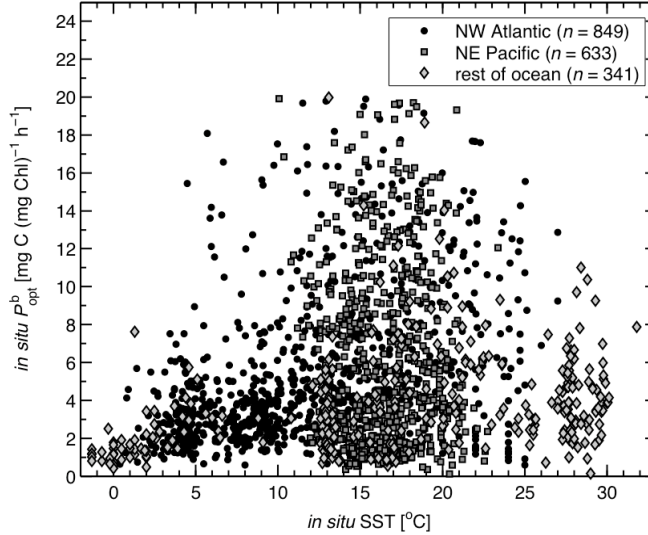
Figure S5.1. Observed values of Chl-specific maximum carbon fixation rate in a water column (*in situ* P^b_{opt}) plotted against coincidental measurements of sea surface temperature (*in situ* SST). Three geographical subsets with corresponding number of observations are indicated: the north-west Atlantic (black dots), the north-east Pacific (dark grey squares) and the rest of the global ocean (light grey diamonds).
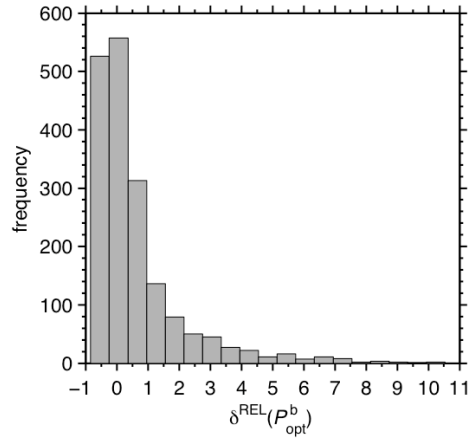
Figure S5.2. Frequency distribution of relative difference between model estimates from Equation (5.4) and matching observed values of P^b_{opt} ($\delta^{REL}(P^b_{opt})$) Five outliers (12.4, 13.9, 17.9, 29.8 and 59.0) are not presented.
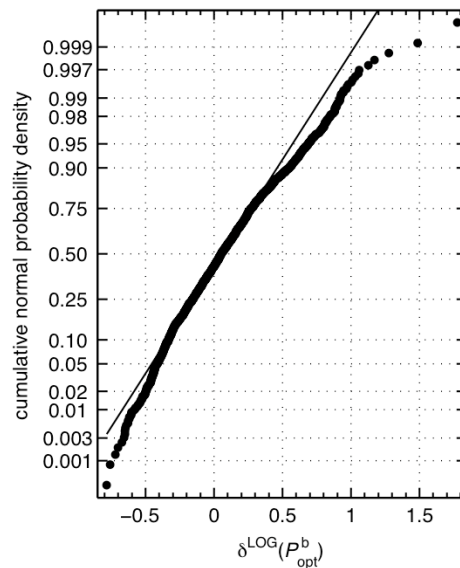
Figure S5.3. Normal probability plot for difference between $\log_{10}$ values of P^b_{opt} estimates from Equation (5.4) and corresponding reference data ($\delta^{LOG}(P^b_{opt})$). To help evaluate conformance of $\delta^{LOG}(P^b_{opt})$ with normality, a reference line is drawn by joining the first and third quartiles of $\delta^{LOG}(P^b_{opt})$ series and extrapolating towards the ends of the sample. This graphical test of normality shows that the left tail is shorter and the right tail longer than expected for a normally distributed variable, but most of $\delta^{LOG}(P^b_{opt})$ values (from ~5th percentile to ~85th percentile conform well to the normal distribution.
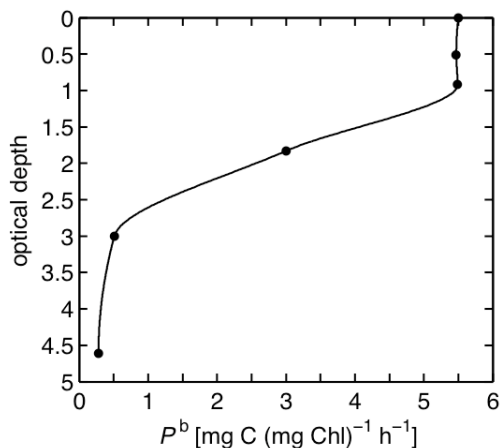
Figure S5.4. Example vertical profile of chlorophyll-normalized primary productivity (P^b) obtained by interpolating between discrete field estimates (dots), shown for a series of optical depths. Optical depth is a dimensionless product of physical depth and mean vertical attenuation coefficient for PAR. Source of measurements: Brookhaven National Laboratory (research vessel Knorr). Station coordinates: 38.46°N, 75.00°W. Date: 31 August 1980.
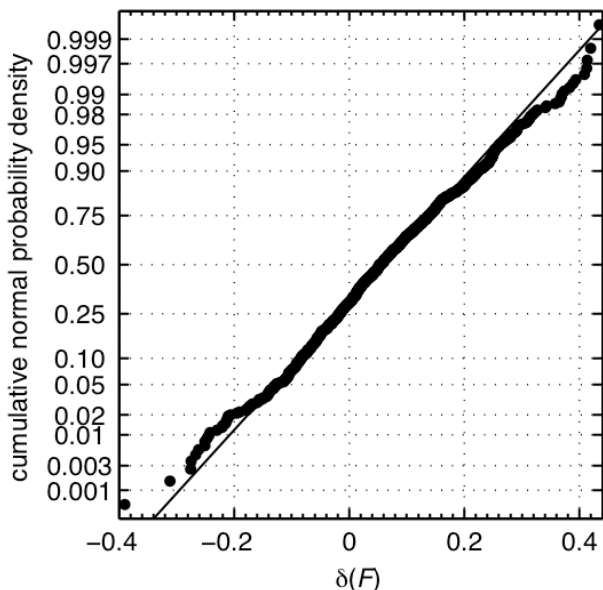
Figure S5.5. Normal probability plot for values of $\delta(F)$ from Figure 5.7, presented as dots. Superimposed on the plot is a line expected for a perfectly normally distributed sample.
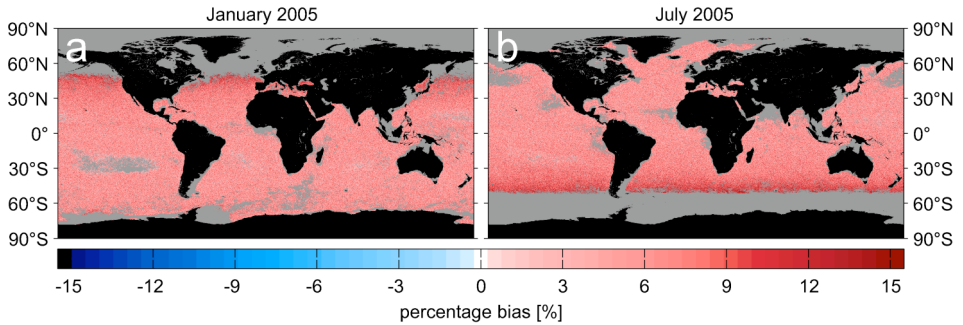
Figure S5.6. Bias of nominal NPP estimates presented as a percentage of the corresponding mean values of NPP uncertainty distributions, i.e. $\left[\left(\mathrm{NPP} - \overline{\mathrm{NPP}_{\mathrm{MC}}}\right)\big/\overline{\mathrm{NPP}_{\mathrm{MC}}}\right] \times 100\%$, in (a) January and (b) July 2005. Grey colour indicates shelf (<200 m), bins without remote sensing data and locations with unreliable statistics.
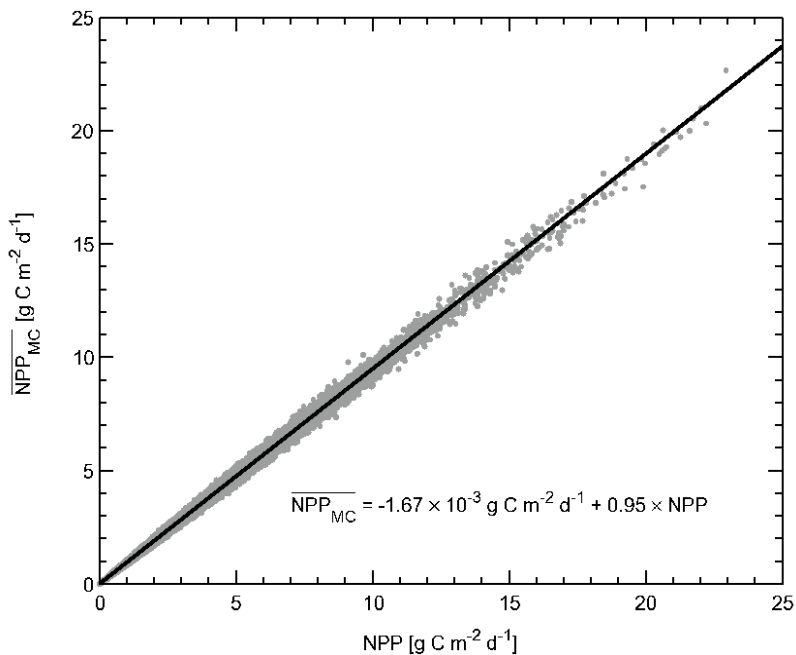
Figure S5.7. Comparison between nominal NPP estimates and the associated mean values of NPP uncertainty distributions ($\overline{\mathrm{NPP}_{\mathrm{MC}}}$) in 2005. The number of data points is 47.8 million. The line and the inserted equation represent the functional relationship between the two variables, obtained using the least-squares linear regression.

The equation shown on the figure:

$$RU(NPP) = 6.01 \times 10^{-3} \text{ g C m}^{-2} \text{ d}^{-1} + NPP$$
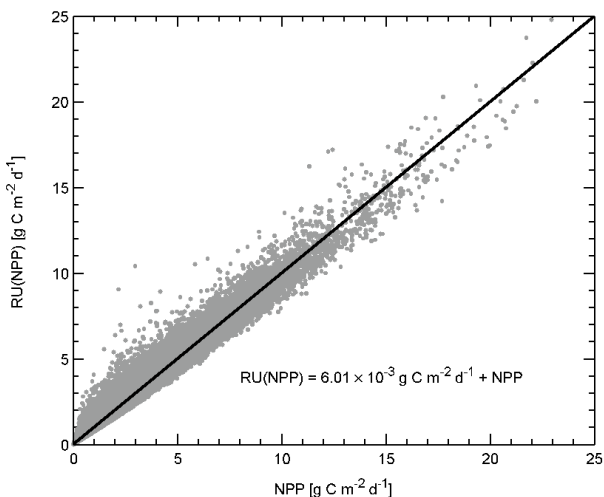
Figure S5.8. The random uncertainty of NPP (RU(NPP)), expressed as standard deviation of NPP uncertainty distributions, plotted against the corresponding nominal NPP values in 2005. There are 47.8 million data points. The line, described by the inserted equation, was fitted to the points using the least-squares regression.
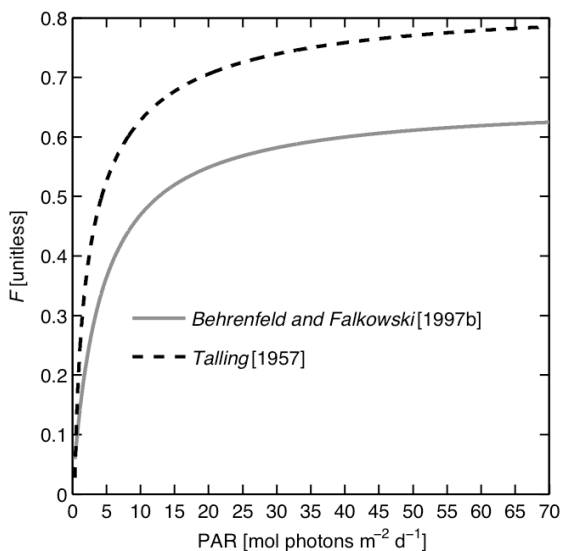
Figure S5.9. Functions devised respectively by *Behrenfeld and Falkowski* [1997b] (Equation (5.5)) and *Talling* [1957] (Equation (5.8)) to describe the relationship between PAR at the sea surface and the parameter *F*, which represents the vertical profile of chlorophyll-normalized photosynthetic rates.

Appendix C: Summary of the Monte Carlo Method

The Monte Carlo method, used to propagate input uncertainties through the VGPM, can be summarized by the following mathematical notation, where random values are indicated in bold type, nominal values in light type and $\mathcal{N}$ symbolizes a particular normal probability distribution, whose mean and standard deviation are given in square brackets:

$$\log_{10}(\mathbf{Chl}) \sim \mathcal{N}\left[\log_{10}(\text{Chl}) - B^{\text{LOG}}(\text{Chl}),\ \text{RMSD}_0^{\ \text{LOG}}(\text{Chl})\right]; \tag{A5.10}$$

$$\mathbf{Z_{eu}} = f(\mathbf{Chl}); \tag{A5.11}$$

$$\log_{10}\left(\mathbf{P_{opt}^b}\right) \sim \mathcal{N}\left[\log_{10}(P_{opt}^b) - B^{\text{LOG}}(P_{opt}^b),\ \text{RMSD}_0^{\ \text{LOG}}(P_{opt}^b)\right]; \tag{A5.12}$$

$$\mathbf{F} \sim \mathcal{N}\left[F - B(F),\ \text{RMSD}_0(F)\right]; \tag{A5.13}$$

$$\mathbf{NPP} = f(\mathbf{Chl}, \mathbf{Z_{eu}}, \mathbf{P_{opt}^b}, \mathbf{F}, \text{DL}). \tag{A5.14}$$

References

Antoine, D., J. M. Andre, and A. Morel (1996), Oceanic primary production 2. Estimation at global scale from satellite (coastal zone color scanner) chlorophyll, *Global Biogeochemical Cycles*, *10*(1), 57-69.

Arrigo, K. R. (2005), Marine microorganisms and global nutrient cycles, *Nature*, *437*(7057), 349-355.

Balch, W., R. Evans, J. Brown, G. Feldman, C. McClain, and W. Esaias (1992), The remote-sensing of ocean primary productivity - use of a new data compilation to test satellite algorithms, *Journal of Geophysical Research-Oceans*, *97*(C2), 2279-2293.

Behrenfeld, M., E. Boss, D. Siegel, and D. Shea (2005), Carbon-based ocean productivity and phytoplankton physiology from space, *Global Biogeochemical Cycles*, *19*(1), GB1006.

Behrenfeld, M. J., and P. G. Falkowski (1997a), A consumer's guide to phytoplankton primary productivity models, *Limnology and Oceanography*, *42*(7), 1479-1491.

Behrenfeld, M. J., and P. G. Falkowski (1997b), Photosynthetic rates derived from satellite-based chlorophyll concentration, *Limnology and Oceanography*, *42*(1), 1-20.

Behrenfeld, M. J., E. Maranon, D. A. Siegel, and S. B. Hooker (2002a), Photoacclimation and nutrient-based model of light-saturated photosynthesis for quantifying oceanic primary production, *Marine Ecology-Progress Series*, *228*, 103-117.

Behrenfeld, M. J., W. E. Esaias, and K. R. Turpie (2002b), Assessment of primary production at the global scale, in *Phytoplankton productivity: Carbon assimilation in marine and freshwater ecosystems*, edited by P. J. leB. Williams, D. N. Thomas and C. S. Reynolds, Blackwell Science.

Bureau International des Poids et Mesures (BIPM), International Electrotechnical Commission (IEC), International Federation of Clinical Chemistry (IFCC), International Laboratory Accreditation Cooperation (ILAC), International Organization for Standardization (ISO), International Union of Pure and Applied Chemistry (IUPAC), International Union of Pure and Applied Physics (IUPAP), and Organisation Internationale de Métrologie Légale (OIML) (2008a), *Evaluation of measurement data — supplement 1 to the 'guide to the expression of uncertainty in measurement' — propagation of distributions using a Monte Carlo method*, Joint Committee for Guides in Metrology, Bureau International des Poids et Mesures, Sèvres, France. Available at http://www.bipm.org/utils/common/documents/jcgm/JCGM_101_2008_E.pdf.

Bureau International des Poids et Mesures (BIPM), International Electrotechnical Commission (IEC), International Federation of Clinical Chemistry (IFCC), International Organization for Standardization (ISO), International Union of Pure and Applied Chemistry (IUPAC), International Union of Pure and Applied Physics (IUPAP), and Organisation Internationale de Métrologie Légale (OIML) (2008b), *Evaluation of measurement data — guide to the expression of uncertainty in measurement (GUM 1995 with minor corrections)*, Joint Committee for Guides in Metrology, Bureau International des Poids et Mesures, Sèvres, France. Available at http://www.bipm.org/utils/common/documents/jcgm/JCGM_100_2008_E.pdf.

Bureau International des Poids et Mesures (BIPM), International Electrotechnical Commission (IEC), International Federation of Clinical Chemistry (IFCC), International Laboratory Accreditation Cooperation (ILAC), International Organization for Standardization (ISO), International Union of Pure and Applied Chemistry (IUPAC), International Union of Pure and Applied Physics (IUPAP), and Organisation Internationale de Métrologie Légale (OIML) (2009), *Evaluation of measurement data – an introduction to the "Guide to the expression of uncertainty in measurement" And related documents*, Joint Committee for Guides in Metrology, Bureau International des Poids et Mesures, Sèvres, France. Available at http://www.bipm.org/utils/common/documents/jcgm/JCGM_104_2009_E.pdf.

Campbell, J., D. Antoine, R. Armstrong, K. Arrigo, W. Balch, R. Barber, M. Behrenfeld, R. Bidigare, J. Bishop, M. Carr, W. Esaias, P. Falkowski, N. Hoepffner, R. Iverson, D. Kiefer, S. Lohrenz, J. Marra, A. Morel, J. Ryan, V. Vedernikov, K. Waters, C. Yentsch, and J. A. Yoder (2002), Comparison of algorithms for estimating ocean primary production from surface chlorophyll, temperature, and irradiance, *Global Biogeochemical Cycles*, *16*(3), 1035.

Campbell, J. W. (1995), The lognormal distribution as a model for bio-optical variability in the sea, *Journal of Geophysical Research-Oceans*, *100*(C7), 13237-13254.

Carr, M.-E., M. A. M. Friedrichs, M. Schmeltz, M. Noguchi Aita, D. Antoine, K. R. Arrigo, I. Asanuma, O. Aumont, R. Barber, M. Behrenfeld, R. Bidigare, E. T. Buitenhuis, J. Campbell, A. Ciotti, H. Dierssen, M. Dowell, J. Dunne, W. Esaias, B. Gentili, W. Gregg, S. Groom, N. Hoepffner, J. Ishizaka, T. Kameda, C. L. Quéré, S. Lohrenz, J. Marra, F. Mélin, K. Moore, A. Morel, T. E. Reddy, J. Ryan,

M. Scardi, T. Smyth, K. Turpie, G. Tilstone, K. Waters, and Y. Yamanaka (2006), A comparison of global estimates of marine primary production from ocean color, *Deep-Sea Research Part II: Topical Studies in Oceanography*, *53*(5-7), 741- 770.

Charlson, R., J. E. Lovelock, M. O. Andreae, and S. G. Warren (1987), Oceanic phytoplankton, atmospheric sulphur, cloud albedo and climate, *Nature*, *326*(6114), 655-661.

Curran, P. J. (2002), Foreword, in *Uncertainty in remote sensing and GIS*, edited by G. M. Foody and P. M. Atkinson, pp. xi-xvi, John Wiley & Sons, Ltd.

Dickey, T., N. Bates, R. H. Byrne, G. Chang, F. P. Chavez, R. A. Feely, A. K. Hanson, D. M. Karl, D. Manov, C. Moore, C. L. Sabine, and R. Wanninkhof (2009), The nopp o-scope and MOSEAN projects: Advanced sensing for ocean observing systems, *Oceanography*, *22*(2), 168-181.

Ducklow, H. W., and S. L. McCallister (2005), The biogeochemistry of carbon dioxide in the coastal oceans, in *The sea: The global coastal ocean—multiscale interdisciplinary processes*, edited by A. R. Robinson and K. H. Brink, pp. 269-315, Harvard University Press, Cambridge, Massachusetts, USA.

Eppley, R. W. (1972), Temperature and phytoplankton growth in the sea, *Fishery Bulletin*, *70*(4), 1063-1085.

Falkowski, P. G., R. T. Barber, and V. Smetacek (1998), Biogeochemical controls and feedbacks on ocean primary production, *Science*, *281*(5374), 200-206.

Falkowski, P. G., and J. A. Raven (2007), *Aquatic photosynthesis*, 2nd ed., 500 pp., Princeton University Press.

Friedrichs, M. A. M., M.-E. Carr, R. T. Barber, M. Scardi, D. Antoine, R. A. Armstrong, I. Asanuma, M. J. Behrenfeld, E. T. Buitenhuis, F. Chai, J. R. Christian, A. M. Ciotti, S. C. Doney, M. Dowell, J. Dunne, B. Gentili, W. Gregg, N. Hoepffner, J. Ishizaka, T. Kameda, I. Lima, J. Marra, F. Mèlin, J. K. Moore, A. Morel, R. T. O'Malley, J. O'Reilly, V. S. Saba, M. Schmeltz, T. J. Smyth, J. Tjiputra, K. Waters, T. K. Westberry, and A. Winguth (2009), Assessing the uncertainties of model estimates of primary productivity in the tropical Pacific ocean, *Journal of Marine Systems*, *76*(1-2), 113-133.

Frouin, R., and S. F. Iacobellis (2002), Influence of phytoplankton on the global radiation budget, *Journal of Geophysical Research-Atmospheres*, *107*(D19).

Frouin, R., B. A. Franz, and P. J. Werdell (2003), The SeaWiFS PAR product, in *Algorithm updates for the fourth SeaWiFS data reprocessing*, edited by S. B. Hooker and E. R. Firestone, pp. 46-50.

Gregg, W. W., and M. E. Conkright (2001), Global seasonal climatologies of ocean chlorophyll: Blending in situ and satellite data for the Coastal Zone Color Scanner era, *Journal of Geophysical Research-Oceans*, *106*(C2), 2499-2515.

Gregg, W. W., N. W. Casey, J. E. O'Reilly, and W. E. Esaias (2009), An empirical approach to ocean color data: Reducing bias and the need for post-launch radiometric re-calibration, *Remote Sensing of Environment*, *113*(8), 1598-1612.

Kirk, J. T. O. (1994), *Light and photosynthesis in aquatic ecosystems*, 2nd ed., 528 pp., Cambridge University Press.

Lee, Z., K. Du, R. Arnone, S. Liew, and B. Penta (2005), Penetration of solar radiation in the upper ocean: A numerical model for oceanic and coastal waters, *Journal of Geophysical Research-Oceans*, *110*, C09019.

Lee, Z., A. Weidemann, J. Kindle, R. Arnone, K. L. Carder, and C. Davis (2007), Euphotic zone depth: Its derivation and implication to ocean-color remote sensing, *Journal of Geophysical Research-Oceans*, *112*(C3), C03009.

Lindeman, R. L. (1942), The trophic-dynamic aspect of ecology, *Ecology*, *23*(4), 399-417.

Maestrini, S. Y., A. Sournia, and A. Herbland (1993), Measuring phytoplankton production in 1992 and the coming years: A dilemma?, in *Measurement of primary production from the molecular to the global scale*, edited by W. K. W. Li and S. Y. Maestrini, pp. 244-259, International Council for the Exploration of the Sea.

Megard, R. O. (1972), Phytoplankton, photosynthesis, and phosphorus in lake Minnetonka, Minnesota, *Limnology and Oceanography*, *17*(1), 68-87.

Milutinović, S., M. J. Behrenfeld, J. A. Johannessen, and T. Johannessen (2009), Sensitivity of remote sensing-derived phytoplankton productivity to mixed layer depth: Lessons from the carbon-based productivity model, *Global Biogeochemical Cycles*, *23*, GB4005.

Minnett, P. J., O. B. Brown, R. H. Evans, E. L. Key, E. J. Kearns, K. Kilpatrick, A. Kumar, K. A. Maillet, and G. Szczodrak (2004), Sea-surface temperature measurements from the moderate-resolution imaging spectroradiometer (MODIS) on Aqua and Terra, paper presented at 2004 IEEE International Geoscience and Remote Sensing Symposium Proceedings, Anchorage, Alaska, USA.

Montes-Hugo, M., S. C. Doney, H. W. Ducklow, W. Fraser, D. Martinson, S. E. Stammerjohn, and O. Schofield (2009), Recent changes in phytoplankton communities associated with rapid regional climate change along the western Antarctic Peninsula, *Science*, *323*(5920), 1470-1473.

Morel, A., and J. F. Berthon (1989), Surface pigments, algal biomass profiles, and potential production of the euphotic layer - relationships reinvestigated in view of remote-sensing applications, *Limnology and Oceanography*, *34*(8), 1545-1562.

Morel, A., and S. Maritorena (2001), Bio-optical properties of oceanic waters: A reappraisal, *Journal of Geophysical Research-Oceans*, *106*(C4), 7163-7180.

O'Reilly, J. E., Maritorena S., Mitchell B.G., Siegel D.A., Carder K.L., Garver S.A., Kahru M., and M. C. (1998), Ocean color chlorophyll algorithms for SeaWiFS, *Journal of Geophysical Research-Oceans*, *103* (C11), 24937-24953.

Pemberton, K. L., K. R. Clarke, and I. Joint (2006), Quantifying uncertainties associated with the measurement of primary production, *Marine Ecology-Progress Series*, *322*, 51-59.

Platt, T., and S. Sathyendranath (1993), Estimators of primary production for interpretation of remotely sensed data on ocean color, *Journal of Geophysical Research-Oceans*, *98*(C8), 14561-14576.

Richardson, A. J., and E. S. Poloczanska (2008), Under-resourced, under threat, *Science*, *320*(5881), 1294-1295.

Roemmich, D., G. C. Johnson, S. Riser, R. Davis, J. Gilson, W. B. Owens, S. L. Garzoli, C. Schmid, and M. Ignaszewski (2009), The Argo program: Observing the global ocean with profiling floats, *Oceanography*, *22*(2), 34-43.

Saba, V. S., M. A. M. Friedrichs, M.-E. Carr, D. Antoine, R. A. Armstrong, I. Asanuma, O. Aumont, N. R. Bates, M. J. Behrenfeld, V. Bennington, L. Bopp, J. Bruggeman, E. T. Buitenhuis, M. J. Church, A. M. Ciotti, S. C. Doney, M. Dowell, J. Dunne, S. Dutkiewicz, W. Gregg, N. Hoepffner, K. J. W. Hyde, J. Ishizaka, T. Kameda, D. M. Karl, I. Lima, M. W. Lomas, J. Marra, G. A. McKinley, F. Mèlin,

J. K. Moore, A. Morel, J. O'Reilly, B. Salihoglu, M. Scardi, T. J. Smyth, S. Tang, J. Tjiputra, J. Uitz, M. Vichi, K. Waters, T. K. Westberry, and A. Yool (2010), Challenges of modeling depth-integrated marine primary productivity over multiple decades: A case study at bats and hot, *Global Biogeochemical Cycles*, *24*(3), GB3020.

Saba, V. S., M. A. M. Friedrichs, D. Antoine, R. A. Armstrong, I. Asanuma, M. J. Behrenfeld, A. M. Ciotti, M. Dowell, N. Hoepffner, K. J. W. Hyde, J. Ishizaka, T. Kameda, J. Marra, F. Mélin, A. Morel, J. O'Reilly, M. Scardi, W. O. Smith Jr, T. J. Smyth, S. Tang, J. Uitz, K. Waters, and T. K. Westberry (2011), An evaluation of ocean color model estimates of marine primary productivity in coastal and pelagic regions across the globe, *Biogeosciences*, *8*(2), 489-503.

Siegel, D. A., T. K. Westberry, M. C. O'Brien, N. B. Nelson, A. F. Michaels, J. R. Morrison, A. Scott, E. A. Caporelli, J. C. Sorensen, S. Maritorena, S. A. Garver, E. A. Brody, J. Ubante, and M. A. Hammer (2001), Bio-optical modeling of primary production on regional scales: The Bermuda BioOptics project, *Deep-Sea Research Part II: Topical Studies in Oceanography*, *48*(8-9), 1865-1896.

Sokal, R. R., and F. J. Rohlf (1995), *Biometry: The principles and practice of statistics in biological research*, 3rd ed., 887 pp., W. H. Freeman and Company, New York.

Talling, J. F. (1957), The phytoplankton population as a compound photosynthetic system, *New Phytologist*, *56*(2), 133-149.

Taylor, J. R. (1997), *An introduction to error analysis: The study of uncertainties in physical measurements*, 327 pp., University Science Books.

Taylor, K. E. (2001), Summarizing multiple aspects of model performance in a single diagram, *Journal of Geophysical Research-Atmospheres*, *106*(D7), 7183-7192.

Thöni, H. (1969), A table for estimating the mean of a lognormal distribution, *Journal of the American Statistical Association*, *64*(326), 632-636.

Westberry, T., M. J. Behrenfeld, D. A. Siegel, and E. Boss (2008), Carbon-based primary productivity modeling with vertically resolved photoacclimation, *Global Biogeochemical Cycles*, *22* GB2024.

Wollast, R. (1998), Evaluation and comparison of the global carbon cycle in the coastal zone and in the open ocean, in *The sea: The global coastal ocean processes and methods*, edited by K. H. Brink and A. R. Robinson, pp. 213-252, John Wiley & Sons, Inc., New York, USA.

CHAPTER 6 ────────────

Uncertainty in a Model for Estimating Euphotic Depth from Satellite Observations of Chlorophyll

VI

Uncertainty in a Model for Estimating Euphotic Depth from Satellite Observations of Chlorophyll

Svetlana Milutinović

6.1. Introduction

Euphotic depth (Z_{eu} [m]) is the depth at which photosynthetically available radiation (spanning the wavelength domain from 400 to 700 nm and thus roughly coinciding with the visible part of the electromagnetic spectrum) decreases to 1% of its value just below the sea surface [*Kirk*, 1994]. Z_{eu} is an important property for primary productivity modelling, as it is generally assumed that photosynthesis below this depth is negligible [*Falkowski and Raven*, 2007]. Various procedures have been developed to estimate Z_{eu} from satellite ocean-colour remote sensing [*Lee et al.*, 2007]. This work presents an approach for calculating Z_{eu} from remotely sensed chlorophyll *a* in Case-1 waters, which was employed by *Milutinović and Bertino* [2011]. The approach combines two formulations devised by *Morel and Berthon* [1989, Equation (3a)] and *Morel and Maritorena* [2001, Figure 6], respectively. The former determines the total chlorophyll *a* content within the productive water column (Chl_{tot} [mg m^{-2}]) as a power-law function of surface chlorophyll *a* concentration, while the latter relates Z_{eu} to a fourth-order polynomial of $\log_{10}(Chl_{tot})$. Naturally, Z_{eu} determined by this model incorporates some uncertainty, a part of which arises from uncertainty in satellite chlorophyll (Chl) estimates. This part was taken into account by *Milutinović and Bertino* [2011] and is not considered here. Instead, the objective of this report is to quantify the portion of uncertainty in the Chl-derived Z_{eu} that is inherent in the modelling approach.

6.2. Method and Results

To evaluate the component of uncertainty in the modelled Z_{eu} (Z_{eu}^{MOD}) that stems from the model itself, 990 *in situ* measurements of chlorophyll *a* concentration just below the sea surface (Chl_{surf} [mg m^{-3}]) and simultaneous reference estimates of Z_{eu} (Z_{eu}^{REF}) were used. Z_{eu}^{REF} values were based on *in situ* measurements of either downward irradiance at discrete wavelengths in the visible domain ($E_d(\lambda)$ [μW cm^{-2} nm^{-1}]) or the total photosynthetically available radiation (PAR [μmol photons cm^{-2} s^{-1}]), taken at a number of depths in the upper water column. The *in situ* Chl_{surf} and radiometric data are distributed via

149

Table 6.1. Summary of information on radiometric measurements and surface chlorophyll data used for evaluation of uncertainty in modelled euphotic depth

Experiment	Principal investigator	Location	Time of measurement	Number of stations
ACE-Asia	G. Mitchell	Japan and western Pacific	Mar–Apr 2001	37
Aerosols/INDOEX	G. Mitchell	Atlantic and Indian Oceans	Jan–Mar 1999	41
AMLR	G. Mitchell	Weddell Sea	Feb–Mar 2000	22
BBOP	D. Siegel	Sargasso Sea	variable 1994–2003	262
CalCOFI	G. Mitchell	California Current	variable 1993–2003	326
JGOFS Arabian Sea	J. Mueller	Arabian Sea	Mar, Apr, Oct, Nov, Dec 1995	129
JGOFS Sea of Japan	G. Mitchell	Japan and western Pacific	Jun–Jul 1999	35
JGOFS Southern Ocean	G. Mitchell	Ross Sea	Nov–Dec 1997, Jan–Feb 1998	8
JGOFS/WOCE	J. Marra	central tropical Pacific	Sep 1991	18
Oceania	D. Stramski	Norwegian and Greenland Seas, Spitsbergen Bank	Jun–Jul 1998–2000	55
OceanLIDAR	M. Lewis	equatorial Pacific	variable 1994–1999, 2001	57

the SeaWiFS Bio-optical Archive and Storage System (SeaBASS) at http://seabass.gsfc.nasa.gov/authorized/seabass_search.cgi [*Werdell et al.*, 2003]. Table 6.1 lists measurement sources, locations, times and number of stations.

Z_{eu}^{REF} was determined in two steps. In the first step, interpolation was done between $E_d(\lambda)$ data to obtain the complete spectral distribution of downwelling irradiance in the photosynthetic waveband (400–700 nm) at a given depth (Figure 6.1). If the shortest measured wavelength was larger than 400 nm, extrapolation of $E_d(\lambda)$ to 400 nm was employed. Similarly, $E_d(\lambda)$ was extrapolated to 700 nm when necessary. PAR was calculated at each discrete depth as the integral $\int_{400\,nm}^{700\,nm} E_d(\lambda)\, d(\lambda)$. When *in situ* measurements of PAR were available, this step was omitted.

In the second step, vertical profile of PAR was computed by interpolating between the PAR values at discrete depths in the upper water column (Figure 6.2). Subsequently, ratio between PAR at a given depth and sea-surface PAR was derived. Finally, Z_{eu}^{REF} was determined as the depth at which this ratio reached 0.01. Sometimes, the radiometric measurements were not taken
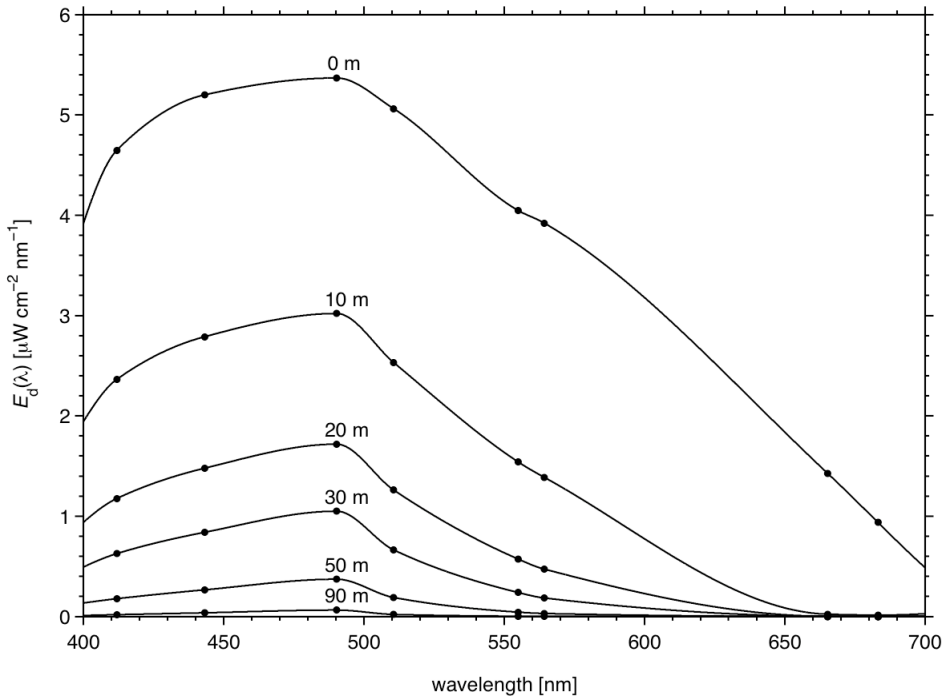
Figure 6.1. An example of the spectral distribution of downward irradiance $E_d(\lambda)$, obtained by interpolating between discrete *in situ* measurements (dots) and extrapolating to 700 nm, shown for a selection of increasing water depths (0, 10, 20, 30, 50 and 90 metres). Source of measurements: The Bermuda Bio-Optics Project (BBOP). Station coordinates: 31.68°N, 64.26°W. Date: 22 January 2002.

immediately beneath the sea surface or did not extend deep enough for the ratio to reach 0.01. In such cases, a polynomial was fitted to common logarithms of the 10 shallowest (or deepest) PAR data and extrapolation was performed to determine sea-surface PAR (or PAR corresponding to the ratio of 0.01). Clearly, PAR computed from $E_d(\lambda)$ in the step one is given in units of radiant power incident on a surface (μW cm^{-2}), while the *in situ* measured PAR is expressed as the amount of quanta (or photons) per unit area of surface per unit time (μmol photons cm^{-2} s^{-1}). Defining Z_{eu} based on PAR in quantum units may be considered more appropriate, because each photon from the waveband 400–700 nm absorbed by photosynthetic biomass, regardless of its energy content, has equal value for photosynthesis [*Kirk*, 1994]. However, *Morel and Gentili* [2004] showed that units in which PAR is expressed have no practical impact on the resulting value of Z_{eu}.
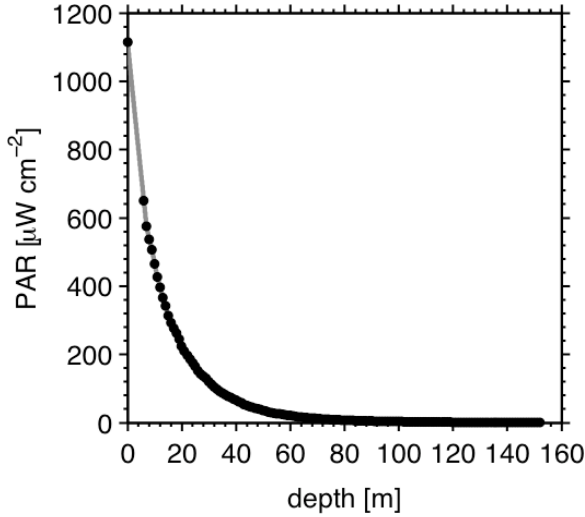
Figure 6.2. Vertical profile of PAR corresponding to the data shown in the previous figure. Black dots represent PAR determined by integrating the 'continuous' $E_d(\lambda)$ values at a given depth over the wavelength domain 400–700 nm. For depths where measurements had not been taken, PAR values were derived by interpolation (denoted by grey line).

Nearly all Chl_{surf} data were measured by fluorometric method. Only those from the Oceania experiment (in total 55 values) were determined spectrophotometrically. Prior to calculating Z_{eu}^{MOD}, inverse prediction was used to find what would Chl_{surf} values be if they were measured by high performance liquid chromatography (HPLC), because HPLC is widely regarded as superior to the other methods [e.g. *Mantoura et al.*, 1997]. For the fluorometrically determined Chl_{surf}, the corresponding HPLC values were predicted from the parameters yielded in a linear regression on $\log_{10}$ scale, using data from the NASA bio-Optical Marine Algorithm Data set (NOMAD) [*Werdell and Bailey*, 2005] (see Figure 6.3). These parameters were assumed to be valid for the fluorometric Chl_{surf} data employed here, since they are, with the exception of 18 points measured in the JGOFS/WOCE experiment (Table 6.1), a subset of the NOMAD data set. For the spectrophotometrically determined Chl_{surf}, the slope and y-intercept of the least squares regression line reported by *Stramska et al.* [2003] for the Oceania experiment were used: Chl_{surf}(spectrophotometric) = 1.0239 Chl_{surf}(HPLC) + 0.0123. The inversely predicted HPLC Chl_{surf} was used to calculate Z_{eu}^{MOD}.

Z_{eu}^{MOD} values are in general slightly overestimated but show good correlation with Z_{eu}^{REF} data (Figure 6.4). However, while the frequency distribution of Z_{eu}^{MOD} is unimodal, that of Z_{eu}^{REF} displays bimodality (Figure 6.5). Figures 6.6a–6.6b show geographic positions of Z_{eu}^{REF} values clustered
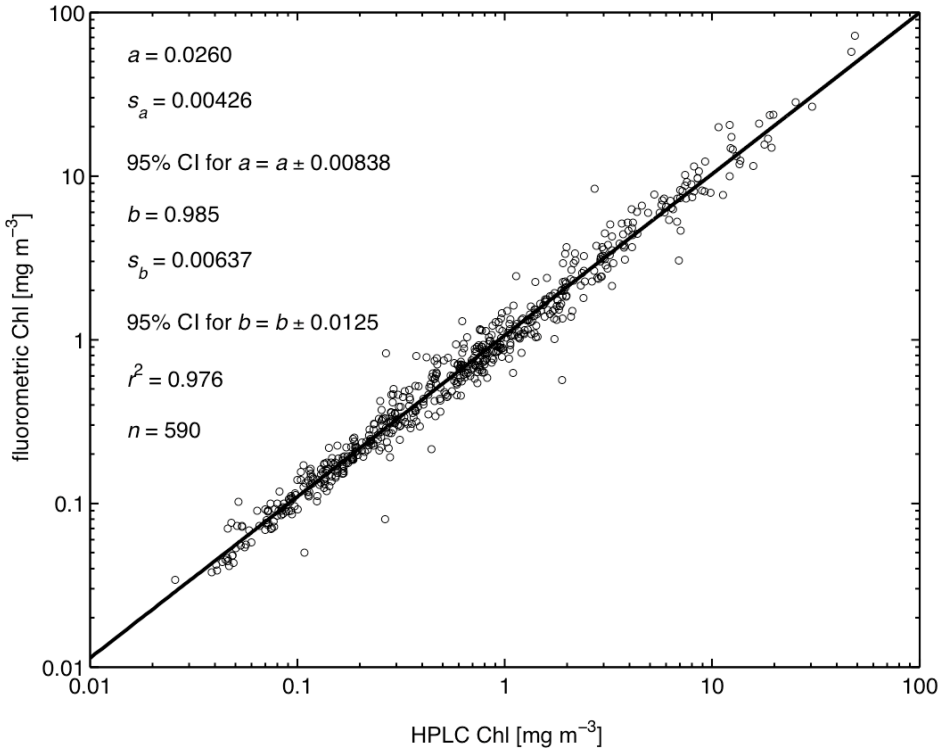
152

Figure 6.3. Comparison between coincident HPLC and fluorometric values of chlorophyll *a* concentration in NOMAD, expressed in mg m^{-3}. The least-squares regression line was fitted to the data in order to enable inverse prediction of HPLC values from fluorometric measurements (note the logarithmic scale). The statistics provided here are: *y*-intercept (*a*), slope (*b*), their standard uncertainties (s_a and s_b) and 95% confidence intervals (CI), coefficient of determination (r^2), and sample size (*n*).

around the lower and the upper mode, respectively. The largest subset of Z_{eu}^{REF} contributing to the lower mode originates from the California Current region, while Z_{eu}^{REF} values from the Sargasso Sea contribute most to the upper mode.

To evaluate the performance of the Z_{eu} model of *Morel and Berthon* [1989] and *Morel and Maritorena* [2001], relative discrepancy between individual Z_{eu}^{MOD} estimates and the corresponding Z_{eu}^{REF} ($\delta^{REL}(Z_{eu})$) was determined as:

$$\delta^{REL}(Z_{eu}) = \frac{Z_{eu}^{MOD} - Z_{eu}^{REF}}{Z_{eu}^{REF}}. \tag{6.1}$$

153
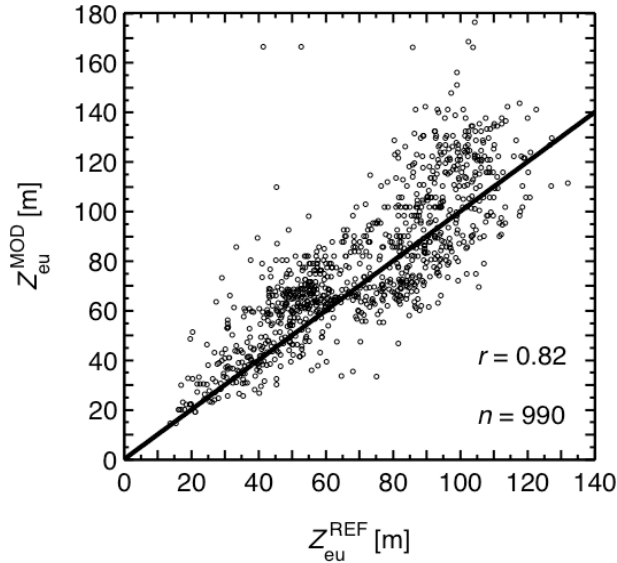
Figure 6.4. Scatterplot of euphotic depth values derived from field measurements of surface chlorophyll concentration (Z_{eu}^{MOD}) against reference euphotic depths based on *in situ* radiometric observations (Z_{eu}^{REF}). The line denotes one-to-one relationship. Correlation coefficient (r) and the number of points (n) are inserted.
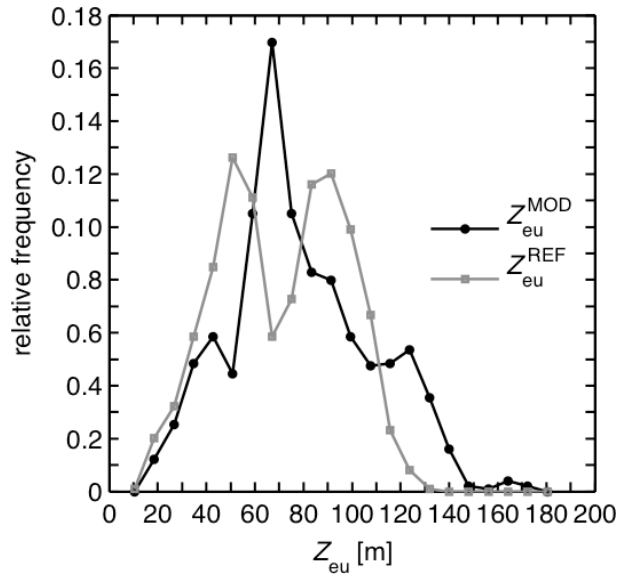

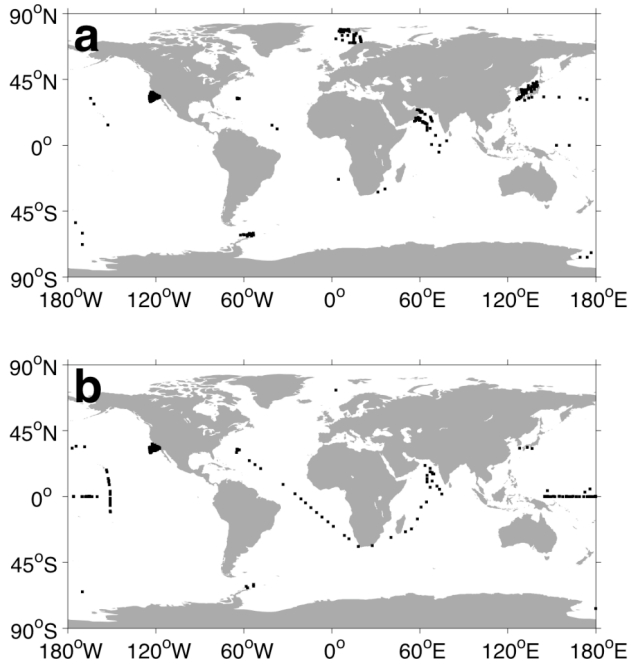**Figure 6.5.** Relative frequency polygons of modelled euphotic depth values (Z_{eu}^{MOD}) and reference data (Z_{eu}^{REF}).

154

Figure 6.6. Locations of reference euphotic depth values (Z_{eu}^{REF}) grouped around (a) the lower mode and (b) the upper mode, shown in Figure 6.5. The values represented in Figure 6.6a are shallower than the mean Z_{eu}^{REF} (70.9 m), while those in Figure 6.6b are deeper.
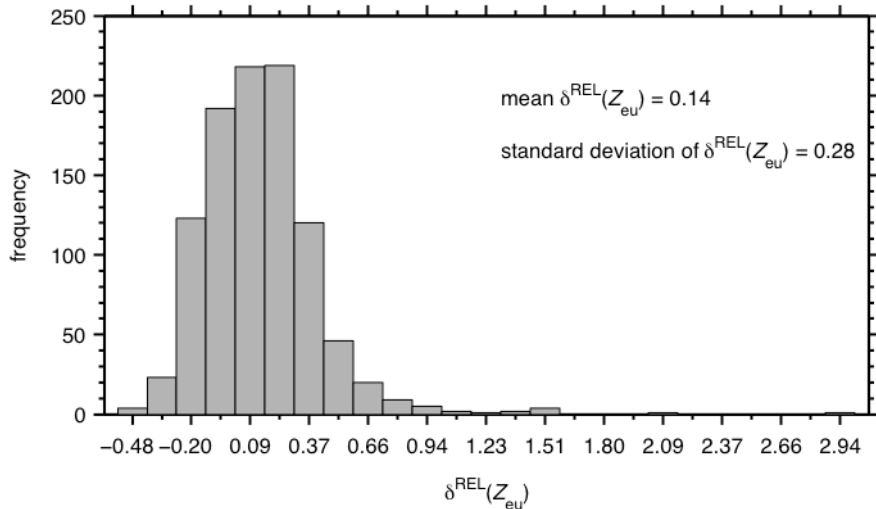

Figure 6.7. Histogram of relative discrepancies between model estimates and matching reference values of the euphotic depth ($\delta^{REL}(Z_{eu})$; see Equation (6.1)).
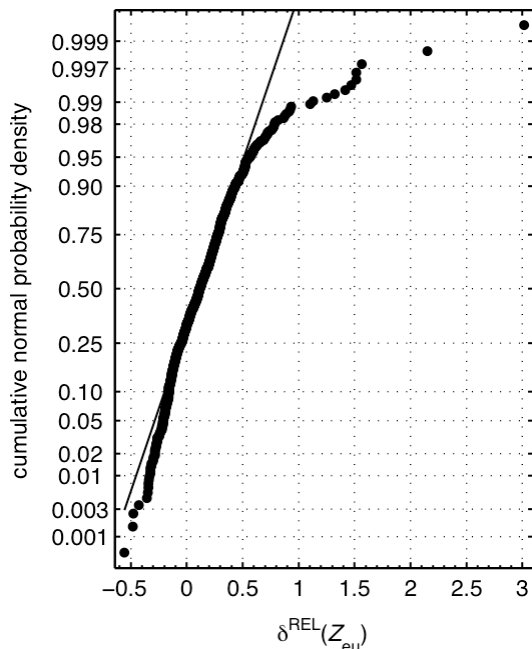
155

Figure 6.8. Normal probability plot of relative discrepancies between Z_{eu}^{MOD} and Z_{eu}^{REF} ($\delta^{REL}(Z_{eu})$), presented as dots. Superimposed on the plot is a line expected for a perfectly normally distributed sample.

The frequency distribution of $\delta^{REL}(Z_{eu})$ (Figure 6.7) is slightly positively skewed, shows a positive bias (mean = 0.14, i.e. 14%) and has a standard deviation of 0.28 (i.e. 28%). A normal probability plot of $\delta^{REL}(Z_{eu})$ (Figure 6.8) reveals that about 80% of $\delta^{REL}(Z_{eu})$ values (between ~10% and ~90% quantiles) comply with normal distribution. Hence, it can be assumed that normal distribution represents the distribution of uncertainties in Z_{eu}^{MOD} fairly realistically.

As seen in Figures 6.6a–6.6b, the geographic coverage by the data sample used here is uneven. This is reflected in the bimodal nature of the Z_{eu}^{REF} frequency distribution, shown in Figure 6.5. The statistics of $\delta^{REL}(Z_{eu})$ thus needed to be weighted. Global monthly Level-3 binned chlorophyll products between September 1997 and December 2005 from the reprocessing 5.1 of the Sea-viewing Wide Field-of-view Sensor (SeaWiFS) data set (provided by the NASA Ocean Biology Processing Group at http://oceancolor.gsfc.nasa.gov) were used to obtain population benchmarks for the weighting. Z_{eu} was computed from SeaWiFS chlorophyll using the approach of *Morel and Berthon* [1989] and *Morel and Maritorena* [2001]. Finally, eight-year average Z_{eu} (Z_{eu}^{AVG}) was calculated for every SeaWiFS grid cell (about 9 km × 9 km in
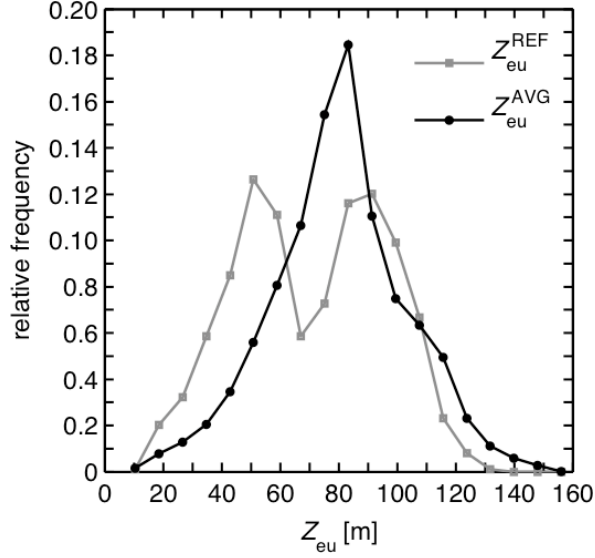
Figure 6.9. Relative frequency polygons of reference euphotic depths (Z_{eu}^{REF}) and average euphotic depths based on SeaWiFS global monthly Level-3 chlorophyll fields from September 1997 to December 2005 (Z_{eu}^{AVG}).

size). Figure 6.9 shows which classes of values are over- or underrepresented by the Z_{eu}^{REF} sample, relative to the frequency distribution of Z_{eu}^{AVG}.

The statistics of $\delta^{REL}(Z_{eu})$ were weighted in the following way: Z_{eu}^{REF} values were grouped in 10 equally wide euphotic depth classes. In each class, $\delta^{REL}(Z_{eu})$ was determined (see Equation (6.1)) and its mean and standard deviation were calculated (Figure 6.10). Weighting factor for these statistics in the ith euphotic depth class (w_i) was determined as the proportion of Z_{eu}^{AVG} belonging to that class:

$$w_i = \frac{n_i}{\sum\limits_{i=1}^{10} n_i},\tag{6.2}$$

where n_i is the number of Z_{eu}^{AVG} values in the ith class (Figure 6.10). Note that the range of Z_{eu}^{AVG} surpasses that of Z_{eu}^{REF} (Figure 6.9). In the weighting procedure, the Z_{eu}^{AVG} values extending beyond the maximum Z_{eu}^{REF} value were not considered, because defining 10 equally wide euphotic depth classes based on the range of Z_{eu}^{AVG} would yield two classes at the deep end of the range without any Z_{eu}^{REF} values. Disregarded values of Z_{eu}^{AVG} constitute only ~1% of the total number of Z_{eu}^{AVG} values. Weighted statistics (S_w) that
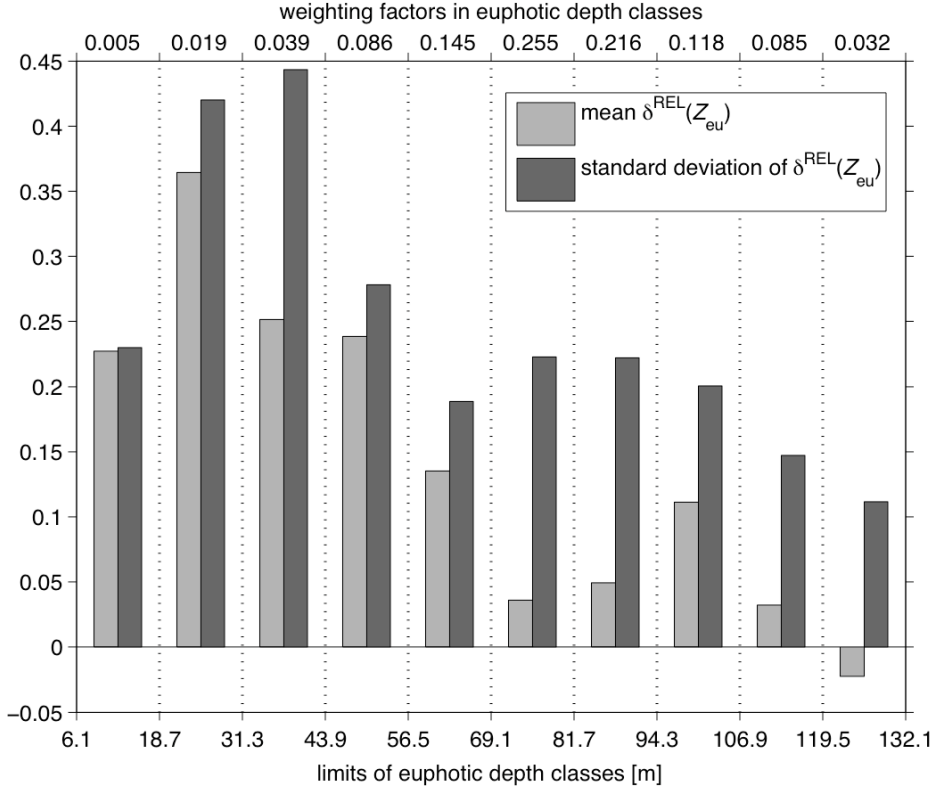
Figure 6.10. Means and standard deviations of relative discrepancies between Z_{eu}^{MOD} and Z_{eu}^{REF} ($\delta^{REL}(Z_{eu})$) in 10 euphotic depth classes. Weighting factors for the statistics in each class (top of the chart) were computed using Equation (6.2).

describe the uncertainty of Z_{eu}^{MOD} estimates were obtained by multiplying the statistics from each depth class (S_i) by their corresponding weighting factor (w_i) and summing the results:

$$S_w = \sum_{i=1}^{10} w_i \times S_i . \tag{6.3}$$

This method resulted in weighted mean $\delta^{REL}(Z_{eu})$ of 0.09 (i.e. 9%) and standard deviation of $\delta^{REL}(Z_{eu})$ equal to 0.22 (i.e. 22%). The former value can be regarded as the relative bias of Z_{eu}^{MOD}. The latter statistic is equivalent to zero-centred root mean square difference in relative terms [*Milutinović and Bertino*, 2011] and can thereby represent the uncertainty in modelling the natural variability of Z_{eu} (hereafter referred to as imprecision).

6.3. Discussion and Conclusions

Z_{eu} is a common input variable for net primary productivity (NPP) algorithms [e.g. *Behrenfeld et al.*, 2005; *Behrenfeld and Falkowski*, 1997; *Longhurst et al.*, 1995; *Mélin and Hoepffner*, 2011; *Smyth et al.*, 2005]. In order to establish the reliability of modelled NPP, it is important to quantify and, in turn, propagate uncertainties in input terms, such as Z_{eu}, through NPP models [*Boss and Maritorena*, 2006; *Lee et al.*, 2007; *Saba et al.*, 2011]. Recently, *Milutinović and Bertino* [2011] propagated uncertainties in input variables (including Z_{eu} modelled by the same approach as in this report) through an NPP algorithm. However, in that study, the component of uncertainty in Chl-based Z_{eu} estimates stemming from the modelling approach was disregarded, and only the component due to uncertainty in Chl derived from SeaWiFS observations was propagated. In future studies similar to that by *Milutinović and Bertino* [2011] both components should be included in uncertainty budgets. The results of this report can be used for such purposes.

Including the bias of Z_{eu}^{MOD} (9%) in the propagation of input uncertainties through the NPP model used by *Milutinović and Bertino* [2011] would not necessarily increase the bias of NPP estimates by 9%. It might be anticipated that the tendency of the method of *Morel and Berthon* [1989] and *Morel and Maritorena* [2001] to overestimate Z_{eu} would be offset to some extent by the positive bias of SeaWiFS Chl, which was reported by *Gregg et al.* [2009] and employed in the study by *Milutinović and Bertino* [2011]. This is because overestimated Chl yields underestimated Z_{eu}^{MOD}. However, the possibility of such an offset is questionable, as the portion of uncertainty in Z_{eu} considered by *Milutinović and Bertino* [2011] did not counteract the bias in SeaWiFS Chl. Quite the contrary, the collective contribution of Chl and Z_{eu} to the bias of NPP was larger than the contribution of Chl alone, probably owing to strong nonlinear effects. On the other hand, the imprecision of NPP resulting from the joint contribution of Chl and Z_{eu} was smaller than that due to Chl only, because the imprecisions of the two input variables partially cancelled one another (a likely effect of using the same quantity, in this case Chl, as input to a model more than once [*Taylor*, 1997]). This compensatory mechanism can hardly be expected to damp the influence of Z_{eu}^{MOD} imprecision on NPP estimates, because that imprecision is independent of Chl. Clearly, this is no more than a tentative speculation and a more rigorous approach is required before any firm conclusions related to this issue can be made.

A few recommendations can be given for future actions towards quantification and minimization of uncertainties related to Z_{eu} modelling. For example, it may prove helpful to derive Chl by the method from *Gregg et al.* [2009]. This could reduce Chl bias that, as discussed above, reflects negatively on Z_{eu} estimates. Furthermore, in a large global evaluation of 21 NPP models, *Saba et al.* [2011] discovered that the overall model skill was particularly poor in Case-2 waters, which they equated to regions where bottom depths were less than 250 m.

Interestingly, this underperformance was not caused by conditions that are challenging for ocean-colour estimates of Chl, because *Saba et al.* [2011] used *in situ* Chl as input to the models. They therefore hypothesized that the NPP model skill might have been impaired at least partly by inaccuracies in Z_{eu} modelling. This hypothesis remains to be tested by performing uncertainty evaluations for Z_{eu} models separately in Case-1 and Case-2 waters. It is probable that those Z_{eu} models which rest upon the first principles [*Lee et al.*, 2007] perform better in the optically complex environments than empirical models, such as the one used in the present report. This, however, awaits further investigation.

Acknowledgements

References

Behrenfeld, M., E. Boss, D. Siegel, and D. Shea (2005), Carbon-based ocean productivity and phytoplankton physiology from space, *Global Biogeochemical Cycles*, *19*(1), GB1006.

Behrenfeld, M. J., and P. G. Falkowski (1997), Photosynthetic rates derived from satellite-based chlorophyll concentration, *Limnology and Oceanography*, *42*(1), 1-20.

Boss, E., and S. Maritorena (2006), Uncertainties in the products of ocean-colour remote sensing, in *Remote sensing of inherent optical properties: Fundamentals, tests of algorithms and applications*, edited by Z. Lee, pp. 19-26, International Ocean-Colour Coordinating Group, Dartmouth, Canada.

Falkowski, P. G., and J. A. Raven (2007), *Aquatic photosynthesis*, 2nd ed., 500 pp., Princeton University Press.

Gregg, W. W., N. W. Casey, J. E. O'Reilly, and W. E. Esaias (2009), An empirical approach to ocean color data: Reducing bias and the need for post-launch radiometric re-calibration, *Remote Sensing of Environment, 113*(8), 1598-1612.

Kirk, J. T. O. (1994), *Light and photosynthesis in aquatic ecosystems*, 2nd ed., 528 pp., Cambridge University Press.

Lee, Z., A. Weidemann, J. Kindle, R. Arnone, K. L. Carder, and C. Davis (2007), Euphotic zone depth: Its derivation and implication to ocean-color remote sensing, *Journal of Geophysical Research-Oceans*, *112*(C3), C03009.

Longhurst, A., S. Sathyendranath, T. Platt, and C. Caverhill (1995), An estimate of global primary production in the ocean from satellite radiometer data, *Journal of Plankton Research*, *17*(6), 1245-1271.

Mantoura, R. F. C., S. W. Jeffrey, C. A. Llewellyn, C. H., and C. E. Morales (1997), Comparison between spectrophotometric, fluorometric and HPLC methods for chlorophyll analysis, in *Phytoplankton pigments in oceanography: Guidelines to*

modern methods, edited by S. W. Jeffrey, R. F. C. Mantoura and S. W. Wright, pp. 361-380, UNESCO Publishing, Paris, France.

Mélin, F., and N. Hoepffner (2011), Monitoring phytoplankton productivity from satellite: An aid to marine resources management, in *Handbook of satellite remote sensing image interpretation: Applications for marine living resources conservation and management*, edited by J. Morales, V. Stuart, T. Platt and S. Sathyendranath, pp. 79-93, EU PRESPO and IOCCG.

Milutinović, S., and L. Bertino (2011), Assessment and propagation of uncertainties in input terms through an ocean-colour-based model of primary productivity, *Remote Sensing of Environment*, in press, doi: 10.1016/j.rse.2011.03.013.

Morel, A., and J. F. Berthon (1989), Surface pigments, algal biomass profiles, and potential production of the euphotic layer - relationships reinvestigated in view of remote-sensing applications, *Limnology and Oceanography*, *34*(8), 1545-1562.

Morel, A., and S. Maritorena (2001), Bio-optical properties of oceanic waters: A reappraisal, *Journal of Geophysical Research-Oceans*, *106*(C4), 7163-7180.

Morel, A., and B. Gentili (2004), Radiation transport within oceanic (case 1) water, *Journal of Geophysical Research-Oceans*, *109*, C06008.

Saba, V. S., M. A. M. Friedrichs, D. Antoine, R. A. Armstrong, I. Asanuma, M. J. Behrenfeld, A. M. Ciotti, M. Dowell, N. Hoepffner, K. J. W. Hyde, J. Ishizaka, T. Kameda, J. Marra, F. Mélin, A. Morel, J. O'Reilly, M. Scardi, W. O. Smith Jr, T. J. Smyth, S. Tang, J. Uitz, K. Waters, and T. K. Westberry (2011), An evaluation of ocean color model estimates of marine primary productivity in coastal and pelagic regions across the globe, *Biogeosciences*, *8*(2), 489-503.

Smyth, T. J., G. H. Tilstone, and S. B. Groom (2005), Integration of radiative transfer into satellite models of ocean primary production, *Journal of Geophysical Research-Oceans*, *110*(C10), C10014.

Stramska, M., D. Stramski, R. Hapter, S. Kaczmarek, and J. Stoń (2003), Bio-optical relationships and ocean color algorithms for the north polar region of the Atlantic, *Journal of Geophysical Research-Oceans*, *108*(C5), 3143.

Werdell, P. J., S. Bailey, G. Fargion, C. Pietras, K. Knobelspiesse, G. Feldman, and C. McClain (2003), Unique data repository facilitates ocean color satellite validation, *Eos, Transactions*, *84*(38), 377, 387.

Werdell, P. J., and S. W. Bailey (2005), An improved in-situ bio-optical data set for ocean color algorithm development and satellite data product validation, *Remote Sensing of Environment*, *98*(1), 122-140.